DAMAGE DETECTION AND RELIABILITY ASSESSMENT OF BUILDING STRUCTURES USING STOCHASTIC APPROACHES

by

Juan **ZHANG**

B. Eng., M. Sc.

A Thesis Submitted for the Degree of **Doctor of Philosophy**

Department of Civil and Structural Engineering

The Hong Kong Polytechnic University, Hong Kong

February 2010

THE HONG KONG POLYTECHNIC UNIVERSITY

Department of Civil and Structural Engineering

DAMAGE DETECTION AND RELIABILITY ASSESSMENT OF BUILDING STRUCTURES USING STOCHASTIC APPROACHES

by

Juan **ZHANG**

A Thesis Submitted in Partial Fulfillment of the Requirements for the

Degree of Doctor of Philosophy

September 2009

To My Family

Declaration

I hereby declare that this dissertation entitled "***Damage Detection and Reliability Assessment of Building Structures Using Stochastic Approaches***" is my own work and that, to the best of my knowledge and belief, it reproduces no material previously published or written, nor material that has been accepted for the award of any other degree or diploma, except where due acknowledgement has been made in the text.

SIGNED

_____

ZHANG Juan

Abstract

Civil structures begin to deteriorate once they are built due to harsh environment such as corrosion, earthquake, and typhoon. Vibration-based structural damage detection methods have thus attracted considerable attention for assessment of functionality and safety of civil structures. Nevertheless, the damage detection of civil structures still remains as a challenging task. One of the main obstacles is that the current damage detection methods are either insensitive to local structural damage or sensitive to measurement noise. In addition, a significant amount of uncertainties are inherently and inescapably associated with structural damage detection of civil structures, which limits the successful application of most deterministic damage detection methods. In this regard, this thesis focuses on the establishment of a framework in which novel stochastic approaches in consideration of the uncertainties involved in measurements, structures and external excitations are proposed to detect damage of building structures and assess their reliability effectively.

This thesis first proposes a novel structural damage detection method using a new damage index based on the statistical moments of dynamic responses of a building structure under random excitation. The principle of the statistical moment-based damage detection (SMBDD) method is first put forward in the frequency domain through a single-degree-of-freedom (SDOF) system under white Gaussian noise

excitation. The sensitivity of statistical moment to structural damage is discussed for various types of structural responses and different orders of statistical moment. The formulae for statistical moment-based damage detection are derived. The effect of measurement noise on damage detection is ascertained. The new damage index and the proposed SMBDD method are then extended to multi-degree-of-freedom (MDOF) systems with resort to the nonlinear least squares method. As numerical studies, the proposed method is applied to both single and multi-story shear buildings in consideration of measurement noise. Numerical results show that the fourth-order statistical moment of story drifts is a more sensitive indicator to structural stiffness reduction than the natural frequencies, the second order moment of story drift, and the fourth-order moments of velocity and acceleration responses of the shear building. The fourth-order statistical moment of story drifts can be used to satisfactorily identify both locations and severities of various damage scenarios of the shear building. Furthermore, a significant advantage of the SMBDD method lies in that it is not only sensitive to local structural damage but also insensitive to measurement noise.

After that, the SMBDD method is advanced in the following three aspects in the frequency domain for its practical application: (1) the type and location of external excitations, (2) the type of building structures, and (3) the number of structural responses measured. The equations of the SMBDD method are accordingly extended to be more general for any type of building structures under any type of random excitation as long as it complies with the Gaussian distribution. The generalized SMBDD method is also extended from the necessity of complete measurements of all DOFs to the proper selection of measurements of incomplete DOFs. Extensive

numerical examples are presented to demonstrate the feasibility and effectiveness of the generalized SMBDD method. A MDOF shear building structure under colored noise excitations at different locations is investigated. Various damage scenarios of a high-rise building and a frame structure using selected measurement responses are investigated. The effect of measurement noise on the quality of identified results is also investigated for all the damage scenarios concerned by numerically contaminating the external excitations and the measured responses with white Gaussian random noises. Numerical analysis results show that the damage locations and severities of all the concerned various damage scenarios can be identified satisfactorily even though the structural responses used are incomplete and the measurement noise has a high noise-to-signal ratio of 15%.

Furthermore, the feasibility and effectiveness of the generalized SMBDD method are explored in the time domain for the building structures under non-Gaussian excitations. The algorithm of the generalized SMBDD method in the time domain is developed. Various damage scenarios of different damage locations and damage severities of shear buildings, high-rise buildings and frame structures are numerically investigated. Numerical results demonstrate that the generalized SMBDD method is feasible and effective for building structures under either Gaussian or non-Gaussian excitations in the time domain. Even with the measurement noise intensity as high as 15%, the structural damage locations in various damage scenarios with incomplete measurements can be identified satisfactorily no matter whether the external excitation is of Gaussian distribution or not. Furthermore, the identified damage severities are exactly equal to the real values when measurement noise is not considered. Otherwise, the quality of the identified damage severities in the time

domain is similar with that in the frequency domain when measurement noise is considered. Nevertheless, the requirement of proper optimization methods in model updating is required for the generalized SMBDD method in the time domain.

Before the generalized SMBDD method can be applied to real building structures, experimental investigations are necessary. This thesis therefore presents an experimental investigation on the generalized SMBDD method through shaking table tests. Three three-story shear building models of different lumped masses are designed and manufactured. The column width of each building model is reduced from both sides of the columns at designated stories to simulate building damage. Different damage severities are simulated by different reductions of column widths. A total of eight damage scenarios of different single or multi damage locations and different damage severities are constructed in the building models step by step. The undamaged and damaged shear building models are subjected to ground motions generated by the shaking table. Two band-limited white noise time histories and two colored noise time histories are randomly simulated and inputted as scheduled into the control system of the shaking table to generate the expected ground excitation to the building models. The ground motion and the displacement responses of each building model at each floor are recorded. The recorded ground motion and building responses as well as identified structural damping ratios are then used to identify damage locations and severities using the generalized SMBDD method in both the frequency domain and the time domain. To provide a basis for the assessment of the proposed damage detection method, the theoretical value of damage severity for a given damage scenario is also computed using the flexibility method and the principle of virtual work. The identified damage locations and severities are

compared with the theoretical values. The comparison is found satisfactory in both the frequency domain and the time domain. The effectiveness and feasibility of the generalized SMBDD method are therefore demonstrated by the shaking table tests.

The research work on structural damage detection then makes further progress by proposing a new stochastic damage detection method based on the generalized SMBDD method in consideration of random parameters or uncertainties which are inescapable for civil structures. Although many researchers have studied statistical structural damage identification to consider the uncertainties involved in civil structures in the last three decades, most of the statistical approaches still stay in primitive forms. Generally speaking, they have one or more of the following problems: computational complex, inherent limitation to identifying presence of damage only, ineffectiveness in dealing with uncertain parameters which are not normally distributed, and prohibitiveness for most practical applications. The new stochastic damage detection method proposed in this thesis can not only locate structural damage but also identify damage severities without the extensive computational efforts, and it can also handle both Gaussian and non-Gaussian random parameters. The algorithm of the stochastic damage detection method is first presented in the thesis. New damage indices are proposed to identify damage locations and damage severities. The numerical investigation is then conducted to demonstrate the proposed method through a shear building structure. The first damping ratio of the shear building is selected as a random parameter with a lognormal distribution. Three damage scenarios including single and multi damage scenarios are explored. Numerical analysis results show that the proposed method in consideration of uncertainties or random parameters can identify both damage

locations and damage severities of the building structures of random parameters satisfactorily.

The last piece of work described in this thesis is concerned with reliability assessment of instrumented building structures. Although the deployment of structural health monitoring systems has now attained some degree of maturity, the application of measured response data of a building structure for evaluating structural reliability is still in its infancy. In most of previous investigations, structural system identification and structural reliability assessment are treated separately. When uncertainties or random parameters are taken into account, the stiffness parameters of all the elements in a building structure identified are random parameters coupled with each other. Under this circumstance, it is prohibitive to evaluate structural reliability by the current reliability analysis methods for civil structures. This study therefore presents two integrated methods to evaluate structural component reliability and structural system reliability, respectively. The integrated methods accept the measurement responses as input and produce as output the reliability of the concerned instrumented structures. Structural system identification is embedded in the procedure of the reliability analysis in the proposed methods. Numerical investigation is conducted on the aforementioned stochastic shear building structure with three damage scenarios under the EL Centro excitation. The computation results manifest that the undamaged shear building has higher reliability than the damaged shear buildings of various damage scenarios. The larger damage severity, the lower is the reliability of the building. In addition, the values of structural system reliability are always no larger than those of structural component reliability. The structural reliability of stochastic building structures integrated with system identification can

be effectively evaluated by the proposed methods using limited measurement responses.

In summary, the research described in this thesis involves the development and application of the SMBDD method, the stochastic damage detection method, and the reliability assessment methods for stochastic structures. Extensive numerical and experimental investigations have demonstrated that the SMBDD method is not only sensitive to local structural damage but also insensitive to measurement noise, and this method can be used in either the frequency domain or the time domain. The stochastic damage detection method enables the damage identification of building structures of uncertainties or random parameters. By using the proposed reliability assessment methods, the reliability of a stochastic structure without explicit damage identification can be obtained by using limited measurement responses.

Publications

Journal Papers:

Xu, Y.L., Zhang, J., and Li, J.C. (2009), "Experimental investigation on statistical moment-based structural damage detection method", *Journal of Structural Health Monitoring*, 8(6), 555-571.

Xu, Y.L., Zhang, J., Li, J. and Wang, X.M. (2009), "Stochastic damage detection method for building structures with parametric uncertainties", submitted.

Zhang, J., Xu, Y.L., Xia, Y., and Li, J. (2008), "A new statistical moment-based structural damage detection method", *Structural Engineering and Mechanics-An International Journal*, 30(4), 445-466.

Zhang, J., Xu, Y.L., Li, J. and Xia, Y. (2009), "Generalization of the statistical moment-based damage detection method", submitted.

Zhang, J., Xu, Y.L. and Li, J. (2009), "Integrated system identification and reliability evaluation of stochastic building structures", submitted.

Zhang, J., Xu, Y.L. and Li, J.C. (2010), "Statistical moment-based structural damage detection method in the time domain", in process.

Conference Papers:

Zhang, J., Xu, Y.L., Xia, Y., and Li, J., (2007), "A new structural damage detection method based on statistical moments", *Proceedings of International Conference on Health Monitoring of Structure, Material and Environmen*t, Nanjing, China, 168-173;

Zhang, J., Xu, Y.L., and Li, J.C., (2008), “Experimental investigation on a new statistical moment-based structural damage detection method”, *The Fourth International Workshop on Advanced Smart Materials and Smart Structures Technologies (ANCRiSST)*, Waseda University, Tokyo, Japan;

Zhang J., Xu, Y.L., Xia, Y. and Li, J.C. (2009), "Statistical moment-based damage detection of building structures," *Proceedings of the Fourth International Conference on Structural Health Monitoring of Intelligent Infrastructure*, 22-24 July, 2009, Zurich, Switzerland, Paper No.342.

Zhang, J., and Xu, Y.L., (2009), “Stochastic damage detection method for building structures of random parameters”, *Proceedings of the ANCER Workshop on Earthquake Engineering Research: Lessons learned from recent earthquakes and contributions from young researchers*, University of Illinois at Urbana-Champaign, Illinois, USA, 13-14 August 2009. CD-ROM: Session VI-B.

Zhang, J., Xu, Y.L., and Li, J., (2009), “Further development of the statistical moment-based structural damage detection method”, *the Sixth International Conference on Advances in Steel Structures (ICASS ’09)*, The Hong Kong Polytechnic University, Hong Kong, 16-18 December 2009.

Acknowledgements

I would like to express my gratitude to all those who made the completion of this thesis possible. First and foremost I am deeply indebted to my supervisor, Prof. Y.L. Xu, for his expert guidance, invaluable discussion and support all the way throughout the course of my research study. Without his inspiration and patience, I would never have achieved the results presented in this thesis. I would also like to express my sincere thanks to my co-supervisor Prof. J. Li of Tongji University for his enthusiastic guidance and kind encouragement throughout the course of this research.

I owe special thanks to Dr. J.C. Li from University of Technology Sydney, Australia, for his excellent cooperation in completing the experimental work during my PhD study. Thanks also to Dr Y. Xia of The Hong Kong Polytechnic University, Dr. X.M. Wang of Commonwealth Scientific and Industrial Research Organization (CSIRO), Australia, and Dr. J.B. Chen of Tongji University for their beneficial discussions. Special thanks are also given to my friends and fellow colleagues in The Hong Kong Polytechnic University for their help and encouragement in the past years. I particularly thank Dr. B. Chen, Dr. Y.F. Duan, Dr. X.J. Hong, Dr. J. Chen, Mr. S. Zhan, Mr. T.T. Wai and Miss W.S. Chan.

I am grateful for the financial support of The Hong Kong Polytechnic University by awarding me a student scholarship over the past three years. The kind help of staff in

the head office and general office of Department of Civil and Structural Engineering during my PhD study is also appreciated.

Last but not least, I wish to thank all my family members and friends for their love and endless support.

Contents

List of Figures

List of Tables

List of Abbreviations

AR	autoregressive
BP	back-propagation
CN	colored noise
COMAC	coordinate modal assurance criterion
DOF	degree of freedom
DS	damage severity
EMD	empirical mode decomposition
FD	frequency domain
FE	finite element
FEM	finite element
FFT	fast Fourier transform
FORM	first-order reliability method
FRF	frequency response functions
GDEE	generalized density evolution equation
HT	Hilbert-transform
MAC	modal assurance criterion
MCS	Monte Carlo simulation
MDOF	multi-degree-of-freedom
MLP	multilayer perceptron
MNI	measurement noise intensity

NDT	non-destructive technique
PCE	polynomial chaos expansion
PDF	probability density function
PDE	probability density evolution
PDEE	probability density evolution equation
PDEM	probability density evolution method
PSD	power spectral density
PMAC	Partial modal assurance criterion
RDT	random decrement technique
RMS	root mean square
SC	stiffness coefficients
SDOF	single degree of freedom
SFEM	stochastic finite element method
SHMS	structural health monitoring system
SMBDD	statistical moment-based damage detection
STRECH	structural translational and rotational error checking
SORM	second-order reliability method
SSFEM	spectral stochastic finite element method
TD	time domain
WN	white noise
WPS	wavelet packet signature

List of Notations

$\mathbf{C}$	$N \times N$ damping matrix of a structure
c	damping coefficient of a SDOF system
C_k	Fourier transform of $f_k(t)$
C_k^*	the conjugates of C_k
E	Young's modulus
$F(\alpha)$	distribution function
$f(\alpha)$	probability density function
$\mathbf{f}(t)$	external excitation of a building structure
$f(\mathbf{x})$	the joint PDF of a random vector $\mathbf{x}$
$f_k(t)$	the k-th element of $\mathbf{f}(t)$
$\mathbf{g}(\mathbf{\Psi}, t)$	external force with random parameters $\mathbf{\Psi}$
h	the length of elements
Hj	the *j*-th hypothesis for a damage event that can contain any number of substructures as damaged
$H(\omega)$	frequency response function
$H_d(\omega)$	displacement frequency response function
$H_v(\omega)$	velocity frequency response function
$H_a(\omega)$	acceleration frequency response function
I	moment of inertia

k	theoretical stiffness coefficient of a building
$\hat{k}$	identified structural stiffness parameter without considering the effect of measurement noise
$\hat{k}_n$	identified structural stiffness parameter considering the effect of measurement noise
$\hat{k}^u$	identified stiffness parameter of an undamaged structure
$\hat{k}^d$	identified stiffness parameter of a damaged structure
$\mathbf{K}$	$N \times N$ stiffness matrix of a structure
M_{n}	The nth-order statistical moment
m	mass coefficient of a SDOF system
$\mathbf{M}$	$N \times N$ mass matrix of a building
N_s	the number of sampling points
$P\{\cdot\}$	probability of a random event
$P(H_j)$	prior probability of the j-th hypothesis H_j
$P(H_j\|\psi)$	posterior probability of H_j, given ψ a set of observed modal parameters
P_f	failure probability
$p_{\mathbf{XZ}}(x,\mathbf{z},t)$	joint probability density function of structural response $\mathbf{X}(t)$ and structural random parameter vector $\mathbf{Z}$
R	radius of curvature
$R(t)$	dynamic reliability
$S(\omega)$	power spectral density
$x(t)$	displacement response
$x_m(t)$	measured displacement response

$x_u(t)$	unmeasured displacement response
$\bar{x}$	the mean value of $x(t)$
$\dot{x}(t)$	velocity response
$\dot{x}_m(t)$	measured velocity response
$\dot{x}_u(t)$	unmeasured velocity response
$\ddot{x}(t)$	acceleration response
$\ddot{x}_m(t)$	measured acceleration response
$\ddot{x}_u(t)$	unmeasured acceleration response
$\ddot{x}_g$	ground acceleration
$X_i(\omega)$	Fourier transform of the displacement response $x_i(t)$
$\bar{X}_{\max}$	equivalent extreme value
$Y(\tau)$	a virtual stochastic process
α	measurement noise intensity
β	reliability index
γ	noise effect ratio
σ	standard deviation
ε	strain
ξ	modal damping ratio
ξ_i	the *i*th modal damping ratio
ω_i	the *i*th circular frequency
ω_o	circular natural frequency
ω_i	the *i*th circular natural frequency
$\boldsymbol{\Theta}$	random parameter vector

$\Omega_{\boldsymbol{\theta}}$	distribution domain of $\boldsymbol{\Theta}$
κ	curvature or 1/R
φ_i	modal displacement at measurement point i
$\boldsymbol{\phi}_r$	the r-th mode shape
ϕ_{ki}	the kth component of the ith mode shape
$\boldsymbol{\Phi}$	mass-normalized modal matrix of a structure
ψ	a set of observed modal parameters
Ω_S	safe domain
μ	theoretical structural damage severity
$\hat{\mu}$	estimated or identified structural damage severity
Γ_i	the ith participation factor

CHAPTER 1

INTRODUCTION

1.1 Background

Civil engineering infrastructures begin to deteriorate once they are built and continuously accumulate damage during their service life due to natural hazard and harsh environment such as earthquake, storm, fire, long-term fatigue and corrosion. Such damage undetected and uncorrected will potentially cause more damage and eventually lead to catastrophic structural failure with loss of human life. To ensure the serviceability and safety of structures, structural damage detection and integrity assessment are very necessary. They not only could indicate potential damage but also are of essential value to the management authorities to make fast and safe decisions on whether or not repair, partial replacement or even demolition of the structure is necessary. Such information on structural damage and integrity is particularly crucial in cases of severe natural hazards and after long-term usage.

Vibration-based structural damage detection methods have therefore attracted considerable attention in recent years for the assessment of health and safety of complex civil engineering structures. Most of currently-used vibration-based structural damage detection methods are built on the idea that the measured modal parameters or the parameters derived from these modal parameters are functions of the physical properties of the structure and, therefore, changes in the physical properties will cause detectable changes in the modal parameters (Doebling et al. 1998). The changes in modal parameters (damage indices) commonly used in

vibration-based structural damage detection include natural frequency changes, mode shape changes, mode shape curvature changes, flexibility matrix changes, and modal strain energy changes. These damage indices are often estimated experimentally from the structural response time histories measured before and after the changes in physical properties of a structure (structural damage). The advantages of the damage detection method based on natural frequency change are that the identification of natural frequency from measured structural response time histories is relatively easy and of relatively higher precision than those based on other modal parameters. Typical resolution error in the identification of natural frequency of a lightly damped structure is 0.1%, while that of mode shape is 10% or more (Friswell and Penny, 1997). Those synthesized derivatives based on mode shape could presumably have more uncertainty. However, the structural damage typically is a local phenomenon, and the change of natural frequency has low sensitivity to local damages (Salawu, 1997). Furthermore, natural frequency is a global property of the structure and it generally can not provide spatial information about damage location. The damage indices based on mode shape changes or those derivatives can give the spatial information on damage location in theory. However, they may not be effective and reliable in consideration of the number of sensors required and the measurement noise arising from the environment conditions during the test, and they generally do not provide the information regarding damage severity (Pandey et al, 1991; Farrar and Jauregui, 1998). Alvandi and Cremona (2006) assessed various damage indices and concluded that the modal strain energy is less affected by measurement noise. However, they found that, even for the modal strain energy method, a 3% noise level has already made it difficult to identify damage location of a structure in practice and should be considered as a high level of noise.

In view of the aforementioned studies, it can be seen that although vibration-based damage detection methods and modal updating methods have demonstrated various degrees of success, the damage detection of complex civil engineering structures still remains a challenging task. The main obstacles are the insensitivity to local structural damage for the methods based on modal properties (particularly modal frequencies and mode shapes) and the high sensitivity to environmental conditions and measurement noise for the methods based on derivatives of modal parameters and other methods which might be sensitive to local structural damage. Therefore, efficient and effective damage detection methods which are sensitive to local structural damage but insensitive to measurement noise need to be pursued.

Furthermore, most of the methods aforementioned are to identify structural damage deterministically by assuming that the finite element (FE) model of a structure can represent actual structural properties and that measurement data have high precision. In practice, however, a significant amount of uncertainties are inevitably involved in damage detection procedure especially for civil structures. If the level of uncertainty is higher than or close to the level of actual changes of structural properties due to structural damage, the real information of structural damage will be concealed and the structural damage can not be accurately identified. For example, the existence of measurement noise may render less pronounced damage undetectable (negative falsity) or may identify some intact structural elements as damaged elements (positive falsity) (Doebling *et al.,* 1998). The uncertainties existing in the model along with the errors in the measured vibration data limit the successful use of those deterministic damage detection methods. Therefore, Housner (1997) indicated that structural identification within a statistical framework appears to be a promising

general approach to structural health monitoring of civil structures in view of the inescapable data and modeling uncertainties.

Although many researchers have studied in the area of structural damage identification with consideration of uncertainties, most of the statistical approaches still stay in primitive forms. The representative approaches to detect structural damage with consideration of the uncertainties are the Bayesian methods, the Monte Carlo simulation (MCS) methods, the perturbation methods and the statistical pattern recognition methods. For the Bayesian probabilistic approaches, the computation could become prohibitive when a large number of substructures of complex civil structures are assumed as damaged because substantive hypotheses should be examined to find more local maximum posterior probabilities and potentially to identify the correct damage event. The problem of computational complex also exists in the stochastic perturbation methods, in which various covariance matrices of updating parameters have to be calculated by the MCS method under many circumstances. The MCS methods are computationally intensive because it requires a large number of simulations to obtain an accurate and valid statistics. For the statistical pattern recognition methods, they can be divided into two classes: supervised learning and unsupervised learning. The unsupervised learning can be applied to data not containing examples from the damaged structure, but this approach is inherently limited to identify presence of damage only. When data are available from both the undamaged and damaged structure, supervised learning approach can be taken to move forward to higher level damage identification to locate and quantify damage. However, the acquisition of data sets from the damaged structure in various damage states is often prohibitive for most applications.

Furthermore, almost all of damage detection techniques with consideration of uncertainties assume the Gaussian distribution of a feature space, and establish decision making threshold values based on this normality assumption. Therefore, they do not always work effectively in dealing with uncertainty parameters which are not normally distributed. In addition, few, if any, of the current probabilistic damage detection methods can give complete probabilistic information such as the probability density function (PDF) of structural damage severity. Therefore, the more efficient and versatile stochastic damage detection method needs to develop for civil structures.

While the development of methods for structural damage detection has now attained much attention and some degree of maturity, the practical use of monitoring data from instrumented structures to help structural inspection, maintenance, and management is still in its infancy. Research efforts devoted to the methodologies that accept the processed monitoring data as input and produce as output the reliability of the concerned structure are still very few in comparison with the myriad of literature addressing on structural damage detection methods. As structural reliability is the major decision factor throughout the life cycle of civil engineering structures, methodologies to assess structural reliability based on monitoring data are indeed desirable. The prominent work is due to Yao and his colleagues (Yao 1979; Yao 1983; Natke and Yao 1988; Yao and Natke 1994; Wong and Yao 2001). They proposed a holistic view where health monitoring, damage detection, and reliability evaluation are defined as the sequential components in a value chain. In order to cater for the reliability analysis of instrumented structures, the symptom-based reliability method compatible with health monitoring technologies was introduced in

their study. Following this study, Stubbs et al. (1998; 2000) developed a methodology to continuously assess the safety of civil engineering structures in which structural damage was first identified using the measurement data of modal parameters and reliability method was then applied to the possibly damaged structure to determine the failure probability and reliability index. However, the deterministic model updating approach they used lacks the capability in accounting for the uncertainties in measurement data, such as measurement errors and inherent randomness. A complete integrity assessment should consider uncertainties of structures and inputs for the damaged or employed structures, especially in dynamic aspects. Therefore, the method to assess structural reliability with consideration of the uncertainties of structures and inputs and based on the measurement data is indeed desirable for instrumented structures.

1.2 Research Objectives

This thesis is devoted to developing a deterministic damage detection method that is both sensitive to local damage and insensitive to measurement noise, proposing a stochastic damage detection method that can effectively and efficiently identify damage locations and damage severities with consideration of the uncertainties involved in civil structures, and establishing a framework to evaluate structural component reliability with only one limit-state function and structural system reliability with multiple limit-state functions. The proposed structural reliability analysis approaches accept the monitoring data as input and produce as output the reliability of the instrumented structure. More specifically, the main objectives of this research are:

(1) To propose the statistical moment-based damage detection (SMBDD) method for deterministic building structures, and numerically demonstrate the proposed method both in the frequency domain and in the time domain for different kinds of building structures with different external excitations. The proposed method should be sensitive to structural damage and at the same time insensitive to measurement noise.

(2) To carry out experimental study on the SMBDD methods to investigate its feasibility and effectiveness both in the frequency domain and in the time domain through shaking table tests on shear building models of multi degrees of freedom (MDOF) with various damage scenarios.

(3) To develop a stochastic damage detection method with consideration of the uncertainties inescapably involved in structural identification especially for civil structures. The stochastic damage detection method can accurately identify damage locations and damage severities without the problem of prohibitive computation.

(4) To proposed the methods which accept the monitoring data as input and produce as output the reliability of the instrumented structure to assess structural component reliability with only one limit-state function and structural system reliability with multiple limit-state functions. The uncertainties of both structures and inputs are considered in the proposed approaches.

1.3 Thesis Layout

This dissertation is comprised by nine chapters.

Chapter 1 introduces the background and motivation of the present research, the main objectives in the PhD project, and the organization of the thesis.

Chapter 2 contains a literature review, which covers three relatively independent subjects. The first subject is on the vibration-based deterministic damage detection methods, including methods based on structure frequency changes, methods based on mode shape changes and their derivatives, methods based on frequency response functions (FRF), methods based on matrix updating, methods based on neural network and genetic algorithm and time-frequency methods. The second subject is on the statistical damage detection method with consideration of the uncertainties resulting from environment, such as temperature, loading and humidity, measurement noise, uncertainty in geometry and boundary conditions, inexact modeling of the material constitutive behavior or damping, uncertainty in external excitations, and so on. The last subject is on the structural reliability analysis methods, including component reliability analysis methods, system reliability analysis methods and time dependent reliability analysis methods.

Chapter 3 proposed a novel structural damage detection method with a new damage index based on the statistical moments of dynamic responses of a structure under a random excitation. After a brief introduction to statistical moment theory, the principle of the new method is put forward in terms of a single-degree-of-freedom (SDOF) system in the frequency domain. The sensitivity of statistical moment to structural damage is discussed for various types of structural responses and different orders of statistical moment. The formulae for statistical moment-based damage

detection are derived in the frequency domain. The effect of measurement noise on damage detection is ascertained. The new damage index and the proposed statistical moment-based damage detection method are then extended to multi-degree-of-freedom (MDOF) systems with resort to the nonlinear least squares method. Numerical studies are conducted for both single and multi-story shear buildings. And the effect of measurement noise on the quality of identified results is investigated by contaminating the measured responses and inputs with Gaussian white noise.

Chapter 4 advances this statistical moment-based damage detection (SMBDD) method in the frequency domain to make it more versatile to various types of structures rather than shear buildings only and to different random excitations other than white noise ground motion only. In this regard, the basic equations of motion involved in the method are firstly generalized so as to be applicable to different random excitations at different locations and to different types of structures. The feasibility of the extended method is then numerically investigated by utilizing both flexible high-rise buildings and relatively stiff frame structures and by considering colored noise ground excitations as well as random excitations acting on other parts of the structures. Various damage scenarios of different damage locations and severities of the high-rise buildings and the frame structures are investigated using the generalized SMBDD method. The effect of measurement noise is also considered for all the concerned cases.

Chapter 5 investigates the feasibility and effectiveness of the SMBDD method in the time domain without the limitation that the external excitation should be stationary and have Gaussian distribution. Firstly, the algorithm of the proposed method is

proposed in the time domain. Then, various damage scenarios of different damage locations and severities of shear buildings, high-rise buildings and frame structures are investigated using the SMBDD method in the time domain. The effect of measurement noise on the quality of damage detection results is also investigated for all the concerned cases.

Chapter 6 presents the experimental investigation on this method both in the frequency domain and in the time domain through shaking table tests of MDOF shear building models. Three three-story shear building models are manufactured and subjected to ground motions generated by a shaking table. The displacement and acceleration responses of each building model at each floor are recorded. Afterwards, various damage scenarios with different damage locations and different damage severities are inflicted on the shear building models step by step. For each damaged building model with a given damage scenario, the shaking table tests are performed in a way similar to that for the undamaged building model. The first two damping ratios of the undamaged and damaged models are estimated by applying the Hilbert transform method to the measured acceleration responses. Then the recorded ground motion and building responses as well as identified structural damping ratios are utilized to identify damage locations and severities using the SMBDD method. The identified damage locations and severities are finally compared with the theoretical values to evaluate the effectiveness of the proposed method.

Chapter 7 establishes a new stochastic damage detection method to solve the problem of structural damage detection involving a significant amount of uncertainties which are escapable especially for civil structures. The proposed

method is implemented by two steps. Firstly, PDFs of structural stiffness parameters before and after earthquake are calculated by utilizing the probability density evolution (PDE) method and the SMBDD method. Then damage locations and damage severities are identified according to the computed values of probability of damage existence and the PDFs of damage severity index. Numerical investigations are performed to demonstrate the feasibility and effectiveness of the proposed method in terms of a shear building structure with different damage scenarios, in which the first damping ratio was regarded as a stochastic parameter with a lognormal distribution.

Chapter 8 develops a new structural reliability analysis method that accepts the measurement data as input and produces as output the reliability of the concerned instrumented structures. The proposed method can consider uncertainties of both damaged structures and dynamic inputs. Firstly, the method to calculate the component reliability of stochastic structures with only one limit state function is proposed based on the SMBDD method in conjunction with the PDEE-based absorbing boundary condition method. Then, the method to calculate the reliability of stochastic structures with multiple limit-state functions is developed based on the measurement data by integrating the SMBDD method with the PDEE-based equivalent extreme value method. Finally, numerical investigation is conducted through a three-story shear building structure under the EL Centro excitation for different damage scenarios. Both the stochastic parameters of structures and those of dynamic inputs are considered in the numerical analysis.

Chapter 9 summarizes the main conclusions achieved in this thesis and presents the recommendations for future research.

CHAPTER 2

LITERATURE REVIEW

2.1 General Concepts of Structural Damage Detection

Maintaining safe and reliable civil infrastructures for daily use is a topic that has received considerable attention to engineers and researchers in recent years. Usual inspection techniques require the portion of the structure being inspected to be readily accessible but it may not be appropriate because of interference with operational conditions. By definition, non-destructive techniques (NDT) are the means by which structures may be inspected without disruption or impairment of serviceability. Many methods have been developed for NDT, and an overview of the various techniques is presented by Witherell (1994). Some techniques are based on visual observations and some are based on the properties of materials. Other techniques are based on the interpretation of the structural condition by observing the change in the global behavior of the structure.

The need of non-destructive and global techniques for structure diagnosis has led to the continuous development of methods examining the changes of dynamic characteristics. Such an approach has been introduced for a number of years in fields like automotive, aeronautical and mechanical engineering. The basic premise of the global damage detection methods that examine changes in the dynamic properties is that modal parameters, notably resonant frequencies, mode shapes, and modal damping, are a function of the physical properties of the structure (mass, damping, stiffness, and boundary conditions). Therefore, changes in physical properties of the

structure, such as its stiffness or flexibility will cause changes in modal properties. An alternative system of classification for damage detection methods, as presented by Rytter (1993), defines four levels of damage identification as follows:

Level 1: Determination of the presentation of damage in a structure;

Level 2: Determination of the presentation and location of damage in a structure;

Level 3: Determination of the presentation, location and severity of damage;

Level 4: Level 3 plus the prediction of remaining service life of a structure.

Most of the damage detection methods developed to date limit themselves to Level 1 to Level 3. Level 4 methods require the knowledge associated with the disciplines such as structural design, fracture mechanics and structural reliability, and are still very limited (Yao and Natke 1994; Park *et al.* 1997; Stubbs *et al.* 2000; Xia and Brownjohn 2003). The field of damage detection is very broad and encompasses both local and global methods. Many different issues are critical to the success of using the vibration characteristics of a structure for damage detection and health monitoring. Among the important issues are excitation and measurement considerations, including the selection of the type and location of sensors, and the type and location of the excitations. Another important topic is signal processing, which includes such methods as Fourier analysis and time-frequency analysis. In this review, the peripheral issues will not be directly addressed. This review will be limited to global methods that are used to infer damage from changes in vibration characteristics of the structure.

2.2 Vibration-based Deterministic Damage Detection Techniques

2.2.1 Methods based on structure frequency changes

In the first stage of structural damage detection research, as far as the structural dynamic properties parameters are concerned, only the damage detection based on structure frequency change is reliable because of the immature mode identification techniques. The amount of literature addressing damage detection using changes in modal frequencies is quite large (Salawu 1997). There are two types of methods. In the first type of methods, the damage detection problem is treated as a forward problem, where the patterns of measured frequency changes are compared with those of analytical frequency changes for all possible damage cases and then the damage case which produces the best match to the measured frequency changes is regarded as the suspect one. This type of methods takes the advantage that some patterns of measured frequency changes are the function of damage location only. The second type of methods, which essentially is the model updating methods, deals with damage detection as an inverse problem and is able to calculate both damage location and damage magnitude.

The advantages of damage detection methods based on structure frequency change are that the identification is relatively easy, which can be performed only using very few sensors and has relatively higher precision than those based on other parameters because the modal frequency has least statistical variation from random error sources than other modal properties. However, it should be noted that frequency shifts have significant practical limitations for applications to the type of structures considered in this review, although ongoing and future work may help resolve these difficulties.

The somewhat low sensitivity of frequency shifts to damage requires either very precise measurements or large levels of damage. For example, in offshore platforms damage-induced frequency shifts are difficult to distinguish from shifts resulting from increased mass from marine growth. Tests conducted on the I-40 bridge (Farrar, et al., 1994) also demonstrate this point. When the cross-sectional stiffness at the center of a main plate girder had been reduced 96.4%, reducing the bending stiffness of the overall bridge cross-section by 21%, no significant reductions in the modal frequencies were observed. Currently, using frequency shifts to detect damage appears to be more practical in applications where such shifts can be measured very precisely in a controlled environment, such as for quality control in manufacturing. As an example, a method known as “resonant ultrasound spectroscopy”, which uses homodyne detectors to make precise sine-sweep frequency measurements, has been used to determine out-of-roundness of ball bearings. In addition, Xu, et al., (2004) established closed-form sensitivity equation which relates the relative change in the stiffness of each story to the relative changes in the natural frequencies of the building using the transfer matrix method. Numerical and experimental investigations on damage detection of monocoupled multistory buildings were then conducted by their proposed method.

Also, because modal frequencies are a global property of the structure, it is not clear that shifts in this parameter can be used to identify more than the mere existence of damage. In other words, the frequencies generally cannot provide spatial information about structural changes. An exception to this limitation occurs at higher modal frequencies, where the modes are associated with local responses. However, the practical limitations involved with the excitation and extraction of these local modes,

caused in part by high modal density, can make them difficult to identify.

2.2.2 Methods based on mode shape changes

As the largest change in mode shapes is expected to occur in the vicinity of damage, it is intuitive to incorporate them for damage localization. Two most commonly used methods to compare two sets of measured mode shapes are the modal assurance criterion (MAC) and the coordinate modal assurance criterion (COMAC) where one set of data is measured from the intact structure and the other is measured after the structure is damaged. MAC indicates the correlation between two sets of mode shapes and COMAC indicates the correlation between the mode shapes at a selected measurement point on the structure.

The first systematic use of mode shape information was presented by West (1984) for the location of structural damage without the use of a prior finite element model. The author uses the MAC to determine the level of correlation between the modes from the test of an undamaged Space Shuttle Orbiter body flap and the modes from the test of the flap after it has been exposed to acoustic loading. The mode shapes are partitioned using various schemes, and the structural damage is localized using the change in MAC across the different partitioning techniques.

Yuen (1985) determined damage locations according to the changes in the mode shape and mode-shape-slope parameters by computing $\{\varphi^*\}_i = \frac{\{\varphi^d\}_i}{\omega_i^d} - \frac{\{\varphi^u\}_i}{\omega_i^u}$, where $\{\varphi\}_i$ and ω_i are respectively the *i*th mode shape and the *i*th circular frequency. Subscript ‘d’ and ‘u’ denote damaged and undamaged structures. The changes in

these parameters were simulated for a reduction in stiffness in each structural element, and then the predicted changes were compared to the measured changes to determine the damage location. The author identified the need for some ortho-normalization process in order to look at higher mode shapes.

Rizos, et al. (1990) developed an analytical model for vibration of a beam with an open crack. The sections on either side of the crack are considered to be standard slender beams in transverse vibration. The compatibility condition between the two sections is derived based on the crack-strain-energy function. The result is a system of equations for the frequencies and mode shapes in terms of crack length and position. To determine the crack length and location, the beam is excited at a natural frequency, and vibration amplitudes at only two locations are measured. The Newton-Raphson method is used to solve the system of equations for the crack parameters.

A project that examines changes in the dynamic properties of a scale model of an offshore platform subjected to damage was reported by Osegueda, *et al.* (1992). Mode shape changes could not be correlated with damage in this study. Fox (1992) shows that single-number measures of mode shape changes such as the MAC are relatively insensitive to damage in a beam with a saw cut. “Node line MAC,” an MAC based on measurement points close to a node point for a particular mode, was found to be a more sensitive indicator of changes in the mode shape caused by damage. Graphical comparisons of relative changes in mode shapes proved to be the best way of detecting the damage location when only resonant frequencies and mode shapes were examined. A simple method of correlating node points—in modes that

show relatively little change in resonant frequencies—with the corresponding peak amplitude points—in modes that show large changes in resonant frequencies—was shown to locate the damage. The author also presents a method of scaling the relative changes in mode shape to better identify the location of the damage.

Kam and Lee (1992) presented an analytical formulation for locating a crack and quantifying its size from changes in the vibration frequency and mode shape. The crack is located by discretizing the structure and looking at the reduced stiffness in each element. The formulation is based on a first-order Taylor expansion of the modal parameters in terms of the elemental parameters. Once located, the crack length is determined by a formulation based on considering the change in strain energy resulting from the presence of a crack. The Newton-Raphson method is used to solve the resulting equations for the crack parameters. Kim, et al. (1992) investigated the use of MAC and its variations in the location of structural damage. They used the Partial MAC (PMAC) to compare the MAC values of coordinate subsets of the modal vectors. By using the Coordinate MAC (COMAC) and the PMAC in conjunction, they are able to isolate the damaged area of the structure. Mayes (1992) presented a method for model error localization based on mode shape changes known as structural translational and rotational error checking (STRECH). By taking ratios of relative modal displacements, STRECH assesses the accuracy of the structural stiffness between two different structural degrees of freedom (DOF). STRECH can be applied to compare the results of a test with an original FEM or to compare the results of two tests. Srinivasan and Kot (1992) found that changes in mode shapes were a more sensitive indicator of damage than changes in resonant frequencies for a shell structure. These changes are quantified by changes in the

MAC values comparing the damaged and undamaged mode shapes.

Ko, et al. (1994) presented a method that uses a combination of MAC, COMAC and sensitivity analysis to detect damage in steel framed structures. The sensitivities of the analytically derived mode shapes to particular damage conditions are computed to determine which DOF is most relevant. The authors then analyzed the MAC between the measured modes from the undamaged structure and the measured modes from the damaged structure to select which mode pairs to use in the analysis. Using the modes and DOF selected with the above criteria, the COMAC is computed and used as an indicator of damage. The results demonstrate that particular mode pairs can indicate damage, but when all mode pairs are used, the indication of damage is masked by modes that are not sensitive to the damage.

Salawu and Williams (1994) compared the results of using mode shape relative change and mode shape curvature change to detect damage. They demonstrated that the relative difference measure does not typically give a good indication of damage using experimental data. They pointed out that the most important factor is the selection of the modes used in the analysis. Salawu and Williams (1995) showed that the MAC values can be used to indicate which modes are being affected most by the damage. Lam, et al. (1995) defined a mode shape normalized by the change in natural frequency of another mode as a "damage signature." The damage signature is a function of crack location but not of crack length. They analytically computed a set of possible signatures by considering all possible damage states. The measured signatures were matched to a damage state by selecting which of the analytical signatures gave the best match to the measurements using the MAC.

Salawu (1997) proposed a global damage integrity index that is based on a weighted ratio of the damaged natural frequency to the undamaged natural frequency. The weights are used to reflect the relative sensitivity of each mode to the damage event. When damage is indicated, local integrity indices are calculated to locate the defective areas. The local integrity index is calculated from the global integrity index by further weighting the global index by the square of the ratio of damaged mode amplitude to the undamaged mode amplitude for a particular measurement point.

One of key issues in implementing damage indicators using changes in mode shapes is the selection of the modes and the optimum placement of sensors in the case of limited sensors. Such an issue has been addressed by Cobb and Liebst (1997) and Shi et al. (2000) via eigenvector sensitivity analysis. The damage index based on mode shapes change can give the information of spaces, but the high modal shapes which are sensitive to structure local damage are very difficult to get.

2.2.3 Methods based on modal damping changes

The damage detection methods based on modal damping change were mostly applied to composite structure. And this method is still in the laboratorial research stage because the precision of structural modal damping change attained by mode parameters identification technique is not enough. Ndambi (2002) investigated the principle of structure modal damping and made use of the modal damping as a damage detection index for pre-stressed concrete beam structures. Salane and Baldwin (1990) tested a steel bridge having a concrete deck. Farrar *et al.* (1998) found that structural damage was not consistent with structural modal damping

change.

2.2.4 Methods based on mode shape curvature changes

An alternative to using mode shapes to obtain spatial information about vibration changes is using mode shape derivatives, such as curvature. It is first noted that for beams, curvature and bending strain are directly related as $\varepsilon = \frac{y}{R} = \kappa y$, where ε is strain, R is radius of curvature, and κ is curvature or 1/R. The practical issues of measuring strain directly or computing it from displacements or accelerations are discussed by some researchers.

Pandey *et al.* (1991) demonstrated that absolute changes in mode shape curvature can be a good indicator of damage for the beam structures they considered. The curvature values are computed from the analytical modal displacements using a finite difference method, as

$$\kappa_i = (\varphi_{i+1} - 2\varphi_i + \varphi_{i-1}) / h^2 \tag{2.1}$$

where φ_i is the modal displacement at measurement point i; and h is the length of elements.

Ratcliffe (1997) extended the method and put forward the damage detection method which did not use fiducial mode. The index is effective when structural damage is very serious. And if mode shape curvature is used for damage detection, testing locations are required close to each other and testing points are in good enough. Otherwise, the estimate value of centre difference will arouse biggish error. This limitation will make the method very difficult to apply to large complicate structures.

2.2.5 Methods based on flexibility matrix changes

Another class of damage detection methods uses the dynamically measured flexibility matrix to estimate changes in the static behavior of the structure. Typically, damage is detected using flexibility matrices by comparing the flexibility matrix synthesized using the modes of the damaged structure to the flexibility matrix synthesized using the modes of the undamaged structure or the flexibility matrix from an FE model. Because of the inverse relationship to the square of the modal frequencies, the measured flexibility matrix is most sensitive to changes in the lower-frequency modes of the structure.

Pandey and Biswas (1994) presented a damage-detection and -location method based on changes in the measured flexibility of the structure. This method is applied to several numerical examples and to an actual spliced beam where the damage is linear in nature. Results of the numerical and experimental examples showed that estimates of the damage condition and the location of the damage could be obtained from just the first two measured modes of the structure. Toksoy and Aktan (1995) computed the measured flexibility of a bridge and examined the cross-sectional deflection profiles with and without a baseline data set. They observed that anomalies in the deflection profile can indicate damage even without a baseline data set.

2.2.6 Methods based on modal strain energy changes

Damage detection method based on modal strain energy changes is one of commonly used methods in the discipline. Some studies indicated that modal strain energy is useful in localizing structural damage. The general definition of modal strain energy of a structure with respect to the *r*-th mode can be expressed as

$$MSE_r = \frac{1}{2}\boldsymbol{\phi}_r{}^T \mathbf{K} \boldsymbol{\phi}_r \tag{2.2}$$

where **K** is the stiffness matrix of a structure and $\boldsymbol{\phi}_r$ is the *r*-th mode shape.

Yao *et al.* (1992) put forward the method to detect damage through examining changes in modal strain energy. The method is based on the hypothesis that structural damage will result in the redistribution of structural internal force and the modal strain energy changes will be large in the structural damage area. However, the internal force redistribution is different between different modes. Therefore, different outcomes will be attained making use of different testing modes. Topole and Stubbs (1995) examined the feasibility of using a limited set of modal properties for structural damage detection. Later, Stubbs and Kim (1996) improved the method by using modal strain energy to localize the damage and estimating the damage size without baseline modal properties.

Despite damage detection methods based on mode shape changes and their derivatives can provide spatial information regarding the location of structural damage, they also suffer from several limitations in application: Firstly, dense array of measurement points is required for an accurate configuration of mode shapes and curvature mode shapes. Secondly, the mode shape has larger statistical variation than does modal frequency. Thirdly, the mode shape based methods, especially the curvature mode shape based methods, are not readily applicable for structures with complex configuration. Finally, it is required to select a mode shape, yet it is a priori unknown which mode suffers from significant change due to particular structural damage.

2.2.7 Methods based on frequency response functions (FRF)

Law *et al.* (1992) developed sensitivity from formulation based on the change in the FRF at any point, rather than just at the resonances. In practice, many points of the FRF around the resonances are taken, and a least-squares fit is used to determine the changes in the physical parameters. This method requires both a before- and after-damage FRF and a physical modal relating the damage parameter to a physical parameter such as stiffness. Wu *et al.* (1992) identified the damage in a three-storey building model by selecting the first 200 points of the frequency response function as input to a back-propagation (BP) neural network. Chaudhry and Ganino (1994) used measured FRF data over a specified frequency range as input to a BP neural network to identify the presence and severity of delamination in debonded beams. Juan, *et al.* (2000) presented and experimentally verified a new technique to identify damage based on changed in the component transfer functions of the structure, or the transfer functions between the floors of a structure. Multiple locations of damage can be identified and quantified using the approach. The peak value of frequency response function can provide spatial information of structural damage. Frequency response function based methods have the advantages as follows:

a. measuring data include modes which are outside the frequency band width;
b. measuring data can provide ample structural information;
c. the error of mode identification can be avoided because of not needing to analyze mode; and
d. it can be applied to structures with high damping and highly close mode

However, the structural input information is required when identifying frequency response function of structure. This is quite difficult for large civil engineering structures. Furthermore, there is still no good method to choose interested frequency

bound and the noise in converse response is large.

2.2.8 Matrix update methods

Another class of damage identification methods is based on the modification of structural model matrices such as mass, stiffness, and damping to reproduce as closely as possible the measured static or dynamic response from the data. These methods solve for the updated matrices (or perturbations to the nominal model that produce the updated matrices) by forming a constrained optimization problem based on the structural equations of motion, the nominal model, and the measured data. Comparisons of the updated matrices to the original correlated matrices provide an indication of damage and can be used to quantify the location and extent of damage. The methods use a common basic set of equations, and the differences in the various algorithms can be classified as follows: 1) objective function to be minimized; 2) constraints placed on the problem; 3) numerical scheme used to implement the optimization. They, either for model improvement or for damage detection applications, can be classified into three categories: 1) optimal matrix updating methods; 2) eigenstructure assignment methods; and 3) sensitivity-based updating methods. Considerable research efforts have been devoted to developing various model updating methods during the past several decades. Survey literature on model updating in structural dynamics began to appear in the early 1970s. Among them, Hart and Yao (1977), Liu and Yao (1978), Natke (1988), Imregun and Visser (1991), Natke (1991), Zimmerman and Smith (1992), Mottershead and Friswell (1993), and Link (2001) are worthy of attention.

It should be noted that model updating algorithms used for model improvement and

damage detection share the similar objectives, i.e. seeking an analytical model that is close to the real structure. The purpose of model improvement is to achieve an analytical model which is dynamically equivalent to the tested structure. The updated model is subsequently utilized for response prediction and structural modification. The model improvement is performed in face of numerous simplifications in FE model building. Often there are complex geometrical features that cannot be modeled accurately. In addition, boundary conditions and joint parameters between components are seldom fully understood. Mottershead and Friswell (1993) summarized three commonly encountered modelling errors, which could give rise to significant discrepancy between analytical predictions and testing values, as: 1) model structure errors, which are liable to occur when there is uncertainty concerning the governing equations of motion; 2) model order errors, which are often arising from discretizing the complex structures and can result in a model with insufficient order; and 3) model parameter errors, which typically include inappropriate boundary conditions, inaccurate assumptions used in order to simplify the model, and inconsistent material properties. These modeling errors may exist only in a few locations or can be extensively distributed in the whole structure.

On the other hand, the damage detection aims to detect and identify the changes in stiffness, mass and damping matrices due to damage instead of modeling errors. The changes in the measured quantities caused by structural damage are often smaller than those observed between the healthy (i.e. undamaged) structure and its FE model. Consequently, it becomes almost impossible to discern between inadequate modeling and actual changes due to damage. To distinguish damage from modeling errors, an original FE model that accurately represents the intact structure is required. This is

accomplished with a first-stage model improvement procedure which is performed in order to correlate this original model with testing data of the intact structure (Titurus et al. 2003a). The improved model is commonly used as the baseline model and can be then further correlated with testing data of possibly damaged structures for damage detection by using a similar updating procedure (Titurus et al. 2003b). Therefore, a two-step scheme is generally required for damage detection application using model updating methods with the first step correcting the modelling errors and the second step detecting structural damage. For a large-scale structure, the modelling errors could spread over the whole structure while the damage generally tends to concentrate on several locations.

2.2.9 Neural network and genetic algorithm based methods

In recent years there has been increasing interest in using neural networks to estimate and predict the extent and location of damage in complex structures. Neural networks have been promoted as universal function approximators for functions of arbitrary complexity. A general overview of neural networks can be found in Bishop (1994). The most common neural network in use is the multilayer perceptron (MLP) trained by back-propagation. In this section, terminology will be defined consistent with common usage by calling a MLP trained by back-propagation a “back-prop neural network.” The back-prop neural network is a system of cascaded sigmoid functions where the outputs of one layer, multiplied by weights, summed, then shifted by a bias are used as the inputs to the next layer. Once architecture for the network is chosen, the actual function represented by the neural network is encoded by the weights and biases. The back-propagation learning algorithm is a way of adjusting the weights and biases by minimizing the error between the predicted and measured outputs. In

the following studies there were typically more adjustable weights than experiments, and the body of data was repeatedly run through the training algorithm until a criterion for the error between the data and the neural network was satisfied. Each error-generating run is called an epoch. The terms neuron and node are used interchangeably in the following discussion.

Kudva, et al. (1991) used a back prop neural network to identify damage in a plate stiffened with a 4 × 4 array of bays. Damage was modeled by cutting holes of various diameters in the plate at the centers of the bays. The bays were sized 305 mm (12 in.) × 203 mm (8 in.) and the holes were from 12.7 mm (0.5 in.) to 63.5 mm (2.5 in.). A static uniaxial load was applied to the structure, and strain gage readings were taken from elements in the bays. The neural network was used to identify the map from the strain gage data to the location and size of the hole. In different experiments 8, 20, and 40 strain gages were used as input. The structure of the network was chosen to be two hidden layers, each with the same number of hidden nodes as the number of inputs. The network was trained with 3, 12, or 32 patterns, depending on which experiment was being tested. The authors claimed the networks converged in less than 10 minutes on a 386 PC, depending on the example. It should be noted that in one example the neural network failed to converge, and the authors were forced to modify their procedure to a two-step algorithm, which first predicted the whole quadrant, then the correct bay within the quadrant. The authors found that the neural network was able to predict the location of the damaged bay without an error but that predicting whole size was more difficult with sometimes erratic results. In the cases where the neural network successfully identified the whole size, typical errors were on the order of 50%. Wu, et al. (1992) used a back prop neural network

to identify damage in a three-story building modeled by a two-dimensional "shear building" driven by earthquake excitation. The damage was modeled by reducing member stiffness by 50% to 75%. The neural network was used to identify the map from the Fourier transform of acceleration data to the level of damage in each of the members. The first 200 points in the fast Fourier transform (FFT) (0 Hz to 20 Hz) were used as network inputs. Network architecture with one hidden layer and 10 hidden nodes was selected, and 42 training cases were used. No information was given on how long it took for the neural net to converge. The first attempt relied on using only acceleration data from the top floor. On test data, the neural network was only able to identify third-floor data with any accuracy. A second network was implemented that used acceleration data from the second two floors as inputs. This network was able to diagnose damage on the first and third floors to within approximately 25% but was still unable to predict damage to the second floor with any accuracy. The latter method relied on a complete knowledge of the time histories of two of the three DOF.

Elkordy, et al. (1993) used back propagation neural networks to identify damage in five-story buildings. Damage was modeled by reducing member stiffness in the bottom two stories from 10% to 70%. The neural network was used to identify the map from the mode shapes to the percent change in member stiffness. The authors chose a network with a single hidden layer of fourteen nodes. The network was trained on two mathematical models and verified with experimental data. The models were two-dimensional, finite element representations of increasing complexity. The first model gave eleven training patterns, the second model gave nine. The authors do not specify how long it took the neural net to converge. The model was reasonably

successful at predicting damage to the first and second stories and predicting the extent of the damage. In general, the neural network trained on the first model of lower complexity made poorer predictions, and it incorrectly diagnosed damage in two of the eleven experiments. The neural network trained on the second model never made an incorrect diagnosis, but it was indeterminate in one example. If the correct diagnosis was made, the predictions of damage were generally correct to within 10%. Elkordy, et al. (1994) is a slightly modified version of this paper.

In addition, Tsou and Shen (1994) used residual force vectors in a neural network based identification process to obtain structural damage location and severity. Mares and Surace (1996) employed the concept of the residual force vectors to specify an objective function for an optimization procedure which is then implemented by using genetic algorithms and identified damage in elastic structures. Friswell *et al.* (1998) proposed a combined genetic and eigensensitivity algorithm to locate damage in structures. Genetic algorithms have also been applied in structural damage identification by Xia and Hao (2001), Chou and Ghaboussi (2001). To overcome the computational complexity of traditional genetic algorithms involved in evaluating the fitness functions for large populations when there are a lot of candidates in the possible damage domain, Au *et al.* (2002) proposed the two-level search strategy and the micro-genetic algorithm to identify structural damage severity.

2.2.10 Time-frequency methods

Many time-frequency methods, such as short time Fourier transform, wavelet transform, Hilbert transform and empirical mode decomposition, have been investigated numerically or experimentally for damage detection purpose. One of the

major reasons for the application of these signal processing techniques is their capturing capability of non-stationary events because many factors will induce non-stationary events in structural response, such as structural nonlinearities, time-varying structural parameters, sudden or cumulative damages and non-stationary excitations. Unlike the Fourier analysis, which spreads out an abrupt change in a non-stationary signal over the whole frequency range, wavelet analysis transforms the non-stationary signal in a way that the abrupt change can be precisely separated from the original signal. This important property of wavelet analysis was used by Hou *et al* (2000) to identify the damage time instant and damage location of the structure subject to a sudden damage. It is illustrated that the sudden damage will induce discontinuities in the structural responses. The occurrence of damage and the moment when it occurs can be identified from the wavelet detail of structural response, which contains the high frequency content of the signal. Noting the similarity of the property between wavelet decomposition and empirical mode decomposition (EMD), the similar damage detection procedure was proposed based on empirical mode decomposition (Vincent et al, 1999; Yang et al, 1999). Only numerical investigations were conducted in the aforementioned wavelet and EMD based damage detection studies. To investigate the applicability of EMD for identifying sudden structural damage in real situation, shaking table tests were carried out by Xu and Chen (2004). Two springs were horizontally connected to the first floor of the tested building. The sudden damage was simulated by suddenly releasing two pre-tensioned springs. It was found that the damage time instant and location can be obtained from the spikes in the first IMF component of the structural responses at different locations. Although for some cases a monotonic relationship could be seen between the spike amplitude and the damage severity, no quantitative

relationship can be found. It is noted that in all these researches, both the wavelet and EMD based spikes are damage location sensitive, which means that the accelerometer should be located in the vicinity of the damage location to capture the discontinuity in response. A disadvantage thus emerges when the number of sensors is small and no sensor is installed near the position where damage occurs. Furthermore, since the spikes caused by linear time-varying damage are not as large and concentrated as sudden damage, the applicability of the aforementioned damage detection techniques for time-varying damage case is not optimistic.

Unlike the aforementioned damage detection methods, which utilize the signal decomposition results directly as the indicator of occurrence and location of damage, Sun and Chang (2002) proposed a wavelet packet decomposition based method for structural damage assessment. A wavelet packet signature (WPS), which represents the energy of predominant frequency component, was proposed as damage index. The structural damage was assessed by comparing the wavelet packet signature before and after damage. The changes of the signature were then input into neural network models to quantify the damage severity of structural components. Numerical examples showed that the signature is sensitive to structural damage. However, since the structure was assumed to be linear before and after damage during the application of this method, WPS based damage detection can hardly be applied for time-varying damage models.

2.3 Structural Damage Detection Methods with Consideration of Uncertainties

Structural damage detection in civil engineering involves a significant amount of uncertainties which may result from environment, such as temperature, loading and

humidity, measurement noise, uncertainty in geometry and boundary conditions, inexact modeling of the material constitutive behavior or damping, uncertainty in external excitations, and so on. To sum up, the uncertainty and errors in structural damage detection are attributed to:

(1). inaccuracy in the FE model discretization;

(2). uncertainties in geometry and boundary conditions;

(3). variations in material properties during manufacture;

(4). inexact modeling of the material constitutive behavior;

(5). uncertainties introduced during the construction process;

(6). environmental variability (such as temperature, wind and traffic);

(7). uncertainties in external excitations;

(8). errors associated with measured signals;

(9). errors in post-processing techniques;

(10). un-modeled features such as neglected nonstructural components;

(11). improper methods applied in damage identification, etc..

According to their sources, these errors can be classified into three groups, namely methodology errors, modeling errors and measurement errors. Methodology errors are generated by the limitation of the method itself in model updating (or damage identification). Modeling errors are related to the uncertainties in modeling the actual structure. Measurement errors mainly come from procedures and equipment related to modal testing. These errors can be divided into two basic categories: systematic errors and random errors. Systematic errors cause the mean of the estimation not to converge to the actual value even when more values are taken. Random errors, on the other hand, are quantified in the form of a standard deviation associated with the

mean of the estimation for the parameters considered. Normally methodology errors belong to systematic errors, but both systematic errors and random errors might exist in modeling and measurement data. And these errors in damage identification can result in false-positive damage identification (identifying the intact element as damaged) and false-negative damage identification (failure to identify the damaged elements). The uncertainties existing in the model along with the errors in the measured vibration data limit the successful use of those deterministic damage detection methods. Therefore, many approaches with consideration of the uncertainties have been developed for detecting structural damage and are reviewed in the following section.

2.3.1 Bayesian methods

The method of statistical identification of structures which is capable of dealing with uncertainties both in FE model and measured modal properties was first developed by Collins *et al.* (1974), and later improved by Friswell (1989) to accelerate the convergence rate. They presented a minimum variance method for statistical estimation of flexural and torsional stiffness based on Bayesian theorem. In their method, both structural parameters and measured modal properties are assumed to have errors given in terms of their variances. The estimation of mean and variance of the updating parameters is iteratively obtained and the iteration will cease if the difference of parameter estimation in two consecutive iterations is small.

Let H_j denote a hypothesis for a damage event that can contain any number of substructures as damaged, and the hypothesis H_j is represented with a prior probability $P(H_j)$. Using Bayes theorem, the posterior probability $P(H_j \mid \psi)$, given a

set of observed modal parameters ψ , can be represented as:

$$P(H_j|\psi) = \frac{P(\psi|H_j)}{P(\psi)} P(H_j) \tag{2.3}$$

The most likely damaged substructures are the ones included in the hypothesis *Hmax* that has the largest posterior probability (Sohn and Law 1997), i.e.

$$P(H_{\max}|\psi) = \max_{\forall H_j} P(H_j|\psi) \tag{2.4}$$

The distribution of measurement noise and modeling error are explicitly considered within the Bayesian probabilistic framework. To avoid permuting all possible damage events *Hj*, a branch-and-bound method was devised to search the results. Sohn and Law (2000) applied this algorithm to detect damages in an RC bridge column. The proposed probabilistic damage detection method was able to locate the damaged region, but two deterministic methods could not. A more rigorous and comprehensive Bayesian updating has been developed by Beck and his co-workers (Beck and Katafygiotis 1998; Katafygiotis and Beck 1998; Yuen and Katafygiotis 2005).

2.3.2 Monte Carlo simulation method

The commonly used method for uncertainty propagation is the Monte Carlo simulation (MCS) method. The basic concept behind the MCS method is: a large number of samples following the given probability distribution of stochastic parameters are generated and then repeatedly used for model updating; the desired statistics are eventually estimated from these resulting updating results.

Agbabian *et al.* (1988) employed the MCS method to identify the statistical

properties of stiffness coefficients in a linear system. In their simulation study, they computed the time histories of the applied excitation as well as the accelerations, velocities, and displacements of a system. The calculated data were then corrupted with a set of Gaussian noise. By separately applying the model updating procedure to different time segments, ensembles of stiffness coefficients were identified. Subsequent statistical analysis yielded statistical measures such as mean, variance, and probability density functions (PDFs). This work has been later extended to statistical identification of a nonlinear system approximated by an equivalent linear one (Smyth *et al.* 2000). Banan *et al.* (1994), Sanayei and Saletnik (1996), Yeo *et al.* (2000), and Zhou *et al.* (2003) adopted similar approaches for studying the effect of measurement noise on identification results. However, the MCS method is computationally intensive as it requires a large number of simulations to obtain an accurate and valid statistics.

2.3.3 Perturbation methods

An alternative approach to uncertainty propagation is the perturbation method. This approach expands a nonlinear function with a truncated Taylor series expansion at a known point and then proceeds to the approximation of the moments of solutions from the expansion.

Perturbation method is another very popular technique for uncertainty propagation. It has been applied very successfully in the discipline of stochastic structural analysis where the perturbation technique in conjunction with the FE analysis is applied to evaluate the response variability and failure probabilities associated with prescribed limit states (Kleiber and Hien 1992). Perturbation method expands the nonlinear

function in terms of random variables either by a linear function or by a quadratic one at a particular point. Second moment technique is then applied to evaluate the mean and standard deviation of the response, or to evaluate the failure probabilities.

Liu (1995) might be the first to adapt this technique to model updating. In her work, the identification of structural parameters is formulated in a linear least squares problem to minimize the modal force residuals. To investigate the influence of measurement errors, the author expanded each term in a system of linear equations in terms of random variables. Making use of the expanded sets of linear equations, the mean and covariance of updating parameters are finally derived. Papadopoulos and Garcia (1998) presented a two-step probabilistic method for damage assessment to determine the statistics of stiffness coefficients of the damaged structure. They first used the measured statistical changes in modal frequencies and mode shapes to obtain the statistics of stiffness reduction factor. These statistics of stiffness reduction factor along with the statistics of stiffness coefficients corresponding to healthy structure are then combined to determine the statistics of stiffness coefficients of the damaged structure. A set of graphical and statistical probability damage quotients was then used to assess the existence of damage by the comparison of statistics of SC before and after damage. Xia *et al.* (2002), and Xia and Hao (2003) updated the statistics of stiffness of the damaged structure in a single step and used the statistics of stiffness before and after structural damage to implement probabilistic damage detection. Araki and Hjelmstad (2001) used the higher-order perturbation method based on the concept of optimum sensitivity.

Intuitively, all model updating algorithms can be combined with MCS method and

perturbation method for uncertainty propagation. The combination of MCS method and model updating techniques has been used by a number of researchers (Agbabian *et al.* 1988; Banan *et al.* 1994; Sanayei and Saletnik 1996; Smyth *et al.* 2000; Yeo *et al.* 2000; Zhou *et al.* 2003).

2.3.4 Statistical pattern recognition methods

In addition, Farrar *et al.* (1999) set up a statistical pattern recognition paradigm for vibration-based structural health monitoring. Sohn *et al.* (2000) developed the technique known as an 'X-bar control chart' and set up the autoregressive (AR) model for vibration-based damage diagnosis in the context of a statistical pattern recognition paradigm. Then, Sohn *et al.* (2001) extended the above statistical pattern recognition method to locate structural damage. Wang *et al.* (2008) employed a statistical pattern recognition method to locate damage of sensitivity-enhanced structures. Probabilistic neural network methods can be regarded as one kind of the statistical pattern recognition methods. Klenke *et al.* (1996) applied the probabilistic neural network to determine whether structural damage had happened or not. Stefano *et al.* (1999) exploited the fundamental learning and generalization capabilities of probabilistic neural networks to obtain an estimate of the vulnerability of structural systems. Ni and his coworkers (Ni YQ, *et al.* 2000; Ni YQ, *et al.* 2001) built adaptive probabilistic neural networks to locate structural damage for a cable stayed bridge and a suspension bridge, respectively.

2.3.5 Other methods

Other researches addressing the statistical parameter estimation using uncertain

modal data include the work of Li and Roberts (2001) who incorporated the uncertainty-propagation approach with extended Kalman filter method for recursive identification of random structural parameters, Farrar and Doebling (1998) who used Monte Carlo method and Bootstrap method to estimate modal parameters, Fonseca *et al.* (2005) who combined the maximum likelihood method with perturbation technique for estimating the statistics of random location of a mass, Xu and Chen (2004) who presented an experimental investigation on the applicability of the empirical mode decomposition for identifying structural damage caused by a sudden change of structural stiffness.

2.4 Structural Reliability Analysis Methods

The essence of the structural reliability problem is the probability integral

$$P_f = \int \cdots \int_D f_{X_1, X_1, \cdots, X_n}(x_1, x_2, \cdots, x_n) dx_1 dx_2 \cdots dx_n \tag{2.5}$$

which may also be written as

$$P_f = \int_D f(\mathbf{x}) d\mathbf{x} \tag{2.6}$$

where P_f denotes the 'failure' probability, $f(\mathbf{x})$ denotes the joint PDF of a vector of random variables $\mathbf{x}$, and D denotes a subset of the outcome space where failure occurs. The term failure used here is in its general sense. It may denote the physical failure of a structure or its member, or the exceeding of a serviceability limit state. In other words, the reliability analysis can be formulated for both the safety and serviceability limit states. And the uncertainties in a structure and its external loadings are assumed to be time-invariant and modeled by continuous random

variables. These random variables include the load-related, resistance-related, and geometry-related quantities (Nowak and Collins 2000). The set of basic random variables describing these uncertainties are represented by the random vector $\mathbf{x} = (x_1, x_2, \cdots, x_n)^T$. Structural reliability analysis methods can be divided into component reliability analysis methods and system reliability analysis methods according to the objects of study. The evaluation of the failure probability for a single failure mode (or a single limit-state function) is called component reliability analysis. The probability due to the combination of numerous failure modes requires a system reliability analysis, for which the component failure probability is the basic ingredient.

For mathematical analysis, it is necessary to describe the failure domain D in an analytical form. A "component' reliability problem is defined when D is described through a single function, *i.e.* $D = \{\mathbf{x} : g(\mathbf{x}) \le 0\}$, where $g(\mathbf{x})$ is known as the limit-state function. The boundary of D is defined by $g(\mathbf{x}) = 0$ and is known as the limit-state surface. The set with $g(\mathbf{x}) > 0$ defines the safe domain and the set with $g(\mathbf{x}) < 0$ defines the failure domain. These definitions are shown in Figure 2.1 for the special case of two variables.

The system reliability problem is defined when D is described as the union and/or intersection of several subsets. In particular, a ‘series system’ reliability problem is defined by $D = \left\{\mathbf{x} : \bigcup_i g_i(\mathbf{x}) \le 0\right\}$, and a ‘parallel system’ reliability problem is defined by $D = \left\{\mathbf{x} : \bigcap_i g_i(\mathbf{x}) \le 0\right\}$, where $g_i(\mathbf{x})$ denote componental limit-state functions (see Figure 2.2). Series systems and parallel systems are the two basic

system types from which any system can be built. Any system can be represented both as a series system of parallel systems and as a parallel system of series systems.

2.4.1 Component reliability analysis methods

A great deal of effort has been devoted to developing efficient algorithms for computing component probability integrals in Equation (2.6). A straightforward integration, by analytical or numerical means, usually is not possible because of the arbitrary nature of the integration domain and the typically high dimension of the problem. Over the past decades, a number of approximation methods have been developed to compute this probability integral as summarized by Melchers (1999).

Several of the methods described below require transformation of a random vector $\mathbf{x}$ into a standard normal vector $\mathbf{u}$, thus enabling the reliability analysis for random variables with arbitrary distribution types. The standard normal space is defined by a set of independent and standard normal variables $\mathbf{u}$ having zero means and unit covariance matrix and the following joint PDF:

$$f_U(\mathbf{u}) = \frac{1}{(2\pi)^{n/2}} e^{-\frac{1}{2}\mathbf{u}^T\mathbf{u}} \tag{2.7}$$

where n denotes the number of random variables.

A general form of the transformation is given by Hobenbichler and Rackwitz (1981) and a more convenient form for a particular class of multivariate distributions is given by Der Kiureghian and Liu (1986). Equation (2.6) is rewritten in the following form after the transformation.

$$P_f = \int_D \phi_n(\mathbf{u}) d\mathbf{u} \tag{2.8}$$

where D is now defined in the $\mathbf{u}$ space and $\phi_n(\mathbf{u})$ denotes the joint PDF of the vector of random variables $\mathbf{x}$ in the standard normal space. For notational convenience, let $G(\mathbf{u}) = g(\mathrm{T}^{-1}(\mathbf{u}))$ denote the transform of the limit-state function in the $\mathbf{u}$ space.

2.4.1.1 First-order and second-order reliability method

Two widely used methods: the first-order reliability method (FORM) and the second-order reliability method (SORM) have been proved satisfactory for most of engineering problems (Rackwitz, 2001). For example, Kareem evaluated the reliability of concrete chimneys under winds by employing the First-order Second-moment approximation (Kareem and Hseih, 1986). The first- and second-order reliability methods (FORM and SORM) take advantage of the fact that the point $\mathbf{u}^*$ located on the limit-state surface with minimum distance from the origin has the highest probability density among all failure points in the standard normal space. This point is known as the 'design point' or the 'most likely failure point' and is defined by the constrained optimization problem

$$\mathbf{u}^* = \arg\min\left\{\|\mathbf{u}\| \,\middle|\, G(\mathbf{u}) = 0\right\} \tag{2.9}$$

where 'argmin' denotes the argument of the minimum of a function.

It is readily evident that probability densities in the standard normal space are rotationally symmetric and decay exponentially with the square of distance in both radial and tangential directions from $\mathbf{u}^*$. It follows that the major contribution to the probability integral in Equation (2.8) comes from the neighborhood of $\mathbf{u}^*$, provided the surface is not strongly nonlinear and there is only one significant design point.

These conditions are satisfied for most structural component reliability problems. Based on this, the limit-state surface in the neighborhood of the design point is approximated by a first- or second-order surface for which the solution of the probability integral is available. Specifically, in the FORM, the limit-state surface is replaced by the tangent hyperplane at $\mathbf{u}^*$. The linearized limit-state function is written as

$$G(\mathbf{u}) \cong G_1(\mathbf{u}) = \nabla G(\mathbf{u}^*)(\mathbf{u}-\mathbf{u}^*) = \left\|\nabla G(\mathbf{u}^*)\right\|(\beta - \alpha\mathbf{u}) \tag{2.10}$$

where $\nabla G(\mathbf{u}) = (\partial G/\partial u_1, \cdots, \partial G/\partial u_n)$ denotes the gradient row vector, $\alpha = -\nabla G(\mathbf{u}^*)/\left\|\nabla G(\mathbf{u}^*)\right\|$ is the normalized negative gradient row vector at the design point (a unit vector normal to the limit-state surface at the design point and pointing toward the failure domain), and $\beta = \alpha\mathbf{u}^*$ is the reliability index. In essence, the linearization replaces the failure domain $G(\mathbf{u}) \le 0$ by the half space $\beta - \alpha\mathbf{u} \le 0$; see Figure 2.3. The first-order approximation of the failure probability is given by the probability content of the half space in the standard normal space, which is completely defined by the distance β; that is,

$$p_f \cong p_{f1} = \Phi(-\beta) \tag{2.11}$$

where the subscript 1 is used to indicate a first-order approximation. There are two conditions under which this approximation may not work well: (1) the surface is strongly nonflat, and (2) the optimization problem in Equation (2.8) has multiple local or global solutions. A recourse for the first condition is to use a higher-order approximation, such as SORM, or a corrective sampling method, such as importance sampling or sampling on the orthogonal plane (Engelund, *et al.*, 1993). All these methods make use of the design point, so they need the FORM solution as a first step. The second condition is quite rare, but it does occur, particularly when dealing with

dynamic problems.

As its name implies, the second-order reliability method, SORM, involves a second-order approximation of the limit-state function. Consider a Taylor series expansion of the component limit-state function $G(\mathbf{u})$ at the design point $\mathbf{u}^*$.

$$\begin{aligned} G(\mathbf{u}) &\cong \nabla G(\mathbf{u}^*)(\mathbf{u}-\mathbf{u}^*) + \frac{1}{2}(\mathbf{u}-\mathbf{u}^*)^{\mathrm{T}}\mathrm{H}(\mathbf{u}-\mathbf{u}^*) \\ &= \left\|\nabla G(\mathbf{u}^*)\right\| \left[(\beta - \alpha\mathbf{u}) + \frac{1}{2\left\|\nabla G(\mathbf{u}^*)\right\|}(\mathbf{u}-\mathbf{u}^*)^{\mathrm{T}}\mathrm{H}(\mathbf{u}-\mathbf{u}^*) \right] \end{aligned} \tag{2.12}$$

where α and β are as defined earlier and H is the second-derivative matrix at the design point having the elements $H_{ij} = \partial^2 G(\mathbf{u}^*)/(\partial u_i \partial u_j),\ i, j = 1, \cdots, n.$ Now consider a rotation of the axes $\mathbf{u}' = \mathbf{P}\mathbf{u}$, where $\mathbf{P}$ is an orthonormal matrix with α as its last row. Such a matrix can be constructed by, for example, the well-known Gram-Schmidt algorithm. This rotation positions the design point on the axis u', such that $\mathbf{u}'^* = [0 \cdots 0\beta]^{\mathrm{T}}$. Keeping only second-order term in Equation (2.12), the limit-state surface can be rewritten as

$$G'(\mathbf{u}') \cong \beta - u_n' + \frac{1}{2}\mathbf{u}_{n-1}'^{\mathrm{T}}\mathbf{A}_{11}\mathbf{u}_{n-1}' \tag{2.13}$$

where $\mathbf{A}_{11}$ is the $(n-1)\times(n-1)$ matrix formed by the first *n*-1 rows and columns of $\mathbf{A}$. Now consider a rotation of the axes around u_n' defined by the transformation $\mathbf{u}_{n-1}'' = \mathbf{Q}\mathbf{u}_{n-1}'$. It follows that by selecting $\mathbf{Q}^{\mathrm{T}}$ as the eigenmatrix of $\mathbf{A}_{11}$, Equation (2.13) reduces to

$$G'(\mathbf{u}') \cong \beta - u_n' + \frac{1}{2}\sum_{i=1}^{n-1}\kappa_i u_i''^2 \tag{2.14}$$

where κ_i are the eigenvalues of $\mathbf{A}_{11}$. The preceding expression defines a paraboloid

through its principal axes with κ_i, i =1, …, n-1, denoting its principal curvatures. This paraboloid is tangent to the limit-state surface at the design point and its principal curvatures match those of the limit-state surface at the design point. In SORM, the probability of failure is approximated by the probability content of the above-defined paraboloid. The SORM approximation can be written as

$$p_f \cong p_{f2}(\beta, \kappa_1, \cdots, \kappa_{n-1}) \tag{2.15}$$

Tvedt (1990) has derived an exact expression for p_{f2} under the condition $-1 < \beta\kappa_i$ as follows.

$$p_{f2} = \phi(\beta)\,\mathrm{Re}\left\{ \mathrm{i}\sqrt{\frac{2}{\pi}} \int_0^{\mathrm{i}\infty} \frac{1}{s} \exp\left[\frac{(s+\beta)^2}{2} \right] \prod_{i=1}^{n-1} \frac{1}{\sqrt{1+\kappa_i s}}\, ds \right\} \tag{2.16}$$

where i= $\sqrt{-1}$. A simpler foumula based on asymptotic approximations derived earlier by Breitung (1984) is

$$p_{f2} \cong \Phi(-\beta) \prod_{i=1}^{n-1} \frac{1}{\sqrt{1+\psi(\beta)\kappa_i}} \tag{2.17}$$

where $\psi(\beta) = \phi(\beta)/\Phi(\beta)$. Note that in the above formula, each term $1/\sqrt{1+\psi(\beta)\kappa_i}$ acts as a correction factor on the FORM approximation to account for the curvature of the limit-state surface in the principal direction u_i'' .

To summarize, the SORM approximation according to the above formulation involves the following steps after the design point has been found: (1) Construct the orthonormal matrix **P** with α as its last row; (2) Compute the second-derivative matrix **H** at the design point by using a finite difference scheme in the **u** space; (3) Compute the matrix $\mathbf{A}_{11}$ and its eigenvalues; (4) Use either of the formulas in

Equation (2.15) or Equation (2.16) to obtain the SORM approximation.

2.4.1.2 Monte Carlo simulation method

Another widely used method for computing probabilities is the MCS method (Rubenstein, 1981; Ang and Tang, 1984). For example, Kareem analyzed the aerodynamic response and reliability of wind sensitive structures with parametric uncertainties by utilizing the MCS method (Kareem, 1988a; Kareem, 1988b; Kareem, 1990). The basic concept behind the MCS method is: a large number of samples following the given probability distribution of stochastic parameters **x** are generated and then repeatedly used for calculating the limit-state function g(**x**); the desired failure probability is eventually estimated as the ratio of the times when g(**x**) < 0 to the sampling number. The MCS method is the most straightforward statistical method and effective for higher-order nonlinear problems of structural reliability. The main disadvantage of the Monte Carlo simulation method lies in its large computational requirement. The direct MCS method normally requires tens or hundreds of thousands of repeated computations of the limit-state function, which is impractical for many engineering applications (Kiureghian, 1994). Therefore, many more efficient simulation methods have been developed, aiming at reducing the variance of the probability estimate for a given number of simulations.

The importance sampling method (Shinozuka, 1983; Harbitz, 1986) appears to be the most promising variance reduction technique for the structural reliability problem. Knowledge of the design point(s) from FORM analysis can be particularly helpful in choosing an appropriate sampling density used in the importance sampling method (Harbitz, 1986; Schueller, 1987). The method that sampling is the normal density

centered at each design point has been advocated by a number of investigators (Melchers, 1987; Maes and Breitung, 1993) when the shape of the limit-state surface is not known in advance. Adaptive importance sampling techniques, where the sampling density is modified during the course of sampling, have also been suggested (Bucher, 1988). It should be noted that the importance sampling method may converge to a wrong probability estimate if the sampling density is not properly selected. Other variance-reduction techniques include the method of antitbetic variates (Rubenstein, 1981), the method of stratified sampling , and in particular the Latin hypercube sampling (McKay, *et al.*, 1979).

Another class of efficient simulation methods is based on the concept of conditioning. Karamchandani and Cornell (1991) have used this method by conditioning on a single variable. One simulation method by conditioning is the so-called directional simulation method, in which various choices for the sampling density using the knowledge of design point(s) from FORM analysis have been suggested by Bjerager (1988) and Melchers (1990). Another, nonradial, directional simulation method has been suggested by Hohenbichler and Rackwitz (1988), which is aimed at improving probability estimates based on FORM and SORM.

2.4.1.3 Response surface method

For large complex structures, it is difficult to obtain the explicit expression of structural limit-state function and its gradient which is necessary in FORM and SORM analysis is difficult to compute. The response surface method (Montgomery, 1976) has been developed for computing probabilities of this kind of problem. The basic principle is to replace the integration boundary by an approximating response

surface and then perform the integration by an approximate means (e.g. FORM, SORM) without having to engage the actual limit-state function. Faravelli (1989) developed the response surface method based on the experimental design. The iterative interpolation technique proposed by Bucher and Bourgund (1990) has high efficiency. Schueller et al. (1989) investigated the precision of the response surface method. Liu et al. (1994) applied the sequential response surface method to aircraft structural system.

To construct the response surface, a number of 'experiment' points $\mathbf{x}_i$, i =1, 2, ..., N, are used to calculate g(**x**) and then fits a polynomial surface to the points by the least squares method. If a second-order polynomial is used, at least $N^2/2+3N/2+1$ points are necessary, which is a formidable number for large N. To reduce this number, the use of polynomial functions excluding cross terms has been suggested by Schueller and Stix (1987). Another suggestion is to reduce the number of random variables by collecting less important variables into a single error term (Faravelli, 1989). The selection of the 'experiment' points, $\mathbf{x}_i$, is important consideration in the response surface methodology. For the structural reliability problem, it is clear that these points should be selected in the neighborhood of the design point, which unfortunately is usually unknown in advance.

2.4.1.4 Stochastic finite element method

Stochastic finite element method (SFEM) which combines probability theory with deterministic FE methods (FEM), provides an efficient alternative to time-costly MCS and allows engineers to estimate the risk of structural systems. SFEM is an extension of deterministic FEM for considering the fluctuation of structural

properties, loads, and responses of stochastic systems. The basic formulation for SFEM is described as follows (Schuëller, 1997; Shinozuka, 1986).

$$\mathbf{K} = \mathbf{K}_0 + \Delta\mathbf{K} = \sum_{e=1}^{N_e} \mathbf{K}_0^{(e)} + \sum_{e=1}^{N_e} \Delta\mathbf{K}^{(e)} \tag{2.18}$$

The global stiffness matrix can be split into two parts: the deterministic part, $\mathbf{K}_0$, and the fluctuation (uncertainty) part, $\Delta\mathbf{K}$. The global stiffness matrix $\mathbf{K}$ is obtained by assembling the element stiffness matrices of N_e elements. There are four typical methods for formulating the fluctuation part of the SFEM procedure: the perturbation method, the Neumann expansion method, the weighted integral method, and the spectral stochastic finite element method.

The perturbation method is also known as the Taylor series expansion method and, generally, its effectiveness is restricted in that the random fluctuations must be small (*i.e.*, COV < 0.2). Hart and Collins (1970) and Cambou (1971) dealt with randomness in FEM modeling using first-order perturbation theory. Handa and Anderson (1981) obtained the variance of the structural response considering the first-order variance of force, displacement, and stiffness. Nakagiri and Hisada (1982) indicate that the second-order perturbation is impractical for large-scale problems because of its huge computational effort in calculating the second-order function gradients. The Neumann expansion method has been used by several researchers within the framework of Monte Carlo simulation (Schuëller, 1997). The main advantage of the Neumann expansion method is that the matrix $\mathbf{K}_0$ has to be decomposed only once for all samples in conjunction with the Monte Carlo simulation. Due to this single matrix decomposition, computing time can be greatly reduced. However, determining the covariance matrix among all elements of the

fluctuation part of the stiffness matrix requires extremely high computational effort (Matthies, *et al.*, 1997). The weighted integral method was proposed by Deodatis and Shinozuka (1988, 1991). The main feature of this method is that it does not require discretization of the random field. Instead, everything is determined by the mesh chosen for the deterministic part of the stiffness matrix. The weighted integral method requires about ten times more computational effort than the perturbation scheme method (Matthies, *et al.*, 1997).

The spectral stochastic finite element method (SSFEM) has been introduced by Ghanem and Spanos (1991) as an extension of the deterministic finite element method for the solution of boundary value problems with random material properties. In most applications, SSFEM is used in conjunction with a Karhunen – Loève (K–L) expansion of the Gaussian random field(s) describing the uncertain parameters of the problem (Schevenels, *et al.*, 2004). This random field must be characterized by a correlation length sufficiently large in order for the corresponding K–L expansion to yield a good approximation for a small number of (<20) terms and a reasonable stochastic dimension is preserved. For non-Gaussian properties, it has been suggested to use polynomial chaos expansion (PCE) for the representation of the input as well (Ghanem and Kruger, 1996; Ghanem, 1999a; Ghanem, 1999b). However, the use of PCE for the representation of both input and output can lead to a loss of accuracy (Sudret and Kiureghian, 2000; 2002). The use of the generalized PCE seems to be the best solution in the case of a general non-Gaussian input (Foo, *et al.*, 2007; Lucor, et al., 2004; Xiu and Karniadakis, 2002). The application of SSFEM is practically limited to linear problems. Geometrical and material non-linearity cannot be taken into account efficiently since PCE has been found to

perform poorly in problems involving sharp non-linearities, discontinuities, slope changes or bifurcations (Field and Grigoriu, 2004; Acharjee and Zabaras, 2006). More recently, a novel stochastic response surface approach has been proposed for solving nonlinear mechanical problems (Baroth, *et al.*, 2006; Baroth, *et al.*, 2007), but its application is limited to problems involving a small number of uncertain parameters. The most recent developments in spectral-Galerkin-based SFEM include the stochastic reduced basis methods (SRBMs) introduced in (Nair and Keane, 2002; Sachdeva, *et al.*, 2006; Mohan, *et al.*, 2008), the non-intrusive approaches proposed in (Baroth, *et al.*, 2006; 2007; Berveiller *et al.*, 2006), the use of the method in a multi-scale setting (Xu, 2007) and the extension to the stochastic framework of the extended finite element method (Nouy, *et al.*,2008).

2.4.2 System reliability analysis methods

Structural system reliability analysis initially arose as an extension of component failure mode analysis when it became apparent that multi-component behavior had a severe impact on the true risk of structure failure. In reality, structure systems have a wide variety of different failure characteristics. In many structures, several components must fail before the structure fails. On the other hand, in some systems, a weakest-link or chain model governs so the failure of one single component is catastrophic. For applications to large-scale realistic structures, the system reliability analysis is divided into two parts: (a) identification and enumeration of the statistically significant collapse modes, and (b) probabilistic calculations to assess each individual model failure probability or safety index and subsequently combining these into a single system risk assessment.

To identify dominant modes of structural failure, the methods of mechanics (Murotsu, *et al*., 1981; Christensen and Murotsu, 1986) and mathematical programming techniques have been employed. Fu and Moses (1988) found a new approach in importance sampling that provided both good accuracy and high efficiency. The major recent extensions of the failure tree system modeling were done by Cornell and his colleagues (1988) supported by an oil industry project. The representative approaches to calculate structural system failure probability include the Probabilistic network evaluation technique (Ang, 1975) and the lower-upper bound method (Vanmarcke, 1973; Ditlevsen, 1979; Feng, 1989). In these methods, major difficulties encountered are how to deal with the combination explosion problem and how to tackle the correlation information among different component random events.

2.4.3 Time dependent reliability analysis methods

Time dependent reliability still complies with the general structural reliability problem defined by Equation (2.6). A new trait lies in that the limit-state function depends on time, which is also said to be time-variant reliability. In general, the time dependent reliability can be given by

$$R(t) = P\left\{X(\tau) \in \Omega_S,\ \tau \in [0,t]\right\} \tag{2.19}$$

where P{·} is the probability of the random event; Ω_S is the safe domain. Equation (2.19) means that the time dependent reliability is the total probability of a random event that is always in the safe domain over the time interval [0, t]. The failure probability of exceeding a limit state can be described as the first-passage probability (Lin, 1967).

The time dependent reliability of deterministic structures can be assessed by the level

crossing theory through the Rice formula (Rice, 1944) or by the diffusion theory through the backward Kolmogorov equation (Crandall, 1970) besides the Monte Carlo simulation (Au and Beck, 2001). These methods have been naturally extended to assess the reliability of structures involving random parameters. For instance, the reliability is assessed by the level crossing theory after the statistical quantities have been gained by the orthogonal polynomial expansion method (Jensen and Iwan, 1992). The similar methodology, to directly employ the level crossing theory after gaining the statistical quantities with the random perturbation, is widely used as well (Chen, et al., 1997; Kawano and Venkataramana, 1999). Brenner and Bucher (1995) embedded the stochastic finite element method in the reliability analysis procedure. However, the joint probability density function of the response and its velocity required in the Rice formula is usually unavailable and can only be assumed, say, to be normal or Rayleigh distribution, with the acquired mean and the standard deviation. Additionally, Poisson or Markov assumption in the traditional probability analysis may lead to irreducible error. The diffusion process theory based method may give more accurate results. For example, Spencer and Elishakoff (1988) used the diffusion theory method to an SDOF system, dealing with the randomness through the conditionization technique, to evaluate the reliability with the backward Kolmogorov equation. Unfortunately, it is still difficult to use the method for practical MDOF systems. Until now, it seems that only Monte Carlo method, including its improvements, is widely accepted as a versatile and practical approach for time dependent reliability assessment of MDOF structures (Au and Beck, 2001).

For the system reliability problems in dynamic aspect, the theory of the extreme value distribution has been extensively studied since pioneering researches of Fisher

and Tippet (1928) and Gumbel (1958). Some approximate approaches to calculate the extreme value distribution were studied based on the level-crossing process theory. The Rayleigh distribution was adopted as the extreme value distribution of a narrow-banded Gaussian stochastic process by Powell (1958). To tackle non-Gaussian processes, the translation processes technique based on nonlinear static transformations were proposed (Grigoriu, 1984; Grigoriu, 1998). Generally speaking, the assumption on properties of the upcrossing events has to be made in these method. In engineering the Poisson's assumption and the Vanmarcke's assumption are widely used (say, Cheong, 1995; Rychlik, *et al.*, 1997; etc.) based on empirical data rather than theoretical analysis. Another approach employed the equivalent statistical quadratization and cubicization in the frame of equivalent Volterra systems gives fair results for SDOF systems with explicit nonlinearities in damping or restoring forces (Tognarelli, *et al.*, 1997).

In recent years, a family of probability density evolution method (PDEM), which is capable of capturing the instantaneous PDF and its evolution of the response of structures involving random parameters, has been developed and used successfully in linear and nonlinear dynamical systems by Li and Chen (2004; 2005; 2006). Based on the generalized density evolution equation (GDEE), the time dependent reliability assessment can be performed in two different ways. One is to investigate the first-passage problem through the transition and absorbing of probability by the absorbing boundary condition method (Li and Chen, 2005), the other is to transform the first-passage problem to the corresponding extreme value (Chen and Li, 2007). The former is effective for component reliability problems, while the latter can be used to solve both the component reliability problems and the system reliability

problems.

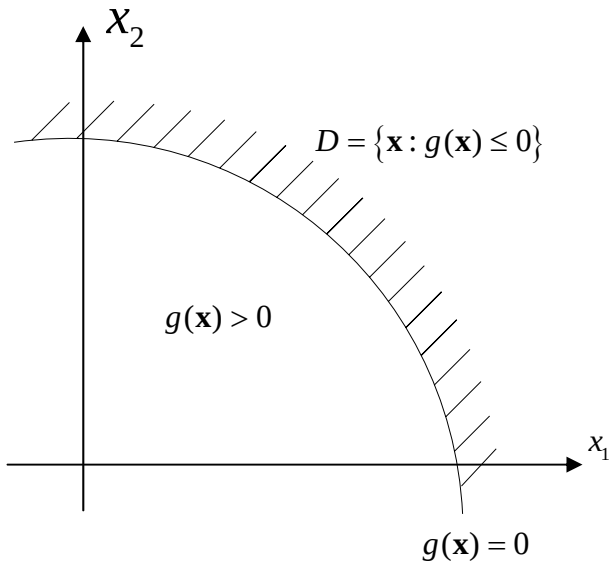

Figure 2.1 Component reliability problem

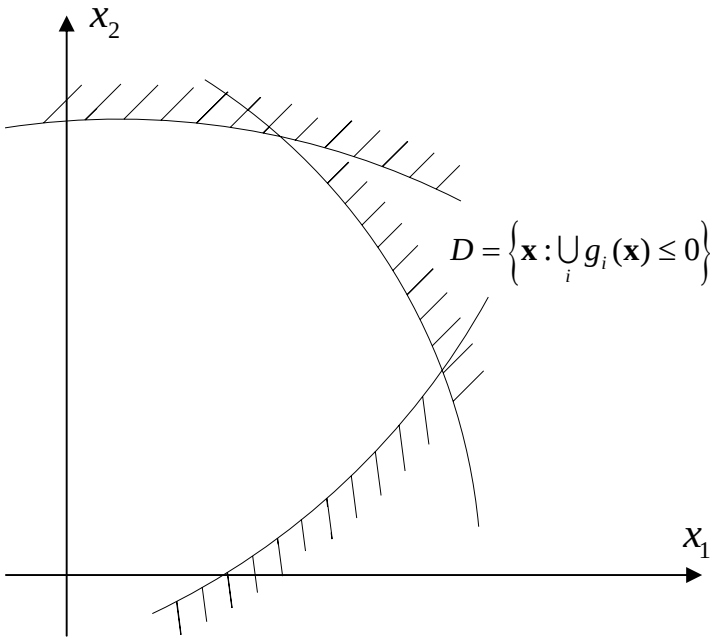

(a) series system

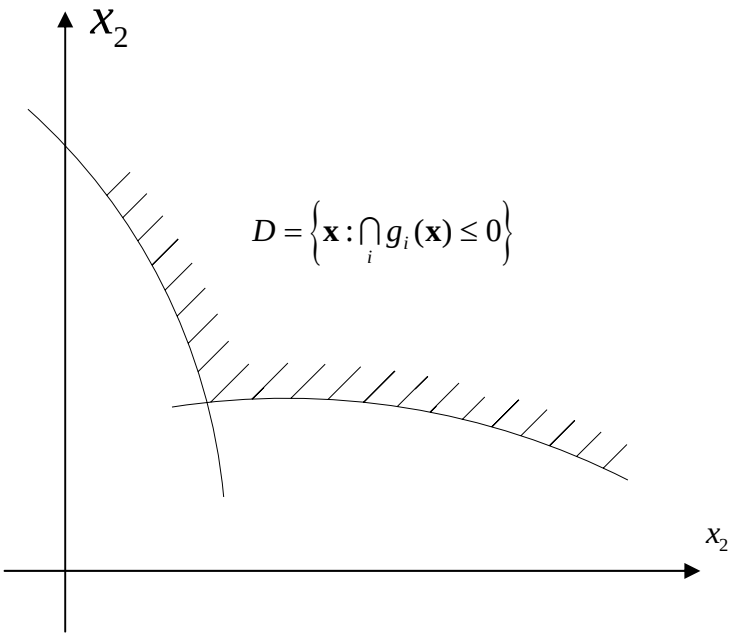

(b) parallel system

Figure 2.2 System reliability problem: (a) series system, (b) parallel system

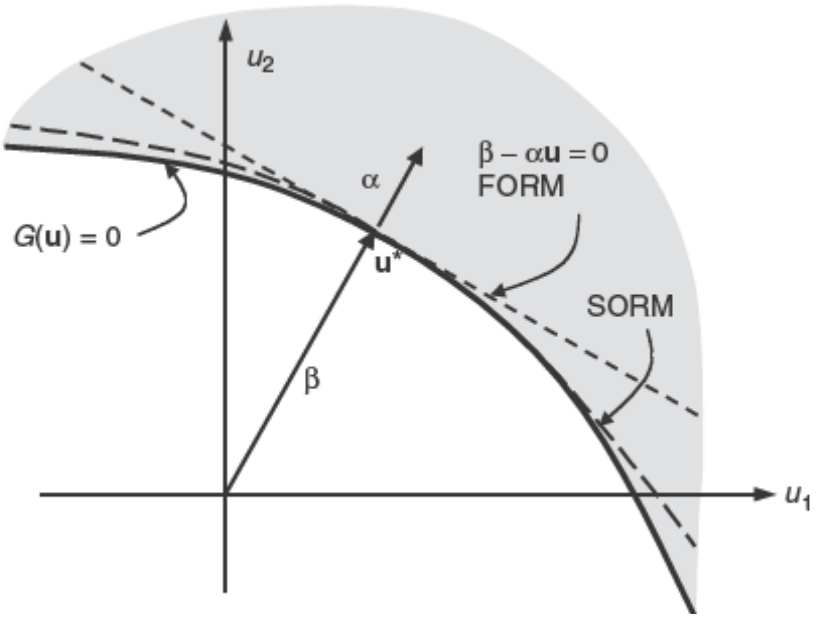

Figure 2.3 FO RM and SORM approximations for a component problem

CHAPTER 3

STATISTICAL MOMENT-BASED DAMAGE DETECTION METHOD IN FREQUENCY DOMAIN

3.1 Introduction

In this chapter, a novel statistical moment-based damage detection (SMBDD) method is proposed in the frequency domain and illustrated through shear building structures. White noise ground motion is employed to excite shear building structures. The principle of the SMBDD method is firstly presented through a single-degree-of-freedom (SDOF) system with a brief introduction of statistical theory. The sensitivity and noise issues of the new method are discussed in relation to various types of responses and different orders of statistical moments. The new method is then extended to MDOF systems. The displacement responses of a MDOF shear building structure are numerically measured and then utilized to calculate the measured statistical moments of story drifts. The measured statistical moments are used as standards to update structural stiffness parameters using the least squares method, by which structural damage can be detected. The theoretical values of the statistical moments which are compared with the measured values in the objective function of the least square method are obtained through dynamic analyses in the frequency domain. Numerical studies on multi-story shear building structures finally show that the SMBDD method is not only sensitive to structural damage but insensitive to measurement noise. The feasibility and robustness of the SMBDD method in detecting damage location and evaluating damage severities for both SDOF and

MDOF systems are demonstrated through various damage scenarios in both SDOF and MDOF shear building structures.

3.2 Statistical Moment Theory

To introduce the statistical moment-based damage detection method, a brief review of statistical moment theory is presented here. For a linear structural system, if the excitation is a stationary Gaussian random process, then the structural response is also a stationary Gaussian random process (Meirovitch, 1975).

The probability density function (PDF) of a structural response x of Gaussian distribution can be expressed by

$$p(x) = \frac{1}{\sqrt{2\pi}\sigma} e^{\frac{-(x-\bar{x})^2}{2\sigma^2}} \tag{3.1}$$

where $p(x)$ is the PDF of structural response x ; σ is the standard deviation of structural response; and $\bar{x}$ is the mean value of structural response. The *n*th-order statistical moment of structural response can be given in terms of PDF by the following integrals:

$$M_n = \int_{-\infty}^{+\infty} (x - \bar{x})^n \, p(x) dx \qquad \text{n = 1, 2, 3, 4,……} \tag{3.2}$$

In general, the odd moments relate to information about the position of the peak of probability density function which is dependent on the mean value for normal distributions, while the even statistical moments indicate the characteristics of the spread of the distribution. Figure 3.1 shows variations of probability density function with the change of variance of a zero-mean structural response of Gaussian distribution. It can be seen that the curve with a large variance tends to be flatter and more spread out than those with small variances. The shape of probability density

function depends on the value of even statistical moments, and the change of the probability density function can be reflected by the even statistical moments. Therefore, when the mean value of a structural response is zero due to a zero-mean ground motion, the odd statistical moments of the structural response are always zeros. Even statistical moments up to sixth order are considered in the following investigation for the statistical moment based structural damage detection.

For a structural response of Gaussian distribution, some relationships exist between the even statistical moments and the variance:

$$M_2 = \int_{-\infty}^{+\infty} (x - \bar{x})^2 \, p(x) dx = \sigma^2 \tag{3.3}$$

$$M_4 = \int_{-\infty}^{+\infty} (x - \bar{x})^4 \, p(x) dx = 3\sigma^4 \tag{3.4}$$

$$M_6 = \int_{-\infty}^{+\infty} (x - \bar{x})^6 \, p(x) dx = 15\sigma^6 \tag{3.5}$$

The differentiation of Equations (3.3), (3.4) and (3.5) with respect to the standard deviation σ then yields

$$\frac{dM_2}{M_2} = \frac{2\sigma \cdot d\sigma}{\sigma^2} = 2\frac{d\sigma}{\sigma} \tag{3.6}$$

$$\frac{dM_4}{M_4} = \frac{12\sigma^3 \cdot d\sigma}{3\sigma^4} = 4\frac{d\sigma}{\sigma} \tag{3.7}$$

$$\frac{dM_6}{M_6} = \frac{90\sigma^5 \cdot d\sigma}{15\sigma^6} = 6\frac{d\sigma}{\sigma} \tag{3.8}$$

The above expressions reveal that the relative change in higher even statistical moments possesses higher sensitivity to the relative change in the standard deviation of a structural response.

3.3 SMBDD Method for SDOF Systems

Structural damage such as stiffness losses in a structure will cause changes in both statistical moments and probability density function of the structure under random excitation. Therefore, the changes in statistical moments, particularly higher even statistical moments, may be sensitive to structural damage. In this regard, the principle of the SMBDD method is firstly put forward in terms of a single-degree-of-freedom (SDOF) system in this section. The sensitivity of statistical moments to structural damage is then discussed for different types of structural responses and different orders of statistical moments. The formulae for statistical moment-based damage detection are derived. The effect of measurement noise on damage detection is finally ascertained.

3.3.1 Statistical moments

Let us consider single-story shear building under zero-mean white-noise ground acceleration of Gaussian distribution as shown in Figure 3.2(a). Considering only a linear-elastic structural system, the equation of motion of the shear building can be expressed as

$$m\ddot{x} + c\dot{x} + kx = -m\ddot{x}_g \tag{3.9}$$

or

$$\ddot{x} + 2\xi\omega_o\dot{x} + \omega_o^2 x = -\ddot{x}_g \tag{3.10}$$

where m , c and k are respectively the mass, damping coefficient and stiffness coefficient of the building;. x , $\dot{x}$ and $\ddot{x}$ are respectively the relative displacement, velocity and acceleration responses of the building to the ground; $\ddot{x}_g$ is the white noise ground acceleration; ξ is the damping ratio of the building; and ω_o is the

circular natural frequency of the building and it is equal to $\sqrt{k/m}$.

If a structure is a linear system, the power spectrum $S(\omega)$ and the variance σ^2 of the structural response can be obtained by

$$S(\omega) = |H(\omega)|^2 S_f(\omega) \tag{3.11}$$

$$\sigma^2 = \int_{-\infty}^{+\infty} S(\omega) d\omega \tag{3.12}$$

where $S_f(\omega)$ is the power spectrum of ground excitation; and $H(\omega)$ stands for the frequency response function (FRF). If the ground excitation is an ideal white noise, $S_f(\omega)$ is then a constant S_0 over the whole frequency zone from $-\infty$ to $+\infty$. For a SDOF system, the module of the displacement FRF, $H_d(\omega)$, the velocity FRF, $H_v(\omega)$, and the acceleration FRF, $H_a(\omega)$, can be obtained as follows:

$$|H_d(\omega)| = \frac{1}{m\sqrt{(\omega_0{}^2 - \omega^2)^2 + (2\xi\omega_0\omega)^2}} \tag{3.13}$$

$$|H_v(\omega)| = \frac{\omega}{m\sqrt{(\omega_0{}^2 - \omega^2)^2 + (2\xi\omega_0\omega)^2}} \tag{3.14}$$

$$|H_a(\omega)| = \frac{\omega^2}{m\sqrt{(\omega_0{}^2 - \omega^2)^2 + (2\xi\omega_0\omega)^2}} \tag{3.15}$$

Substituting Equation (3.13) to Equation (3.11) and then Equation (3.12) leads to the variance or second-order moment of displacement response $\sigma_d{}^2$.

$$M_2{}^{dis} = \sigma_d{}^2 = \int_{-\infty}^{+\infty} |H_d(\omega)|^2 S_f(\omega) d\omega = \frac{\pi S_0}{2\xi\sqrt{mk^3}} \tag{3.16}$$

In a similar way, the variance or second-order moment of velocity, $\sigma_v{}^2$ and acceleration, $\sigma_a{}^2$ can be obtained as follows:

$$M_2{}^{v} = \sigma_v{}^2 = \frac{\pi S_0}{2\xi\sqrt{m^3 k}} \tag{3.17}$$

$$M_2{}^{a} = \sigma_a{}^2 = \frac{\pi S_0 (1-4\xi^2)\sqrt{k}}{2\xi\sqrt{m^5}} \tag{3.18}$$

The fourth-order and sixth-order moments of displacement, velocity and acceleration can then be given as

$$M_4{}^{dis} = \frac{3\pi^2 S_0{}^2}{4m\xi^2 k^3} \tag{3.19}$$

$$M_4{}^{v} = \frac{3\pi^2 S_0{}^2}{4m^3\xi^2 k} \tag{3.20}$$

$$M_4{}^{a} = \frac{3\pi^2 S_0{}^2}{4m^5\xi^2}(1-4\xi^2)^2 k \tag{3.21}$$

$$M_6{}^{dis} = \frac{15\pi^3 S_0{}^3}{8\xi^3\sqrt{m^3 k^9}} \tag{3.22}$$

$$M_6{}^{v} = \frac{15\pi^3 S_0{}^3}{8\xi^3\sqrt{m^9 k^3}} \tag{3.23}$$

$$M_6{}^{a} = \frac{15\pi^3 S_0{}^3}{8\xi^3\sqrt{m^{15}}}(1-4\xi^2)^3\sqrt{k^3} \tag{3.24}$$

3.3.2 Sensitivity analysis

Based on Equations (3.17) to (3.24), the following sensitivity equations can be derived:

$$\frac{dM_2{}^{dis}}{M_2^{dis}} = -\frac{3}{2}\frac{dk}{k}, \quad \frac{dM_2{}^{v}}{M_2{}^{v}} = -\frac{1}{2}\frac{dk}{k}, \quad \frac{dM_2{}^{a}}{M_2{}^{a}} = \frac{1}{2}\frac{dk}{k} \tag{3.25}$$

$$\frac{dM_4{}^{dis}}{M_4{}^{dis}} = -3\frac{dk}{k}, \quad \frac{dM_4{}^{v}}{M_4{}^{v}} = -\frac{dk}{k}, \quad \frac{dM_4{}^{a}}{M_4{}^{a}} = \frac{dk}{k} \tag{3.26}$$

$$\frac{dM_6^{dis}}{M_6^{dis}} = -\frac{9}{2}\frac{dk}{k}, \quad \frac{dM_6^{v}}{M_6^{v}} = -\frac{3}{2}\frac{dk}{k}, \quad \frac{dM_6^{a}}{M_6^{a}} = \frac{3}{2}\frac{dk}{k} \tag{3.27}$$

From the above equations, it can be observed that the relative changes of the statistical moments of displacement and velocity are negatively proportional to the relative change of stiffness while the relative change of the statistical moment of acceleration is positively proportional to the relative change of stiffness. The ratio of the relative change of the second-order, fourth-order and six-order moments of displacement to the relative change of stiffness are always three times of the counterparts of velocity and acceleration positively or negatively. This result reflects that the relative change of the statistical moment of displacement is two times more sensitive to the relative change of stiffness than those of velocity and acceleration. Thus, the statistical moment of displacement is considered in this study. Furthermore, it can be observed that the relative change of higher order moment of displacement is more sensitive to the relative change of stiffness.

3.3.3 Damage detection

Based on Equations (3.16), (3.19) and (3.22), the stiffness of the structure can be obtained from the second-order, fourth-order, and sixth-order statistical moments of displacement response, respectively.

$$k = \sqrt[3]{\frac{\pi^2 S_0^{\,2}}{4m\xi^2 (M_2^{dis})^2}} \tag{3.28}$$

$$k = \sqrt[3]{\frac{3\pi^2 S_0^{\,2}}{4m\xi^2 M_4^{dis}}} \tag{3.29}$$

$$k = \sqrt[9]{\frac{225\pi^6 S_0^{\,6}}{64\xi^6 m^3 (M_6^{dis})^2}} \tag{3.30}$$

The above equations reflect the relationships between the stiffness and the statistical moments of the displacement responses for a SDOF system in the frequency domain. From a practical point of view, the *i*th-order statistical moment can be estimated directly from the measured displacement response of the single-story shear building, denoted as $\hat{M}_i$ (*i*=2,4,6). Assuming that the measured discrete time history of the displacement response is $\mathbf{x}=[x_1, x_2, \cdots, x_{N_s}]$, where N_s is the number of sampling points, the statistical moments of the measured displacement response can be calculated as follows.

$$\hat{M}_2 = \frac{1}{N_s}\sum_{i=1}^{N_s} x_i^{\,2} - (\frac{1}{N_s}\sum_{i=1}^{N_s} x_i)^2 \tag{3.31}$$

$$\hat{M}_4 = 3(\hat{M}_2)^2 \tag{3.32}$$

$$\hat{M}_6 = 15(\hat{M}_2)^3 \tag{3.33}$$

The statistical moment-based damage detection of a SDOF system can be carried out according to the following steps:

(1) Measure the displacement response of the undamaged single-story shear building under ground acceleration which can be assumed to be a zero-mean Gaussian white noise random process;

(2) Calculate the measured statistical moments, $\hat{M}_2$, $\hat{M}_4$ and $\hat{M}_6$, using Equations (3.31) to (3.33);

(3) Substitute $\hat{M}_2$, $\hat{M}_4$ or $\hat{M}_6$ into Equations (3.28) to (3.30), and the structural stiffness $\hat{k}^u$ of the undamaged structure can be obtained;

(4) For the same building with damage (stiffness reduction), repeat Steps (1) to (3) to find out the structural stiffness $\hat{k}^d$ of the damaged structure ;

(5) The structural damage severity μ can then be identified by

$$\hat{\mu} = \frac{\hat{k}^d - \hat{k}^u}{\hat{k}^u} \times 100\% \tag{3.34}$$

In the above, the symbol '^' represents 'estimated' in contrast with 'theoretical'. The superscript 'u' and 'd' stand for 'undamaged' and 'damaged', respectively.

3.3.4 Effect of measurement noise

In order to investigate the effect of measurement noise on the quality of damage detection, white noise is used as measurement noise to contaminate the displacement response of a SDOF system. The measurement noise intensity is defined as the ratio of the root mean square (RMS) of measurement noise ε to the RMS of displacement response x.

$$\alpha = \frac{RMS(\varepsilon)}{RMS(x)} \times 100\%, \tag{3.35}$$

The effect of measurement noise on the quality of damage detection is measured in terms of the noise effect ratio γ.

$$\gamma = \frac{\hat{k}_n - \hat{k}}{\hat{k}} \times 100\% \tag{3.36}$$

where $\hat{k}_n$ is the identified structural stiffness considering the effect of measurement noise while $\hat{k}$ is the counterpart without considering the effect of measurement noise. By defining the structural response with measurement noise as y, there is a relationship

$$y = x + \varepsilon \tag{3.37}$$

where x is the actual structural response; ε is the measurement noise independent of x. Then, by taking a noise intensity of 15%, for example, one may have

$$\sigma_y{}^2 = \sigma_x{}^2 + \sigma_\varepsilon{}^2 = 1.0225\sigma_x{}^2 \tag{3.38}$$

As a result, the statistical moments of the structural responses with measurement noise can be obtained as

$$M_{2y} = 1.0225M_{2x} \tag{3.39}$$

$$M_{4y} = 3(\sigma_y{}^2)^2 = 3\times(1.0225)^2\sigma_x{}^4 = (1.0225)^2 M_{4x} \tag{3.40}$$

$$M_{6y} = 15(\sigma_y{}^2)^3 = 15\times(1.0225)^3\sigma_x{}^6 = (1.0225)^3 M_{6x} \tag{3.41}$$

where M_{2y}, M_{4y} and M_{6y} are respectively the second-order, fourth-order and sixth-order moment of y; M_{2x}, M_{4x} and M_{6x} are the counterparts of x, respectively. Using Equations (3.28) to (3.30) leads to

$$k^n = \left\{ \begin{array}{l} \sqrt[3]{\dfrac{\pi^2 S_0{}^2}{4m\xi^2 M_{2y}{}^2}} = \dfrac{1}{\sqrt[3]{1.0225^2}}\sqrt[3]{\dfrac{\pi^2 S_0{}^2}{4m\xi^2 M_{2x}{}^2}} \\ \sqrt[3]{\dfrac{3\pi^2 S_0{}^2}{4m\xi^2 M_{4y}}} = \dfrac{1}{\sqrt[3]{1.0225^2}}\sqrt[3]{\dfrac{3\pi^2 S_0{}^2}{4m\xi^2 M_{4x}}} \\ \sqrt[9]{\dfrac{225\pi^6 S_0{}^6}{64\xi^6 m^3 M_{6y}{}^2}} = \dfrac{1}{\sqrt[3]{1.0225^2}}\sqrt[9]{\dfrac{225\pi^6 S_0{}^6}{64\xi^6 m^3 M_{6x}{}^2}} \end{array} \right\} = 0.9853k \tag{3.42}$$

where k^n is the theoretically identified stiffness with considering measurement noise; and k is the corresponding stiffness without considering measurement noise. It can be seen that the theoretical noise effect ratio is only 1.47% even at the noise intensity of 15%. This result indicates that the statistical moment of displacement response is not sensitive to measurement noise.

3.4 SMBDD Method for MDOF Systems

In this section, the statistical moment-based damage detection method is extended to a MDOF system. Let us consider an N-story linear shear building subjected to

ground acceleration $\ddot{x}_g$ as shown in Figure 3.2 (b). The lumped mass, horizontal stiffness coefficient, and structural damping coefficients of *i*th story of the building are denoted as m_i, k_i and c_i, respectively, where $i = 1, 2,\ldots,N$. The equation of motion in the matrix form for this shear building can be expressed as

$$\mathbf{M}\ddot{\mathbf{x}}(t) + \mathbf{C}\dot{\mathbf{x}}(t) + \mathbf{K}\mathbf{x}(t) = -\mathbf{M}\mathbf{I}\ddot{x}_g(t) \tag{3.43}$$

where $\mathbf{M}$, $\mathbf{C}$ and $\mathbf{K}$ are the mass matrix, damping matrix and stiffness matrix of the building structure, respectively; $\ddot{\mathbf{x}}(t)$, $\dot{\mathbf{x}}(t)$ and $\mathbf{x}(t)$ are the acceleration, velocity and displacement response vectors relative to the ground, respectively; and $\mathbf{I}$ is the column vector with all its elements equal to unity. The ground acceleration $\ddot{x}_g$ is taken as zero-mean white noise ground excitation whose power spectral density is a constant S_0.

By adopting the Rayleigh damping assumption, Equation (3.43) can be decoupled through the following transformation:

$$\mathbf{x} = \mathbf{\Phi}\mathbf{z} \tag{3.44}$$

where $\mathbf{\Phi}$ is the mass-normalized modal matrix of the system. The uncoupled equations of motion of the system can then be expressed as

$$\ddot{z}_i(t) + 2\xi_i\omega_i\dot{z}_i(t) + \omega_i^2 z_i(t) = \Gamma_i\ddot{x}_g(t) \qquad i=1, 2, 3,\ldots, N \tag{3.45}$$

$$\Gamma_i = \sum_{k=1}^{N} m_k\phi_{ki} \tag{3.46}$$

where Γ_i is the *i*th participation factor; ξ_i is the *i*th modal damping ratio; ω_i is the *i*th circular natural frequency; and ϕ_{ki} is the *k*th component of the *i*th mode shape. By using the mode superposition method and taking the Fourier transform, the Fourier transform of the displacement response $x_i(t)$ of the *i*th floor can be obtained

$$X_i(\omega) = \sqrt{S_o}\sum_{k=1}^{N}\alpha_{ik}(\omega)m_k \tag{3.47}$$

$$\alpha_{ik}(\omega) = \sum_{j=1}^{N}\frac{\phi_{ij}(\mathbf{K})\cdot\phi_{kj}(\mathbf{K})}{\omega_j(\mathbf{K})^2 - \omega^2 + 2i\omega\omega_j(\mathbf{K})\xi_j} \tag{3.48}$$

Because story drifts are directly related to horizontal stiffness reduction, the statistical moments of story drifts other than floor displacements are considered in this section. The Fourier transform of the *i*th story drift can be obtained by

$$\Delta X_i(\omega) = X_i(\omega) - X_{i-1}(\omega) = \sqrt{S_o}\sum_{k=1}^{N}\Delta\alpha_{ik}(\omega)m_k, \quad i = 1,2,3...N \tag{3.49}$$

$$\Delta\alpha_{ik}(\omega) = \alpha_{ik}(\omega) - \alpha_{(i-1)k}(\omega), \quad \text{and} \quad \alpha_{0k}(\omega) = 0 \tag{3.50}$$

The power spectral density (PSD) function of the *i*th story drift Δx_i can be expressed as

$$S_{\Delta x_i}(\omega) = S_o(\sum_{k=1}^{N}\Delta\alpha_{ik}(\omega)m_k)(\sum_{k=1}^{N}\Delta\alpha_{ik}(\omega)^*\cdot m_k) \tag{3.51}$$

where $\Delta\alpha_{ik}(\omega)^*$ is the conjugate of $\Delta\alpha_{ik}(\omega)$. Therefore, the variance of the *i*th story drift can be calculated by

$$\sigma_{\Delta x_i}{}^2 = \int_{-\infty}^{+\infty} S_{\Delta x_i}(\omega)d\omega = \int_{-\infty}^{+\infty} S_o(\sum_{k=1}^{N}\Delta\alpha_{ik}(\omega)m_k)(\sum_{k=1}^{N}\Delta\alpha_{ik}(\omega)^*\cdot m_k)d\omega \tag{3.52}$$

Since the *i*th story drift is a stationary random process, its statistical moments can be computed by

$$M_{2i} = \sigma_{\Delta x_i}{}^2, \quad M_{4i} = 3\sigma_{\Delta x_i}{}^4, \quad M_{6i} = 15\sigma_{\Delta x_i}{}^6, \qquad i=1,2,\ldots,N \tag{3.53}$$

The second-order, fourth-order, and sixth-order statistical moment vectors can be expressed as

$$\mathbf{M}_2 = [M_{21}, M_{22}, \cdots, M_{2N}] \tag{3.54}$$

$$\mathbf{M}_4 = [M_{41}, M_{42}, \cdots, M_{4N}] \tag{3.55}$$

$$\mathbf{M}_6 = [M_{61}, M_{62}, \cdots, M_{6N}] \tag{3.56}$$

Based on the above derivation, it can be seen that if the mass matrix and the damping ratios of the system are kept invariant, the statistical moments of story drifts are the function of the horizontal stiffness. Therefore, the *i*th-order moment vector of story drift, denoted as $\mathbf{M}_i$ (*i*=2,4,6), can be theoretically calculated for the given stiffness vector $\mathbf{k} = [k_1, k_2, ..., k_N]$. For damage detection, the *i*th-order statistical moment vector shall be estimated from the measured displacement responses based on Equations (3.31) to (3.33), denoted as $\hat{\mathbf{M}}_i$. The residual vector between $\mathbf{M}_i$ and $\hat{\mathbf{M}}_i$ can be written as

$$\mathbf{F}(\mathbf{k}) = \mathbf{M}_i(\mathbf{k}) - \hat{\mathbf{M}}_i \tag{3.57}$$

Ideally, if the given stiffness vector **k** is equal to the actual value, the 2-norm of the residual vector, $\|\mathbf{F}(\mathbf{k})\|^2$, will be zero. Practically, the optimal stiffness vector can be identified by the nonlinear least-squares method, that is, giving **k** an initial value and minimizing $\|\mathbf{F}(\mathbf{k})\|^2$. Since it is physically impossible that the stiffness parameters of the damaged building are larger than those of the corresponding undamaged building, the constrained optimization method is utilized to identify the lateral stiffness value of the damaged building. That is, the structural stiffness parameter vector of the damaged building is identified by the nonlinear least-squares method under the constrained condition that the stiffness parameters of the damaged building shall be less than the identified stiffness parameters of the corresponding undamaged building. The quasi-Newton method and the trust-region method are respectively used to solve the unconstrained optimization problem and the constrained optimization problem (Dennis, Gay and Welsch, 1981; Byrd, Schnabel and Shultz, 1988). The finite difference

method is utilized to approximate the Jacobian matrix of the objective function through many additional function evaluations in the aforementioned two methods.

The statistical moment-based damage detection method for a MDOF system can be carried out according to the following steps:

(1) The actual statistical moments of story drifts $\hat{\mathbf{M}}_i$ are estimated from the measured displacements for undamaged and damaged building respectively by using Equations (3.31) ~ (3.33);

(2) Give the horizontal stiffness of the building structure an initial value, the theoretical statistical moments of story drifts $\mathbf{M}_i$ can be calculated by the above Equations (3.44) ~ (3.53) in the frequency domain.

(3) Substitute $\hat{\mathbf{M}}_i$ and $\mathbf{M}_i$ into Equation (3.57), the structural stiffness vector can be identified by the nonlinear least-squares method for the undamaged and damaged building respectively;

(4) The structural damage including damage existence, location and severity can be detected by comparing the identified stiffness vector $\hat{\mathbf{k}}^u$ of the undamaged building with the identified stiffness vector $\hat{\mathbf{k}}^d$ of the damaged building.

In addition, to investigate the effect of measurement noise on the statistical moment-based damage detection, the measurement noise can be added to the numerically measured displacement response and ground excitation. The contaminated displacement responses and excitation can be then used to estimate the actual statistical moment vector in the above Step (1) and the power spectral density of the contaminated excitation which is utilize to calculate the theoretical statistical moments in the above Step (2). The noise effect can be finally assessed by

comparing the identified damage severity values with their corresponding preset ones.

3.5. Numerical Example of SDOF System

3.5.1 Numerical model

A single-story shear building model (see Figure 3.2(a)) is utilized in this section to examine the feasibility of the statistical moment-based damage detection method. The mass and horizontal stiffness of the SDOF system are taken as 230.2 kg and 5.46×10^5 N/m, respectively. The damping ratio is 1%. The ground excitation is taken as a zero-mean white-noise stationary process. The duration of the ground excitation time history is 1000s with a sampling frequency of 256 Hz. The ground excitation time history is generated using the method of digital simulation of a random processes developed by Shinozuka and Jan (1972), which is used to obtain numerically measured structural responses. The excitation time history generated is ergodic regardless of the number of frequency intervals. This makes the method directly applicable to a time domain analysis in which the ensemble average can be evaluated in terms of the temporal average. Note that the simulated process is of Gaussian distribution by virtue of the central limit theorem. Figure 3.3 presents the attributes of a simulated band-limited white Gaussian excitation, which includes its time history, power spectrum density and probability density distribution. The intensity of the power spectral density is $2.1801\times10^{-3}(\text{m/s}^2)^2$/Hz with a frequency band from 0.5Hz to 70Hz.

3.5.2 Sensitivity of PDF to structural damage

The sensitivity of PDF of different responses of the building to structural damage severity is numerically investigated. The displacement, velocity and acceleration responses of the building with different stiffness k_0, $0.98k_0$, $0.95k_0$, $0.90k_0$, $0.80k_0$ and $0.70k_0$ are computed for the same ground excitation. These stiffness coefficients represent different damage severities, that is, 0%, 2%, 5%, 10%, 20% and 30%, correspondingly. The displacement, velocity and acceleration response time histories are then used to compute their PDF curves. The PDF curves are finally fitted by the Gaussian PDF curves and shown in Figures 3.4 (a), (b) and (c) for displacement, velocity, and acceleration responses, respectively, in which DS stands for damage severity.

It can be seen that the PDF curves of displacement and velocity responses become flatter with the increase of structural damage severity but the PDF curves of acceleration responses show the contrary phenomenon. With reference to Figure 3.1, one may conclude that the statistical moments of displacement and velocity responses get bigger with the decrease of structural stiffness but those of acceleration responses become smaller. Furthermore, the PDF curves of displacement responses present more apparent and consistent changes with respect to different damage severities than those of velocity and acceleration responses. Accordingly, the PDF curve of displacement response is more sensitive to structural damage severity than those of velocity and acceleration responses. These results are all consistent with the previous conclusions drawn from theoretical analysis given in Section 3.2. The displacement responses will be therefore utilized hereinafter in order to effectively conduct damage detection.

3.5.3 Sensitivity of statistical moments to structural damage

As mentioned above, changes in the structural stiffness values are clearly illustrated in the PDF of displacement responses which would take the form of well known Gaussian bell shaped curve for a linear SDOF structural system under the ground excitation of zero-mean white noise. The theoretical second-order, fourth-order and sixth-order statistical moments which represent the characteristics of distribution are now computed for the undamaged building and the damaged building with the stiffness reduction of 2%, 5%, 10%, 20% and 30% (Scenario 1 to Scenario 5) respectively using Equations (3.16), (3.19), and (3.22), respectively. The corresponding circular frequencies of the undamaged building and the damaged building are also computed. The theoretical circular frequency and the theoretical second-order, fourth-order and sixth-order statistical moments of the undamaged building calculated by Equations (3.16), (3.19) and (3.22) are denoted as $\omega_0^{\ u}$, $M_2^{\ u}$, $M_4^{\ u}$, and $M_6^{\ u}$, respectively. The counterparts of the damaged building are denoted as $\omega_0^{\ d}$, $M_2^{\ d}$, $M_4^{\ d}$ and $M_6^{\ d}$, respectively. The change ratios of these values to those of the undamaged building are listed in Table 3.1.

Table 3.1 Change ratios of natural frequency and statistical moments

(SDOF system)

Scenario	$\frac{\omega_0^{\ d}-\omega_0^{\ u}}{\omega_0^{\ u}}(\%)$	$\frac{M_2^{\ d}-M_2^{\ u}}{M_2^{\ u}}(\%)$	$\frac{M_4^{\ d}-M_4^{\ u}}{M_4^{\ u}}(\%)$	$\frac{M_6^{\ d}-M_6^{\ u}}{M_6^{\ u}}(\%)$
1	-1.00	3.08	6.25	9.52
2	-2.53	8.00	16.64	25.96
3	-5.13	17.12	37.17	60.66
4	-10.55	39.75	95.31	172.96
5	-16.33	70.75	191.55	397.80

It can be seen that statistical moments are more sensitive to structural damage than circular natural frequency. Furthermore, the higher-order statistical moment is more sensitive to structural damage than lower-order moment. This has also been theoretically interpreted in Section 3.2. It seems that the higher-order statistical moment would be a good index for structural damage detection. However, the statistical moments are calculated in the frequency domain based on the assumption that the responses are stationary Gaussian time histories resulting from the external random excitation which satisfies the stationary Gaussian distribution. Thus, the statistical moments intend to be unstable in the actual numerical calculation due to the effects of limited time duration and the transitory unstable dynamic responses at the initial stage. It is, therefore, necessary to investigate the stability of higher statistical moment value. 20 stationary Gaussian ground acceleration time histories with the same preset power spectral density function are generated randomly and then employed as external excitations and respectively input to the undamaged single story shear building structure. The statistical moments of displacement response are computed. The mean value and standard deviation of the 20 values of the *i*th statistical moment and then the coefficient of variation δ_i are calculated.

$$\delta_i = \frac{std(\hat{M}_i^u)}{mean(\hat{M}_i^u)} \times 100\% \tag{3.58}$$

where $std(\hat{M}_i^u)$ is the standard deviation of the *i*th statistical moment and $mean(\hat{M}_i^u)$ is its mean value. The results show that the coefficients of variance of the second-order, fourth-order and sixth-order moments are 8.9%, 16.9% and 24.2%, respectively. The coefficient of variance is larger for higher statistical moment. Namely, higher statistical moment is less stable. Therefore, as far as a damage index is concerned, the fourth-order moment may be a good choice which represents a

compromise measure between sensitivity and stability. In the following study, the fourth-order moments are adopted for damage detection. In addition, the stability of the identified structural stiffness using the mean value of 20 fourth-order moments is also investigated. The mean value of corresponding structural stiffness identified is 549880N/m which only has a bias of 0.71% and the coefficients of variance 0.42%, comparing with the true value. This promising result paves the way for the following damage detection.

3.5.4 Damage detection results

In this section, the damage detection is carried out without considering the effect of measurement noise. The identified stiffness from the fourth-order moment of displacement response of the undamaged building, $\hat{k}^u$, is 547244 N/m, which is very close to the theoretical stiffness k^u of 546000 N/m. The identified stiffness $\hat{k}^d$ from the fourth-order moments of displacement responses of the damaged building, $\hat{M}_4{}^d$, is tabulated in Table 3.2 for Scenario 1 to Scenario 5. In the table, $\hat{M}_4{}^d$ stands for the estimated fourth-order moment of the damaged building using Equation (3.11) while $M_4{}^d$ is the theoretical value derived by Equation (3.19) using the theoretical stiffness k^d. The maximum difference between the identified and theoretical stiffness among all the five cases is 0.88 % only. The identified damage severities for the five damage cases are 2.20%, 4.12%, 9.38%, 19.83% and 29.64%, which correspond to the preset values, 2%, 5%, 10%, 20%, and 30% respectively. It can be seen that even for the damage severity of 2%, the proposed statistical moment-based damage detection method produces a satisfactory result if measurement noise is not

considered.

Table 3.2 Damage detection results and preset values (SDOF system)

Scenario	$\hat{M}_4^d$ $(10^{-13}m^4)$	M_4^d $(10^{-13}m^4)$	$\hat{k}^d$ (N/m)	k^d (N/m)	$\hat{\mu}$ (%)	μ (%)
1	2.5516	2.5530	535218	535080	-2.20	-2
2	2.1644	2.2310	524683	518700	-4.12	-5
3	3.2873	3.3646	495871	491400	-9.38	-10
4	3.8272	3.8841	438702	436800	-19.83	-20
5	7.2024	7.3511	385054	382200	-29.64	-30

3.5.5 Effect of measurement noise

Random white measurement noises are now introduced into the structural displacement responses to investigate the effect of measurement noise on damage detection. Five noise intensities are considered and they are 1%, 2%, 5%, 10% and 15%, respectively. Table 3.3 displays the noise effect ratio γ obtained for the aforementioned five damage cases and five noise intensities. As shown in the table, the noise effect ratio is only related to noise intensity and has almost nothing to do with damage severity. The measurement noise has only small effects on the damage detection. Even when the noise intensity is as high as15%, the absolute γ values for the five damage cases are only 1.88%, 1.63%, 1.72%, 1.39% and 1.65%.

It can be concluded that the fourth statistical moment is a sensitive measure but it is insensitive to measurement noise. By using the fourth moment as a damage index, the proposed statistical moment–based damage detection method can provide not only reliable damage detection results but explicit estimation of noise effects on damage detection results.

Table 3.3 Noise effect ratio γ (SDOF system)

α	Scenario 1	Scenario 2	Scenario 3	Scenario 4	Scenario 5
1%	-0.01%	-0.01%	-0.01%	-0.01%	-0.01%
2%	-0.03%	-0.03%	-0.03%	-0.03%	-0.03%
5%	-0.21%	-0.19%	-0.19%	-0.13%	-0.17%
10%	-0.90%	-0.80%	-0.76%	-0.57%	-0.71%
15%	-1.88%	-1.63%	-1.72%	-1.39%	-1.65%

3.6 Numerical Example of MDOF System

In this section, the robustness of the statistical moment-based damage detection method is numerically demonstrated based on a real three-story shear building model. Various damage cases with different damage severities and locations are investigated by making use of the inherent relationship between the fourth-order moments of structural responses and structural properties. Random white measurement noises are also introduced into the structural responses to investigate the effect of measurement noise on the damage detection quality.

3.6.1 Numerical model

To demonstrate the feasibility and the effectiveness of the new damage detection method for MDOF systems, a three-story shear building structure is investigated in this section. The mass and horizontal stiffness coefficients of the three-story shear building are respectively 350250 kg and 4728400 kN/m for the first story, 262690 kg and 315230 kN/m for the second story, and 175130 kg and 157610 kN/m for the third story. The mass of each floor is assumed to be invariant. The first damping ratio is taken as 1%. The second and third modal damping ratios are 2.14% and 5.56%,

respectively. The ground acceleration is simulated as a white noise whose magnitude is chosen such that the maximum absolute value of acceleration is 2.0 m/sec^2. To simulate the white noise excitation, a method of digital simulation random processes developed by Shinozuka M and Jan CM (1972) is utilized. The duration of the excitation time history is 1000s with the sampling frequency of 256 Hz.

Listed in Table 3.4 are the values of the fourth-order moments for all the three stories of the undamaged building, $\hat{M}_{4i}^{u}$ ($i = 1,2,3$), obtained using Equations (3.30) and (3.31). The identified stiffness values of the undamaged building, $\hat{k}_i^u$ ($i = 1,2,3$) using the corresponding values of the fourth-order moments and the least-squares method are also listed in Table 3.4. It can be seen that the identified horizontal stiffness coefficients of the undamaged building $\hat{k}_i^u$ are very close to the theoretical values k_i^u . The relative errors of the identified horizontal stiffness values are respectively 0.93%, 0.38% and 0.35% for the three stories compared with the real values, which lays down a good foundation for the coming damage detection.

Table 3.4 Identified statistical moments and stiffness of undamaged building (MDOF system)

Story	$\hat{M}_{4i}^{u}$ (m^4)	$\hat{k}_i^u$ (kN/m)	k_i^u (kN/m)
1	6.9171×10^{-16}	4772490.31	4728400.00
2	1.3412×10^{-11}	316418.04	315230.00
3	2.6322×10^{-11}	158158.31	157610.00

3.6.2 Damage detection results: different damage severities at the same damage location

The main purpose of this section is to demonstrate the sensitivity of the proposed statistical moment-based damage detection method to structural damage severities at the same damage locations. Five single-damage cases with different damage severities at the first story are considered. The details of the five damage cases are listed in Table 3.5 in which the theoretical stiffness values k_1^u, k_2^u and k_3^u of the undamaged building can be found in Table 3.4. The theoretical damage severities are actually 2%, 5%, 10%, 20% and 30%, respectively, for the first story of the building.

For each damage case, the fourth-order moments of story drift are computed for each story of the damaged building and then used to identify stiffness coefficients of the damaged building using the least-squares method. With reference to the identified stiffness coefficients of the undamaged building (see Table 3.4), the damage severities of each story are finally calculated for each damage case. The results are listed in Table 3.6 and the result of Scenarios 2 is also plotted in Figure 3.5. In comparison with the actual damage severities shown in Table 3.5, it can be seen that the identified damage severities are quite close to the actual damage severities. Even for the small damage Scenario 1, the identified damage severity is 1.99% versus the actual value of 2%. The effectiveness and sensitivity of the proposed method to structural damage are demonstrated here.

Table 3.5 Details of five single-damage scenarios (MDOF system)

Scenario	Story 1	Story 2	Story 3
1	$0.98\,k_1^u$	k_2^u	k_3^u
2	$0.95\,k_1^u$	k_2^u	k_3^u
3	$0.90\,k_1^u$	k_2^u	k_3^u
4	$0.80\,k_1^u$	k_2^u	k_3^u
5	$0.70\,k_1^u$	k_2^u	k_3^u

Table 3.6 Identified damage severities μ (%) for Scenarios 1-5 (MDOF system)

Scenario	Story 1	Story 2	Story 3
1	-1.99	0.00	0.00
2	-4.92	0.00	0.00
3	-9.90	0.00	0.00
4	-19.75	0.00	0.00
5	-29.77	0.00	0.00

3.6.3 Damage detection results: different damage locations and severities

To demonstrate the accuracy of the statistical moment-based damage detection method for identifying more complicated damage of the three-story building, other 11 damage scenarios with combination of various damage severities and locations are further considered in this section. The details of damage cases are presented in Table 3.7 in which the theoretical stiffness values of the undamaged building k_1^u, k_2^u and k_3^u can be found in Table 3.4. Scenarios 6 and 7 simulate single damage in the second story with damage severities of 5% and 10%, respectively. Scenario 8 has single damage in the third story with damage severity of 10%. Scenarios 9 to 15 simulate two damages at different stories with the same or different damage severities. In Scenario 16, the three stories all have damage but with different severities.

Table 3.7 Details of eleven more damage scenarios (MDOF system)

Scenario	Story 1	Story 2	Story 3
6	k_1^u	$0.95\,k_2^u$	k_3^u
7	k_1^u	$0.90\,k_2^u$	k_3^u
8	k_1^u	k_2^u	$0.90\,k_3^u$
9	$0.98\,k_1^u$	$0.98\,k_2^u$	k_3^u
10	$0.90\,k_1^u$	$0.95\,k_2^u$	k_3^u
11	$0.90\,k_1^u$	$0.90\,k_2^u$	k_3^u
12	k_1^u	$0.95\,k_2^u$	$0.90\,k_3^u$
13	k_1^u	$0.80\,k_2^u$	$0.90\,k_3^u$
14	k_1^u	$0.70\,k_2^u$	$0.90\,k_3^u$
15	$0.90\,k_1^u$	k_2^u	$0.70\,k_3^u$
16	$0.95\,k_1^u$	$0.90\,k_2^u$	$0.80\,k_3^u$

Table 3.8 Identified damage severities $\hat{\mu}$ (%) vs. μ (%) for Scenarios 6 -16

(MDOF system)

Scenario	Story 1		Story 2		Story 3	
	μ (%)	$\hat{\mu}$ (%)	μ (%)	$\hat{\mu}$ (%)	μ (%)	$\hat{\mu}$ (%)
6	0.00	0.00	-5.00	-5.02	0.00	0.00
7	0.00	0.00	-10.00	-9.84	0.00	0.00
8	0.00	0.00	0.00	0.00	-10.00	-9.65
9	-2.00	-1.56	-2.00	-1.44	0.00	0.00
10	-10.00	-9.80	-5.00	-4.75	0.00	0.00
11	-10.00	-9.79	-10.00	-9.68	0.00	0.00
12	0.00	0.00	-5.00	-4.38	-10.00	-9.50
13	0.00	-0.25	-20.00	-20.22	-10.00	-10.20
14	0.00	0.00	-30.00	-29.97	-10.00	-9.93
15	-10.00	-10.13	0.00	-0.02	-30.00	-29.97
16	-5.00	-4.52	-10.00	-9.26	0.00	0.00

By using the same procedure as used in Section 3.6.2, the damage severities μ are identified for these damage scenarios and listed in Table 3.8. It can be seen that the structural damage can be effectively detected out for all these damage scenarios with different damage locations and severities. The large damage at one story of the shear building structure hardly has any effect on the identified results of adjacent locations, in other words, there are no negative falsity (less pronounced damage undetectable) and positive falsity (identifying intact stories as damaged ones) resulting from the large damage at adjacent stories. For example, the situations of Story 1 and 3 can be quite accurately identified according to the analytical result even when the damage severity of Story 2 is 30% in Scenario 14. In addition, the small multi-damage can also be detectable by utilizing the proposed method, say, Scenario 9. The identification results for Scenarios 7, 14 and 16 are also plotted in Figure 3.5. The damage locations can be apparently identified for these damage scenarios seen from these figures. It can be seen that the identified results only have very small relative errors compared with the actual values. The robustness of the proposed method for identifying complicated damage of multi-story shear buildings is demonstrated without considering measurement noise in this section.

3.6.4 Effect of measurement noise

To assess the effect of measurement noise on the damage detection of the three-story building, each displacement response is contaminated with a random Gaussian white noise. The ground excitation is also contaminated with a random Gaussian white noise. The added Gaussian white noises are different with and independent to each other. Two noise intensities, $\alpha = 5\%$ and 15%, are considered, respectively. The story drifts are calculated from the contaminated displacement responses. The fourth-

order moments of the story drifts are then computed and utilized for the structural damage detection. The horizontal stiffness coefficients of the undamaged building are firstly identified by the proposed method. The results are listed in Table 3.9. Compared with the results of the scenarios without considering measurement noise presented in Table 3.4, it can be seen that the effects of measurement noise on the fourth-order moments and horizontal stiffness coefficients are very minimal. Even when noise intensity is as high as 15%, the relative differences between the identified horizontal stiffness values and the actual stiffness values are only 0.27%, 0.92% and 0.89% for the three stories of the undamaged structure, respectively.

Table 3.9 Identified statistical moments and stiffness of undamaged building with noise (MDOF system)

Story	$\alpha = 5\%$		$\alpha = 15\%$	
	$\hat{M}_{4i}^{un}\ (m^4)$	$\hat{k}_i^{un}(kN/m)$	$\hat{M}_{4i}^{un}\ (m^4)$	$\hat{k}_i^{un}(kN/m)$
1	6.9529×10^{-16}	4772351.56	7.2476×10^{-16}	4715438.96
2	1.3475×10^{-11}	316536.42	1.4034×10^{-11}	312336.05
3	2.6441×10^{-11}	158220.87	2.7490×10^{-11}	156200.23

Five scenarios of the three-story building are explored with consideration of measurement noise. The identified results with 5% and 15% noise intensities are listed in Tables 3.10 and 3.11, respectively. Four of the five scenarios with 15% measurement noise intensities are also plotted in Figures 3.6. Compared with the actual values, it can be seen that even the measurement noise intensity is as high as 15%, it has only very little impact on the identified damage results: the damage severities and damage locations can still be properly identified. Therefore, the proposed method is insensitive to measurement noise. Its robustness and reliability

are demonstrated again.

Table 3.10 Identified damage severities μ^n (%) for Scenarios 2, 7, 11, 14 and 16 with noise intensity α =5% (MDOF system)

Scenario	Story 1	Story 2	Story 3
2	-5.11	-0.10	-0.10
7	0.00	-9.95	0.00
11	-9.86	-9.74	0.00
14	-0.28	-30.25	-10.28
16	-4.90	-9.76	-19.75

Table 3.11 Identified damage severities μ^n (%) for Scenarios 2, 7, 11, 14 and 16 with noise intensity α =15% (MDOF system)

Scenario	Story 1	Story 2	Story 3
2	-4.81	0.00	0.00
7	0.00	-9.58	0.00
11	-9.76	-9.61	0.00
14	-0.31	-30.25	-10.28
16	-5.13	-10.00	-19.96

3.7 Conclusions

A new structural damage detection method has been proposed in the frequency domain in this chapter based on the analysis of statistical moments of displacement responses of a shear building structure under white noise ground excitation in the frequency domain.

The basic equations for sensitivity analysis of damage indices and damage detection

have been derived for a single-story shear building. It is found that the relative change of the statistical moment of structural displacement response is two times more sensitive to the relative change of building stiffness than those of velocity and acceleration. Therefore, the displacement responses are employed in the numerical analysis rather than the velocity and acceleration responses. In addition, the relative change of higher order moments is more sensitive to that of the natural frequency and the second-order moment. However, the higher statistical moments may not be numerically stable. As a result, the fourth-order moment has been proposed as a new damage index by making a balance between the sensitivity to structural damage and the numerical stability to random excitation. Analytical results of the single-story shear building show that the new method is sensitive to structural damage. Even when the damage severity is only 2%, the identified result is very close to the actual value. In addition, the effect of measurement noise on the quality of damage detection is explored in terms of the noise effect ratio. Analytical results of the single-story shear building show that the noise effect ratio is only related to noise intensity and has almost nothing to do with damage severity. Even when the noise intensity is as high as 15%, the maximal value of the noise effect ratio for the numerically evaluated damage cases is only 1.88%. Therefore, the damage index of the fourth-order statistical moment is also very insensitive to measurement noise for the SDOF system.

Then the proposed method is applied to a multi-story shear building. A three-story shear building is investigated for various damage scenarios with different damage locations and damage severities. Numerical results show that the fourth order moments of story drifts can be used to accurately identify both damage locations and

damage severities for all the damage scenarios concerned. Furthermore, a significant advantage of the proposed damage detection method lies in that it is insensitive to measurement noise. Even when the measurement noise intensity is as high as 15%, the SMBDD method still gives highly reliable results on damage severities and damage locations of the multi-story shear building structure. The robustness of the proposed method is also demonstrated through the multi-story shear building.

However, only shear building structures are explored to demonstrate the feasibility and effectiveness of the SMBDD method in this chapter. More complicated structures should be investigated before the practical application of the proposed method. Furthermore, the Gaussian white noise excitation is employed in this chapter, which is only a very special dynamic excitation. It is necessary to explore the feasibility of other dynamic excitations, such as colored noise excitations. Other types of structures and colored noise excitations will be addressed in Chapter 4. In addition, the SMBDD method can also be applied in the time domain. In other words, the theoretical fourth-order statistical moment in Equation (3.57) can also be obtained in the time domain. The feasibility and effectiveness of the SMBDD method in the time domain will be addressed in Chapter 5.

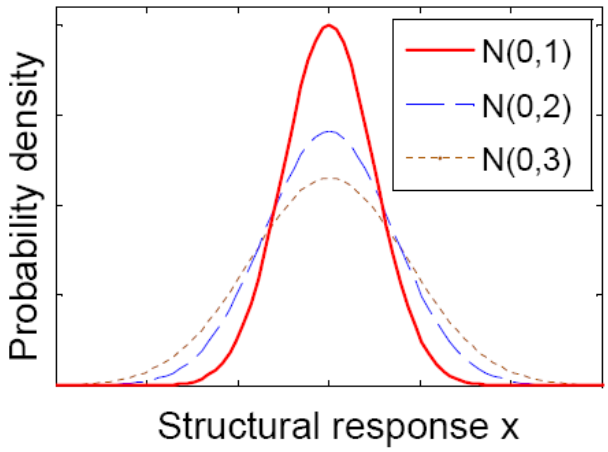

Figure 3.1 Variations of zero-mean Gaussian probability density functions

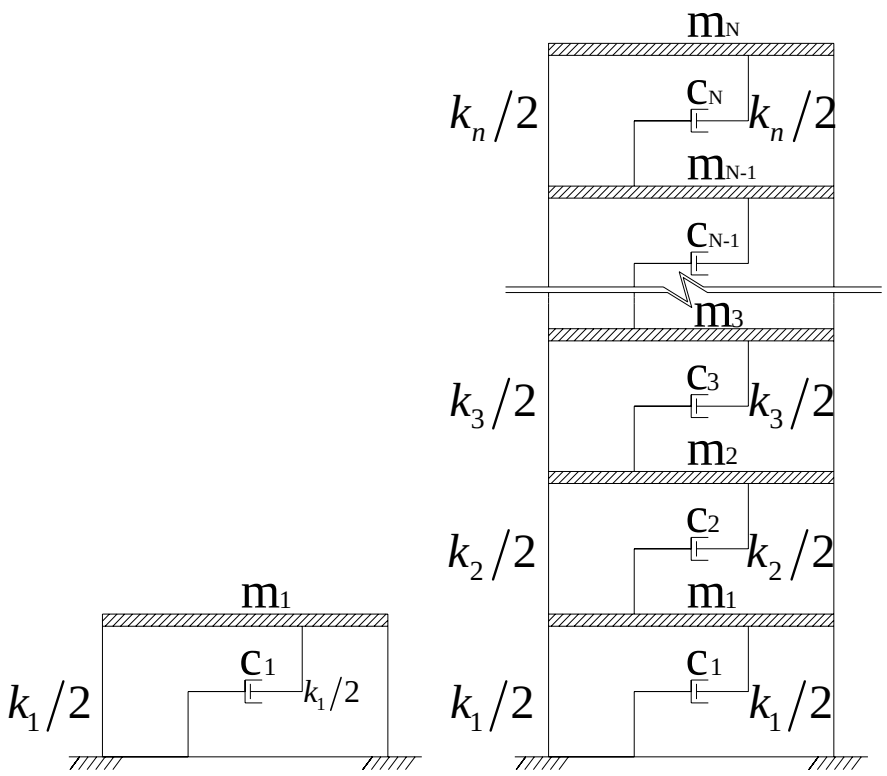

(a). Single-story shear building; (b). N-story shear building

Figure 3.2 Building models: (a) single-story shear building, (b) N-story shear building

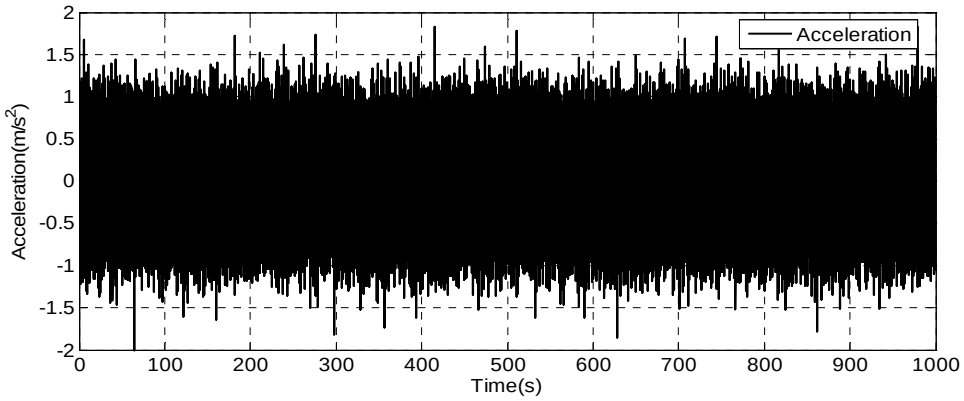

(a) time history

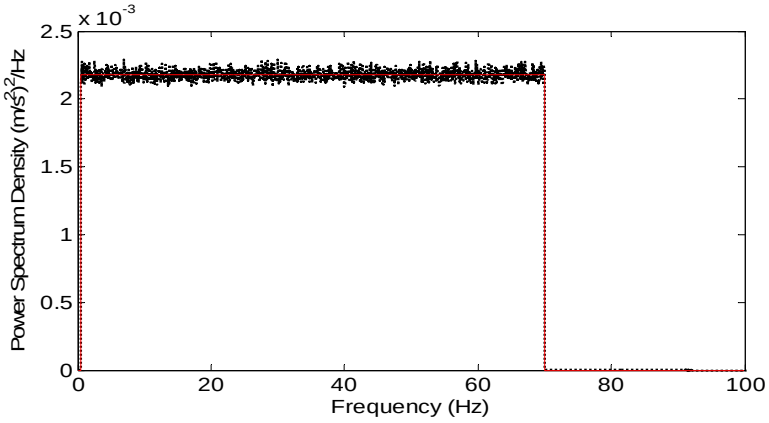

(b) power spectrum density

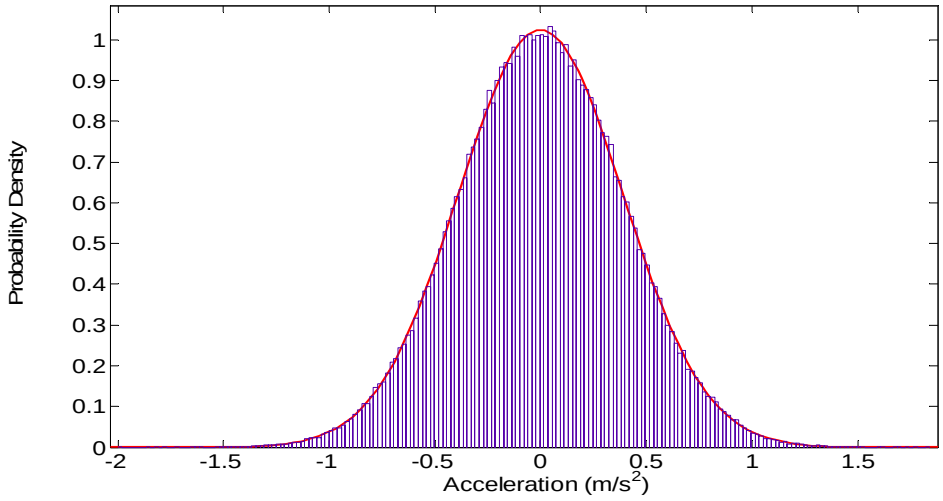

(c) probability density distribution

Figure 3.3 Simulated band-limited Gaussian white noise excitation: (a) time history, (b) power spectrum density, (c) probability density distribution

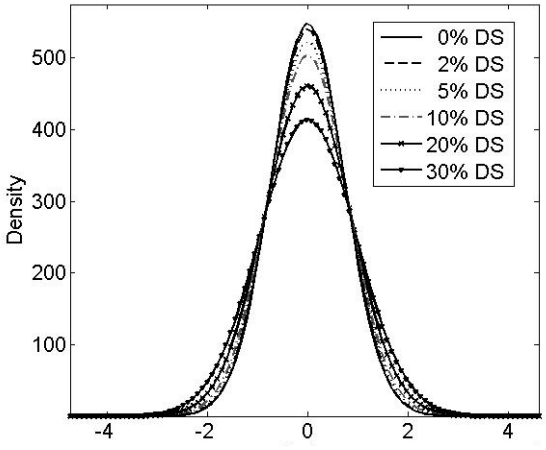

(a) displacement ($\times 10^{-3}$ m)

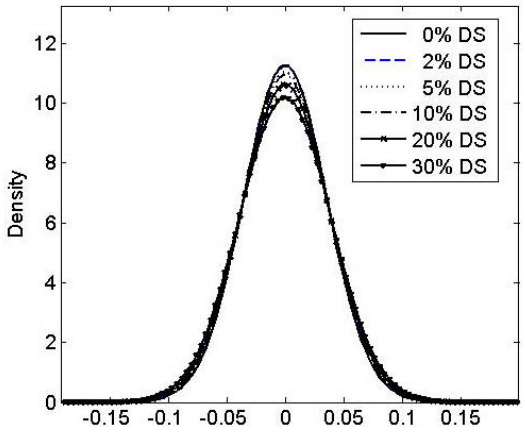

(b) velocity (m/s)

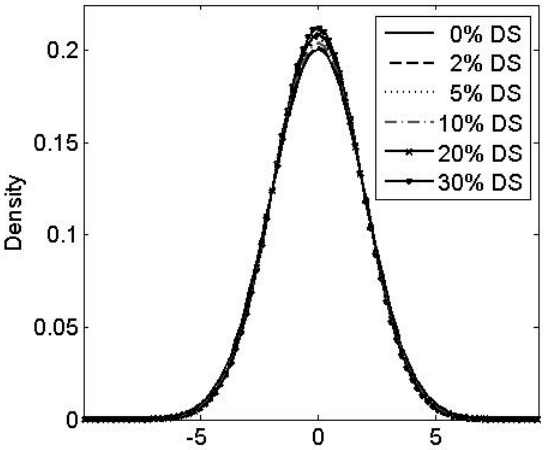

(c) acceleration (m/s^2)

Figure 3.4 Probability density functions of different responses for different stiffness values: (a) displacement ($\times 10^{-3}$ m), (b) velocity (m/s), (c) acceleration (m/s^2)

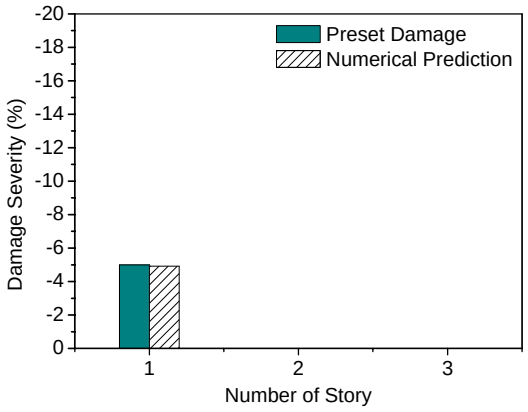

(a) Scenario 2

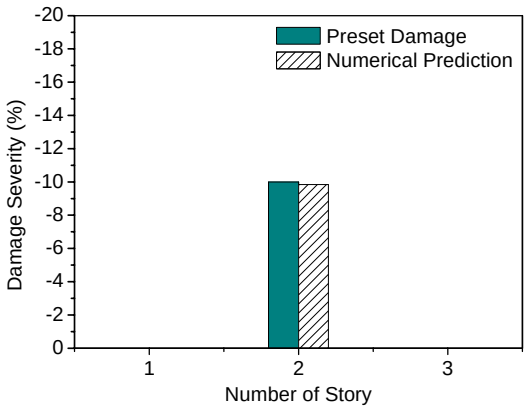

(b) Scenario 7

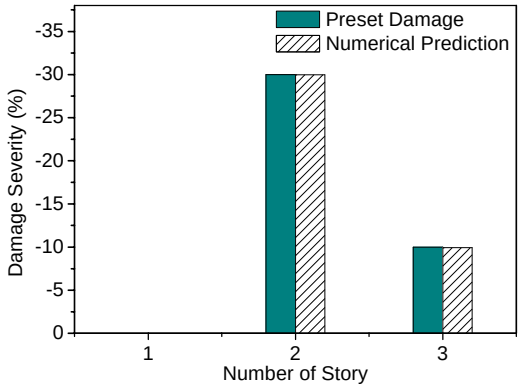

(c) Scenario 14

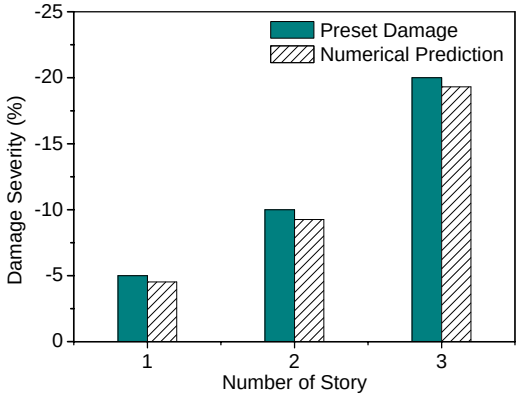

(d) Scenario 16

Figure 3.5 Identified results with noise free: (a) Scenario 2, (b) Scenario 7, (c) Scenario 14, (d) Scenario 16

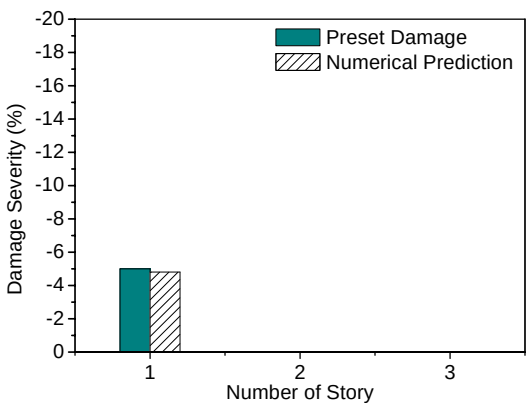

(a) Scenario 2

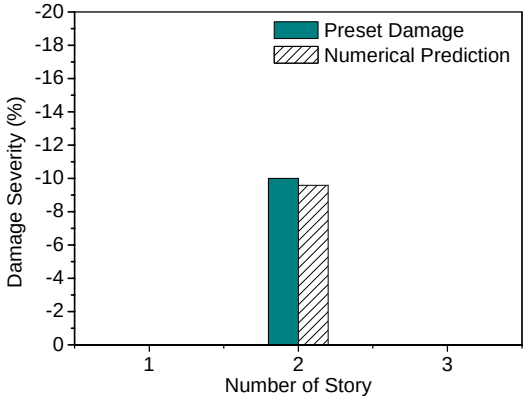

(b) Scenario 7

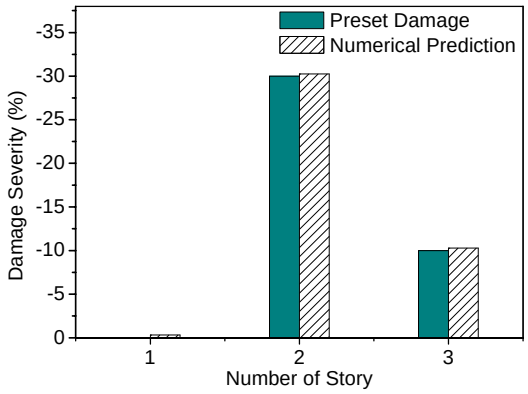

(a) Scenario 14

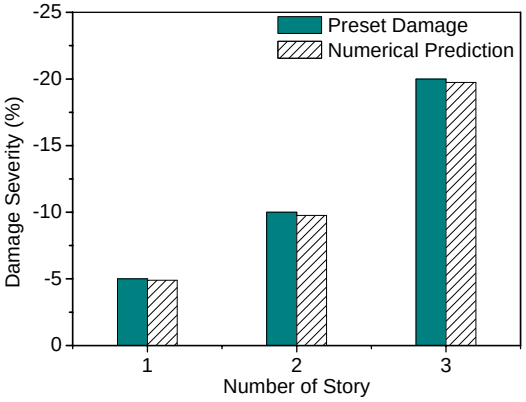

(b) Scenario 16

Figure 3.6 Identified results with the measurement noise intensity of 15%: (a) Scenario 2, (b) Scenario 7, (c) Scenario 14, (d) Scenario 16

CHAPTER 4

GENERALIZATION OF SMBDD METHOD IN FREQUENCY DOMAIN

4.1 Introduction

The basic equations of the statistical moment-based damage detection (SMBDD) method have been derived based on shear building structures by making use of Gaussian white noise ground excitation in Chapter 3. The feasibility and effectiveness of the proposed method have also been numerically demonstrated through various damage scenarios with different damage locations and damage severities of a three-story shear building. The major advantage of the proposed method is that it is not only sensitive to structural damage but also insensitive to measurement noise. However, the white noise ground excitation is an idealized excitation which is hard to obtain in practical application. The application of the proposed method by utilizing other more realistic excitations is worthwhile to investigate. In addition, most building structures are more complicated than shear buildings and generally analyzed by finite element (FE) methods. Therefore, further study is necessary to extend the proposed method from shear building structures to more general structures based on FE models.

Furthermore, shared with all developed approaches for damage detection and model correlation, incomplete measurement is a problem. For large structures, it is usually not feasible to measure the responses of a structure at all DOFs of the FE model, and

to collect the data from all natural modes that the FE model possesses because of a limited number of sensors being placed at accessible locations on the real structure. The current approach of addressing the problem practically is either to reduce the FE model to the measured degrees of freedom or to expand the measured modal data to all degrees of freedom included in the FE model. Unfortunately, both of these approaches cause troubles when performing damage detection. An observed problem with model reduction is that localized changes in the full model may become "smeared" throughout the reduced model. The problem observed with mode shape expansion is that errors introduced in the expansion process lead to false positive indications of damage. However, neither mode shape expansion nor model reduction is theoretically required by the SMBDD method because the objective function of model updating is based on errors between the components of statistical moments of the measured responses and the associated analytical statistical moments only. Therefore, it is also worthwhile to investigate the feasibility of the proposed method for practical application with only incomplete measurement responses.

In this regard, the equations of the proposed method are generalized for not only more kinds of excitations acting at various locations but also more types of structures based on the FE models with considering of the incomplete measurement problem in this chapter. Numerical investigation is first conducted to demonstrate the feasibility of the generalized method by using colored noise excitations acting at different locations of a shear building structure without considering the incomplete measurement problem. Then, various damage scenarios of high-rise buildings and frame structures with only partially measured DOFs are respectively investigated by the generalized method in the frequency domain. The effects of measurement noise

on the quality of identified results are also investigated for all the concerned damage cases by contaminating the fully or partially measured responses and external excitations with Gaussian white noise.

4.2 The Generalized SMBDD Method

The basic principle of the generalized SMBDD method is to first identify the stiffness parameters of a building before and after the occurrence of damage through FE model updating based on the statistical moments of fully or, most probably, partially measured building responses and then determine damage locations and damage severities by comparing the structural stiffness parameters identified at the two stages. A planar FE model of a building structure with N DOFs and N_e elements plotted in Figure 4.1 is utilized here to illustrate the generalized SMBDD method. There are three DOFs at every node: the horizontal displacement x, the vertical displacement y and the angular displacement θ. From the viewpoint of engineering, the time history of angular displacement is hard to measure. Therefore, only the horizontal displacement or the vertical displacement responses or both are assumed to be available and utilized to detect frame structures' damage by the generalized SMBDD method as long as the total number of measured displacement responses, denoted as N_m, is larger than or at least equal to the number of unknown stiffness parameters, N_e. The equation of motion in the matrix form for the structure can be expressed as

$$\mathbf{M}\ddot{\mathbf{x}}(t) + \mathbf{C}\dot{\mathbf{x}}(t) + \mathbf{K}\mathbf{x}(t) = \mathbf{f}(t) \tag{4.1}$$

where $\mathbf{M}$, $\mathbf{C}$ and $\mathbf{K}$ are the global mass matrix, damping matrix and stiffness matrix of the structure, respectively. $\ddot{\mathbf{x}}(t)$, $\dot{\mathbf{x}}(t)$ and $\mathbf{x}(t)$ are the acceleration,

velocity and displacement response vectors, respectively. Only part of displacement responses are measured, that is, $\mathbf{x}(t) = [\mathbf{x}_m(t)\ \mathbf{x}_u(t)]^T$, where subscript 'm' and 'u' denote respectively measured and unmeasured quantities. $\mathbf{x}_m(t) = [x_{m1}(t), x_{m2}(t), \cdots, x_{mN_m}(t)]^{\mathrm{T}}$, $\mathbf{x}_u = [x_{u1}(t), x_{u2}(t), \cdots, x_{u(N-N_m)}(t)]^{\mathrm{T}}$, where ($N$-$N_m$) is the number of unmeasured displacement responses. $\mathbf{f}(t)$ is the external excitation, $\boldsymbol{f}(t) = [\boldsymbol{f}_1(t), \boldsymbol{f}_2(t), \cdots, \boldsymbol{f}_N(t)]^{\mathrm{T}}$. The Fourier transform of $f_k(t)$ is denoted as $C_k(\omega)$.

By adopting the Rayleigh damping assumption, Equation (4.1) can be decoupled through the following transformation:

$$\mathbf{x} = \mathbf{\Phi z} \tag{4.2}$$

where $\mathbf{\Phi}$ is the mass-normalized modal matrix of the system. The uncoupled equations of motion of the system can then be expressed as

$$\ddot{\mathrm{z}}_{\mathrm{i}}(\mathrm{t}) + 2\xi_{\mathrm{i}}\omega_{\mathrm{i}}(\mathbf{K})\dot{\mathrm{z}}_{\mathrm{i}}(\mathrm{t}) + \omega_{\mathrm{i}}(\mathbf{K})^2\mathrm{z}_{\mathrm{i}}(\mathrm{t}) = \mathrm{p}_{\mathrm{i}}(\mathrm{t}) \quad i=1, 2, 3,\ldots, N \tag{4.3}$$

where $p_i(t) = \sum_{j=1}^{N} \phi_{ji}(\mathbf{K})\, f_j(t)$; $\phi_{ji}(\mathbf{K})$ is the jth component of the ith theoretical mode shape and $\omega_i(\mathbf{K})$ is the ith theoretical circular natural frequency; ξ_i is the ith modal damping ratio. In most cases, the first two modal damping ratios are estimated from the measured acceleration responses, while the higher modal damping ratios are derived according to the Rayleigh damping assumption.

Denote the Fourier transform of the displacement response corresponding to measured DOFs $\mathbf{x}_m$ as $\mathbf{X}_m(\omega)$, $\mathbf{X}_m(\omega) = [X_{m1}(\omega), X_{m2}(\omega), \cdots, X_{mN_m}(\omega)]^{\mathrm{T}}$. By using the mode superposition method, the Fourier transform of the displacement response

x_{mi} can be obtained

$$X_{mi}(\omega) = \sum_{k=1}^{N} C_k(\omega)\alpha_{ik}(\omega),\ i = 1, 2, \cdots, N_m \tag{4.4}$$

$$\alpha_{ik}(\omega) = \sum_{j=1}^{N} \frac{\phi_{ij}(\mathbf{K}) \cdot \phi_{kj}(\mathbf{K})}{\omega_j(\mathbf{K})^2 - \omega^2 + 2i\omega\omega_j(\mathbf{K})\xi_j} \tag{4.5}$$

The conjugate of $X_{mi}(\omega)$, denoted as $X^*_{mi}(\omega)$, is calculated by

$$X^*_{mi}(\omega) = \sum_{k=1}^{N} C^*_k(\omega)\alpha^*_{ik}(\omega) \tag{4.6}$$

where $C_k^*(\omega)$ and $\alpha^*_{mk}(\omega)$ are respectively the conjugates of $C_k(\omega)$ and $\alpha_{mk}(\omega)$.

It should be noted that not only the statistical moments of the measured absolute displacement responses, $\mathbf{x}_m = [x_{m1}, x_{m2}, \cdots, x_{mN_m}]^{\mathrm{T}}$, but also the relative displacement responses, denoted as $\mathbf{y}_m = [y_{m1}, y_{m2}, \cdots, y_{mN_m}]^{\mathrm{T}}$, can be utilized to identify structural stiffness by the generalized SMBDD method. The relative displacement responses can be calculated from the measured absolute displacement responses. For example, if the *k*th relative displacement responses y_{mk} is the *i*th absolute displacement response x_{mi} relative to the *j*th absolute displacement response x_{mj}, y_{mk} can be calculated as follow.

$$y_{mk} = x_{mi} - x_{mj} = \mathbf{P}\mathbf{x}_m \tag{4.7}$$

where $\mathbf{P} = [0, \cdots, 0, \underset{i}{1}, 0, \cdots, 0, \underset{j}{-1}, 0, \cdots, \underset{N_m}{0}]$. When the *j*th element of **P,** denoted as P_j, equals to 0**,** y_{mk} represents the *i*th absolute displacement response. In addition, the Fourier transform of y_{mk} can be obtained by

$$Y_{mk}(\omega) = \mathbf{P}\mathbf{X}_m(\omega) \quad k=1,2,3,\ldots, N_m \tag{4.8}$$

Therefore, the power spectral density (PSD) function of the *k*th relative displacement

($P_j = -1$) or the *k*th absolute displacement ($P_j = 0$) y_{mk} can be uniformly expressed as

$$S_{y_{mk}}(\omega) = \left[\mathbf{P}\mathbf{X}_m(\omega)\right]\left[\mathbf{P}\mathbf{X}^*_m(\omega)\right] \tag{4.9}$$

where $\mathbf{X}^*_m(\omega)$ is the conjugate of $\mathbf{X}_m(\omega)$, $\mathbf{X}^*_m(\omega) = [X^*_{m1}(\omega), X^*_{m2}(\omega), \cdots, X^*_{mN_m}(\omega)]^{\mathrm{T}}$. The variance of y_{mk} can be calculated by

$$\sigma_{y_{mk}}{}^2 = \int_{-\infty}^{\infty} S_{y_{mk}}(\omega) d\omega \tag{4.10}$$

The external excitations are taken as stationary Gaussian random processes in this study. Therefore, the structural responses are also stationary Gaussian random processes in terms of a linear structural system. Its statistical moments can be computed by

$$M_{2k} = \sigma_{y_{mk}}{}^2, \quad M_{4k} = 3\sigma_{y_{mk}}{}^4, \quad M_{6k} = 15\sigma_{y_{mk}}{}^6, \; k=1,2,3,\ldots, N_m \tag{4.11}$$

The theoretical second-order, fourth-order, and sixth-order statistical moment vectors can be expressed as

$$\mathbf{M}_i = [M_{i1}, M_{i2}, \cdots, M_{iN_m}], \; i=2, 4, 6 \tag{4.12}$$

Based on the above derivation, it can be seen that if the mass matrix and the damping ratios of the building structure are kept invariant, the statistical moments of displacement responses are the function of lateral stiffness of the building. Therefore, the *i*th-order statistical moment vector of the associated responses, denoted as $\mathbf{M}_i$ (*i*=2,4,6), can be theoretically calculated for a given stiffness vector $\mathbf{k} = [k_1, k_2, ..., k_{Ne}]$ in the frequency domain. On the other hand, the actual *i*th-order statistical moment vector can be directly estimated from the measured displacement responses as follows, denoted as $\hat{\mathbf{M}}_i = [\hat{M}_{i1}, \hat{M}_{i2}, \cdots, \hat{M}_{iN_r}]$ (*i*=2,4,6).

Denote the *k*th actually measured displacement response corresponding to y_{mk} as $\hat{y}_{mk}$, $\hat{y}_{mk} = [\hat{y}_{mk1,}\hat{y}_{mk2,}\cdots,\hat{y}_{mkNs}]$, where N_s is the number of sampling points, the statistical moments of $\hat{y}_{mk}$ can be calculated as follows.

$$\hat{M}_{2k} = \frac{1}{N_s}\sum_{i=1}^{N_s}\hat{y}_{mki}{}^2 - (\frac{1}{N_s}\sum_{i=1}^{N_s}\hat{y}_{mki})^2 \tag{4.13}$$

$$\hat{M}_{4k} = 3(\hat{M}_{2k})^2 \tag{4.14}$$

$$\hat{M}_{6k} = 15(\hat{M}_{2k})^3 \tag{4.15}$$

Therefore, the residual vector between the theoretical statistical moment vector, $\mathbf{M}_i$, for a given stiffness vector and the actual statistical moment vector, $\hat{\mathbf{M}}_i$ estimated from the measured building responses can be calculated and written as

$$\mathbf{F}(\mathbf{k}) = \mathbf{M}_i(\mathbf{k}) - \hat{\mathbf{M}}_i \tag{4.16}$$

Once the objective function has been established, the system identification of the undamaged or damaged building structure can be interpreted as a nonlinear least-squares problem, that is, giving $\mathbf{k}$ an initial value $\mathbf{k}_0$ and minimizing $\|\mathbf{F}(\mathbf{k})\|^2$ through optimization algorithms. Detailed information about the optimization algorithms for undamaged and damaged building structures can be found in Chapter 3 and will not be reiterated here.

In brief, the generalized SMBDD method for a building structure can be implemented according to the following steps:

(1) Decide the number and locations of displacement responses of a building structure needed to measure before and after damage and record the measurement data of the building structure under external excitations;

(2) The actual statistical moments of the measured displacement responses, $\hat{\mathbf{M}}_i$, are estimated from the measured displacements for undamaged and damaged building respectively by using Equations (4.13) ~ (4.15);

(3) Give the stiffness parameter vector of the building structure an initial value, the theoretical statistical moments $\mathbf{M}_i$ corresponding to $\hat{\mathbf{M}}_i$ can be calculated by the above Equations (4.4) ~ (4.12) in the frequency domain;

(4) Substitute $\hat{\mathbf{M}}_i$ and $\mathbf{M}_i$ into Equation (4.16), the structural stiffness vector can be identified by the unconstrained and constrained nonlinear least-squares methods for the undamaged and damaged building, respectively;

(5) The structural damage including damage existence, location and severity can be detected by comparing the identified stiffness vector $\hat{\mathbf{k}}^u$ of the undamaged building with the identified stiffness vector $\hat{\mathbf{k}}^d$ of the damaged building.

The procedure of the generalized SMBDD method to detect structural damage is presented in Figure 4.2. The fourth-order moment other than the second-order or the sixth-order moment is used in the following investigation which makes a tradeoff between the sensitivity of an index to structural damage and its stability to random excitation as discussed in Chapter 3.

4.3 Different Types and Locations of External Excitation

4.3.1 Different types of external excitation

In this section numerical investigation is made to extend the SMBDD method from Gaussian white noise ground excitation to colored noise ground excitation. The

three-story shear building model used in Chapter 3 is employed here to demonstrate the feasibility and effectiveness of the proposed method by utilizing colored noise ground excitation. In the following numerical investigation, the power spectral density (PSD) of the colored noise excitation is the Kanai–Tajimi spectral density function which has the form of

$$S_g(\omega) = \frac{1+4\zeta_g^{\,2}(\frac{\omega}{\omega_g})^2}{[1-(\frac{\omega}{\omega_g})^2]^2+4\zeta_g^{\,2}(\frac{\omega}{\omega_g})^2} S_0 \tag{4.17}$$

where ω_g, ζ_g and S_0 may be regarded as the characteristics and the intensity of an external excitation. The parameters in Equation (4.17) are selected as ω_g =15.0 rad/s, ζ_g =0.6, and S_0 =4.65×10^{-4} m^2/rad s^3. The time duration of the simulated acceleration is 1000s and the sampling frequency is 256Hz. The PSD function of the simulated acceleration is estimated and compared with the preset Kanai–Tajimi spectral density function in Figure 4.3 (b). The probability density functions (PDFs) of simulated ground acceleration with Gaussian and nonparametric fitting are presented in Figure 4.3 (c). It can be seen that the PDF of simulated ground acceleration can be regarded as a Gaussian distribution. Displacement responses of the undamaged and damaged buildings are measured and then their story drifts are calculated.

The undamaged shear building is firstly identified by the SMBDD method. Listed in Table 4.1 are the values of the fourth-order moments of the story drifts of the undamaged building $\hat{M}_{4i}^{\,u}$ ($i=1,2,3$) calculated by Equation (4.14) and the identified stiffness values of the undamaged building $\hat{k}_i^{\,u}$ ($i=1,2,3$) using the least-squares method. It can be found that the identified horizontal stiffness coefficients of

the undamaged building $\hat{k}_i^u$ are very close to the real values k_i^u. Compared with the real values, the relative errors of the three identified horizontal stiffness values are only 0.36%, 0.32% and 0.30%, respectively, which lays down a good foundation for the coming damage detection. Furthermore, comparing the identified horizontal stiffness parameters using colored noise excitation with those using white noise excitation listed in Table 3.4, it can be seen that the type of external excitations has no much effect on the quality of the identified results. The maximum relative error between them is only 0.57%. It indicates that different types of external excitations can be utilized to identify structural stiffness parameters before and after damage and then to detect structural damage.

Table 4.1 Analysis results of the undamaged shear building by utilizing colored noise ground excitation

Story	$\hat{M}_{4i}^{u}$ (m^4)	$\hat{k}_i^u$ (kN/m)	k_i^u (kN/m)
1	2.3546×10^{-14}	4745423.61	4728400.00
2	9.0875×10^{-10}	316236.44	315230.00
3	1.6514×10^{-9}	158080.95	157610.00

Then ten damage scenarios with different damage locations and damage severities are examined to demonstrate the robustness of the proposed method by employing the colored noise ground excitation. The details of these damage scenarios are presented in Table 4.2, in which Scenarios 1 ~7 have been investigated by the proposed method utilizing white noise ground excitation in Chapter 3. And two more scenarios with very small damage severity of 2%, Scenario 8 and 9, are also examined to check the sensitivity of the proposed method to structural damage by using the colored noise ground excitation. Very adverse circumstances for damage detection are considered in the multi-damage scenarios. For example, in Scenario 10,

a small damage of 5% at Story 2 is set to be in the middle of two large damages of 20% and 30% at Story 1 and Story 3, respectively.

Table 4.2 Details of damage scenarios 1-10 of a three-story shear building

Scenario	Story 1	Story 2	Story 3
1	$0.98k_1^u$	k_2^u	k_3^u
2	k_1^u	$0.95k_2^u$	k_3^u
3	k_1^u	k_2^u	$0.90k_3^u$
4	$0.90k_1^u$	$0.95k_2^u$	k_3^u
5	$0.90k_1^u$	k_2^u	$0.70k_3^u$
6	k_1^u	$0.95k_2^u$	$0.90k_3^u$
7	$0.95k_1^u$	$0.90k_2^u$	$0.80k_3^u$
8	k_1^u	$0.98k_2^u$	k_3^u
9	k_1^u	$0.90k_2^u$	$0.98k_3^u$
10	$0.80k_1^u$	$0.95k_2^u$	$0.70k_3^u$

For each damage scenario, the fourth-order moments of story drifts are computed from the measured displacement responses of the damaged building and then utilized to identify the horizontal stiffness values of the damaged building. With reference to the identified horizontal stiffness values of the undamaged building (see Table 4.1), the damage locations and their corresponding damage severities are determined. The identified results are presented in Figure 4.4 and also listed in Table 4.3. As seen from Figure 4.4, the damage locations can be accurately identified out for both single damage and multi-damage scenarios by using the colored noise excitations. In comparison with the actual damage severities shown in Table 4.3, it can be seen that the identified damage severities are quite close to the actual damage severities. Even for the small damage of 2% in Scenarios 1, 8 and 9 with single or multi damage, the identified damage severities are respectively 1.95% at Story 1 for Scenario 1, 1.49% at Story 2 for Scenario 8 and 1.65% at Story 3 for Scenario 9. The effectiveness and

sensitivity of the proposed method to structural damage are demonstrated through these damage scenarios by using colored noise excitations.

Table 4.3 Identified damage severities by colored noise ground excitation

Scenario	Story 1		Story 2		Story 3	
	μ (%)	$\hat{\mu}$ (%)	μ (%)	$\hat{\mu}$ (%)	μ (%)	$\hat{\mu}$ (%)
1	-2.00	-1.95	0.00	0.00	0.00	0.00
2	0.00	0.00	-5.00	-4.60	0.00	0.00
3	0.00	0.00	0.00	0.00	-10.00	-9.82
4	-10.00	-9.74	-5.00	-4.71	0.00	0.00
5	-10.00	-10.23	0.00	-0.17	-30.00	-30.08
6	0.00	0.00	-5.00	-4.56	-10.00	-9.66
7	-5.00	-4.88	-10.00	-9.79	-20.00	-19.77
8	0.00	0.00	-2.00	-1.49	0.00	0.00
9	0.00	0.00	-10.00	-9.61	-2.00	-1.65
10	-20.00	-20.82	-5.00	-5.95	-30.00	-30.67

The influence of measurement noise on the quality of damage detection results is considered by contaminating measured displacement responses and external excitations with white Gaussian random noises in the following numerical investigation. The superimposed random noises are independent to and different with each other. The measurement noise intensity (MNI) is adopted as 15%. The calculated fourth-order moments and the identified horizontal stiffness coefficients of the undamaged building with the effects of measurement noise are listed in Table 4.4. The relative errors between the identified horizontal stiffness values and the actual ones are respectively only 0.37%, 0.43% and 0.43% for the three stories. The measurement noise has no much effect on the quality of identified results. The identified results of the ten aforementioned damage scenarios with the MNI of 15% are presented in Figure 4.4 and Table 4.5.

Table 4.4 Identified results of the undamaged building (MNI of 15%)

Story	$\hat{M}_{4i}^{u}$ (m^4)	$\hat{k}_i^{u}$ (kN/m)	k_i^{u} (kN/m)
1	2.3546×10^{-14}	4710815.11	4728400.00
2	9.0875×10^{-10}	313889.28	315230.00
3	1.6514×10^{-9}	156935.12	157610.00

Table 4.5 Identified results by colored noise ground excitation (MNI of 15%)

Scenario	Story 1		Story 2		Story 3	
	μ (%)	$\hat{\mu}$ (%)	μ (%)	$\hat{\mu}$ (%)	μ (%)	$\hat{\mu}$ (%)
1	-2.00	-1.88	0.00	0.00	0.00	0.00
2	0.00	0.00	-5.00	-4.88	0.00	0.00
3	0.00	0.00	0.00	0.00	-10.00	-9.92
4	-10.00	-10.23	-5.00	-5.21	0.00	-0.19
5	-10.00	-10.71	0.00	-0.70	-30.00	-30.45
6	0.00	0.00	-5.00	-4.81	-10.00	-9.84
7	-5.00	-5.29	-10.00	-10.19	-20.00	-20.14
8	0.00	0.00	-2.00	-1.63	0.00	0.00
9	0.00	0.00	-10.00	-9.70	-2.00	-1.73
10	-20.00	-20.89	-5.00	-6.00	-30.00	-30.70

As seen from Figure 4.4, there are no much difference among the identified results without measurement noise, those with measurement noise and the real values even when the MNI is as high as 15%. Accurate damage locations and reliable damage severities are obtained at such a high measurement noise level. The insensitiveness of the SMBDD method to measurement noise is demonstrated again by employing colored noise ground excitations.

4.3.2 Different locations of external excitation

In terms of practical application, it is sometimes more convenient to excite a structure at its floor by using an exciter. Therefore, it is necessary to investigate the feasibility and effectiveness of the proposed SMBDD method by utilizing non-ground excitations. The colored noise excitations aforementioned are employed and imposed at the first floor of the three-story shear building in the following numerical analysis.

Firstly, the undamaged shear building is identified by the proposed method. The fourth-order moments of the story drifts of the undamaged building, $\hat{M}_{4i}^{u}$ ($i = 1,2,3$), calculated by Equation (4.14) and the identified stiffness values of the undamaged building, $\hat{k}_i^u$ ($i = 1,2,3$) are presented in Table 4.6. It can be seen that the identified horizontal stiffness coefficients of the undamaged building $\hat{k}_i^u$ are very close to the real values k_i^u. The relative errors of the identified horizontal stiffness values to the real values are only 0.63%, 0.30% and 0.44%, respectively.

Table 4.6 Identified results of the undamaged building by colored noise excitation at the first floor

Story	$\hat{M}_{4i}^{u}$ (m^4)	$\hat{k}_i^u$ (kN/m)	k_i^u (kN/m)
1	2.3094×10^{-17}	4758184.60	4728400.00
2	1.6873×10^{-15}	314270.49	315230.00
3	3.5300×10^{-15}	156921.92	157610.00

Then the ten damage scenarios presented in Table 4.2 are examined to demonstrate the applicability of the proposed method for damage detection by using the non-ground colored noise excitation. The horizontal stiffness values of the damaged

building are identified. With reference to the identified horizontal stiffness values of the undamaged building (see Table 4.6), the damage locations and damage severities are determined for every damage scenario. The identified results are presented in Figure 4.5 and also listed in Table 4.7. The damage locations are accurately identified for both single damage and multi-damage scenarios according to Figure 4.5. In comparison with the actual damage severities shown in Table 4.7, the identified damage severities by the colored noise excitation acting at the first floor are quite close to the actual damage severities. Even for very small damage cases, satisfactory identified results are obtained. For example, the identified results for the small damage of 2% in Scenarios 1, 8 and 9 are respectively 1.99% at Story 1 for Scenario 1, 2.01% at Story 2 for Scenario 8 and 1.24% at Story 3 for Scenario 9. The effectiveness and sensitivity of the proposed method to structural damage are demonstrated again by using the non-ground colored noise excitation.

Table 4.7 Identified damage severities by colored noise excitation at the first floor

Scenario	Story 1		Story 2		Story 3	
	μ (%)	$\hat{\mu}$ (%)	μ (%)	$\hat{\mu}$ (%)	μ (%)	$\hat{\mu}$ (%)
1	-2.00	-1.99	0.00	0.00	0.00	0.00
2	0.00	0.00	-5.00	-5.02	0.00	0.00
3	0.00	-0.02	0.00	0.00	-10.00	-9.99
4	-10.00	-10.00	-5.00	-5.01	0.00	0.00
5	-10.00	-10.41	0.00	0.00	-30.00	-29.76
6	0.00	0.00	-5.00	-4.17	-10.00	-9.24
7	-5.00	-5.09	-10.00	-9.47	-20.00	-19.48
8	0.00	0.00	-2.00	-2.01	0.00	0.00
9	0.00	0.00	-10.00	-9.26	-2.00	-1.24
10	-20.00	-20.92	-5.00	-5.25	-30.00	-30.01

The influence of measurement noise on the damage detection results is also numerically investigated. Random white noises are utilized to contaminate the measured displacement responses of the building and the external excitation. The MNI of 15% is adopted here. The calculated fourth-order moments and the identified horizontal stiffness coefficients of the undamaged building with the effects of measurement noise are listed in Table 4.8. The relative errors between the identified horizontal stiffness values and the actual ones are respectively 0.56%, 1.44% and 1.87% for the three stories. The measurement noise has no much effect on the identified horizontal stiffness values. The identified damage severities are presented in Figure 4.5 and Table 4.9 for all damage scenarios with MNI of 15%.

Table 4.8 Identified results of the undamaged building with MNI of 15%

Story	$\hat{M}_{4i}^{u}\ (m^4)$	$\hat{k}_i^{u}\ (kN/m)$	$k_i^{u}\ (kN/m)$
1	2.4150×10^{-17}	4754794.57	4728400.00
2	1.7251×10^{-15}	310687.53	315230.00
3	3.6432×10^{-15}	154662.48	157610.00

As seen from Figure 4.5, the identified results without measurement noise and those with measurement noise are very close to the actual ones. Even when the MNI is as high as 15%, satisfactory results are also obtained for both damage locations and damage severities by the proposed method utilizing colored noise excitation at the first floor. The stability and insensitivity of the proposed method to measurement noise are demonstrated through the shear building structure utilizing the colored noise excitation acting on upper structures. In addition, comparing the horizontal stiffness values of the undamaged shear building identified by colored noise excitations at the first floor with consideration of MNI of 15% (see Table 4.8) with those identified by white noise ground excitations with consideration of MNI of 15%

(see Table 3.9), the maximum relative error among them is only 0.98%. Therefore, different types and different locations of external excitations can be utilized to vibrate building structures before and after damage by the proposed damage detection method.

Table 4.9 Identified results of damage scenarios by colored noise excitation at the first floor with MNI of 15%

Scenario	Story 1		Story 2		Story 3	
	μ (%)	$\hat{\mu}$ (%)	μ (%)	$\hat{\mu}$ (%)	μ (%)	$\hat{\mu}$ (%)
1	-2.00	-2.14	0.00	-0.02	0.00	0.00
2	0.00	-0.07	-5.00	-5.97	0.00	-0.96
3	0.00	-0.15	0.00	-0.88	-10.00	-10.76
4	-10.00	-10.05	-5.00	-5.04	0.00	0.00
5	-10.00	-10.33	0.00	-1.53	-30.00	-31.11
6	0.00	-0.02	-5.00	-4.14	-10.00	-9.17
7	-5.00	-5.34	-10.00	-11.76	-20.00	-21.44
8	0.00	0.00	-2.00	-2.05	0.00	0.00
9	0.00	-0.01	-10.00	-9.84	-2.00	-1.82
10	-20.00	-21.52	-5.00	-4.96	-30.00	-29.34

4.4 Damage Detection on High-rise Buildings with Incomplete Measurement

4.4.1 Numerical model

In this section, the generalized SMBDD method is applied to a high-rise building. The analysis model of a MDOF flexible building structure is presented in Figure 4.6. Two degrees of freedom are considered for every node in the FE model: the horizontal displacement x and the angular displacement θ. But only the horizontal displacement responses are measured and utilized to detect structural damage in the

following investigation. The *i*th element stiffness matrix of the flexible model can be expressed as

$$\mathbf{K}_e^{\,i} = \begin{bmatrix} \frac{12(EI)_i}{h_i^3} & \frac{6(EI)_i}{h_i^2} & -\frac{12(EI)_i}{h_i^3} & \frac{6(EI)_i}{h_i^2} \\ \frac{6(EI)_i}{h_i^2} & \frac{4(EI)_i}{h_i} & -\frac{6(EI)_i}{h_i^2} & \frac{2(EI)_i}{h_i} \\ -\frac{12(EI)_i}{h_i^3} & -\frac{6(EI)_i}{h_i^2} & \frac{12(EI)_i}{h_i^3} & -\frac{6(EI)_i}{h_i^2} \\ \frac{6(EI)_i}{h_i^2} & \frac{2(EI)_i}{h_i} & -\frac{6(EI)_i}{h_i^2} & \frac{4(EI)_i}{h_i} \end{bmatrix} \tag{4.18}$$

where $(EI)_i$ is the product of the modulus of elasticity and the moment of inertia of the *i*th element. h_i is the length of the *i*th element. For the special case of the element with uniformly distributed mass, the mass matrix of the *i*th element is:

$$\mathbf{M}_e^{\,i} = \frac{\bar{m}L}{420}\begin{bmatrix} 156 & 22L & 54 & -13L \\ 22L & 4L^2 & 13L & -3L^2 \\ 54 & 13L & 156 & -22\mathrm{L} \\ -13L & -3L^2 & -22\mathrm{L} & 4L^2 \end{bmatrix} \tag{4.19}$$

where $\bar{m}$ is the mass density (mass per unit height) of the flexible building. Then the stiffness matrix and the mass matrix for the entire system can be obtained by respectively assembling the stiffness matrix and mass matrix of each beam element of the structure. The global mass matrix and stiffness matrix are then substituted into Equation (4.1). In the following numerical investigation, the explored flexible building is a 20-story high-rise building with height $h_T = 80\,\mathrm{m}$. The mass density is 4×10^5kg/m. The stiffness parameter for the flexible building is $(EI)_T = 8.18\times10^{10}$ kN.m^2, where E is Young's Modulus and I is the moment of inertia of the building. The high-rise building is discretized into five elements with the length of 16m. The ground acceleration is modeled as a colored noise with the Kanai-Tajimi spectrum

having parameters ω_g =15.6 rad/s and ζ_g =0.6. The magnitude is chosen such that the maximum ground acceleration is 2.0 m/sec^2.

4.4.2 Damage detection on high-rise buildings with incomplete measurement and without measurement noise

In the following numerical investigation, the five story drifts of the high-rise building are calculated from the measured horizontal displacement responses and utilized to detect structural damage. Firstly, structural identification is carried out on the undamaged building without considering the effect of measurement noise on detected results. The fourth-order moments of the story drifts, $\hat{M}_{4i}^{u}$ ($i = 1,2,3$), are calculated by Equation (4.13) and then used to identify the stiffness parameters of the undamaged building, $(\hat{EI})_i^u$ ($i = 1,2,3$). The fourth-order moments and the identified stiffness parameters of all elements are presented in Table 4.10. The maximum relative errors of the identified stiffness parameters is only 0.14% for Element 5, while the other four relative errors are 0.02%, 0.01%, 0.04% and 0.06%, respectively. It can be seen that the identified horizontal stiffness coefficients of the undamaged building $(\hat{EI})_i^u$ are almost the same as the theoretical values $(EI)_i^{u}$.

Then six damage scenarios are designed and examined to demonstrate the robustness of the proposed method for high-rise buildings with incomplete measurement. The details of the six damage scenarios are presented in Table 4.11. Scenarios 1 and 2 are single damage cases, while there are two or three damage elements in Scenario 3, 4 and 5 and all elements are damaged in Scenario 6. For each damage scenario, the fourth-order moments of the story drifts are computed according to Equation (4.13).

The horizontal stiffness parameters of the damaged building for every damage scenarios are identified by the constrained least-squares method. With reference to the identified horizontal stiffness values of the undamaged building (see Table 4.10), the damage locations and damage severities are identified for every damage scenario. The identified results without considering the effect of measurement noise are presented in Figure 4.7 and Table 4.12.

According to Figure 4.7, the damage locations can be apparently and accurately identified out for both the single damage and the multi-damage scenarios. Even for the very small damage of 2%, the damage locations can also be accurately detected, say, Element 3 in Scenario 2, Element 4 in Scenario 3 and Element 5 in Scenario 6. In comparison with the actual damage severities shown in Table 4.12, the identified damage severities are quite close to the actual values for these damage scenarios. The feasibility and effectiveness of the proposed method are demonstrated again through the high-rise building structure even when only the horizontal displacement responses are measured.

Table 4.10 Identified results of the undamaged building by colored noise ground excitation

Element	$\hat{M}_{4\mathrm{i}}^{\mathrm{u}}\ (m^4)$	$(EI)_i^{\mathrm{u}}\ (\times 10^5 kN/m)$	$(\hat{EI})_i^{\mathrm{u}}\ (\times 10^5 kN/m)$
1	1.0319757×10^{-10}	818000.00	817836.65
2	4.6951913×10^{-9}	818000.00	817907.89
3	1.7689435×10^{-8}	818000.00	817698.12
4	3.0304883×10^{-8}	818000.00	817468.40
5	3.5325220×10^{-8}	818000.00	816855.31

Table 4.11 Details of damage scenarios of a high-rise building

Scenario No.	Damage severity	Damage location
1	5%	1st element
2	2%	3rd element
3	10%	1st element
	2%	4th element
4	5%	2nd element
	10%	5th element
5	20%	1st element
	10%	3rd element
	5%	5th element
6	10%	1st element
	5%	2nd element
	5%	3rd element
	5%	4th element
	2%	5th element

Table 4.12 Identified damage severities of a high-rise building with noise free

Scenario No.	Element 1	Element 2	Element 3	Element 4	Element 5
1	-5.13	-0.14	-0.14	-0.14	-0.14
2	-0.03	-0.03	-2.03	-0.03	-0.03
3	-10.30	-0.34	-0.34	-2.34	-0.33
4	-0.13	-5.13	-0.13	-0.13	-10.11
5	-19.03	0.00	-8.94	0.00	-3.92
6	-10.38	-5.41	-5.41	-5.43	-2.41

4.4.3 Damage detection on high-rise buildings with measurement noise

The influence of measurement noise on the quality of the damage detection results is numerically investigated through the high-rise building structure. Random white noises are added to both the measured horizontal displacement responses of the building and the external acceleration excitation. The MNI of 15% is adopted here.

Similar procedure is adopted to detect structural damage as that without considering measurement noise. The identified stiffness parameters of the undamaged building with the effects of measurement noise are listed in Table 4.13. The maximum relative error between the identified stiffness parameters and the actual ones are only 1.44% for the five elements even when the MNI is 15%, which demonstrate the reliability of the generalized SMBDD method under measurement noise and incomplete measurement.

Table 4.13 Identified results of the undamaged high-rise building with MNI of 15%

Element	$\hat{M}_{4i}^{\ u}\ (m^4)$	$(\hat{EI})_i^{\ u}\ (\times 10^5 kN/m)$	$(EI)_i^{\ u}\ (\times 10^5 kN/m)$
1	1.5065×10^{-10}	806943.46	818000.00
2	6.8538×10^{-9}	806978.22	818000.00
3	2.5822×10^{-8}	806924.45	818000.00
4	4.4237×10^{-8}	806827.05	818000.00
5	5.1566×10^{-8}	806226.68	818000.00

Then the six damage scenarios presented in Table 4.11 are explored to evaluate the effect of measurement noise on the quality of identified results. For each damage scenario, the measured horizontal displacement responses and the external excitation are contaminated by independent white Gaussian random noises. The noise intensity is adopted as 15%. The horizontal stiffness parameters of the damaged building for every damage scenarios are identified by utilizing the fourth-order moments of the contaminated responses and the contaminated external excitation. With reference to the identified horizontal stiffness values of the undamaged building (see Table 4.13), the damage severity of each element is finally calculated for every damage scenario. The identified results are presented in Figure 4.8 and Table 4.14.

As seen from Figure 4.8, there is no much difference between the identified results without measurement noise and those with measurement noise which are at the same time very close to the actual ones. Even when the MNI is as high as 15%, satisfactory results are also obtained for both damage locations and damage severities by the proposed method. In other words, the proposed method is insensitive to measurement noise. The reliability and robustness of the proposed method are demonstrated through the high-rise building structure with considering the effect of measurement noise.

Table 4.14 Identified damage severities of a high-rise building with MNI of 15%

Scenario No.	Element 1	Element 2	Element 3	Element 4	Element 5
1	-5.84	-0.90	-0.88	-0.87	-0.83
2	-0.15	-0.16	-2.16	-0.17	-0.17
3	-10.73	-0.83	-0.82	-2.81	-0.78
4	-0.03	-5.04	-0.05	-0.06	-10.04
5	-19.03	0.00	-8.94	0.00	-3.96
6	-11.05	-6.13	-6.11	-6.12	-3.11

4.5 Damage Detection on Frame Structures with Incomplete Measurement

4.5.1 Numerical model

The feasibility and robustness of the SMBDD method being applied to frame structures are investigated in this section. A 2-D moment resisting one-story and one-bay steel frame (see Figure 4.9) is employed to illustrate the application of the proposed method. The frame consists of two columns (W14×257 and W14×311) and one beam (W33×118). The columns are made of 345 MPA (50ksi) steel and the beam is made of 248 MPA (36ksi) steel. The bay width L is 9.15m (30ft) and the

height h is 3.96m (13 ft). The mass density of the left column (W14×257) is 382.46 Kg/m, while that of the right column (W14×311) is 462.82 Kg/m and that of the beam is 17235.7 Kg/m. The Rayleigh damping is assumed and the first two damping ratios are adopted as 2%. The external excitations are simulated as zero-mean colored noise acceleration represented by the Kanai-Tajimi spectrum having parameters ω_g =15.6 rad/s and ζ_g =0.6 . The locations of the external excitations are presented in Figure 4.9. The magnitude is chosen such that the maximum acceleration is 2.0 m/sec^2. The duration of the external excitation time history is 1000s with a sampling frequency of 256 Hz. The FE model of the frame structure is presented in Figure 4.9. Each column or beam is divided into two elements. These elements are numbered and marked in Figure 4.9. The bar element is adopted in the finite element model of the frame structure. The element stiffness matrix, $\mathbf{K}_e$, is given as

$$\mathbf{K}_e = \begin{bmatrix} \frac{EA}{l} & 0 & 0 & -\frac{EA}{l} & 0 & 0 \\ 0 & \frac{12EI}{l^3} & \frac{6EI}{l^2} & 0 & -\frac{12EI}{l^3} & \frac{6EI}{l^2} \\ 0 & \frac{6EI}{l^2} & \frac{4EI}{l} & 0 & \frac{6EI}{l^2} & \frac{2EI}{l} \\ -\frac{EA}{l} & 0 & 0 & \frac{EA}{l} & 0 & 0 \\ 0 & -\frac{12EI}{l^3} & -\frac{6EI}{l^2} & 0 & \frac{12EI}{l^3} & -\frac{6EI}{l^2} \\ 0 & \frac{6EI}{l^2} & \frac{2EI}{l} & 0 & -\frac{6EI}{l^2} & \frac{4EI}{l} \end{bmatrix} \tag{4.20}$$

where E, A and I are respectively the elastic modulus, the area and the inertia moment of the element. The mass matrix of the *i*th element with the uniformly distributed mass is:

$$\mathbf{M}_e = \frac{\bar{m}L}{420}\begin{bmatrix} 140 & 0 & 0 & 70 & 0 & 0 \\ 0 & 156 & 22L & 0 & 54 & -13L \\ 0 & 22L & 4L^2 & 0 & 13L & -3L^2 \\ 70 & 0 & 0 & 140 & 0 & 0 \\ 0 & 54 & 13L & 0 & 156 & -22\mathrm{L} \\ 0 & -13L & -3L^2 & 0 & -22\mathrm{L} & 4L^2 \end{bmatrix} \tag{4.21}$$

where $\bar{m}$ is the mass density (mass per unit height) of the *i*th element. Then the mass matrix and the stiffness matrix for the entire system can be obtained by assembling all the element mass matrices and the element stiffness matrices, respectively.

4.5.2 Damage detection on frame structures without measurement noise

In the following numerical investigation, only the horizontal and vertical displacement responses are measured and utilized to detect frame structures' damage by the generalized SMBDD method. Firstly, structural identification is carried out on the undamaged frame structure without considering the effect of measurement noise. The identified stiffness parameters of the undamaged frame structure, $(\hat{EI})_i^u$ ($i = 1,2,3,4,5,6$) are presented and compared with real values $(EI)_i^{\mathrm{u}}$ in Table 4.15. The maximum relative error of the identified stiffness parameters is only 0.69%. The high accuracy of the identified stiffness parameters of the undamaged building paves a good foundation for the following damage detection of the frame structure.

Then six damage scenarios are designed and examined to demonstrate the robustness of the proposed method for frame structures. The details of the six damage scenarios are presented in Table 4.16. Scenarios 1, 2 and 3 are single damage in which Scenarios 1and 3 have damage in column elements and Scenarios 2 have damage in a beam element (see Figure 4.9). The other three damage scenarios have multi-damage

with different locations and different damage severities. The actual locations of all damaged elements can be found in Figure 4.9. For each damage scenario, the actual fourth-order moments of displacement responses are directly computed from the measured displacement responses of the damaged buildings by Equation (4.14). Then the stiffness parameters of the damaged building for every damage scenarios are identified by the constrained least-squares method. With reference to the identified stiffness parameters of the undamaged building (see Table 4.15), damage locations and their corresponding damage severities of damage scenario are identified. The identified results are presented in Figure 4.10 and listed in Table 4.17.

Table 4.15 Identified results of the undamaged frame structure with noise free

Element	$(EI)_i^{\mathrm{u}}$ $(N \cdot m^2)$	$(\hat{EI})_i^{\mathrm{u}}$ $(N \cdot m^2)$	Relative Error
1	491153082.21	494203217.52	0.62%
2	491153082.21	489363945.78	0.36%
3	283037369.41	283104171.25	0.02%
4	283037369.41	281073515.95	0.69%
5	360456414.57	360771944.64	0.09%
6	360456414.57	358373464.68	0.58%

As seen from Figure 4.10, the damage locations of the frame structure can be accurately identified out for both single damage and multi-damage scenarios no matter whether the damage is in beam elements or in column elements. Even for the very small damage of 2% in Scenario 3, the damage locations can also be detected out. In comparison with the real damage severities shown in Table 4.16 for every damage scenario, it can be seen that the identified damage severities in Table 4.17 are quite close to the real values for both single damage and multi-damage scenarios. The feasibility and robustness of the proposed method are demonstrated through the

frame structure with incomplete measurement when measurement noise is not considered.

Table 4.16 Details of damage scenarios of the frame structure

Scenario No.	Damage severity	Damage location
1	5%	3rd element
2	5%	2nd element
3	2%	6th element
4	5%	1st element
	10%	5th element
5	10%	2nd element
	10%	3rd element
	20%	5th element
6	5%	1st element
	10%	2nd element
	15%	4th element
	20%	5th element

Table 4.17 Identified damage severities (%) of the frame structure with noise free

Scenario No.	Element 1	Element 2	Element 3	Element 4	Element 5	Element 6
1	0.00	0.00	-5.13	-0.03	-0.08	0.00
2	0.00	-5.06	0.00	-0.14	-0.01	-0.06
3	0.00	0.00	0.00	-0.05	0.00	-2.07
4	-4.97	-0.04	0.00	-0.45	-10.02	0.00
5	0.00	-9.07	-9.51	-2.25	-20.36	0.00
6	-3.95	-9.97	0.00	-16.42	-20.06	0.00

4.5.3 Damage detection on frame structures with measurement noise

Then the influence of measurement noise on the quality of damage detection results is numerically investigated through frame structures. Gaussian white noises are added to both the measured displacement responses of the building and the external

acceleration excitation. The added random noises are independent to and different with each other. The MNI of 15% is adopted here. The identified stiffness parameters of the undamaged building with the effects of measurement noise are listed and compared with the real values in Table 4.18. The maximum relative error between the identified stiffness parameters and the actual ones is 1.58%, which is larger than that without the effects of measurement noise but still acceptable in consideration of the high measurement noise intensity of 15%.

Table 4.18 Identified results of the undamaged frame structure with MNI of 15%

Element	$(EI)_i^{\mathrm{u}}$ $(N \cdot m^2)$	$(\hat{EI})_i^{\mathrm{u}}$ $(N \cdot m^2)$	Relative Error
1	491153082.21	495524388.89	0.89%
2	491153082.21	489843679.41	0.27%
3	283037369.41	283513318.58	0.17%
4	283037369.41	278577259.14	1.58%
5	360456414.57	361059562.66	0.17%
6	360456414.57	355794388.97	1.29%

Then the six damage scenarios aforementioned are explored again to evaluate the effect of measurement noise. For each damage scenario, the measured displacement responses and the external excitation are contaminated by the measurement noise. The noise intensity is adopted as 15%. The stiffness parameters of the damaged building for every damage scenarios are identified by utilizing the fourth-order moments of the contaminated responses and the contaminated external excitation. With reference to the identified stiffness parameters of the undamaged building (see Table 4.18), the damage severity of each element is finally calculated for every damage scenario. The identified results are presented in Figure 4.10 and compared with real values and those without considering measurement noise. The damage severity values of the six damage scenarios can be found in Table 4.19.

Table 4.19 Identified damage severities of the frame structure with MNI of 15%

Scenario No.	Element 1	Element 2	Element 3	Element 4	Element 5	Element 6
1	0.00	-0.08	-4.99	0.00	-0.02	-0.02
2	0.00	-3.92	0.00	-0.32	-0.58	0.00
3	0.00	0.00	0.00	0.00	0.00	-1.10
4	-4.35	0.00	0.00	-1.00	-9.89	0.00
5	0.00	-8.91	-9.52	-1.96	-20.36	0.00
6	-4.48	-9.25	-0.32	-16.35	-20.15	0.00

It can be seen from Figure 4.10 that even when the MNI is as high as 15%, the damage locations of these scenarios are accurately detected out for the frame structure with incomplete measurement. The location of very small damage of 2% in Scenario 3 is also identified out. In addition, as seen from Table 4.19, the identified damage severity values with measurement noise are close to the real ones. Compared with the identified results without measurement noise, the measurement noise has small effect on the identified results. The feasibility and robustness of the proposed method are demonstrated through the frame structure with incomplete measurement and with high level of measurement noise.

4.6 Conclusions

In this chapter research efforts are made to extend the SMBDD method from Gaussian white noise ground excitation to colored noise excitation, from shear building structures to more general building structures represented by FE models and from complete measurements to incomplete measurements. The more general equations of the SMBDD method are derived in the frequency domain. Then the generalized SMBDD method is numerically investigated in the frequency domain for

the aforementioned extension cases.

In the numerical investigation, the colored noise acceleration with the Kanai–Tajimi power spectral density is firstly employed as ground external excitation. Various damage scenarios of a multi-story shear building are explored by the proposed method. Numerical results show that the damage locations and damage severities of these damage scenarios are accurately detected by using the colored noise ground excitation. The effect of measurement noise is explored by contaminating the displacement responses and external excitations with Gaussian white noise. Even when the measurement noise intensity is as high as 15%, the SMBDD method still gives highly reliable results on damage severities and damage locations of the multi-story shear building structure. Then the locations of the colored noise excitation change from ground to the upper structure. Various damage scenarios aforementioned and the effect of measurement noise are examined again. It is shown that the proposed method is still feasible and effective to detect both damage locations and damage severities when colored noise excitations acting on the upper structures are utilized and high level of measurement noise is considered. The types and locations of external excitations have no much effect on the quality of the identified stiffness parameters of building structures. Therefore, before and after damage, different types and different locations of external excitations can be utilized to vibrate building structures by the proposed damage detection method.

After that, the generalized SMBDD method is applied to high-rise buildings with incomplete measurement. A 20-story high-rise building with height $h_T = 80$ m is employed to demonstrate the feasibility and robustness of the SMBDD method. In

the numerical investigation, only the horizontal displacement responses of the high-rise building is measured and utilized to detect damage, which is much less than the number of the DOFs. Various damage scenarios with different damage locations and damage severities of the high-rise building are identified by the proposed method. It is shown that the method can effectively identify damage locations and damage severities of various damage scenarios under the influences of measurement noise and incomplete measurement.

Finally, a frame structure is numerically investigated by the proposed method. Only the horizontal and vertical displacement responses are measured and utilized to detect structural damage. The advantage of the proposed method that is both sensitive to structural damage and insensitive to measurement noise is manifested through various damage scenarios of the frame structure with incomplete measurement. The feasibility and robustness of the proposed method are demonstrated again through the frame structure.

In conclusion, the generalized SMBDD method is sensitive to both damage states and to damage levels. Theoretically speaking, it can be applied to any structures by utilizing any Gaussian external excitations with no limitation of locations. In addition, it has the capability to cope with the incomplete measurement problem. Such features of the proposed method show great potential for industrial applications.

Nevertheless, the research efforts up to now only focus on the SMBDD method in the frequency domain which requires that the external excitations should be stationary and have Gaussian distributions. Such a requirement prevents the SMBDD

method from practical application under other external loads of non-Gaussian nature. To make the proposed method more versatile, the SMBDD method in the time domain without such a limitation will be explored in the next chapter.

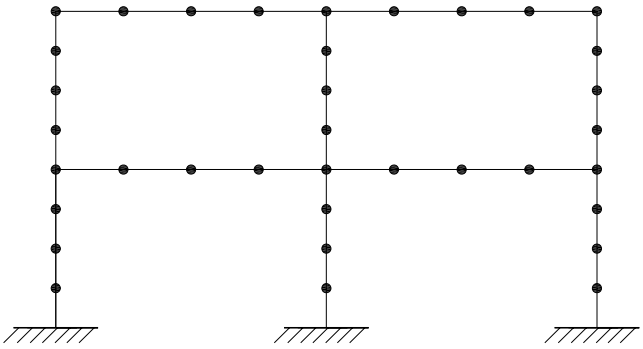

Figure 4.1 Finite element model of a building structure

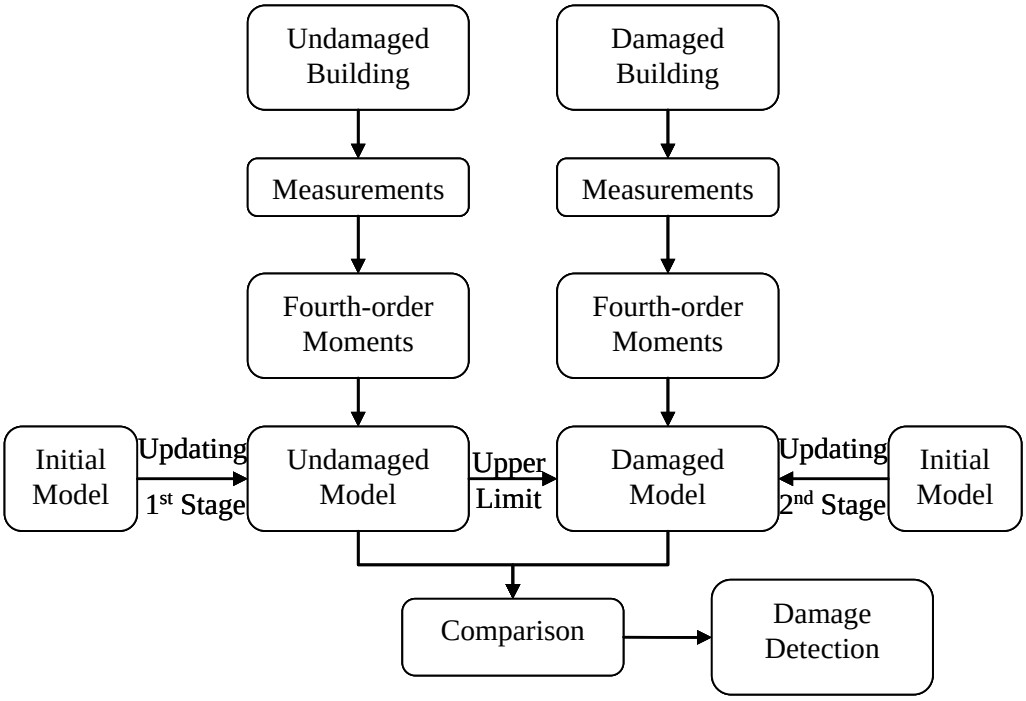

Figure 4.2 Procedure of the generalized SMBDD method

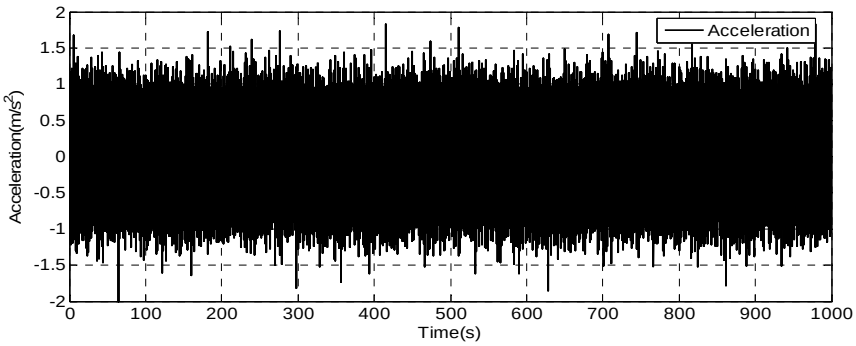

(a) time history

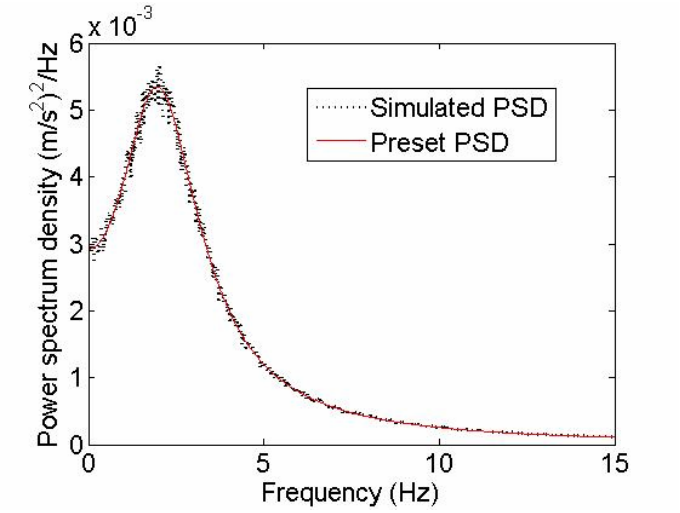

(b) power spectrum density

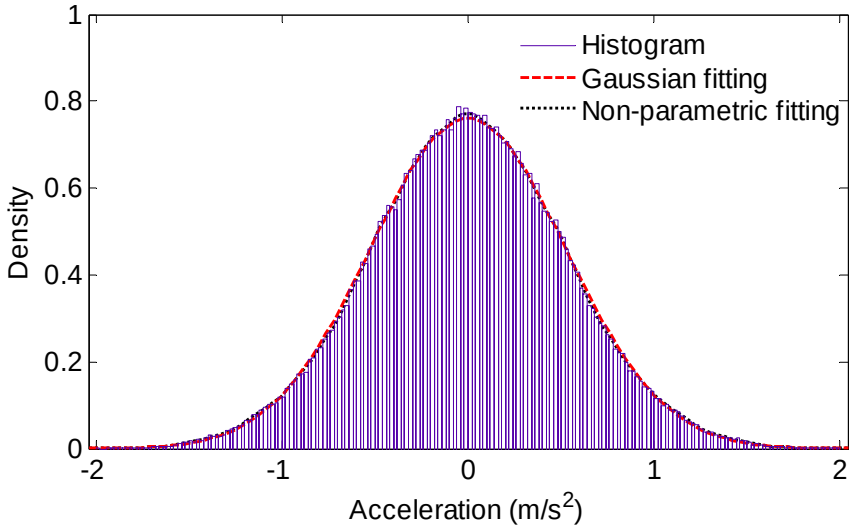

(c) probability density distribution

Figure 4.3 Simulated colored noise excitation: (a) time history, (b) power spectrum density, (c) probability density distribution

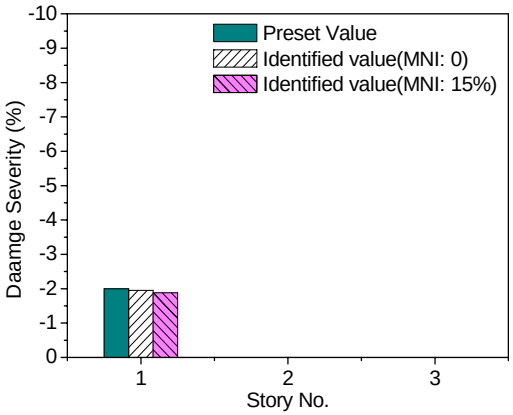

(a) Scenario 1

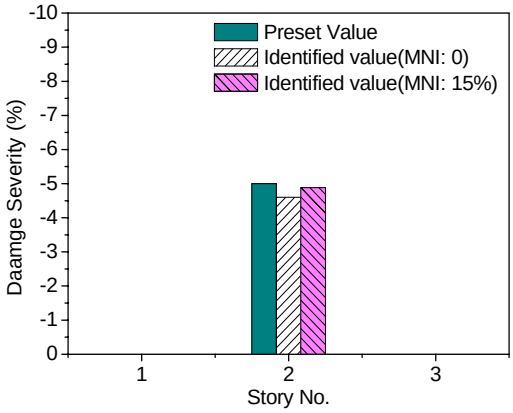

(b) Scenario 2

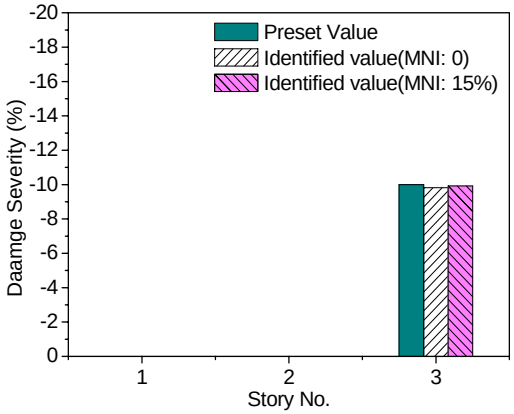

(c) Scenario 3

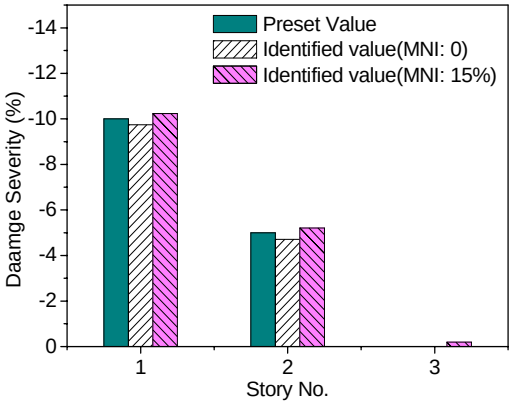

(d) Scenario 4

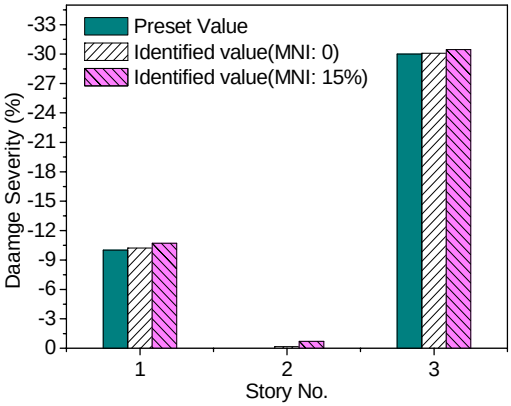

(e) Scenario 5

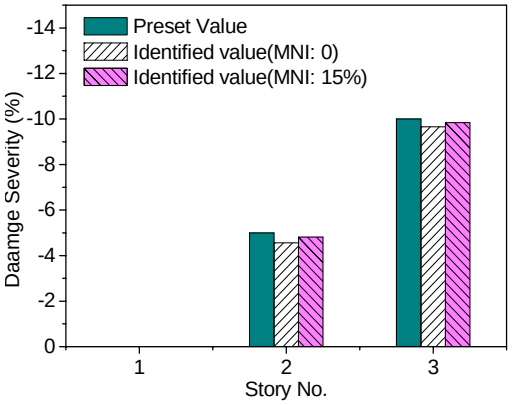

(f) Scenario 6

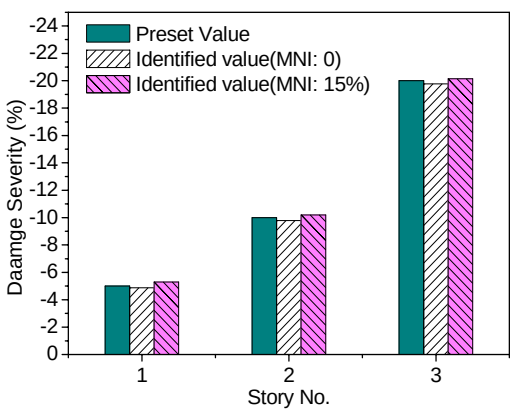

(g) Scenario 7

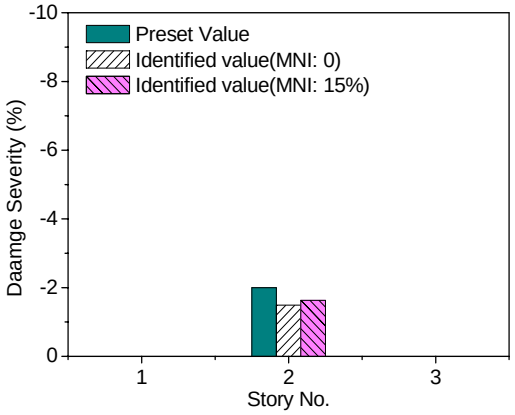

(h) Scenario 8

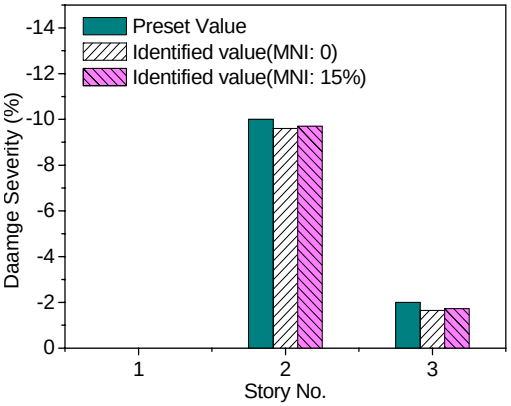

(j) Scenario 9

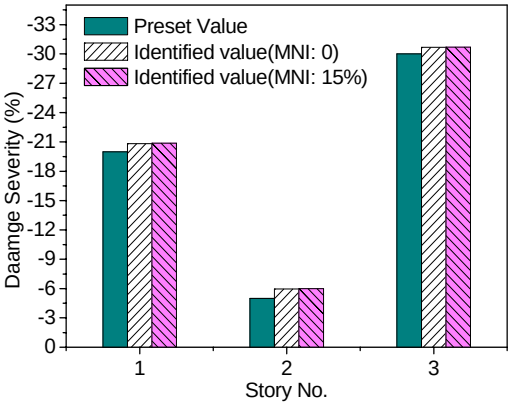

(k) Scenario 10

Figure 4.4 Identified results of shear building structures using colored noise ground excitation: (a) Scenario 1, (b) Scenario 2, (c) Scenario 3, (d) Scenario 4, (e) Scenario 5, (f) Scenario 6, (g) Scenario 7, (h) Scenario 8, (j) Scenario 9, (k) Scenario 10

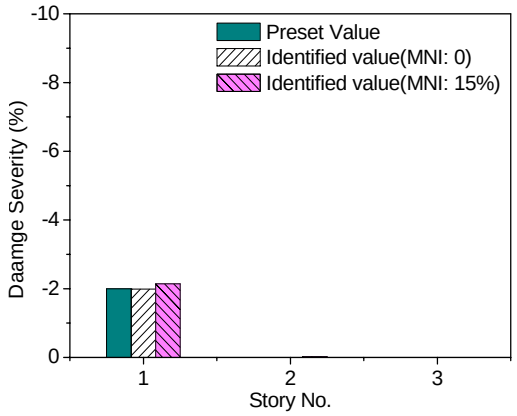

(a) Scenario 1

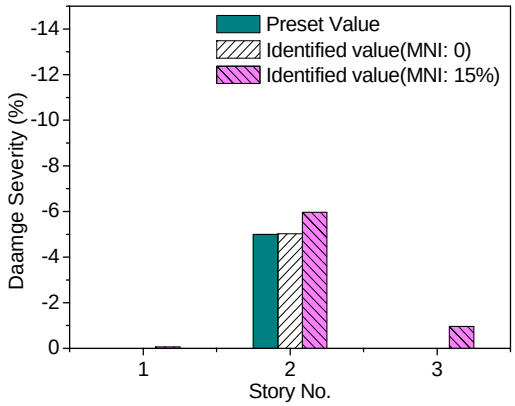

(b) Scenario 2

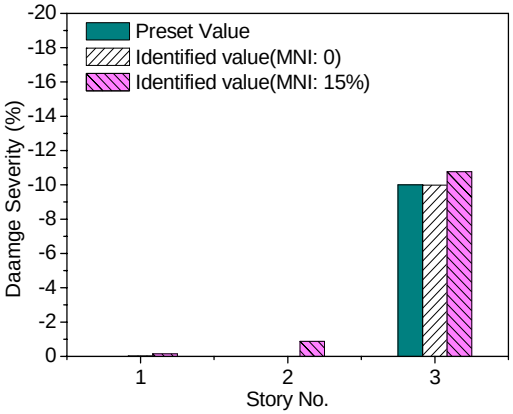

(c) Scenario 3

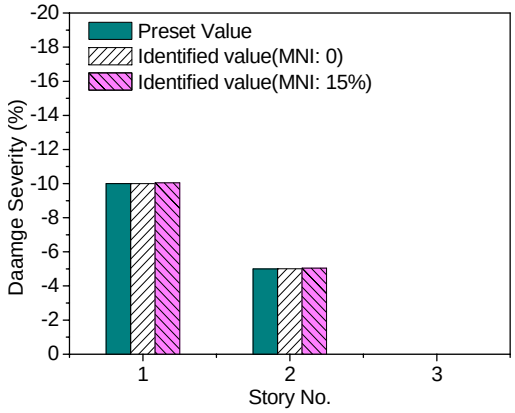

(d) Scenario 4

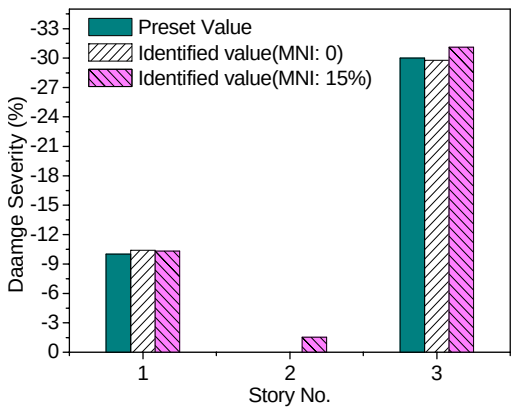

(e) Scenario 5

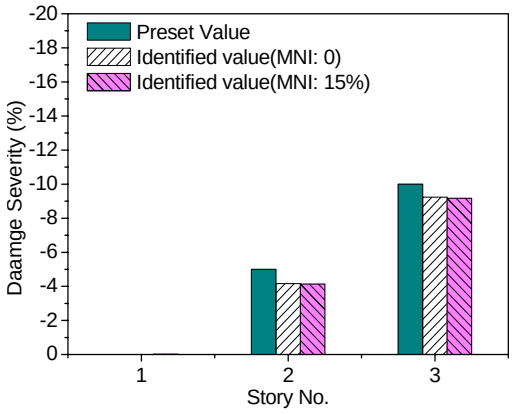

(f) Scenario 6

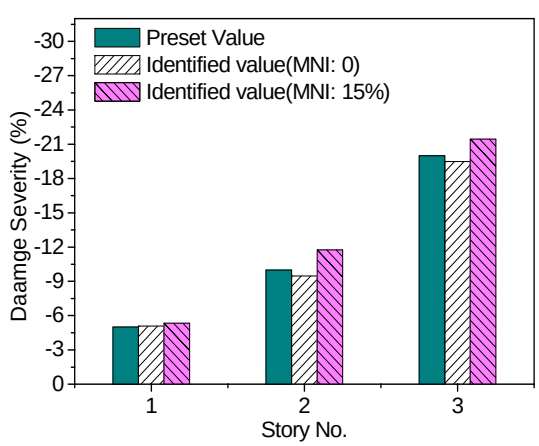

(g) Scenario 7

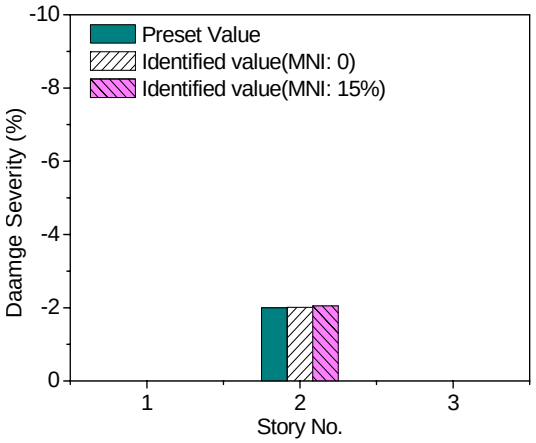

(h) Scenario 8

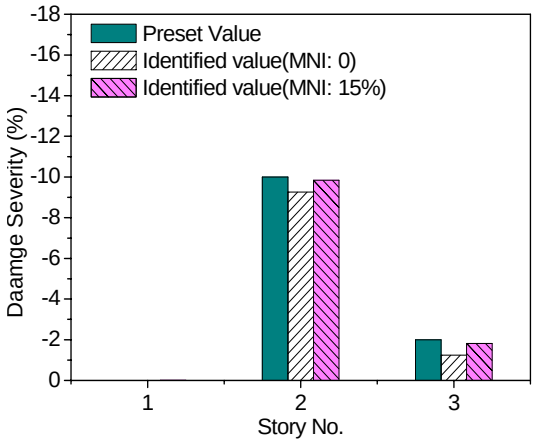

(j) Scenario 9

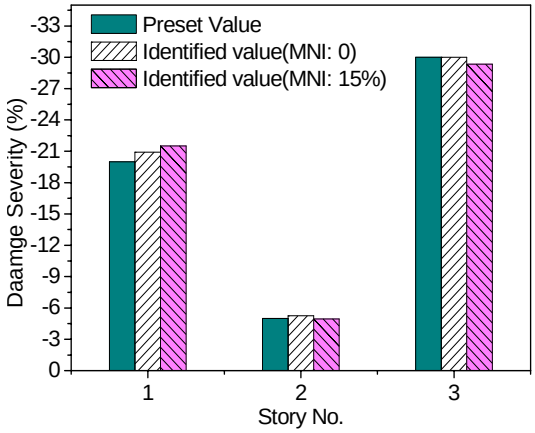

(k) Scenario 10

Figure 4.5 Identified results of shear building structures using colored noise excitation at the first floor: (a) Scenario 1, (b) Scenario 2, (c) Scenario 3, (d) Scenario 4, (e) Scenario 5, (f) Scenario 6, (g) Scenario 7, (h) Scenario 8, (j) Scenario 9, (k) Scenario 10

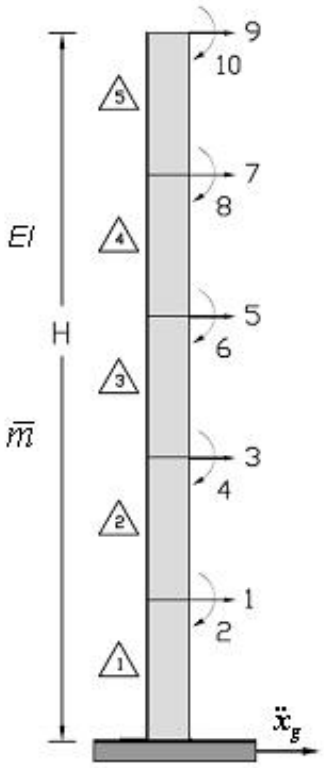

Figure 4.6 Configuration of a high-rise building structure

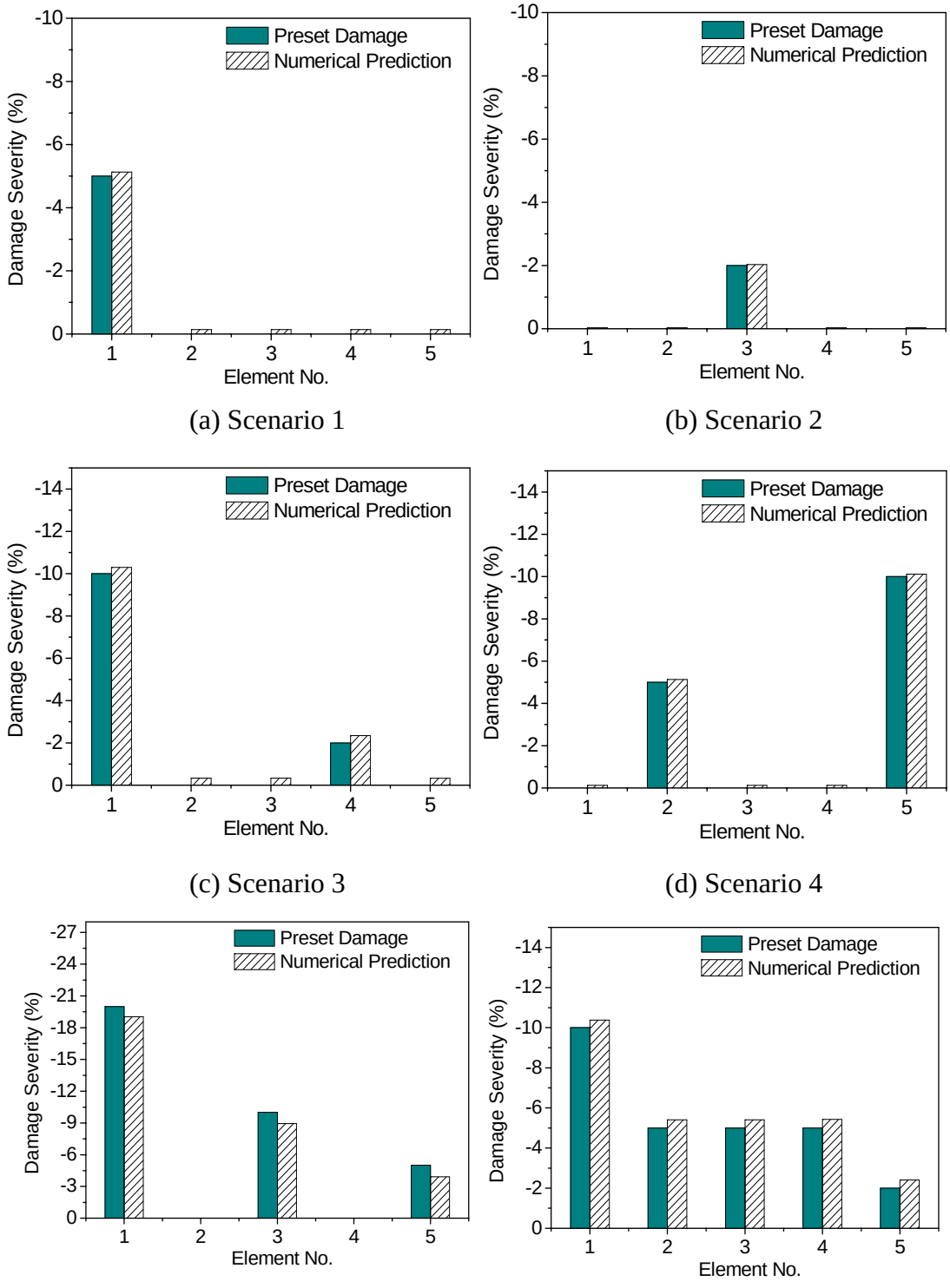

Figure 4.7 Identified results of a high-rise building with noise free: (a) Scenario 1, (b) Scenario 2, (c) Scenario 3, (d) Scenario 4, (e) Scenario 5, (f) Scenario 6

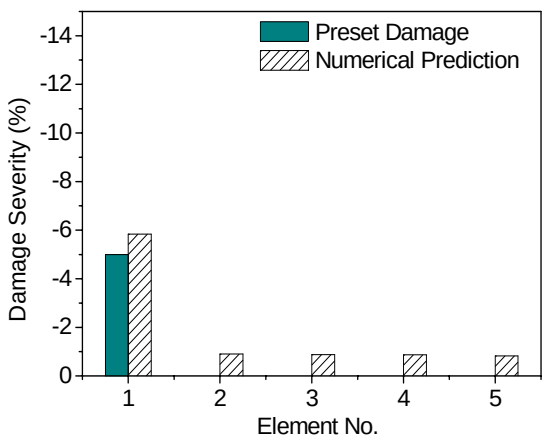

(a) Scenario 1

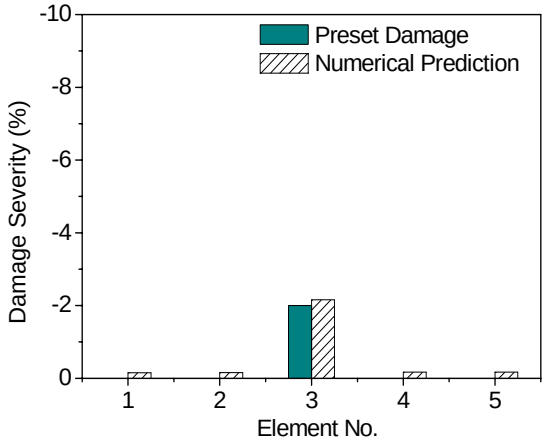

(b) Scenario 2

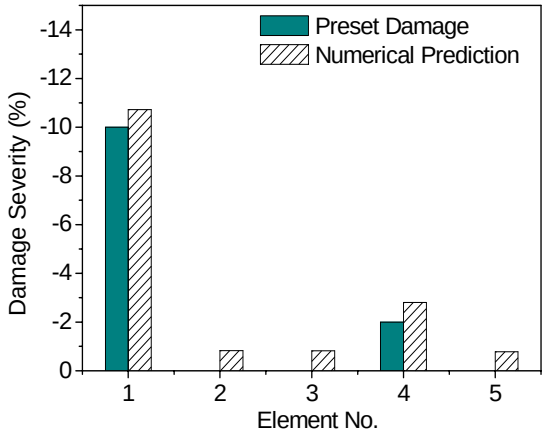

(c) Scenario 3

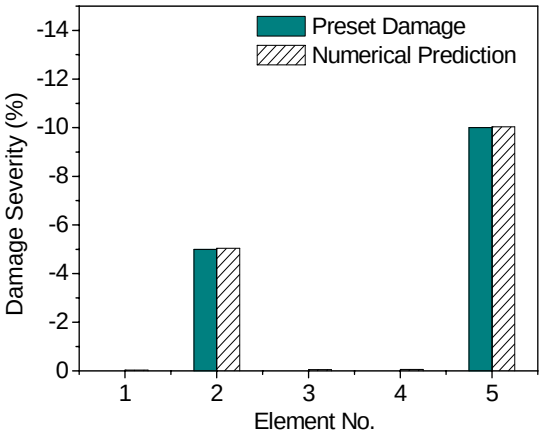

(d) Scenario 4

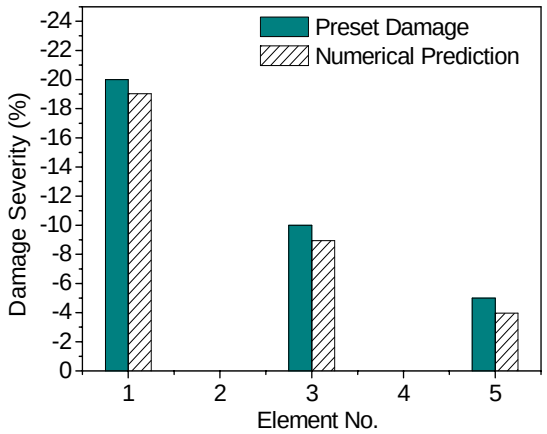

(e) Scenario 5

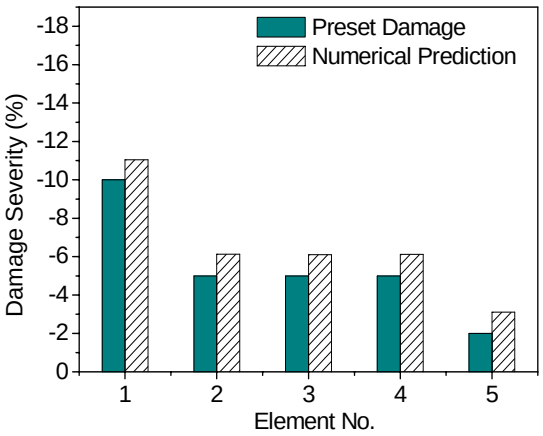

(f) Scenario 6

Figure 4.8 Identified results of a high-rise building with the MNI of 15%: (a) Scenario 1, (b) Scenario 2, (c) Scenario 3, (d) Scenario 4, (e) Scenario 5, (f) Scenario 6

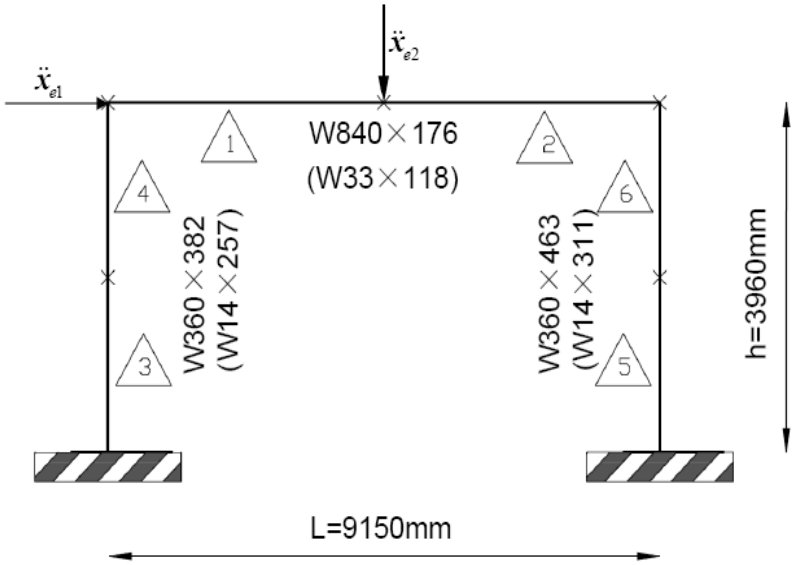

Figure 4.9 Configuration of a steel frame structure

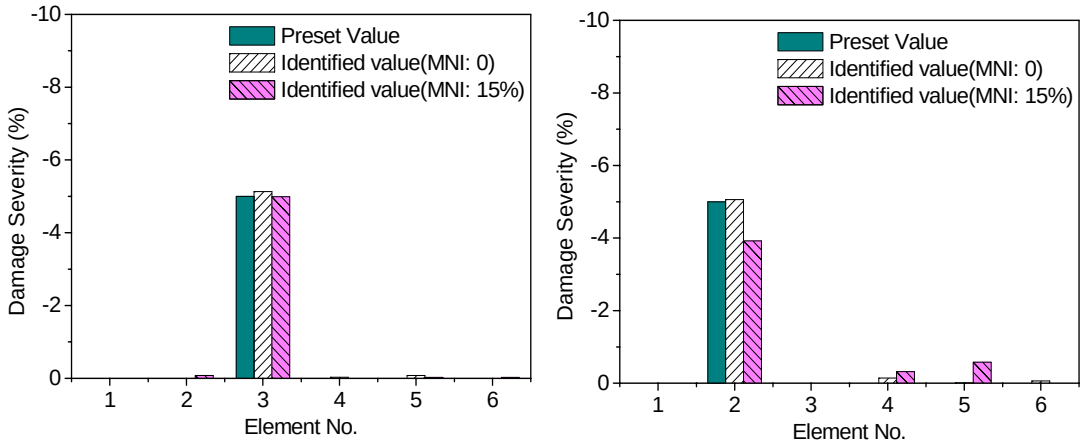

(a) Scenario 1 (b) Scenario 2

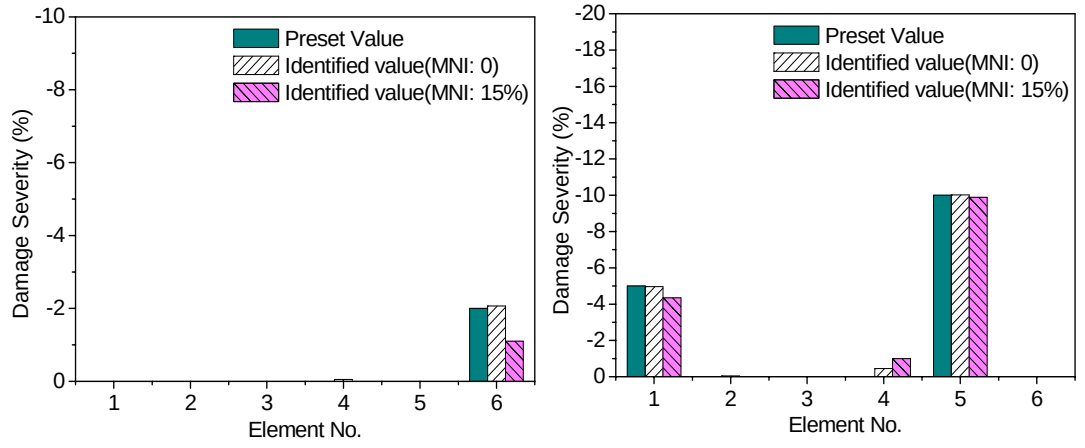

(c) Scenario 3 (d) Scenario 4

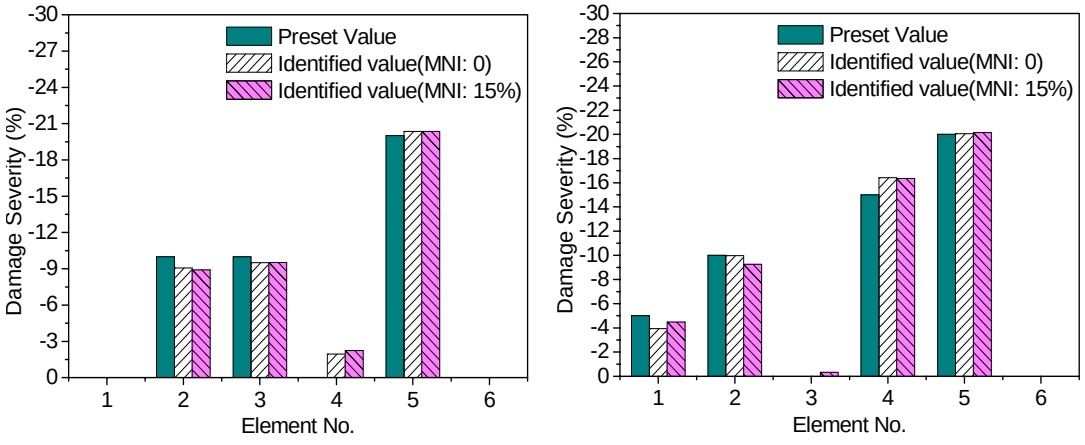

(e) Scenario 5 (f) Scenario 6

Figure 4.10 Identified results of the frame structure with the MNI of 15%(a) Scenario 1, (b) Scenario 2, (c) Scenario 3, (d) Scenario 4, (e) Scenario 5, (f) Scenario 6

CHAPTER 5

STATISTICAL MOMENT-BASED DAMAGE DETECTION METHOD IN TIME DOMAIN

5.1 Introduction

The feasibility and robustness of the SMBDD method have been numerically demonstrated in the frequency domain through shear buildings, tall buildings and frame structures with consideration of the problems of incomplete measurements and measurement noise in Chapters 3 and 4. However, the SMBDD method can be applied to practical structures in the frequency domain only when external excitations have Gaussian distributions. This requirement limits the application of the SMBDD method to other non-Gaussian external excitations. In this regard, the SMBDD method is further explored in the time domain in this chapter.

Firstly, the algorithm of the SMBDD method is proposed in the time domain for any Gaussian, non-Gaussian and non-stationary external excitations with consideration of the problem of incomplete measurements. Then various damage scenarios of shear buildings, high-rise buildings and frame structures are numerically investigated in the time domain by the SMBDD method. The feasibility and effectiveness of the SMBDD method are first investigated in the time domain by using Gaussian external excitations. Then non-Gaussian and non-stationary external excitations are utilized to demonstrate the versatility of the SMBDD method in the time domain through shear building structures. The effect of measurement noise on the quality of identified

results is finally studied for all the concerned damage scenarios. Analysis results show that various damage scenarios with consideration of the incomplete measurements and measurement noise can be accurately identified in the time domain by the SMBDD method using Gaussian, non-Gaussian and nonstatioary external excitations.

5.2 The SMBDD Method in Time Domain

Let us consider an N-DOFs building structure which is under an external excitation $\boldsymbol{f}(t) = [\boldsymbol{f}_1(t), \boldsymbol{f}_2(t), \cdots, \boldsymbol{f}_N(t)]$. Without loss of generality, the equation of motion in the matrix form for the building structure can be expressed as

$$\mathbf{M}\ddot{\mathbf{x}}(t) + \mathbf{C}\dot{\mathbf{x}}(t) + \mathbf{K}\mathbf{x}(t) = \mathbf{f}(t) \tag{5.1}$$

where $\mathbf{M}$, $\mathbf{C}$ and $\mathbf{K}$ are the mass matrix, damping matrix and stiffness matrix of the building structure, respectively, $\ddot{\mathbf{x}}(t)$, $\dot{\mathbf{x}}(t)$ and $\mathbf{x}(t)$ are the acceleration, velocity and displacement response vectors, respectively. The problem of incomplete measurements is also considered by the SMBDD method in the time domain. The displacement responses $\mathbf{x}(t)$ include the measured ones $\mathbf{x}_m(t)$ and the unmeasured ones $\mathbf{x}_u(t)$. $\mathbf{x}_m(t) = [x_{m1}(t), x_{m2}(t), \cdots, x_{mN_m}(t)]^T$, where N_m is the total number of measured displacement responses. Denote the number of unknown stiffness parameters as N_e. N_m should be larger than or at least equal to N_e. Otherwise, it will result in an unidentifiable problem for the model updating. $\mathbf{f}(t)$ is the external excitation vector which can be Gaussian and non-Gaussian random excitation acting at any locations of the building structure.

Denote the time history of the *j*th measured response as $\mathbf{x}_j = [x_{1j}, x_{2j}, \cdots, x_{N_s j}]$, where N_s is the number of sampling points. Its statistical moments, denoted as $\hat{\mathbf{M}}_i$ (*i*=2,4,6), can be calculated by using summation-type relationships as follows whenever it fits the Gaussian distribution or not (Martin, 1989).

$$M_{1j} = \overline{x}_j = \frac{1}{N}\sum_{i=1}^{Ns} x_{ij} \tag{5.2}$$

$$M_{2j} = \frac{1}{N}\sum_{i=1}^{Ns} {x_{ij}}^2 - {\overline{x}_j}^2 \tag{5.3}$$

$$M_{4j} = \frac{1}{N}\sum_{i=1}^{Ns} {x_{ij}}^4 - \frac{4}{N}\overline{x}_j \sum_{i=1}^{Ns} {x_{ij}}^3 + \frac{6}{N}{\overline{x}_j}^2 \sum_{i=1}^{Ns} {x_{ij}}^2 - 3{\overline{x}_j}^4 \tag{5.4}$$

$$M_{6j} = \frac{1}{N_s}\sum_{i=1}^{Ns} {x_{ij}}^6 - \frac{6}{N_s}\overline{x}_j \sum_{i=1}^{Ns} {x_{ij}}^5 + \frac{15}{N_s}{\overline{x}_j}^2 \sum_{i=1}^{Ns} {x_{ij}}^4 - \frac{20}{N_s}{\overline{x}_j}^3 \sum_{i=1}^{Ns} {x_{ij}}^3 + \frac{15}{N_s}{\overline{x}_j}^4 \sum_{i=1}^{Ns} {x_{ij}}^2 - 5{\overline{x}_j}^6 \tag{5.5}$$

Given the structural stiffness parameter vector an initial value, the stiffness matrix and the damping matrix can be calculated through the FE model of the building structure by adopting the Rayleigh damping assumption. Substituting them into Equations (5.1), the displacement response corresponding to the *j*th measured displacement response can be obtained by solving the equation. Then the statistical moments of the obtained displacement response can be directly calculated by using the above Equations (5.2) ~ (5.5) in the time domain, denoted as $\mathbf{M}_i$ (*i*=2,4,6). Therefore, the residual vector between the theoretical statistical moment vector, $\mathbf{M}_i$ (*i*=2,4,6), for a given stiffness parameter vector $\mathbf{k}$ and the actual statistical moment vector of the measured building responses, $\hat{\mathbf{M}}_i$ (*i*=2,4,6), can be calculated and written as

$$\mathbf{F}(\mathbf{k}) = \mathbf{M}_i(\mathbf{k}) - \hat{\mathbf{M}}_i \tag{5.6}$$

Ideally, if the given stiffness vector $\mathbf{k}$ is equal to the actual value, the 2-norm of the residual vector, $\|\mathbf{F}(\mathbf{k})\|^2$, will be zero. Practically, the optimal stiffness vector can be identified by the least-squares method, that is, giving $\mathbf{k}$ an initial value $\mathbf{k}_0$ and minimizing $\|\mathbf{F}(\mathbf{k})\|^2$.

In brief, the SMBDD method can be implemented in the time domain according to the following steps:

(1) Measure the displacement responses of the undamaged and damaged building under external acceleration;

(2) The actual statistical moments of the measured displacement responses of the undamaged and damaged building, $\hat{\mathbf{M}}_i$, are respectively estimated by using Equations (5.2) ~ (5.5);

(3) Given the stiffness parameter vector an initial value, the theoretical statistical moments of displacement responses $\mathbf{M}_i$ can be calculated based on FE models of the building structure and the above Equations (5.2) ~ (5.5) in the time domain.

(4) Substitute $\hat{\mathbf{M}}_i$ and $\mathbf{M}_i$ into Equation (5.6), the structural stiffness vector can be identified by the constrained nonlinear least-squares method for the undamaged and damaged building respectively;

(5) The structural damage including damage existence, damage location and damage severity can be detected by comparing the identified stiffness vector $\hat{\mathbf{k}}^u$ of the undamaged building with the identified stiffness vector $\hat{\mathbf{k}}^d$ of the damaged building.

It should be noted that the constrained nonlinear least-squares method is utilized by the SMBDD method in the time domain for both undamaged and damaged building structures other than for damaged building structures only. In piratical application, the upper limit of the stiffness parameter vector of the undamaged building should be first estimated and then utilized by the constrained nonlinear least-squares method in model updating. Otherwise, under some circumstances, the unconstrained least-squares method will converge to the local optimum value other than the global optimum value of the stiffness parameter vector for some undamaged buildings. Generally speaking, higher requirement is put forward for the optimization method used by the SMBDD method in the time domain than in the frequency domain. In addition, since the stiffness parameters of the damaged building are physically impossible to be larger than those of the corresponding undamaged building, the upper limit of the structural stiffness parameter vector of the damaged structures is adopted as the identified stiffness parameters of the corresponding undamaged building. The fourth-order moment other than the second-order or the sixth-order moment is used in this following investigation, which makes a tradeoff between the sensitivity of an index to structural damage and its stability to random excitation.

In summary, the algorithm of the SMBDD method in the time domain is similar to that of the SMBDD method in the frequency domain. The only difference between them lies in that the statistical moments $\mathbf{M}$ for a given initial stiffness parameter vector are directly calculated in the time domain without any limitation, while the relationship between the variance and the statistical moments of a Gaussian response need to be utilized in the frequency domain. Therefore, there is no such limitation

that the external excitation should have normal distribution for the SMBDD method in the time domain as that in the frequency domain.

5.3 Numerical Investigation by Gaussian Excitations

5.3.1 Damage detection of shear buildings

The three-story shear building model (see Figure 5.1) is employed here to illustrate the application of the proposed method in the time domain. The mass and horizontal stiffness coefficients of the three-story shear building are respectively 350250 kg and 4728400 kN/m for the first story, 262690 kg and 315230 kN/m for the second story, and 175130 kg and 157610 kN/m for the third story. The mass of each floor is assumed to be invariant. The first damping ratio is taken as 1%. The second and third modal damping ratios are 2.14% and 5.56%, respectively. The ground acceleration is modeled as a colored noise corresponding to the Kanai-Tajimi spectrum having parameters ω_g =15.6 rad/s and ζ_g =0.6. The magnitude is chosen such that the maximum ground acceleration is 2.0 m/sec^2. The time duration of the simulated acceleration is 1000s and the sampling frequency is 256Hz. The time history of the ground excitation is generated using the method of digital simulation of a random processes developed by Shinozuka and Jan (1972).

5.3.1.1 Damage detection of shear buildings in the time domain without consideration of measurement noise

The undamaged shear building is firstly identified in the time domain by the proposed method using Gaussian external excitations. The effect of measurement noise is not considered at first. Listed in Table 5.1 are the values of the fourth-order

moments of the measured three story drifts of the undamaged building, $\hat{M}_{4i}^{u}$ ($i = 1,2,3$), calculated by Equations (5.2) ~ (5.5). Given the stiffness parameter vector an initial value, the horizontal stiffness values of the undamaged building, $\hat{k}_i^{u}$ ($i = 1,2,3$) are identified by using the constrained nonlinear least-squares method. The identified results are presented in Table 5.1. It can be found that the identified horizontal stiffness coefficients of the undamaged building $\hat{k}_i^{u}$ in the time domain are the same as the real values k_i^{u}, which have the higher precision than the results identified in the frequency domain.

Table 5.1 Identification results of the undamaged shear building in the time domain

Story	$\hat{M}_{4i}^{u}$ (m^4)	k_i^{u} (kN/m)	$\hat{k}_i^{u}$ (kN/m)
1	4.0380×10^{-14}	4728400.00	4728400
2	1.6151×10^{-9}	315230.00	315230
3	2.9936×10^{-9}	157610.00	157610

Then six damage scenarios are investigated. The details of these damage scenarios are presented in Table 5.2. Both single damage scenarios and multi-damage scenarios with different damage locations and damage severities are considered. All these damage scenarios of the shear building have been investigated in the frequency domain by the proposed method in Chapter 4. For each damage scenario, the fourth-order moments of story drifts are computed in the time domain through the measured displacement responses of the damaged building. Then the horizontal stiffness values of the damaged building are identified by the SMBDD method. With reference to the identified horizontal stiffness values of the undamaged building (see Table 5.1), the damage severity of each story is obtained for every damage scenario. The identified results are presented in Table 5.3 and compared with the actual

damage severities. It can be seen that the identified damage severities are the same as the actual damage severities for all the six damage scenarios. The accurateness and sensitivity of the proposed method are demonstrated in the time domain when measurement noise is not taken into account.

Table 5.2 Details of damage scenarios 1-6 of a three-story shear building

Scenario	Story 1	Story 2	Story 3
1	$0.98\,k_1^u$	k_2^u	k_3^u
2	k_1^u	$0.95\,k_2^u$	k_3^u
3	$0.90\,k_1^u$	$0.95\,k_2^u$	k_3^u
4	k_1^u	$0.95\,k_2^u$	$0.90\,k_3^u$
5	$0.90\,k_1^u$	k_2^u	$0.70\,k_3^u$
6	$0.95\,k_1^u$	$0.90\,k_2^u$	$0.80\,k_3^u$

Table 5.3 Identified results of damage scenarios of a three-story shear building in the time domain with noise free

Scenario	Story 1		Story 2		Story 3	
	μ (%)	$\hat{\mu}$ (%)	μ (%)	$\hat{\mu}$ (%)	μ (%)	$\hat{\mu}$ (%)
1	-2.00	-2.00	0.00	0.00	0.00	0.00
2	0.00	0.00	-5.00	-5.00	0.00	0.00
3	-10.00	-10.00	-5.00	-5.00	0.00	0.00
4	0.00	0.00	-5.00	-5.00	-10.00	-10.00
5	-10.00	-10.00	0.00	0.00	-30.00	-30.00
6	-5.00	-5.00	-10.00	-10.00	-20.00	-20.00

5.3.1.2 Damage detection of shear buildings with measurement noise

The effect of measurement noise on the quality of damage detection results is numerically investigated in this section. Random white Gaussian noises are added into the measured displacement responses and the external excitations of the

undamaged and damaged shear buildings. The added random noises are independent to and different with each other. The measurement noise intensity (MNI) is adopted as 15%. The calculated fourth-order moments and the identified horizontal stiffness coefficients of the undamaged building with the effects of measurement noise are listed in Table 5.4. The relative errors between the identified horizontal stiffness values and the actual ones are respectively 0.34%, 0.48% and 0.35% for the three stories. It can be said that the measurement noise has no much effect on the identified horizontal stiffness values in the time domain by using the proposed method. The identified damage severities of the six damage scenarios aforementioned with the MNI of 15% are presented in Table 5.5. The identified results are also compared with the real values, the identified results in the time domain with noise free and the identified results in the frequency domain with the MNI of 15% in Figure 5.2.

Table 5.4 Identified results of the undamaged shear building with MNI of 15%

Story	$\hat{M}_{4i}^{u}\ (m^4)$	$k_i^{u}\ (kN/m)$	$\hat{k}_i^{u}\ (kN/m)$
1	2.4921×10^{-14}	4728400	4712127
2	9.6735×10^{-10}	315230	313722
3	1.7432×10^{-9}	157610	157066

Table 5.5 Identified results by colored noise ground excitation with MNI of 15%

Scenario	Story 1		Story 2		Story 3	
	μ (%)	$\hat{\mu}$ (%)	μ (%)	$\hat{\mu}$ (%)	μ (%)	$\hat{\mu}$ (%)
1	-2.00	-2.08	0.00	0.00	0.00	-0.11
2	0.00	0.00	-5.00	-4.86	0.00	-0.25
3	-10.00	-10.67	-5.00	-4.51	0.00	0.00
4	0.00	-0.17	-5.00	-5.07	-10.00	-10.21
5	-10.00	-10.30	0.00	-0.17	-30.00	-30.22
6	-5.00	-3.76	-10.00	-8.38	-20.00	-18.67

As seen from Figure 5.2, the damage locations can be accurately detected out even when the MNI is as high as 15%. There is no much difference among the four kinds of identified results. In other words, the SMBDD method is insensitive to measurement noise and effective both in the frequency domain and in the time domain. In addition, the identified damage severities have no much difference with the real values according to Table 5.5 even when the MNI is as high as 15%. The robustness of the proposed method in the time domain is demonstrated through the shear building structure.

5.3.2 Damage detection of tall buildings with incomplete measurements

In this section, the proposed SMBDD method is applied to high-rise buildings or flexible buildings in the time domain with consideration of the problem of incomplete measurements. In the following numerical investigation, the concerned flexible building is a 20-story high-rise building with height $h_T = 80\,\text{m}$. The mass density is $4 \times 10^5 \text{kg/m}$. The stiffness parameter for the flexible building is $(EI)_T = 8.18 \times 10^{10}\ \text{kN.m}^2$, where E is the Young's modulus and I is the moment of inertia of the building. The high-rise building (see Figure 5.3) is discretized into five elements with the length of 16m. The colored noise simulated in Section 5.3.1 is utilized as external ground excitation. The problem of incomplete measurements is considered in the numerical investigation. Therefore, only half of the DOFs of the high-rise building are measured and utilized to detect structural damage in the time domain by the SMBDD method.

5.3.2.1 Damage detection of high-rise buildings without measurement noise

Firstly, structural identification is carried out on the undamaged building without considering the effect of measurement noise on detected results. The fourth-order moments of the horizontal displacement responses, $\hat{M}_{4i}^{u}$ ($i = 1,2,3,4,5$), are calculated by Equations (5.2) ~ (5.5) and then used to identify the stiffness parameters of the undamaged building, $(\hat{EI})_i^u$ ($i = 1,2,3,4,5$). The fourth-order moments and the identified stiffness parameters of all elements are presented in Table 5.6. It can be seen that the identified horizontal stiffness coefficients of the undamaged building $(\hat{EI})_i^u$ in the time domain are identical with the theoretical values $(EI)_i^{u}$ when measurement noise is not taken into account.

Table 5.6 Identified results of the undamaged building

Element	$\hat{M}_{4i}^{u}$ (m^4)	$(EI)_i^{u}$ $(\times 10^5 kN/m)$	$(\hat{EI})_i^{u}$ $(\times 10^5 kN/m)$
1	1.4848×10^{-10}	818000.00	818000.00
2	6.7453×10^{-9}	818000.00	818000.00
3	2.5381×10^{-8}	818000.00	818000.00
4	4.3449×10^{-8}	818000.00	818000.00
5	5.0632×10^{-8}	818000.00	818000.00

Then six damage scenarios are examined to explore the feasibility of the proposed method in the time domain through the high-rise building. Both single damage scenarios and multiple damage scenarios are explored. The details of the six damage scenarios are presented in Table 5.7. For each damage scenario, the fourth-order moments of the relative horizontal displacement responses between two elements are computed from the measured horizontal displacement responses of the damaged

building. The horizontal stiffness parameters of the damaged building for every damage scenarios are identified by the constrained nonlinear least-squares method. With reference to the identified horizontal stiffness values of the undamaged building (see Table 5.6), the damage severity of each element is calculated for every damage scenario. The identified results without considering the effect of measurement noise are presented in Table 5.8.

Table 5.7 Details of damage scenarios of a high-rise building

Scenario No.	Damage severity	Damage location
1	5%	1st element
2	2%	3rd element
3	10%	1st element
	2%	4th element
4	5%	2nd element
	10%	5th element
5	20%	1st element
	10%	3rd element
	5%	5th element
6	10%	1st element
	5%	2nd element
	5%	3rd element
	5%	4th element
	2%	5th element

According to Table 5.8, the damage locations and damage severities can be apparently and accurately identified out for both single damage scenarios and multi-damage scenarios when measurement noise is not taken into account. Even for the very small damage of 2%, the damage can also be accurately detected. In comparison with the actual damage severities shown in Table 5.7, the identified damage severities are the same as the actual values when measurement noise is taken

into account. The sensitivity of the proposed method is demonstrated in the time domain through high-rise buildings.

Table 5.8 Identified damage severities (%) of a high-rise building with noise free

Scenario No.	Element 1	Element 2	Element 3	Element 4	Element 5
1	-5.00	0	0	0	0
2	0	0	-2.00	0	0
3	-10.00	0	0	-2.00	0
4	0	-5.00	0	0	-10.00
5	-20.00	0	-10.00	0	-5.00
6	-10.00	-5.00	-5.00	-5.00	-2.00

5.3.2.2 Damage detection of high-rise buildings with measurement noise

The influence of measurement noise on the quality of the damage detection results is then numerically investigated for the high-rise building structure. Random white Gaussian noises are added to both the measured displacement responses and the external acceleration excitation. The added random noises are independent and different with each other. The MNI of 15% is adopted here. The calculated fourth-order moments and the identified stiffness parameters of the undamaged building with the effects of measurement noise are listed in Table 5.9. The maximum relative error between the identified stiffness parameters and the actual ones is only 0.89% for the five elements.

Then the six damage scenarios presented in Table 5.7 are explored to evaluate the effect of measurement noise. For each damage scenario, the measured displacement responses and the external excitation are contaminated by the measurement noise. The noise intensity is still adopted as 15%. The horizontal stiffness parameters of the

damaged building for every damage scenarios are identified by utilizing the fourth-order moments of the contaminated responses and the contaminated external excitation. With reference to the identified horizontal stiffness values of the undamaged building (see Table 5.9), the damage severity of each element is finally calculated for every damage scenario. The identified results are presented in Table 5.10. The identified results are also compared with the real values, the identified results in the time domain with noise free and the identified results in the frequency domain with the MNI of 15% in Figure 5.4.

Table 5.9 Identified results of the undamaged high-rise building with MNI of 15%

Element	$\hat{M}_{4i}^{\ u}\ (m^4)$	$(EI)_i^{\ u}\ (\times 10^5 kN/m)$	$(\hat{EI})_i^{\ u}\ (\times 10^5 kN/m)$
1	1.5514×10^{-10}	818000	811073
2	7.0481×10^{-9}	818000	811168
3	2.6521×10^{-8}	818000	811195
4	4.5399×10^{-8}	818000	811261
5	5.2905×10^{-8}	818000	810759

Table 5.10 Identified damage severities of a high-rise building with MNI of 15%

Scenario No.	Element 1	Element 2	Element 3	Element 4	Element 5
1	-4.80	-0.74	-1.00	-0.99	-1.69
2	-0.19	-0.20	-2.19	-0.18	-0.16
3	-12.28	-2.60	-2.57	-4.56	-2.43
4	0	-4.96	0	0	-9.88
5	-21.20	-1.58	-11.38	-1.56	-6.31
6	-8.21	-3.09	-3.10	-3.09	-0.81

As seen from Figure 5.4, the damage locations of these damage scenarios can be accurately determined even when the MNI is as high as 15%. Taking Scenario 2 for

example, the damage location is accurately determined as the third element by the proposed method although its damage severity is very small and only 2%. There is no much difference between the identified damage severities and the real values. The reliability and robustness of the proposed method are demonstrated in the time domain through the high-rise building structure. In addition, the precision of the identified results in the time domain is similar with that of the identified results in the frequency domain. In other words, although the higher precision of the identified severities is obtained by the SMBDD method in the time domain when the effect of measurement noise is not considered, the identified results with consideration of measurement noise are not distinctly improved compared with those obtained by the SMBDD method in the frequency domain.

5.3.3 Damage detection of frame structures with incomplete measurements

The feasibility and robustness of the SMBDD method are investigated in the time domain through frame structures in this section. A 2-D moment resisting one-story and one-bay steel frame (see Figure 5.5) is employed to illustrate the application of the proposed method in the time domain. The frame consists of two columns (W14×257 and W14×311) and one beam (W33×118). The columns are 345 MPA (50ksi) steel and the beam is 248 MPA (36ksi). The bay width *L* is 9.15m (30ft) and the height h is 3.96m (13 ft). The mass density of the left column (W14×257) is 382.46 Kg/m, while that of the right column (W14×311) is 462.82 Kg/m and that of the beam is 17235.7 Kg/m. Each column or beam is divided into two elements. These elements are numbered and marked in Figure 5.5. There are three DOFs at every node: the horizontal displacement x, the vertical displacement y and the angular

displacement θ. The Rayleigh damping is assumed and the first two damping ratios are adopted as 2%. The colored noise simulated in Section 5.3.1 is utilized as external ground excitation. The locations of the external excitations are in the middle of the beam and at the top of the left column. The problem of incomplete measurements is considered. Only the horizontal and vertical displacement responses no angular displacement responses of frame structures are measured and utilized in the following numerical investigation.

5.3.3.1 Damage detection of frame structures without measurement noise

Firstly, structural identification is carried out on the undamaged frame structure without considering the effect of measurement noise. The identified stiffness parameters of the undamaged frame structure, $(\hat{E}I)_i^u$ ($i = 1, 2, 3, 4, 5, 6$) are presented and compared with real values $(EI)_i^u$ in Table 5.11. The former is almost the same as the latter. The high accuracy of the identified stiffness parameters of the undamaged building paves a good foundation for the following damage detection of the frame structure.

Then six damage scenarios are examined in the time domain by the proposed method. The details of the six damage scenarios are presented in Table 5.12. All of them which include single and multiple damage scenarios have been investigated in the frequency domain by the proposed method in Chapter 4. For each damage scenario, the actual fourth-order moments of displacement responses are directly computed from the measured displacement responses of the damaged buildings by Equations (5.2)~ (5.5). Then the stiffness parameters of the damaged building for every damage

scenarios are identified by the constrained nonlinear least-squares method. With reference to the identified horizontal stiffness values of the undamaged building (see Table 5.11), the damage severity of each element is calculated for every damage scenario. The identified results are presented in Table 5.13.

Table 5.11 Identified results of a frame structure with noise free

Element	$(EI)_i^{\mathrm{u}}$ $(N \cdot m^2)$	$(\hat{EI})_i^{\mathrm{u}}$ $(N \cdot m^2)$
1	491153082	491152980
2	491153082	491152940
3	283037369	283037340
4	283037369	283037560
5	360456415	360456380
6	360456415	360456700

Table 5.12 Details of damage scenarios of the frame structure

Scenario No.	Damage severity	Damage location
1	5%	3rd element
2	5%	2nd element
3	2%	6th element
4	5%	1st element
	10%	5th element
5	10%	2nd element
	10%	3rd element
	20%	5th element
6	5%	1st element
	10%	2nd element
	15%	4th element
	20%	5th element

Table 5.13 Identified damage severities (%) of the frame structure with noise free

Scenario No.	Element 1	Element 2	Element 3	Element 4	Element 5	Element 6
1	0	0	-5.00	0	0	0
2	0	-5.00	0	0	0	0
3	0	0	0	0	0	-2.00
4	-5.00	0	0	0	-10.00	0
5	0	-10.00	-10.00	0	-20.00	0
6	-5.00	-10.00	0	-15.00	-20.00	0

As seen from Table 5.13, the damage locations and damage severities of the frame structure can be accurately identified out for all these damage scenarios no matter whether the damage is in beam elements or in column elements. Even for the very small damage of 2%, the damage can also be accurately detected out. The identified damage severities in Table 5.13 are the same as the real values listed in Table 5.12 for every damage scenario. The sensitivity and accurateness of the proposed method are demonstrated in the time domain through the frame structures when measurement noise is not taken into account.

5.3.3.1 Damage detection on frame structures with measurement noise

The influence of measurement noise on the quality of damage detection results is then numerically investigated for the frame structure. Random white noises are added to both the measured displacement responses and the external acceleration excitation. The MNI of 5% and 15% are respectively investigated for the frame structure in this section. The identified stiffness parameters of the undamaged building with the effects of measurement noise are listed and compared with the real values in Table 5.14. The maximum relative error between the identified stiffness

parameters and the actual ones is only 0.26% when the MNI is of 5% and 1.42% when the MNI is of 15%.

Then the effects of measurement noise on the quality of the identified results of the six damage scenarios aforementioned are explored. For each damage scenario, the measured displacement responses and the external excitation are contaminated by white Gaussian noise. The MNI of 5% and 15% are considered respectively. The stiffness parameters of the damaged building for every damage scenarios are identified by utilizing the fourth-order moments of the contaminated responses and external excitation. With reference to the identified stiffness parameters of the undamaged building (see Table 5.14), the damage severity of each element is finally calculated for every damage scenario. The identified damage severities are respectively presented in Table 5.15 and Table 5.16 for the two levels of measurement noise. The identified results with consideration of the two kinds of measurement nose levels are also compared with the actual values in Figure 5.6.

Table 5.14 Identified results of the undamaged frame structure with noise

Element	Preset value	Identified value with MNI of 5%		Identified value with MNI of 15%	
	$(EI)_i^{\mathrm{u}}\ (N\cdot m^2)$	$(\hat{EI})_i^{\mathrm{u}}\ (N\cdot m^2)$	Relative Error	$(\hat{EI})_i^{\mathrm{u}}\ (N\cdot m^2)$	Relative Error
1	491153082	4916991.23	0.11%	491346309	0.04%
2	491153082	4924055.39	0.26%	490327349	0.17%
3	283037369	2825623.28	0.10%	282647167	0.14%
4	283037369	2826226.71	0.15%	284223829	0.42%
5	360456415	3599515.46	0.14%	359533793	0.26%
6	360456415	3612725.28	0.23%	365578356	1.42%

It can be seen from Figure 5.6 that when the MNI is of 5%, the damage locations of all the concerned damage scenarios can be accurately identified. The detected

damage severities are almost the same as the actual values. There is almost no positive falsity which identifies some intact structural elements as damaged elements. When the MNI is increased to 15%, small positive falsities are observed for some damage scenarios. However, the identified results are still satisfactory in view of such a high measurement noise level. The insensitiveness of the proposed method to measurement noise is manifested in the time domain.

Table 5.15 Identified damage severities of the frame structure with MNI of 5%

Scenario No.	Element 1	Element 2	Element 3	Element 4	Element 5	Element 6
1	-0.16	0	-4.92	-0.37	0	-0.08
2	-0.15	-4.70	0	-0.54	0	-0.31
3	-0.08	0	0	-1.04	0	-2.38
4	-5.09	-0.27	-0.08	0	-10.05	0
5	0	-10.08	-9.87	-0.60	-19.98	0
6	-5.06	-10.21	0	-15.24	-20.07	0

Table 5.16 Identified damage severities of the frame structure with MNI of 15%

Scenario No.	Element 1	Element 2	Element 3	Element 4	Element 5	Element 6
1	-0.55	0	-4.45	-2.22	0	-3.23
2	0	-7.18	0	-2.05	-0.07	-1.06
3	-0.22	-0.85	0	-1.98	0	-3.45
4	-6.83	0	-1.90	0	-10.58	-3.61
5	0	-9.79	-9.28	-2.85	-19.65	-2.71
6	-4.11	-13.25	-1.36	-15.51	-22.35	-0.70

In addition, the results identified in the time domain with the MNI of 15% are also compared with those identified in the frequency domain with the same level of measurement noise in Figure 5.7. It can be seen that the precision of the results identified in the time domain is similar with that of the results identified in the

frequency domain. The effectiveness and feasibility of the proposed method are demonstrated both in the frequency domain and in the time domain through the frame structure.

5.4 Numerical Investigation by Non-Gaussian Excitations

In this section, the robustness of the SMBDD method is demonstrated in the time domain through the aforementioned three-story shear building model by using non-Gaussian external excitations. Details of the shear building model can be found in Section 5.3.1. A random process with Log-normal distribution is simulated and utilized as an external excitation. Its magnitude is chosen such that the maximum absolute value of acceleration is 2.0 m/sec^2. The time duration of the simulated acceleration is 1000s and the sampling frequency is 256Hz. The time history and the probability density distribution of the random process are presented in Figure 5.8. It can be seen that the random process has highly skewed non-Gaussian probability distribution in comparison with the normal distribution.

The undamaged shear building and the four damage scenarios listed in Table 5.2, Scenarios 1, 3, 4 and 6, are firstly identified by the non-Gaussian external excitation without considering the effect of measurement noise. The fourth-order moments of the measured three story drifts of the undamaged building, $\hat{M}_{4i}^{u}$ ($i = 1,2,3$), and the identified horizontal stiffness values of the undamaged building, $\hat{k}_i^{u}$ ($i = 1,2,3$) are presented in Table 5.17. The identified stiffness parameters are identical to the real values when the effect of measurement noise is not taken into account. The high precision of the SMBDD method in the time domain is manifested by the

non-Gaussian external excitation. The identified results of the four damage scenarios without considering the measurement noise are presented in Table 5.18 and compared with the real values in Figure 5.8. The damage locations of the four damage scenarios are all accurately identified. The identified damage severities are exactly the same as the prescribed values.

Table 5.17 Identification results of the undamaged shear building in the time domain

Story	$\hat{M}_{4i}^{u}\ (m^4)$	$k_i^{u}\ (kN/m)$	$\hat{k}_i^{u}\ (kN/m)$
1	4.4704×10^{-19}	4728400	4728400
2	8.7034×10^{-15}	315230	315230
3	1.6937×10^{-14}	157610	157610

Then the effect of the measurement noise on the quality of identified results is explored in the time domain by the SMBDD method using the non-Gaussian external excitation. The measured displacement responses and the external excitation are all contaminated by white noise. The MNI of 15% is considered here. The identified stiffness parameters of the undamaged shear building are listed in Table 5.19. The maximum relative error between the identified stiffness parameters and the real values is only 1.91% even when the MNI is as high as 15%. The damage detection results of the four damage scenarios are presented in Figure 5.9 and Table 5.20. It can be seen from Figure 5.8 that the damage locations of the four scenarios can be accurately identified. The identified damage severities are very close to the real values. The sensitivity of the proposed method to structural damage and its stability to measurement noise are demonstrated in the time domain by utilizing the non-Gaussian external excitation.

Table 5.18 Identified results of damage scenarios of a three-story shear building in the time domain with noise free

Scenario	Story 1		Story 2		Story 3	
	μ (%)	$\hat{\mu}$ (%)	μ (%)	$\hat{\mu}$ (%)	μ (%)	$\hat{\mu}$ (%)
1	-5.00	-5.00	0.00	0.00	0.00	0.00
3	-10.00	-10.00	-5.00	-5.00	0.00	0.00
4	0.00	0.00	-20.00	-20.00	-10.00	-10.00
6	-5.00	-5.00	-10.00	-10.00	-20.00	-20.00

Table 5.19 Identified results of the undamaged shear building with MNI of 15%

Story	$\hat{M}_{4i}^{\,u}$ (m^4)	$k_i^{\,u}$ (kN/m)	$\hat{k}_i^{\,u}$ (kN/m)
1	5.4991×10^{-19}	4728400	4700622
2	9.8948×10^{-15}	315230	318342
3	2.6444×10^{-14}	157610	160616

Table 5.20 Identified results by colored noise ground excitation with MNI of 15%

Scenario	Story 1		Story 2		Story 3	
	μ (%)	$\hat{\mu}$ (%)	μ (%)	$\hat{\mu}$ (%)	μ (%)	$\hat{\mu}$ (%)
1	-5.00	-4.64	0.00	-0.28	0.00	0.00
3	-10.00	-10.75	-5.00	-6.49	0.00	-1.16
4	0.00	-0.48	-20.00	-20.21	-10.00	-10.09
6	-5.00	-6.17	-10.00	-10.80	-20.00	-20.38

5.5 Numerical Investigation by Non-stationary Excitations

In addition, non-stationary time histories are further adopted as external excitations of the three-story shear building model to identify structural damage by the SMBDD method in the time domain. The utilized non-stationary external excitation takes the form of

$$\ddot{x}_g(t) = \ddot{x}_{gG}(t) \bullet g(t) \tag{5.7}$$

in which $g(t)$ is a specified envelope or modulation function as shown in Figure 4 (a).

$$g(t) = \begin{cases} 0.0 & t < 0 \\ 2.5974[\exp(-0.2t) - \exp(-0.6t)] & t \geq 0 \end{cases} \tag{5.8}$$

$\ddot{x}_{gG}$ is the aforementioned Gaussian colored noise. The time history and probability density distribution of the simulated non-stationary external excitation are presented in Figure 5.10.

The undamaged shear building is first identified by the SMBDD method in the time domain using the non-stationary external excitation without considering the effect of measurement noise. The identified stiffness parameters are 4728400 kN/m, 315230 kN/m and 157610 kN/m, respectively, which are the same as the real values. When the MNI is 15%, the identified stiffness parameters are 4724838 kN/m, 315029 kN/m and 157493 kN/m, respectively. The maximum relative error of all the identified horizontal stiffness values in comparison with the actual ones is only 0.08%. The measurement noise has no much effect on the identified horizontal stiffness values by using the proposed method in the time domain.

Then scenarios 1, 3, 4 and 6 of the shear building structure are investigated. The identified results of the damage shear building structure under non-stationary external excitations are presented in Table 21, in which $\hat{\mu}$ stands for the identified results without considering the effect of measurement noise and $\hat{\mu}_n$ stands for the identified results when the MNI is 15%. In addition, the identified results in Table 21 are also more clearly presented in Figures 5.11 and compared with the corresponding real values. It can be seen from Table 21 that the identified damage severities of the

four damage scenarios are the same as the actual damage severities when the effect of measurement noise is not taken into account. As seen from Figure 5.11, the damage locations can be accurately detected out when the external excitations are non-stationary. Furthermore, the identified results have no much difference with the actual values even when the MNI is as high as 15%. The sensitivity of the SMBDD method to structural local damage, its insensitivity to measurement noise and its applicability to non-stationary external excitations are demonstrated.

Table 5.21 Identified results using non-stationary excitations

Scenario	Story 1		Story 2		Story 3	
	$\hat{\mu}$ (%)	$\hat{\mu}_n$ (%)	$\hat{\mu}$ (%)	$\hat{\mu}_n$ (%)	$\hat{\mu}$ (%)	$\hat{\mu}_n$ (%)
1	-5.00	-5.00	0.00	-0.01	0.00	0.00
2	-10.00	-10.04	-5.00	-5.04	0.00	-0.03
3	0.00	0.00	-20.00	-19.53	-10.00	-9.60
4	-5.00	-4.36	-10.00	-9.57	-20.00	-19.54

5.6 Conclusions

The algorithm of the SMBDD method is proposed in the time domain in this chapter. The effectiveness and feasibility of the SMBDD method are numerically investigated in the time domain by using Gaussian, non-Gaussian and non-stationary external excitations. The problem of incomplete measurements and the effect of measurement noise on the quality of identified results are considered in the time domain by the proposed method.

Firstly, the feasibility of the SMBDD method is explored in the time domain by using Gaussian external excitations. The three-story shear building is first

investigated. Various damage scenarios with different damage locations and different damage severities are examined. Numerical results show that the damage locations of these damage scenarios are accurately detected and the identified damage severities are the same as the real values when the effect of measurement noise is not considered. The effect of measurement noise is then explored by contaminating measured dynamic responses and external excitations. Even when the measurement noise intensity is as high as 15%, the damage locations and damage severities of various damage scenarios are still accurately identified in the time domain by the SMBDD method.

Then a 20-story high-rise building with height $h_T = 80\,\text{m}$ is employed to investigate the feasibility and effectiveness of the SMBDD method in the time domain with consideration of the incomplete measurements. In the numerical investigation, only the horizontal displacement responses of the high-rise building are measured and utilized to detect damage, which is only half of the number of the degrees of freedom. A frame structure with incomplete measurements is also numerically investigated by the proposed method in the time domain using the Gaussian excitations. The damage locations of various damage scenarios of the high-rise building and the frame structure are accurately determined. And the identified damage severities are identical to the real values when the effect of measurement noise is not taken into account. The higher quality of analyzed results is obtained in the time domain by the proposed method when the effect of measurement noise is not taken into account. However, there is no much change or apparent improvement in the quality of the identified results by the SMBDD method in the time domain compared with those obtained by the proposed method in the frequency domain when the effect of

measurement noise is considered.

Finally, the feasibility and effectiveness of the SMBDD method in the time domain are investigated by non-Gaussian and non-stationary external excitations. Several damage scenarios of the shear building structure are explored. Numerical analysis results show that the damage locations of the various damage scenarios are accurately determined and the identified damage severities are the same as the real values when the effect of measurement noise is not considered. The stability of the proposed method in the time domain to the measurement noise is also demonstrated by using the non-Gaussian and non-stationary external excitations. Even when the MNI is as high as 15%, the damage locations can still be accurately detected and the identified damage severities are very close to the real values.

In conclusion, the numerical results of various damage scenarios of different structures demonstrate that the proposed method is sensitive to local structural damage and insensitive to measurement noise in the time domain. Gaussian, non-Gaussian and non-stationary external excitations can be utilized in the time domain by the SMBDD method to detect structural damage. However, higher requirement is put forward for the optimization method used by the SMBDD method in the time domain than in the frequency domain. In addition, before this method can be applied to real structures the experimental investigation is necessary. The next chapter will present an experimental investigation on this method both in the frequency domain and in the time domain.

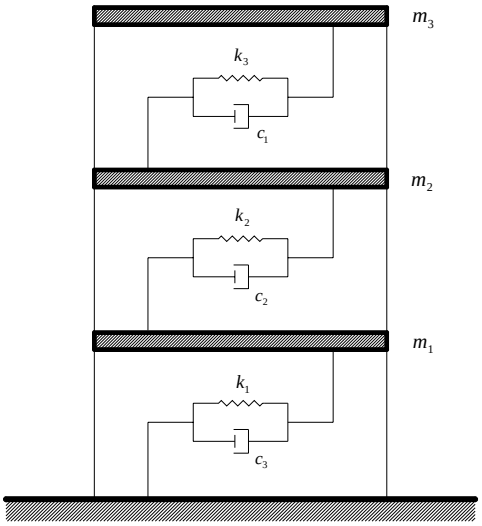

Figure 5.1 Three-story shear building model

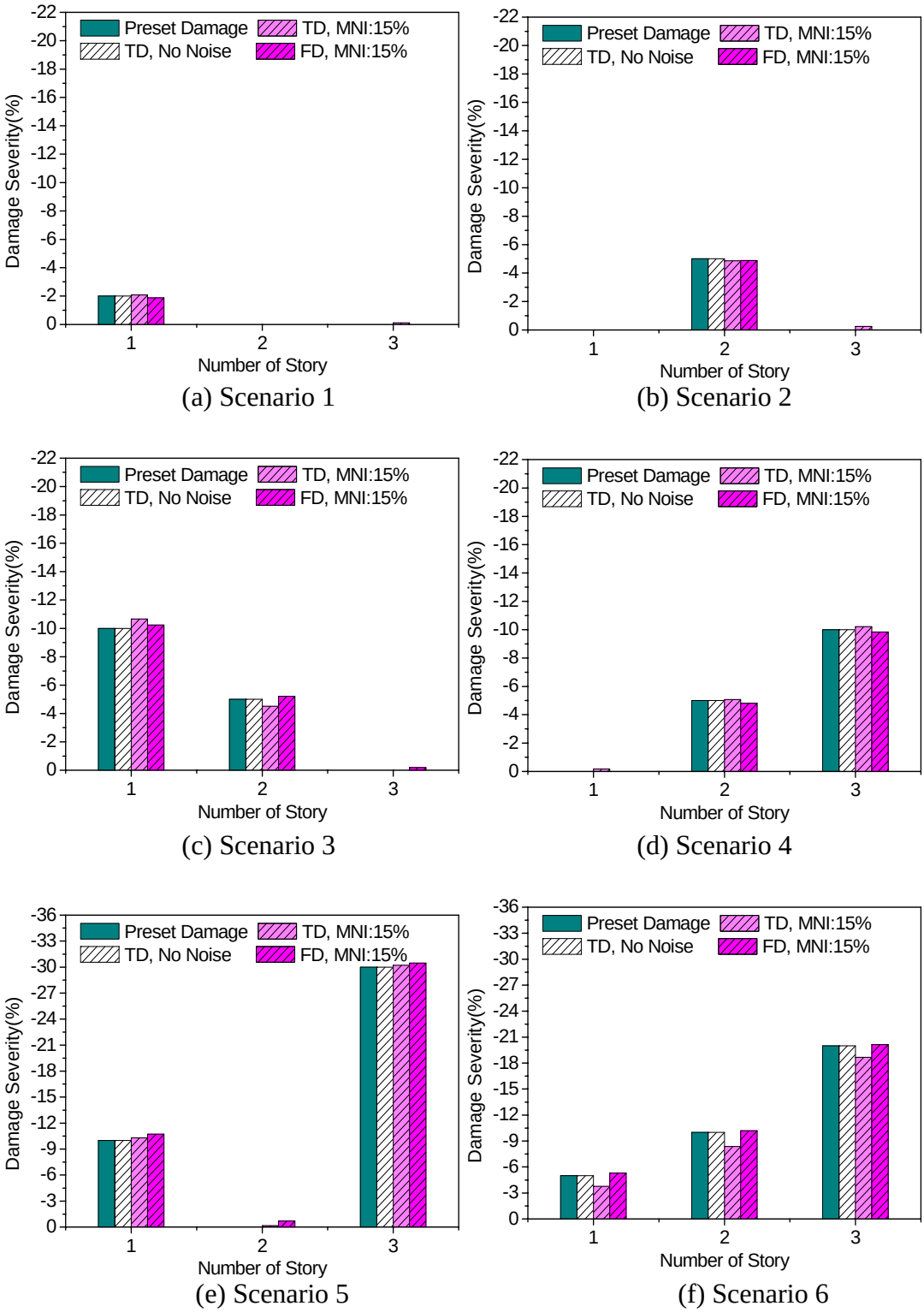

Figure 5.2 Comparison of the identified results of the shear buildings (TD: time domain, FD: frequency domain, MNI: measurement noise intensity): (a) Scenario 1, (b) Scenario 2, (c) Scenario 3, (d) Scenario 4, (e) Scenario 5, (f) Scenario 6

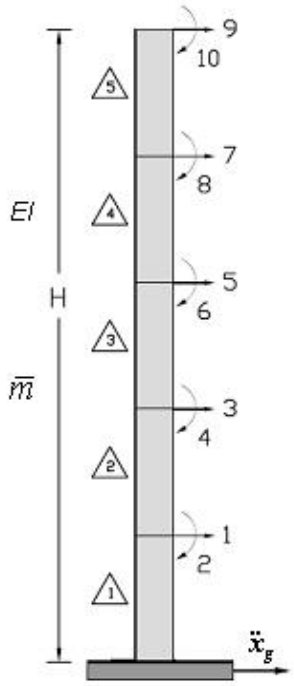

Figure 5.3 Configuration of a high-rise building structure

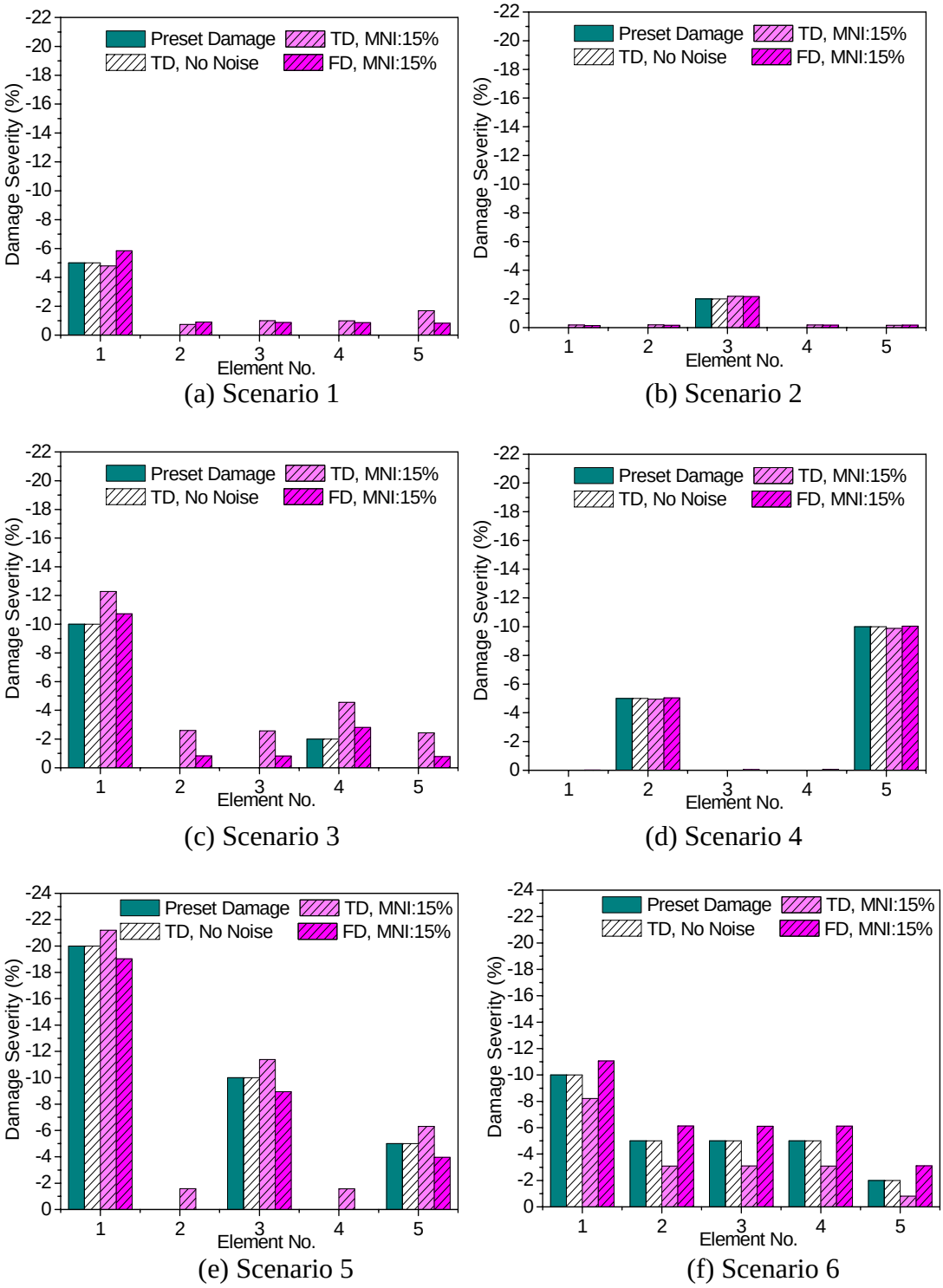

(a) Scenario 1 (b) Scenario 2

(c) Scenario 3 (d) Scenario 4

(e) Scenario 5 (f) Scenario 6

Figure 5.4 Comparison of the identified results of the tall buildings (TD: time domain; FD: frequency domain; MNI: measurement noise intensity) : (a) Scenario 1, (b) Scenario 2, (c) Scenario 3, (d) Scenario 4, (e) Scenario 5, (f) Scenario 6

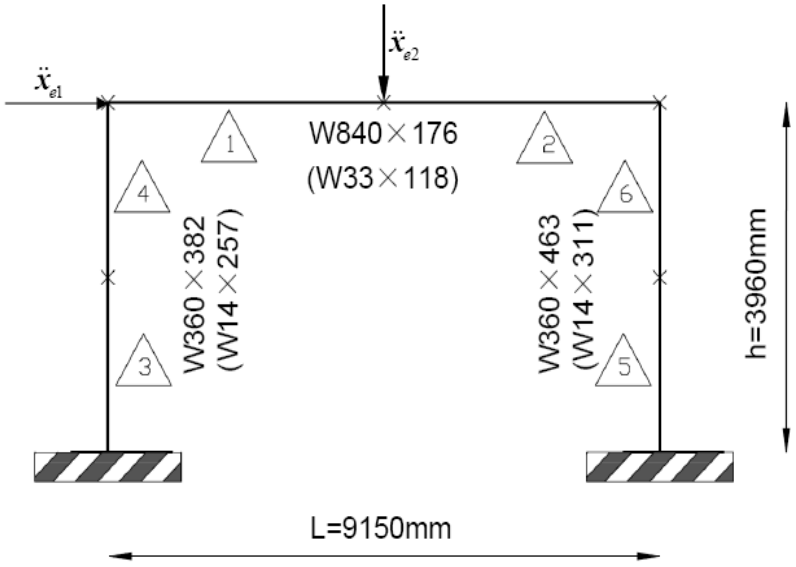

Figure 5.5 Configuration of a steel frame structure

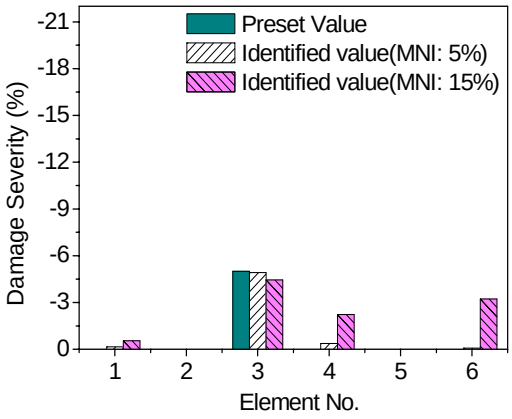

(a) Scenario 1

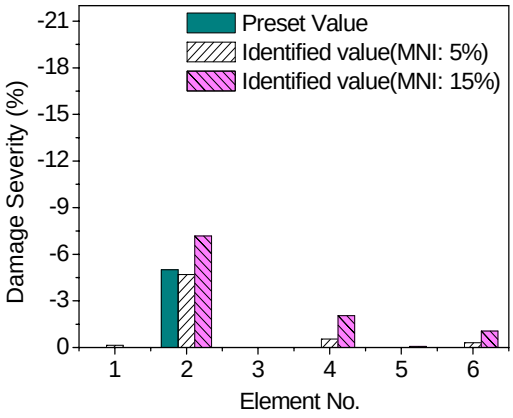

(b) Scenario 2

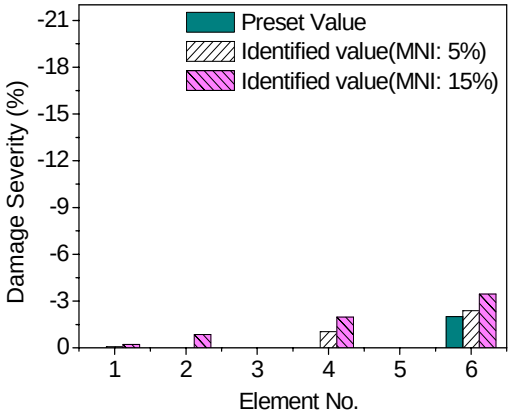

(c) Scenario 3

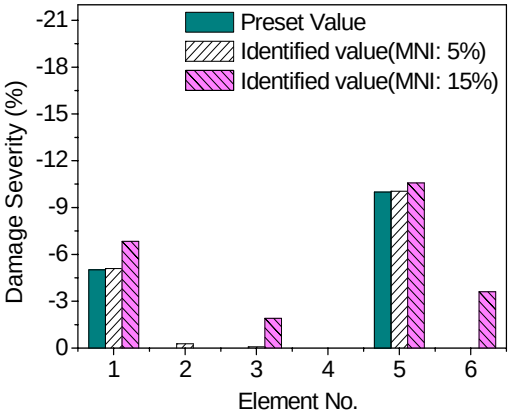

(d) Scenario 4

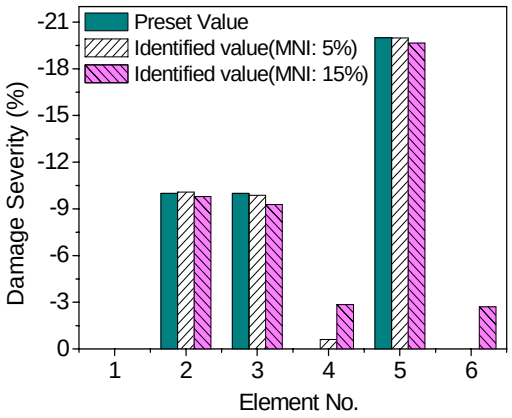

(e) Scenario 5

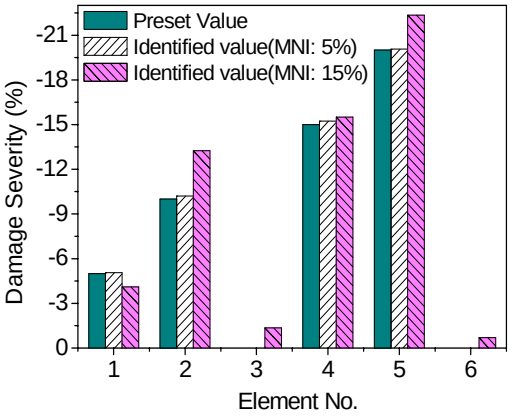

(f) Scenario 6

Figure 5.6 Identified results of a frame structure in the time domain: (a) Scenario 1, (b) Scenario 2, (c) Scenario 3, (d) Scenario 4, (e) Scenario 5, (f) Scenario 6

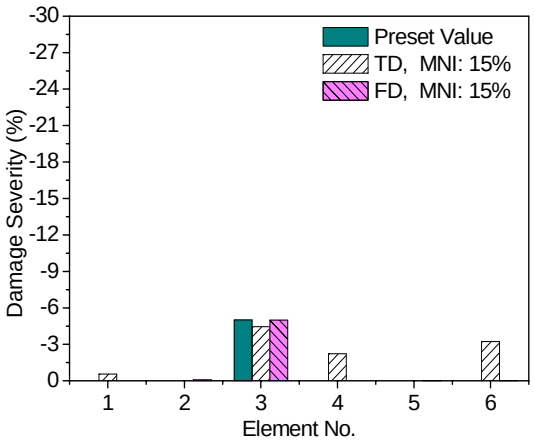

(a) Scenario 1

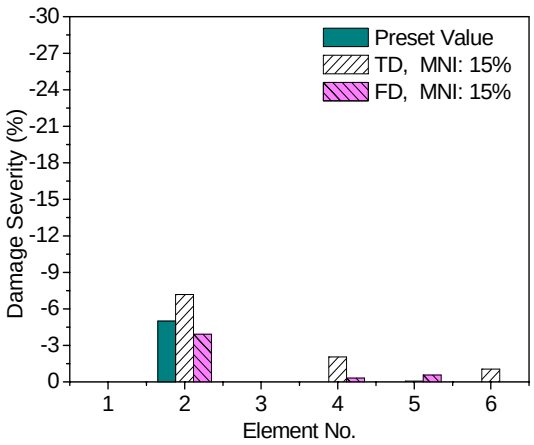

(b) Scenario 2

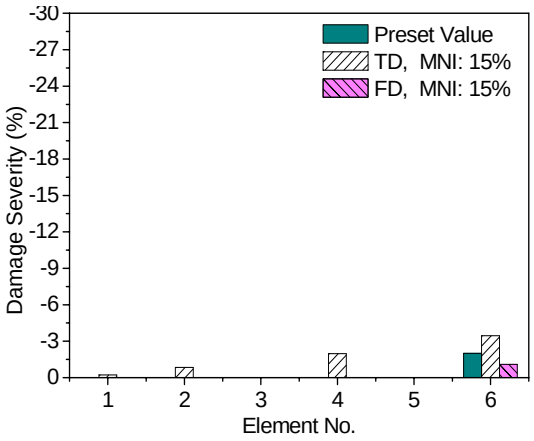

(c) Scenario 3

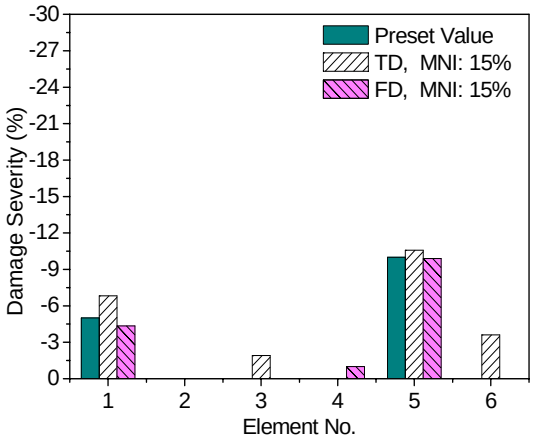

(d) Scenario 4

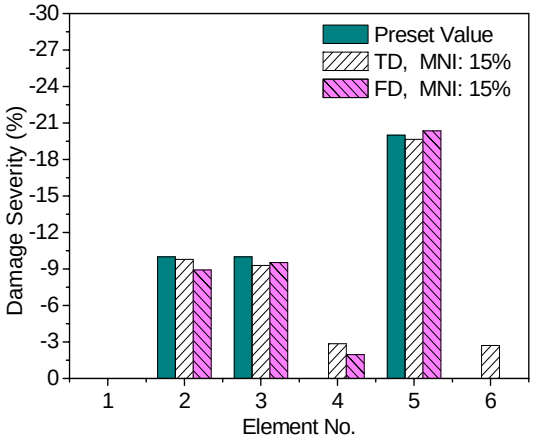

(e) Scenario 5

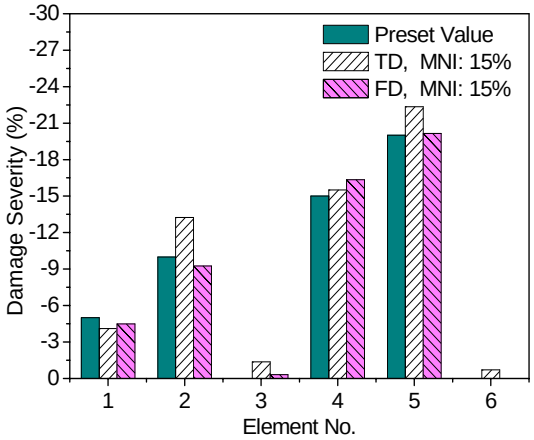

(f) Scenario 6

Figure 5.7 Comparison of the identified results of the frame structures in the time domain with those in the frequency domain with the same MNI of 15%: (a) Scenario 1, (b) Scenario 2, (c) Scenario 3, (d) Scenario 4, (e) Scenario 5, (f) Scenario 6

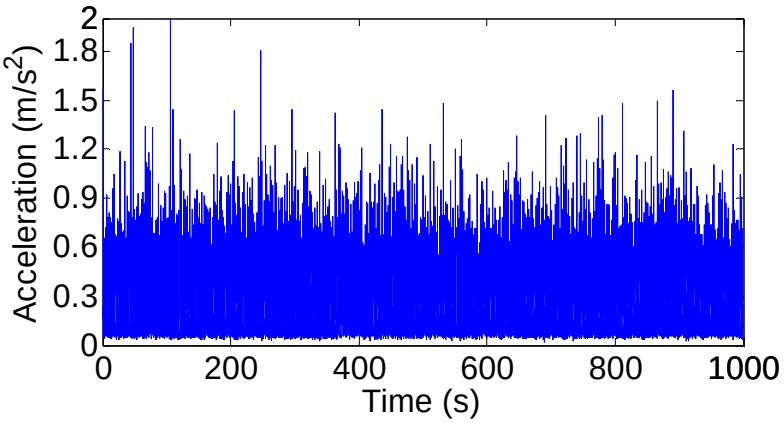

(a) time history

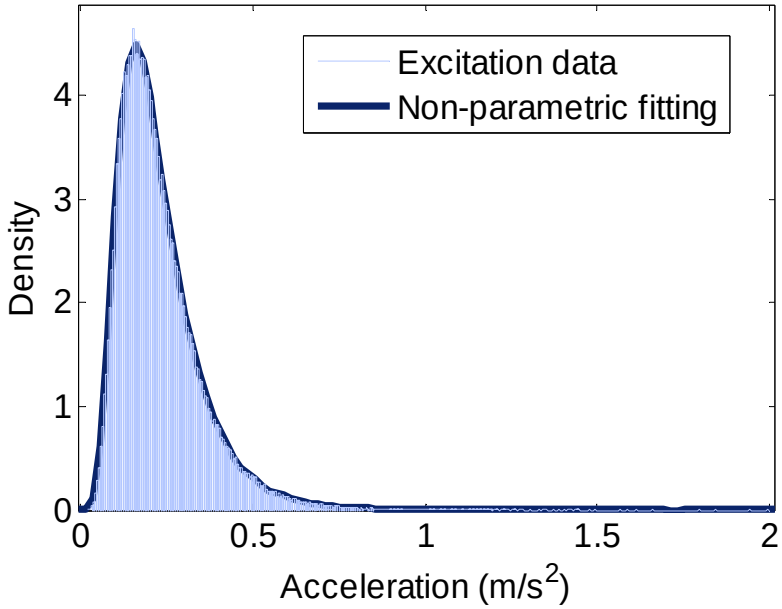

(b) probability density distribution

Figure 5.8 A simulated non-Gaussian external excitation: (a) time history, (b) probability density distribution

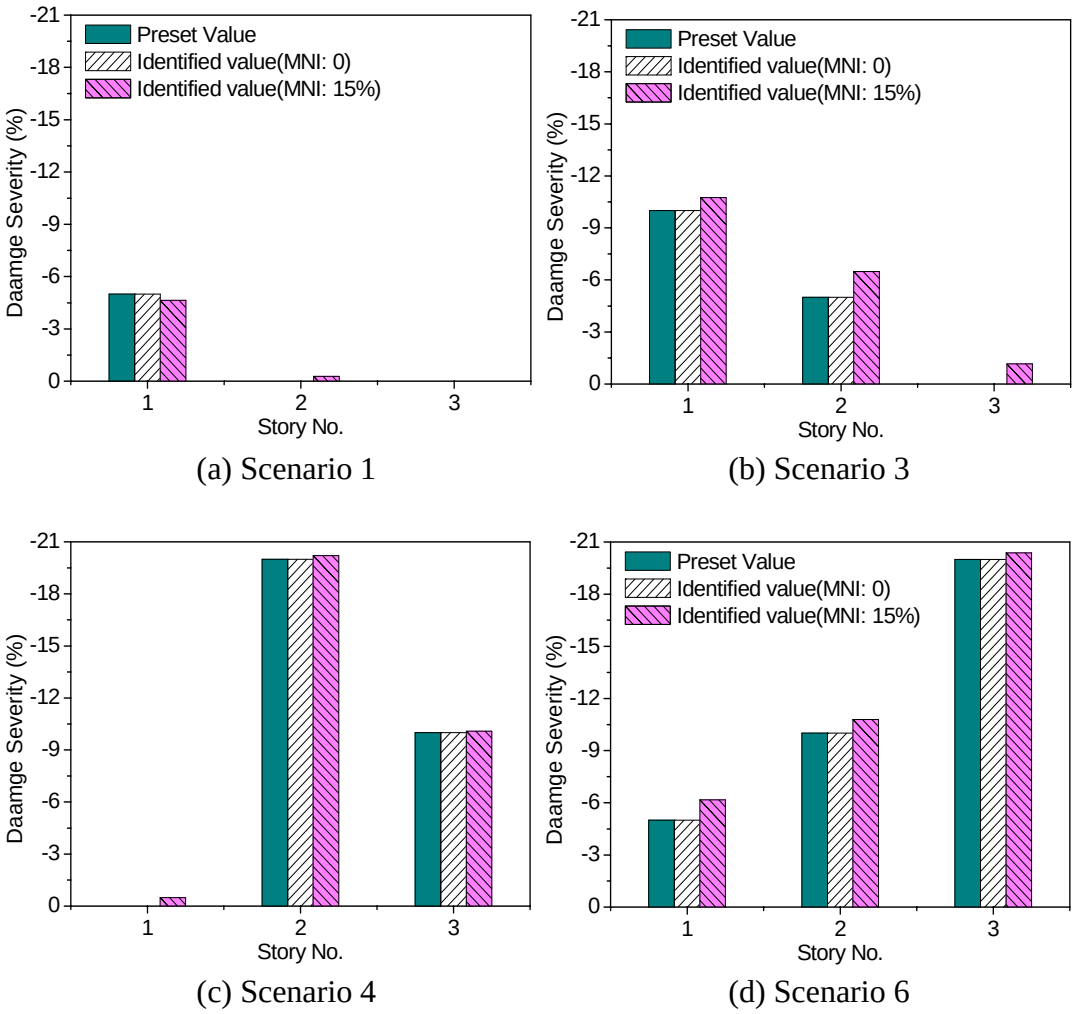

(a) Scenario 1 (b) Scenario 3

(c) Scenario 4 (d) Scenario 6

Figure 5.9 Identified results of the shear building by non-Gaussian excitation: (a) Scenario 1, (b) Scenario 3, (c) Scenario 4, (d) Scenario 6

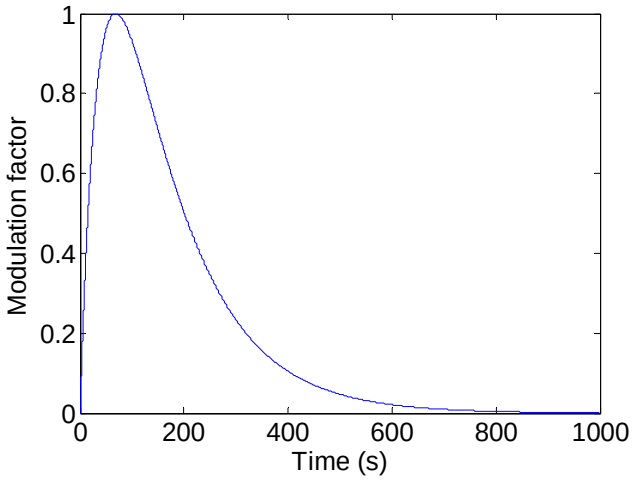

(a) modulation function

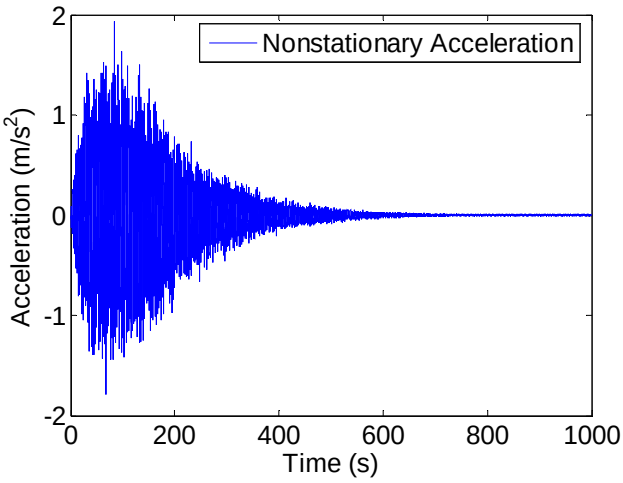

(b) time history

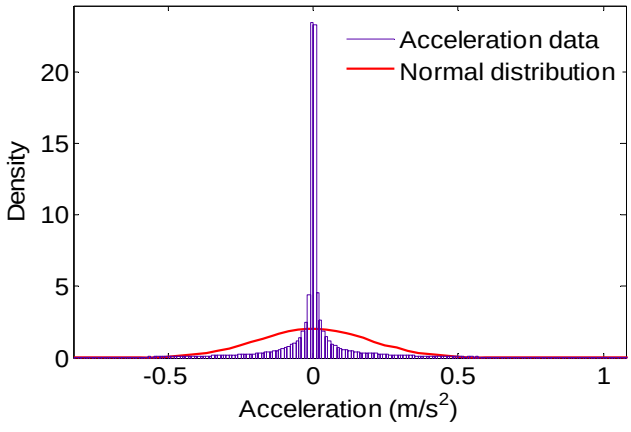

(c) probability density distribution

Figure 5.10 A non-stationary excitation: (a) modulation function, (b) time history, (c) probability density distribution

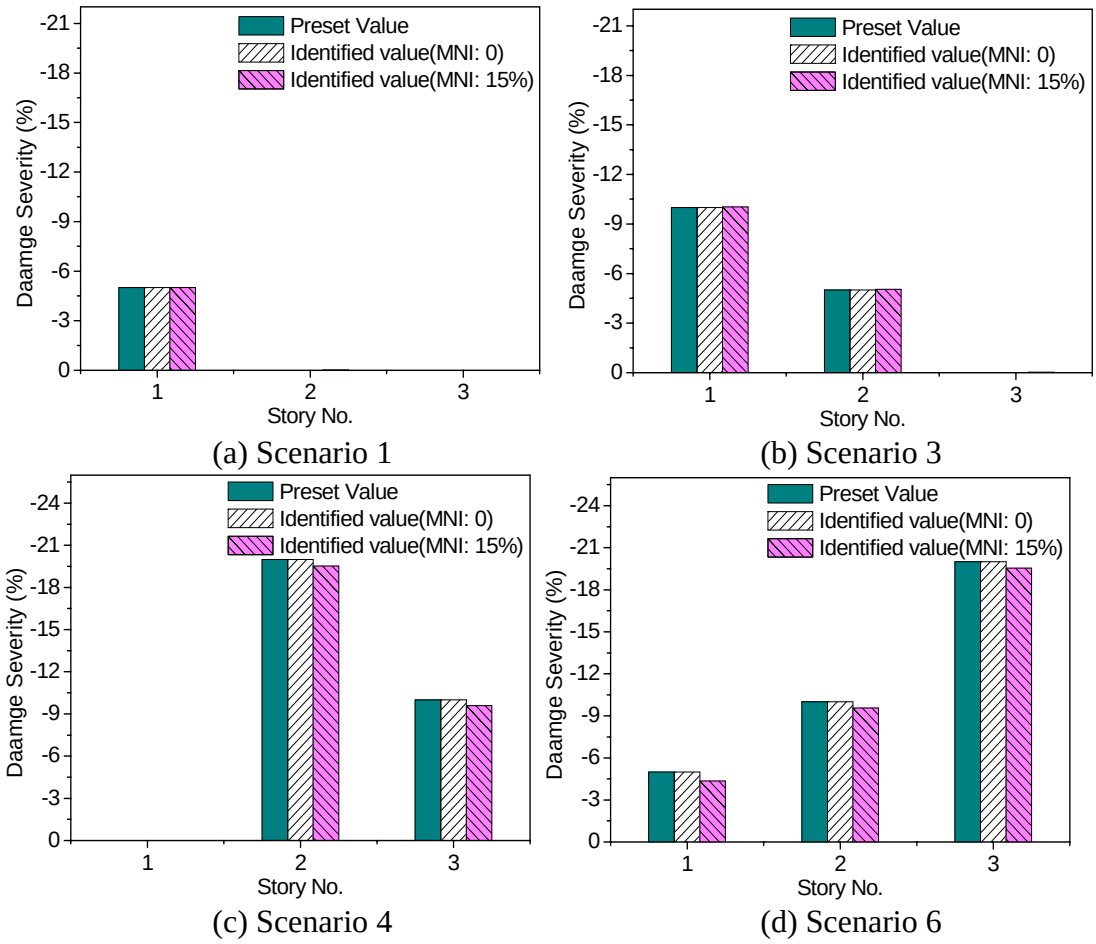

Figure 5.11 Identified results of the shear building by non-stationary excitation: (a) Scenario 1, (b) Scenario 3, (c) Scenario 4, (d) Scenario 6

CHAPTER 6

EXPERIMENTAL INVESTIGATION ON STATISTICAL MOMENT-BASED DAMAGE DETECTION METHOD

6.1 Introduction

A new structural damage detection method based on the statistical moments of dynamic responses of a structure has been proposed in both the frequency domain and the time domain, and extensive numerical studies have been performed in the previous three chapters. The numerical results demonstrated that the proposed method is sensitive to local structural damage and insensitive to measurement noise, and it can identify both location and severity of structural stiffness reduction of a building satisfactorily. Nevertheless, before this method can be applied to real structures the experimental investigation is necessary. This chapter therefore presents an experimental investigation on this method.

Three shear building models were manufactured and mounted on a shaking table. Shaking table tests were firstly conducted on the undamaged building models. The displacement and acceleration responses of the building model at each floor were recorded by laser displacement transducers and accelerometers, respectively. The statistical moments of story drifts were calculated from the measured displacement responses. The first two damping ratios of the undamaged models were estimated by applying the Hilbert transform method to the measured acceleration responses. Afterwards, various damage scenarios with different damage locations and different

damage severities were inflicted on the shear building models step by step. For each damaged building model with a given damage scenario, the shaking table tests were performed in a way similar to that for the undamaged building model.

Then, the data of the shaking table tests were analyzed by the SMBDD method both in the frequency domain and in the time domain. Firstly, the calculated statistical moments and the estimated damping ratios as well as the recorded ground excitation were used as inputs to identify the lateral stiffness values of the undamaged building models in the frequency domain. The lateral stiffness values of the damaged model were obtained accordingly and compared with those of the corresponding undamaged model, from which the damage locations and damage severities were identified by the proposed method in the frequency domain. The identified damage locations and severities were finally compared with the theoretical values to assess the accuracy of the proposed method. Moreover, the lateral stiffness values of the undamaged models and the damaged models were calculated by the proposed method but in the time domain. The damage locations and damage severities were then identified by the proposed method in the time domain. The results demonstrate that the damage locations and their corresponding damage severity values of all the damage scenarios were satisfactorily identified by the proposed method both in the frequency domain and in the time domain. They again demonstrated the reliability and effectiveness of the SMBDD method.

6.2 Experimental Arrangement

To assess the feasibility and accuracy of the proposed damage detection method, an experimental investigation program was initiated and implemented. Three building models were manufactured and mounted on a shaking table. Shaking table tests were conducted on the undamaged building models first. Single and multi damage scenarios of different damage locations and severities were then created in the building models step by step. The damaged building models were finally subjected to the shaking table tests. By comparing undamaged with damaged case, the damage locations and damage severities were identified and compared with the preset theoretical values to assess the accuracy of the proposed method. In this experiment, two band-limited white noise time histories and two colored noise time histories of 1000s duration and a frequency range from 0.5 to 40 Hz were numerically generated using a random process simulation method (Shinozuka et al., 1972). They were input, one by one, into the control system of the shaking table with an appropriate scaling factor for amplitude to generate the expected ground excitations to the building models. Different amplitude scaling factors were utilized for the building models of different damage scenarios to avoid plastic deformation and structural nonlinearity. Since this study intends to demonstrate the feasibility and accuracy of the proposed method through the comparison of stiffness identified from the two cases, no particular length and time scales were followed by the experiment.

6.2.1. Building models

Three shear building models of three stories (the building model 1, 2 and 3) were designed and constructed as shown in Figure 6.1. Each three-story building model consisted of mainly three steel beams of 394 (length)$\times$50 (width) $\times$ 30 (thickness)

mm and two identical columns of a 50 x 3 mm cross section and a 900 mm length. The nominal story height is 300mm. The three beams and two columns were tightly connected by using six steel blocks (50 x 30 x 12 mm) and twenty four screws to form connections as rigid as possible. The building model was then fixed on a steel base plate of 15 mm thickness through four angle bars (50 x 50 x 5 mm) and eight screws. For each support, the inner two angle bars were welded on the steel plate to form rigid support and the outer two ones were fixed on the steel plate by screws. The steel base plate was in turn bolted firmly on the shaking table using a total of eight bolts of high tensile strength. All the columns and beams were made of high strength steel of 435 MPa yield stress and 200 GPa modulus of elasticity. Each steel beam could be regarded as a rigid beam in the horizontal direction, leading to a shear-type building model. An additional mass of about 10 kg was placed on each beam of the building model 1 using bolts and nuts to change the building mass. The lumped mass of each story of a building model was determined through the measurement and summation of the weights of the corresponding beam, connection accessories and part of the column. Without additional masses, the mass was 5.48 kg, 5.48 kg and 5.15 kg for the first, second and third floor of the building model 2 and 3, respectively. With additional masses, the corresponding mass was 15.41 kg, 15.63 kg and 15.26 kg for the building model 1. To simulate inherent energy dissipation capacity of a real structure, a shear-type viscous damper was installed in the first story of all the building models as shown in Figure 6.2.

6.2.2. Damage scenarios

To simulate building damage, the column width of each building model was reduced from both sides at a designated story. Two kinds of column width reductions were

used in this experiment: 2.5 mm reduction from each side of the column to lead to a 10% reduction of the column width, and 5 mm reduction from each side of the column to yield a 20% reduction of the column width. Figures 6.3a-6.3c show respectively the damage scenarios of the building model at the first story with 20% column width reduction, the building model at the second story with 20% column width reduction, and the building model at the third story with 10% column width reduction. A total of eight damage scenarios were designed in this experimental investigation and listed in Table 6.1. The scenarios 1, 2, 3 and 4 represent single damage at either first or second story of the building model. The scenarios 5, 6 and 7 incorporate damage at two different stories while the scenario 8 contains damage at all three stories. The building model 1 was used in the sequence of the scenarios 1, 2 and 5. The building model 2 was used in the sequence of the scenarios 3, 4 and 6 whereas the building model 3 was used in the sequence of the scenarios 7 and 8.

To provide a basis for the assessment of the proposed damage detection method, the theoretical value of damage severity for a given damage scenario was computed using the flexibility method and the principle of virtual work. For a column with a reduced width in the given story, the lateral stiffness values before and after damage are denoted as k^u and k^d respectively, and the theoretical damage severity μ is expressed as follows.

$$\mu = \frac{k^u - k^d}{k^u} \times 100\% \tag{6.1}$$

where k^u is the summation of the lateral stiffness of the undamaged columns in the given story of the building model and k^d is the same quantity but for the building model with the damaged columns. The computed theoretical damage severities for

various damage scenarios are presented in Table 6.1. It is noted that the so-obtained theoretical values of damage severity are only approximations of the real ones of building models but they can be taken as references for comparison with the damage severity identified from the experiments.

Table 6.1 Details of damage scenarios

Scenario No.	Building Model	Ground Excitation	Location of Damage	One-side Width Reduction (mm)	Theoretical damage severity (%)
1	1	W. N.	Story 1	2.5	5.36
2	1	W. N. C. N.	Story 1	5.0	11.26
3	2	C. N.	Story 2	2.5	7.45
4	2	W. N. C. N.	Story 2	5.0	15.33
5	1	W. N.	Story 1	5.0	11.26
			Story 3	2.5	7.45
6	2	W. N. C. N.	Story 2	5.0	15.33
			Story 3	2.5	7.45
7	3	C. N.	Story 1	5.0	11.26
			Story 2	2.5	7.45
8	3	C. N.	Story 1	5.0	11.26
			Story 2	2.5	7.45
			Story 3	5.0	15.33

Note: W.N. and C.N. respectively stand for white noise and colored noise excitation

6.2.3. Experimental equipment and data acquisition

The unidirectional shake table at the Hong Kong Polytechnic University used in this study was manufactured by the MTS Corporation with a dimension of 3 x 3 m in plane (MTS 469DU). The maximum acceleration of the shaking table is ±1 g with

the maximum proof specimen mass of 10 tons, where g is the acceleration due to gravity in m/s^2. The frequency of the input wave ranges from 0.1 to 200 Hz. The horizontal acceleration and displacement responses of the building model at each floor in the x-direction were measured using accelerometers and laser displacement transducers as shown in Figure 6.2. The measured acceleration responses from B&K 4370 accelerometers were used to estimate the first two modal damping ratios of the building model. One more B&K 4370 accelerometer was installed on the base plate of the building model to measure the acceleration in the x-direction as the ground motion. Laser displacement transducers with a maximum range of 100 mm and a resolution of ±0.01 mm were used to measure the absolute displacements of each floor of the building model as well as the shake table. The 32 channel data acquisition system was used to acquire the data during the shaking table tests. The sampling rate was set as 500 samples per second.

6.2.4. Experiment procedure

In the stage 1, the building models 1 and 2 without any damage were mounted on the shake table for simultaneous tests. The two white noise and two colored noise time histories of ground motion randomly generated were input to the shake table to excite the two undamaged models. For each shaking table test of the building models, the fourth-order statistical moment vectors of story drift were computed based on the absolute displacement responses measured from the laser displacement transducers. The first two modal damping ratios of each building model were identified based on the acceleration responses measured from the accelerometers using the Hilbert-transform (HT) method in conjunction with the random decrement technique (RDT) (Yang et al.,1999, Xu et al., 2003). The measured statistical moment vectors, the

estimated masses and damping ratios and the recorded ground motion were used as inputs to identify the lateral stiffness values of the undamaged building models using the proposed method.

In the stage 2, the shake table tests were performed on the building model 1 in the sequence of the scenarios 1 (white noise), 2 (white noise and colored noise) and 5 (white noise) and then on the building model 2 in the sequence of the scenarios 3 (colored noise), 4 (white noise and colored noise), and 6 (white noise and colored noise) (see Table 6.1). Based on the measurement results from each shake table test and following the same procedure as used in the stage 1, the lateral stiffness values of the damaged building models for a given damage scenario could be identified. The identified lateral stiffness of the damaged building model was then compared with that of the corresponding undamaged building model. The damage location and damage severity of the building model could be found. The results were then compared with the aforementioned theoretical values to assess the feasibility and accuracy of the proposed damage detection method.

In the stage 3, the shake table tests were first conducted on the undamaged building model 3 and then on the damaged building model 3 in the sequence of the scenarios 7 (colored noise) and 8 (colored noise). Based on the measurement results from the shake table tests and following the same procedure as used in the stages 1 and 2, the damage location and damage severity of the building model 3 could be found and compared with the theoretical values.

6.3 Experimental Analysis in Frequency Domain

The experimental data were analyzed by the SMBDD method in the frequency domain in this section at first. The time histories of ground motions were studied and their power spectral density functions were estimated and prepared for the following damage identification. Then, the first two modal damping ratios of a building model for each shaking table test were estimated by applying the HT method in conjunction with the RDT. Finally, the power spectral density functions of the ground motions and the recorded building responses as well as the identified structural damping ratios were used to identify damage locations and severities using the SMBDD method in the frequency domain. The identified damage locations and severities were compared with the theoretical values.

6.3.1. Ground motions

In this experiment, two band-limited white noise time histories of a 5 m/s^2 peak ground acceleration (PGA) and two colored noise time histories of a 2 m/s^2 PGA were randomly generated within a frequency range from 0.5 to 40 Hz and for 1000s duration. They were input as scheduled into the control system of the shaking table to generate the expected ground excitation to the building model with an amplitude scaling factor of 0.75, 0.5, and 0.3 for the white noise ground motions and 0.5 for the colored noise ground motions. The selection of the amplitude scaling factor depends on the building model and the damage scenario concerned. Figures 6.4 and 6.5 present the simulated and measured time histories and power spectral density functions of a white noise ground motion and a colored noise ground motion respectively. It can be seen that the measured time histories and power spectral density functions match the simulated ones in general, but the spectral amplitude of

the white noise ground motion is not ideally constant. Furthermore, the background noise of the experimental site was measured by accelerometers with the shake table being closed. The background noise intensity ranged from about 8% to 10% of the PGA, a high level of background noise which may make it difficult to identify damage location of a structure by other detection methods (Alvandi et al., 2006).

6.3.2. Estimation of damping ratios

The first two modal damping ratios of a building model were estimated by applying the HT method in conjunction with the RDT to the structural acceleration responses measured from the accelerometers. The details of the identification procedure used for structural damping ratio could be found in the literature (Yang et al., 1999, Xu et al., 2003). The identified first two modal damping ratios for the three undamaged building models under either white noise excitations or colored noise excitations are listed in Table 6.2.

It can be seen that the structural damping ratio varies within a certain range for the three building models due to various uncertainties. Different excitations of different intensities may cause slightly different damping ratios even for the same building model. The averaged damping ratio is suggested to be used for the subsequent damage detection. The same procedure was applied to the damaged building models to estimate their modal damping ratios.

Table 6.2 Identified structural damping ratios

Test No.	Building Model	Ground Excitation	GPA(m/s^2)	$\hat{\xi}_1$	$\hat{\xi}_2$
1	1	W.N. 1	4.11	0.0169	0.0134
2	1	W.N. 2	3.96	0.0133	0.0112
3	1	C.N. 1	1.01	0.0128	0.0112
4	1	C.N. 2	1.19	0.0136	0.0128
5	2	W.N. 1	4.11	0.0100	0.0092
6	2	W.N. 2	3.96	0.0091	0.0082
7	2	C.N. 1	1.01	0.0076	0.0090
8	2	C.N. 2	1.19	0.0081	0.0084
9	3	C.N. 1	0.99	0.0113	0.0079
10	3	C.N. 2	1.11	0.0105	0.0069

6.3.3. Stiffness identification of undamaged building models

The averaged first two modal damping ratios for the three building models are listed in Table 6.3 for different ground excitations. It can be seen that the modal damping ratio ranges from 0.74% to 1.51%. The averaged modal damping ratios, the measured statistical moment vectors, the estimated masses, and the recorded ground motion were used as inputs to identify the lateral stiffness values of the undamaged building models using the proposed method. The identified results are listed in Table 6.3. It can be seen that the identified lateral stiffness values from the two separate tests using either white noise or colored noise ground excitation are very close to each other. The mean values of identified stiffness vectors of the building model 1 are [45592, 26128, 24574] N/m and [46580, 26772, 24157] N/m for the white noise excitation and the colored noise excitation, respectively. The relative difference of stiffness vectors of the building model 1 identified from the two cases is [2.48%, 2.78%, 1.41%], which indicates that the effect of the type of ground excitation on the

identified stiffness is small. For the building model 2, the mean values of identified stiffness vectors are [40149, 23864, 23236] N/m and [40650, 24110, 23898] N/m for the white noise excitation and the colored noise excitation, respectively. The relative difference of stiffness vectors identified from the two cases is [1.25%, 1.03%, 2.85%]. The small difference of identified stiffness implies some degree of feasibility of the statistical moment-based damage detection method. For the building model 3, the mean value of identified stiffness vector is [37379, 23232, 24347] N/m.

Table 6.3 Identified results of undamaged building models in the frequency domain

Building Model	**Ground Excitation**	**Mean Damping Ratio**		**Identified Stiffness** (N/m)		
		$\hat{\xi}_1$	$\hat{\xi}_2$	$\hat{k}_1$	$\hat{k}_2$	$\hat{k}_3$
1	W.N. 1	0.0151	0.0123	45592	26120	24485
	W.N. 2			45591	26136	24663
	C.N. 1	0.0132	0.0120	46443	26694	23986
	C.N. 2			46717	26849	24327
2	W.N. 1	0.0096	0.0087	40297	23999	23210
	W.N. 2			40002	23729	23262
	C.N. 1	0.0079	0.0087	40746	24101	23930
	C.N. 2			40554	24119	23866
3	C.N. 1	0.0109	0.0074	37047	23080	24088
	C.N. 2			37710	23383	24605

6.3.4. Damage detection results-white noise excitation

A total of five damage scenarios (see Table 6.4) were investigated on the building models 1 and 2 with white noise excitation input. The scenario 1 and scenario 2 have the single damage in the first story of the building model 1 but with different damage severities. The theoretical damage severity of the scenario 1 is 5.36% while that of the scenario 2 is 11.26%. In the scenario 5, a dual damage scenario was inflicted on

the building model 1 with the damage in the first and third story, and the theoretical damage severity is respectively 11.26% and 7.45%. The scenario 4 has the single damage in the second story of the building model 2 with a theoretical damage severity of 15.33% while the scenario 6 investigated the dual damage of the building model 2 in the second and third stories with the theoretical damage severities of 15.33% and 7.45%, respectively.

Table 6.4 Identified stiffness values of damaged building models under W.N.excitation (N/m) in the frequency domain

Scenario	**Building Model**	**Ground Excitation**	**Mean Damping Ratio**		**Identified Stiffness**		
			$\hat{\xi}_1$	$\hat{\xi}_2$	$\hat{k}_1$	$\hat{k}_2$	$\hat{k}_3$
1	1	W.N. 1	0.0155	0.0132	42815	25647	24574
		W.N. 2			43669	26128	24574
2	1	W.N. 1	0.0168	0.0141	40341	25986	24663
		W.N. 2			40670	26136	24663
4	2	W.N. 1	0.0077	0.0098	40149	19970	22993
		W.N. 2			40149	20039	23056
5	1	W.N. 1	0.0146	0.0129	39883	26128	22257
		W.N. 2			39062	26128	21812
6	2	W.N. 1	0.0095	0.0085	40149	19287	21942
		W.N. 2			40149	18943	21539

The first two modal damping ratios of either the building model 1 or the building model 2 were estimated for each damage scenario under white noise excitation, and the mean modal damping ratios estimated are listed in Table 6.4. They are slightly different from the mean modal damping ratios of the corresponding undamaged building model (see Table 6.3) because of the reassembly and reinstallation of the building models after the designated damage scenario was made. The identified

lateral stiffness values of the building models 1 and 2 for each damage scenario are also presented in Table 6.4. It can be seen that the identified results from the two different white noise excitations are again very close to each other for each damage scenario.

Table 6.5 Identified and theoretical damage severities in the frequency domain (white noise excitation)

Scenario	**Building Model**	**Damage Severity (DS)**			
		Category	$\hat{\mu}_1(\%)$	$\hat{\mu}_2(\%)$	$\hat{\mu}_3(\%)$
1	1	Theoretical DS	-5.36	0	0
		Identified DS	-5.15	-0.92	0
2	1	Theoretical DS	-11.26	0	0
		Identified DS	-11.16	-0.27	0
4	2	Theoretical DS	0	-15.33	0
		Identified DS	0	-16.17	-0.91
5	1	Theoretical DS	-11.26	0	-7.45
		Identified DS	-13.42	0	-10.33
6	2	Theoretical DS	0	-15.33	-7.45
		Identified DS	0	-19.90	-6.44

The mean lateral stiffness values of the damaged building model were then compared with those of the corresponding undamaged building model for each damage scenario, from which the damage location and severity were identified. The identified damage location and severity were finally compared with the theoretical ones, as listed in Table 6.5 and plotted in Figure 6.6. It can be seen from Figure 6.6 that the locations of either single damage case or multi-damage case could be identified correctly, even for the minor damage cases such as the 5.36% damage in the first story in the scenario 1 (single damage) and the 7.45% damage in the third story in the scenarios 5 and 6 (multi-damage). Although the theoretical damage severity values may be different from the real damage severity values, the identified

damage severity values are close to the theoretical values except for the scenario 6. The aforementioned results demonstrate the feasibility and accuracy of the statistical moment-based damage detection method.

6.3.5. Damage detection results-colored noise excitation

A total of six damage scenarios (the scenarios 2, 3, 4, 6, 7 and 8) were investigated based on the building models 1, 2 and 3 with the input of colored noise excitation. The scenario 2 has the single damage in the first story of the building model 1 with a theoretical damage severity of 11.26%. The scenarios 3 and 4 have the single damage in the second story of the building model 2 but with different theoretical damage severities of 7.45% for the former and 15.33% for the latter. The scenarios 6 and 7 have dual damage but with different damage locations. In the scenario 6, the damage was inflicted in the second and third stories of the building model 2, and the theoretical damage severities are respectively 15.33% and 7.45%. In the scenario 7, the damage was made in the first and second stories of the building model 3 with the theoretical damage severities of 11.26% and 7.45%, respectively. The scenario 8 has the damage in all the three stories of the building model 3 with the theoretical damage severities of 11.26%, 7.45% and 15.33% for story 1, 2 and 3, respectively.

The first two modal damping ratios of the building models 1, 2 and 3 were estimated for each damage scenario under colored noise excitation, and the mean modal damping ratios estimated are listed in Table 6.6. They are slightly different from the mean modal damping ratios of the corresponding undamaged building model (see Table 6.3) and the corresponding damaged building model under white noise excitation (see Table 6.4) because of the reassembly and reinstallation of the building

models after the designated damage scenario was made. The identified lateral stiffness values of the building models 1, 2 and 3 for each damage scenario are also presented in Table 6.6. It can be seen that the identified results from the two different colored noise excitations are very close to each other for each damage scenario, indicating again the feasibility of the proposed damage detection method.

Table 6.6 Identified stiffness values of damaged building models under C. N. excitation (N/m) in the frequency domain

Scenario	**Building Model**	**Ground Excitation**	**Mean Damping Ratio**		**Identified Stiffness**		
			$\hat{\xi}_1$	$\hat{\xi}_2$	$\hat{k}_1$	$\hat{k}_2$	$\hat{k}_3$
2	1	C.N. 1	0.0166	0.0139	40612	26524	24156
		C.N. 2			41154	26772	24156
3	2	C.N. 1	0.0100	0.0095	40650	21509	23898
		C.N. 2			40650	21969	23898
4	2	C.N. 1	0.0077	0.0099	40650	19753	23129
		C.N. 2			40650	20142	23898
6	2	C.N. 1	0.0097	0.0092	40650	19440	21901
		C.N. 2			40650	19755	22296
7	3	C.N. 1	0.0165	0.0152	33154	21531	23678
		C.N. 2			32838	21236	23938
8	3	C.N. 1	0.0142	0.0110	34023	21304	19569
		C.N. 2			33234	20707	19144

The mean lateral stiffness values of the damaged building model listed in Table 6.6 were then compared with those of the corresponding undamaged building model for each damage scenario, from which the damage location and severity were identified. The identified damage location and severity were finally compared with the theoretical ones, as listed in Table 6.7 and plotted in Figure 6.7. It can be seen from Figure 6.7 that the locations of either single damage case or multi-damage case could be identified satisfactorily although there are small stiffness values identified for the

undamaged third story in the scenarios 4 and 7. Many factors such as high level of measurement noise and uncertainties in damping identification and numerical modeling could all result in these small false identifications. It can also be seen form Figure 6.7 that even for the minor damage cases such as the 7.45% damage in the second floor in the scenario 3 (single damage), the scenario 7 (dual damage) and the scenario 8 (multi-damage), the satisfactory location identification results can be obtained by the statistical moment-based damage detection method. Again, although the theoretical damage severity values may be different from the real damage severity values, the identified damage severity values are close to the theoretical values in most of the cases. The feasibility and accuracy of the statistical moment-based damage detection method are demonstrated again by the colored noise tests.

Table 6.7 Identified and theoretical damage severities and locations (colored noise excitation) in the frequency domain

Scenario	**Building Model**	**Damage Severity (DS)**			
		Category	$\hat{\mu}_1(\%)$	$\hat{\mu}_2(\%)$	$\hat{\mu}_3(\%)$
2	1	Theoretical DS	-11.26	0	0
		Identified DS	-12.23	-0.46	0
3	2	Theoretical DS	0	-7.45	0
		Identified DS	0	-9.83	0
4	2	Theoretical DS	0	-15.33	0
		Identified DS	0	-17.26	-1.61
6	2	Theoretical DS	0	-15.33	-7.45
		Identified DS	0	-18.72	-7.53
7	3	Theoretical DS	-11.26	-7.45	0
		Identified DS	-11.72	-7.95	-2.21
8	3	Theoretical DS	-11.26	-7.45	-15.33
		Identified DS	-10.03	-9.58	-20.50

The damage severities and locations of the building models identified using colored noise excitations are compared with those using white noise excitations to see

whether the type of external excitations affects the identification results or not. This can be done in terms of the scenarios 2, 4 and 6. The identification results of the three scenarios are presented and compared with the corresponding theoretical values in Figure 6.8. It can be seen that the identified results using the white noise excitations are close to those using the colored noise excitations and they all match the theoretical values well. In addition, according to the identified stiffness parameters of the undamaged building models by white noise excitation (see Table 6.3) and the identified stiffness parameters of the damaged building models by colored noise excitation (see Table 6.6), damage locations and damage severities of Scenarios 2, 4 and 6 are obtained and presented in Table 6.8. The identified results by the excitations of different types before and after damage are also compared with theoretical values and those identified by the excitations of the same type in Figure 6.8. It can be seen from Figure 6.8 that there is no much difference in the precision of all the identified results. Therefore, before and after damage, different types of external excitations can be utilized to vibrate building structures by the proposed method.

Table 6.8 Identified damage severities by the excitations of different types before and after damage in the frequency domain

Scenario	**Building Model**	**Damage Severity (DS)**			
		Category	$\hat{\mu}_1(\%)$	$\hat{\mu}_2(\%)$	$\hat{\mu}_3(\%)$
2	1	Theoretical DS	-11.26	0	0
		Identified DS	-10.33	0	-1.70
4	2	Theoretical DS	0	-15.33	0
		Identified DS	0	-16.41	0
6	2	Theoretical DS	0	-15.33	-7.45
		Identified DS	0	-17.88	-4.90

Note: before damage: white noise excitation, after damage: colored noise excitation

6.4 Experimental Analysis in the Time Domain

The experimental data were analyzed by the SMBDD method in the time domain in this section. The recorded ground motions and building responses as well as the identified structural damping ratios in Section 6.3.2 were utilized to identify damage locations and severities using the SMBDD method in the time domain. The identified damage locations and severities were also compared with the theoretical values.

6.4.1. Stiffness identification of undamaged building models

Firstly, the stiffness values of the undamaged shear building models were identified by the SMBDD method in the time domain. The averaged modal damping ratios, the measured statistical moment vectors, the estimated masses, and the recorded ground motion were used as inputs to identify the lateral stiffness values of the undamaged building models. The identified results are listed in Table 6.9.

Table 6.9 Identified results of undamaged building models in the time domain (N/m)

Building Model	**Ground Excitation**	**Mean Damping Ratio**		**Identified Stiffness**		
		$\hat{\xi}_1$	$\hat{\xi}_2$	$\hat{k}_1$	$\hat{k}_2$	$\hat{k}_3$
1	W.N. 1	0.0151	0.0123	45236	25966	24038
	W.N. 2			43783	25099	23659
	C.N. 1	0.0132	0.0120	44231	24811	23235
	C.N. 2			47172	27143	24597
2	W.N. 1	0.0096	0.0087	38974	23029	22560
	W.N. 2			40662	24164	23615
	C.N. 1	0.0079	0.0087	41136	24342	24152
	C.N. 2			41211	24556	24306
3	C.N. 1	0.0109	0.0074	35845	22173	22955
	C.N. 2			37942	23517	24744

Then the mean values of the identified lateral stiffness from the two separate tests using either white noise or colored noise ground excitation are calculated and compared with those computed in the frequency domain in Table 6.10. It can be seen that the results calculated in the time domain are very close to those obtained in the frequency domain. The maximum relative difference between the two kinds of results is only 3.06% which is less than 5% and acceptable. It also indicates that both the identified results in the frequency domain and those in the time domain should be reliable for all the three undamaged shear building models.

Table 6.10 Comparison between identified results of undamaged building models in the FD and those in the TD

Building Model		**Method**	**Mean value of Identified Stiffness (N/m)**		
			$\hat{k}_1$	$\hat{k}_2$	$\hat{k}_3$
1	W.N.	FD	45592	26128	24574
		TD	44510	25533	23849
		Error (%)	2.43	2.33	3.04
	C.N.	FD	46580	26772	24157
		TD	45702	25977	23916
		Error (%)	1.92	3.06	1.01
2	W.N.	FD	40150	23864	23236
		TD	39818	23597	23088
		Error (%)	0.83	1.13	1.01
	C.N.	FD	40650	24110	23898
		TD	41174	24449	24229
		Error (%)	1.27	1.39	1.37
3	C.N.	FD	37379	23232	24347
		TD	36894	22845	23850
		Error (%)	1.31	1.69	2.08

6.4.2. Damage detection results-white noise excitation

The five damage scenarios (the scenarios 1, 2, 4, 5 and 6) which were investigated on the building models 1 and 2 with white noise excitation input were examined by the proposed method in the time domain. Details of the five damage scenarios could be found in Section 6.3.4. The first two modal damping ratios of either the building model 1 or the building model 2 estimated before were also utilized here. The identified lateral stiffness values of the building models 1 and 2 for each damage scenario were presented in Table 6.11. The mean lateral stiffness values of the damaged building model were then compared with those of the corresponding undamaged building model for each damage scenario, from which the damage location and severity were identified. The identified damage location and severity were finally compared with the theoretical ones, as listed in Table 6.12 and plotted in Figure 6.9.

It can be seen from Figure 6.9 that the locations of either single damage cases or multi-damage cases could be identified correctly. In addition, the locations of the minor damage cases such as the 5.36% damage in the first story in the scenario 1 (single damage) and the 7.45% damage in the third story in the scenarios 5 and 6 (multi-damage) were identified correctly. As far as the identified damage severity values in the time domain are concerned, they are close to the theoretical ones. The difference between the identified values in the time domain and the corresponding theoretical values is either decreased or increased for a structural location in comparison with that between the identified values in the frequency domain and the corresponding theoretical values. For example, the difference for the first story and the second story of Scenario 1 in the frequency domain is respectively 0.21% and

0.92% according to Table 6.5. However, the corresponding difference in the time domain listed in Table 6.12 is respectively 1.42% and 0.15%. The difference for the first story of Scenario 2 in the frequency domain and the time domain is respectively 0.10% and 2.7% (see Tables 6.5 and 6.11). However, the difference for the third story of Scenario 5 identified in the frequency domain and the time domain is respectively 2.88% and 0.15% (see Tables 6.5 and 6.11). Therefore, it is difficult to say in which domain the proposed method is more reliable or accurate for the experimental analysis with white noise excitations. In other words, the conclusion can be made that the analyzed results in the time domain also demonstrate the feasibility and effectiveness of the SMBDD method.

Table 6.11 Identified stiffness values of damaged building models under W.N. excitation in the time domain (N/m)

Scenario	**Building Model**	**Ground Excitation**	**Mean Damping Ratio**		**Identified Stiffness**		
			$\hat{\xi}_1$	$\hat{\xi}_2$	$\hat{k}_1$	$\hat{k}_2$	$\hat{k}_3$
1	1	W.N. 1	0.0155	0.0132	42944	25532	23849
		W.N. 2			42565	25455	23849
2	1	W.N. 1	0.0168	0.0141	41043	25533	23849
		W.N. 2			40360	25533	23849
4	2	W.N. 1	0.0077	0.0098	39684	19243	22696
		W.N. 2			39706	21439	23088
5	1	W.N. 1	0.0146	0.0129	37878	25326	21575
		W.N. 2			39849	25533	22497
6	2	W.N. 1	0.0095	0.0085	39706	19387	21932
		W.N. 2			39706	18185	21192

Table 6.12 Identified and theoretical damage severities in the time domain (White Noise Excitation)

Scenario	Building Model	Damage Severity (DS)			
		Category	$\hat{\mu}_1(\%)$	$\hat{\mu}_2(\%)$	$\hat{\mu}_3(\%)$
1	1	Theoretical DS	-5.36	0	0
		Identified DS	-3.94	-0.15	0.00
2	1	Theoretical DS	-11.26	0	0
		Identified DS	-8.56	0.00	0.00
4	2	Theoretical DS	0	-15.33	0
		Identified DS	-0.31	-13.80	-0.85
5	1	Theoretical DS	-11.26	0	-7.45
		Identified DS	-12.68	-0.40	-7.60
6	2	Theoretical DS	0	-15.33	-7.45
		Identified DS	-0.28	-20.39	-6.61

6.4.3. Damage detection results-colored noise excitation

The six damage scenarios (the scenarios 2, 3, 4, 6, 7 and 8) investigated based on the building models 1, 2 and 3 with the input of colored noise excitation were also examined by the proposed method in the time domain. Details of the six damage scenarios could be found in Section 6.3.5. The first two modal damping ratios of either the building model 1 or the building model 2 estimated before, the measured displacement responses and the recorded ground motion were used as inputs to identify the lateral stiffness values of the damaged building models using the proposed method in the time domain. The identified lateral stiffness values of the building models 1 and 2 for each damage scenario were presented in Table 6.13.

Table 6.13 Identified stiffness values of damaged building models under C. N. excitation (N/m) in the time domain

Scenario	Building Model	Ground Excitation	Mean Damping Ratio		Identified Stiffness		
			$\hat{\xi}_1$	$\hat{\xi}_2$	$\hat{k}_1$	$\hat{k}_2$	$\hat{k}_3$
2	1	C.N. 1	0.0166	0.0139	40517	25977	23916
		C.N. 2			40329	25977	23916
3	2	C.N. 1	0.0100	0.0095	41174	21683	23699
		C.N. 2			41174	22120	24229
4	2	C.N. 1	0.0077	0.0099	41174	20622	23072
		C.N. 2			41174	20439	23700
6	2	C.N. 1	0.0097	0.0092	41174	18875	21283
		C.N. 2			41174	21695	22139
7	3	C.N. 1	0.0165	0.0152	33444	21695	23849
		C.N. 2			33482	21661	23850
8	3	C.N. 1	0.0142	0.0110	34065	21319	19571
		C.N. 2			32980	20523	18983

Table 6.14 Identified and theoretical damage severities and locations (colored noise excitation) in the time domain

Scenario	Building Model	Damage Severity (DS)			
		Category	$\hat{\mu}_1(\%)$	$\hat{\mu}_2(\%)$	$\hat{\mu}_3(\%)$
2	1	Theoretical DS	-11.26	0	0
		Identified DS	-11.55	0	0
3	2	Theoretical DS	0	-7.45	0
		Identified DS	0.00	-10.42	-1.09
4	2	Theoretical DS	0	-15.33	0
		Identified DS	0.00	-16.03	-3.48
6	2	Theoretical DS	0	-15.33	-7.45
		Identified DS	0.00	-17.03	-10.39
7	3	Theoretical DS	-11.26	-7.45	0
		Identified DS	-9.30	-5.11	0.00
8	3	Theoretical DS	-11.26	-7.45	-15.33
		Identified DS	-9.14	-8.42	-19.17

The mean lateral stiffness values of the damaged building models listed in Table 6.13 were then compared with those of the corresponding undamaged building model for each damage scenario, from which the damage location and severity were identified. The identified damage location and severity were finally compared with the theoretical ones, as listed in Table 6.14 and plotted in Figure 6.10. Seen from Figure 6.10, the locations of either single damage case or multi-damage could be identified satisfactorily although there were small damage severity values identified for the undamaged locations. As mentioned before, many factors such as high level of measurement noise and uncertainties in damping identification and numerical modeling could all result in such small false identification. In addition, the identified damage severity values in the time domain are also close to the theoretical values according to Table 6.14. Generally speaking, the identified results by the proposed method in the time domain with colored noise excitations remain the same high quality as those identified by the proposed method in the frequency domain. Therefore, the analyzed results of colored noise tests in the time domain demonstrate the feasibility and effectiveness of the SMBDD method again.

6.5. Conclusions

The structural damage detection method developed in the previous chapters based on the statistical moments of dynamic responses of a building structure was experimentally examined in this chapter. Three shear building models were constructed for the shaking table tests under either band-limited white noise excitation or the Kanai-Tajimi filtered white noise (colored noise) excitation. The background noise intensity of about 8% to 10% of the peak ground acceleration was involved in the shake table tests. A total of eight damage scenarios of different

damage locations and severities were created on the three building models to examine the feasibility and accuracy of the proposed damage detection method. Among the eight damage scenarios, there were five damage scenarios that were investigated on the building models 1 and 2 by using two randomly-generated white noise ground excitations, six damage scenarios that were explored by using two randomly-generated colored noise ground excitations and three damage scenarios that were examined by both white noise tests and colored noise tests.

Firstly, the experimental data were analyzed by the proposed method in the frequency domain. It was found that that the identified results from the two different white noise ground excitations were very close to each other for all the damage scenarios concerned. The damage locations and severities of either single damage case or multi-damage case could be identified correctly by the proposed method, even for the minor damage cases. Although the theoretical damage severity values may be different from the real damage severity values, the fact that the identified damage severity values are close to the theoretical values demonstrates the feasibility and effectiveness of the SMBDD method.

Then, the experimental data were analyzed by the proposed method in the time domain. The damage locations and severities of either single damage case or multi-damage case were also accurately identified by the proposed method in the time domain, even for the minor damage cases. Furthermore, the identified results by the proposed method in the time domain almost have the same high quality in comparison with those identified by the proposed method in the frequency domain. It

can be concluded that the proposed statistical moment-based damage detection method is feasible and accurate both in the frequency domain and in time domain.

However, most civil structures involve a certain amount of uncertainties caused by environment or modeling. These uncertainties in damage identification may result in false-positive damage identification (identifying the intact element as damaged) and false-negative damage identification (failure to identify the damaged elements). Therefore, when some uncertainties exist in the structural damage detection, it is definitely necessary to take the uncertainties into account. This will be investigated in the next chapter.

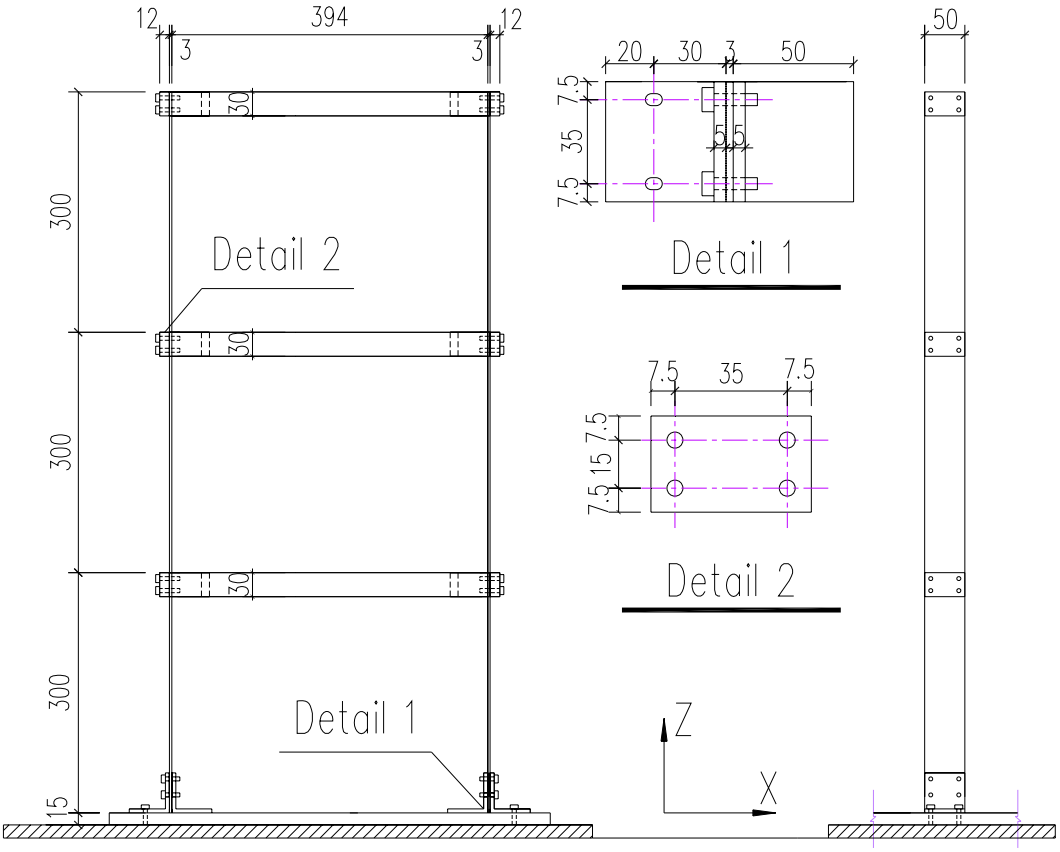

(a) Front view (b) Side view

Figure 6.1 Configuration of building model

Figure 6.2 Experimental arrangement

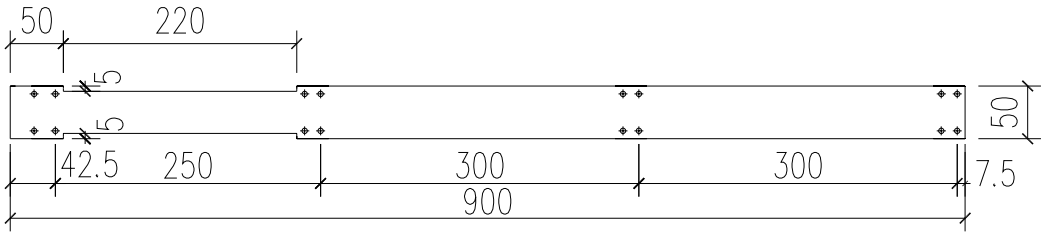

(a) 5 mm reduction from both sides of a column at the first story

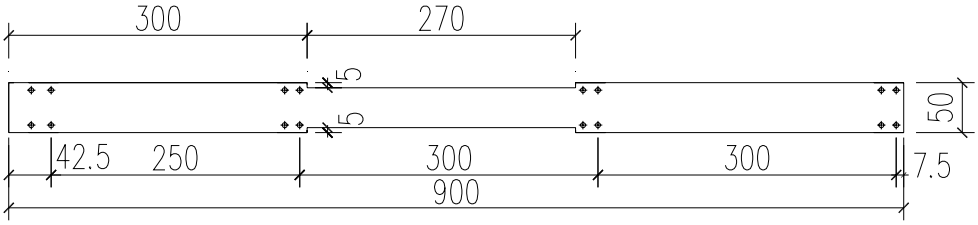

(b) 5 mm reduction from both sides of a column at the second story

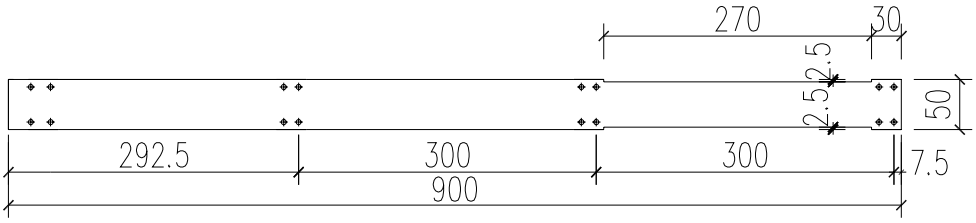

(c) 2.5 mm reduction from both sides of a column at the third story

Figure 6.3 Schematic typical damage scenarios: (a) 5 mm reduction from both sides of a column at the first story, (b) 5 mm reduction from both sides of a column at the second story, (c) 2.5 mm reduction from both sides of a column at the third story

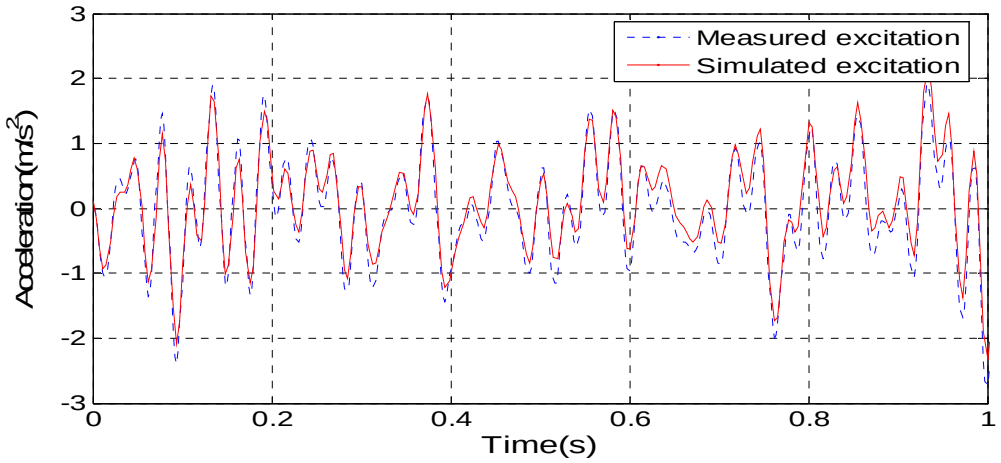

(a) time histories

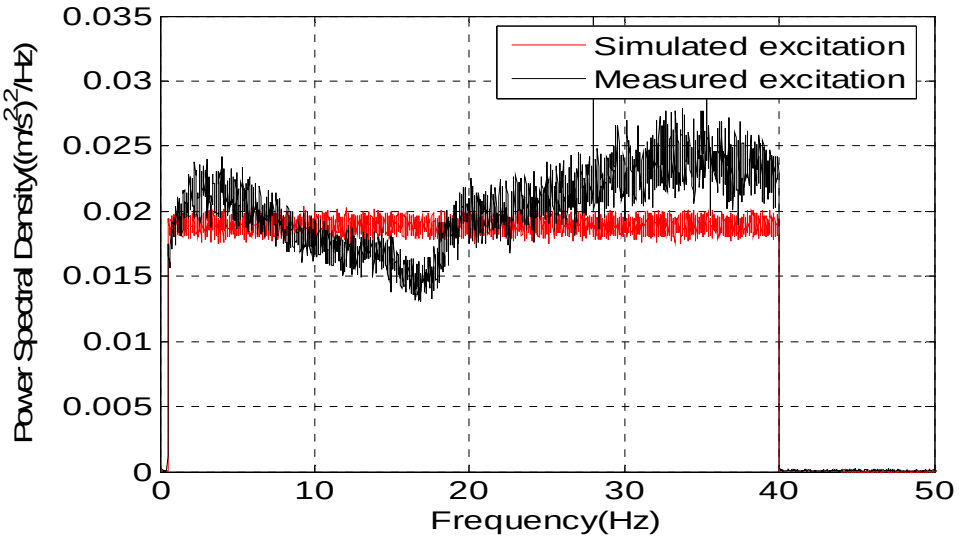

(b) power spectral density functions

Figure 6.4 Typical white noise ground excitation: (a) time histories, (b) power spectral density functions

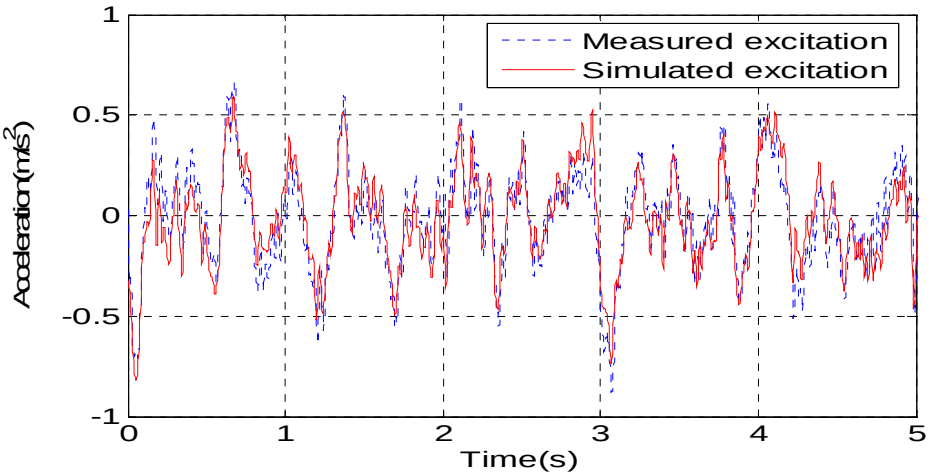

(a) time histories

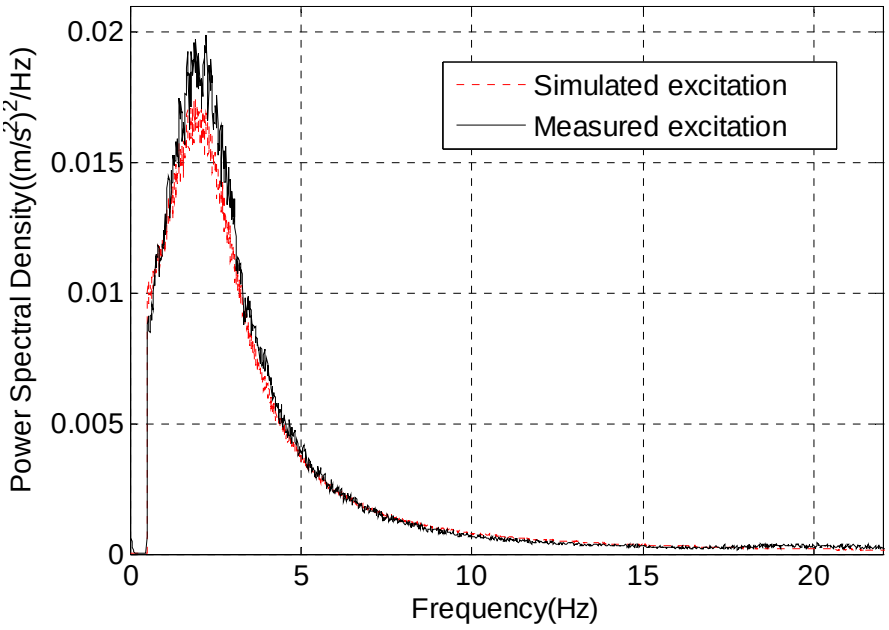

(b) power spectral density functions

Figure 6.5 Typical colored noise ground excitation: (a) time histories, (b) power spectral density functions

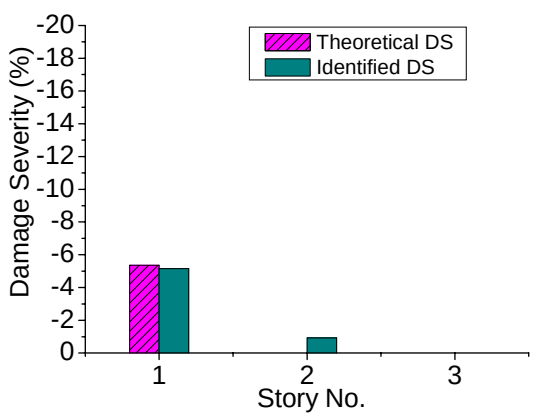

(a) Scenario 1

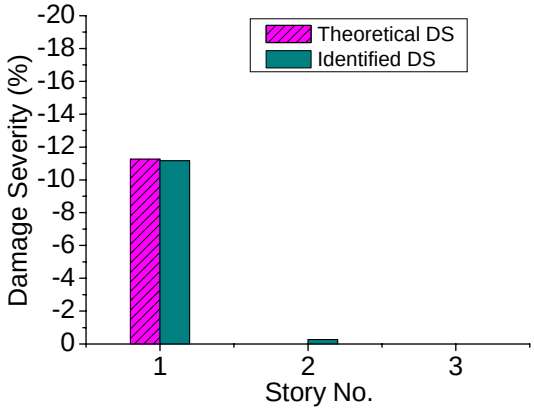

(b) Scenario 2

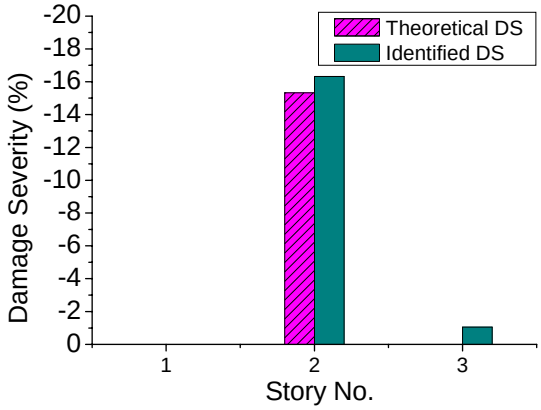

(c) Scenario 4

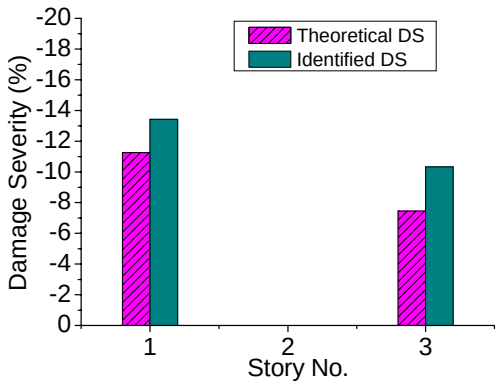

(d) Scenario 5

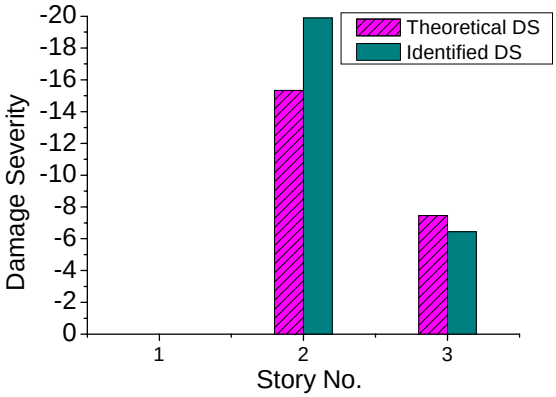

(e) Scenario 6

Figure 6.6 Identified results in the frequency domain using white noise excitations: (a) Scenario 1, (b) Scenario 2, (c) Scenario 4, (d) Scenario 5, (e) Scenario 6

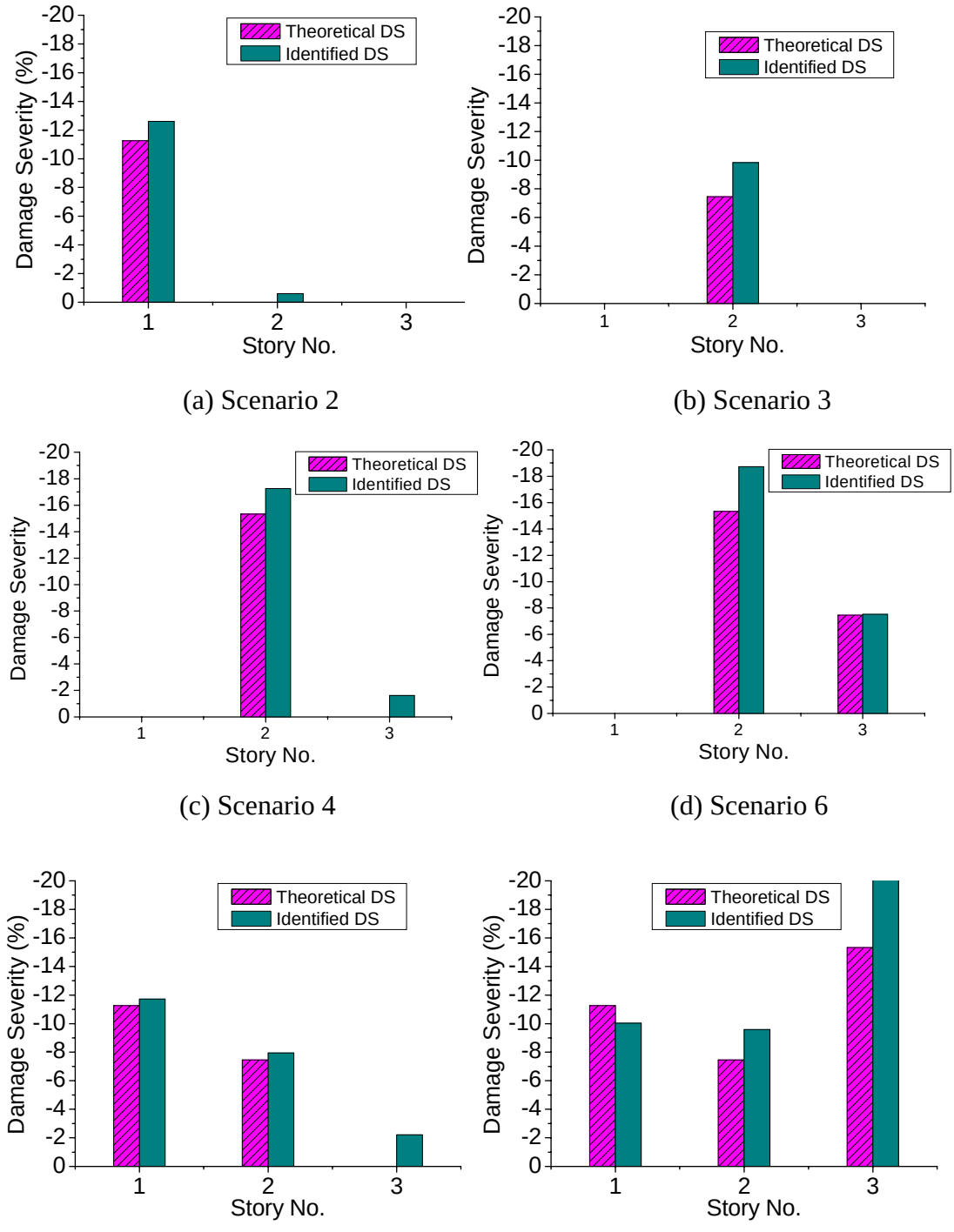

(a) Scenario 2 (b) Scenario 3

(c) Scenario 4 (d) Scenario 6

(e) Scenario 7 (f) Scenario 8

Figure 6.7 Identified results in the frequency domain using colored noise excitations: (a) Scenario 2, (b) Scenario 3, (c) Scenario 4, (d) Scenario 6, (e) Scenario 7, (f) Scenario 8

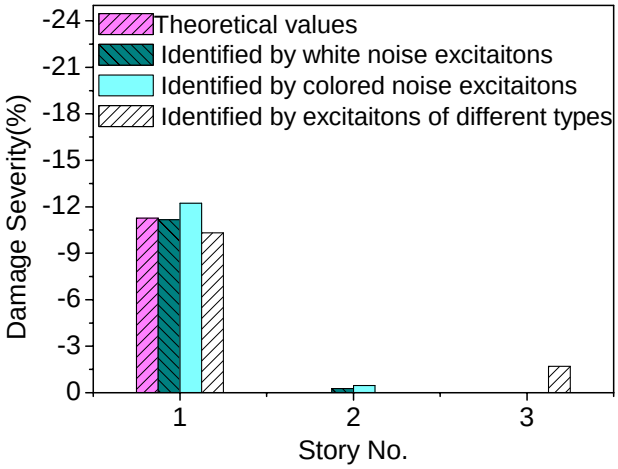

(a) Scenario 2

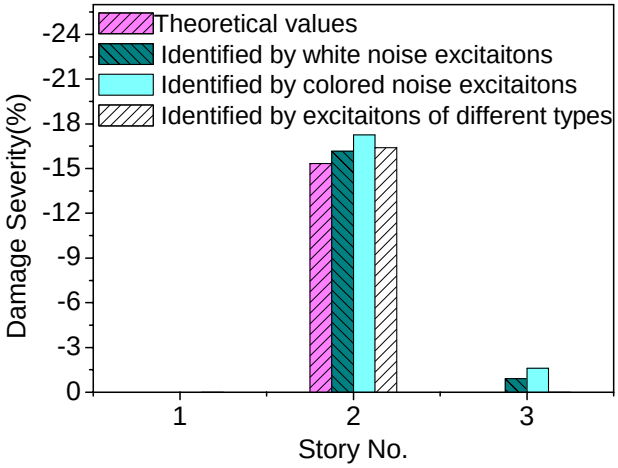

(b) Scenario 4

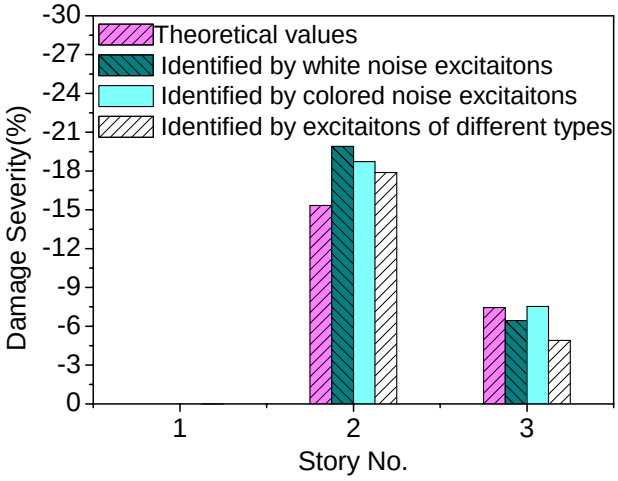

(c) Scenario 6

Figure 6.8 Identified results using white noise excitations before damage and colored noise excitations after damage and those using excitations of the same type before and after damage: (a) Scenario 2, (b) Scenario 4, (c) Scenario 6

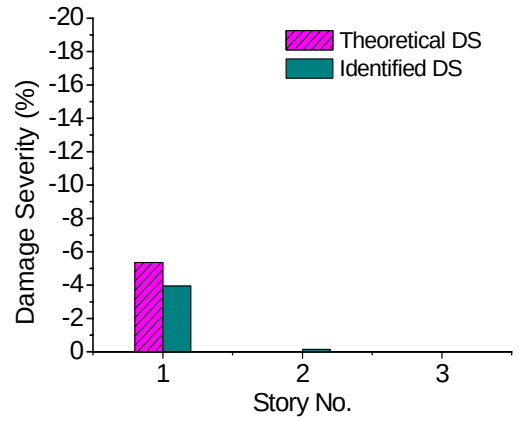

(a) Scenario 1

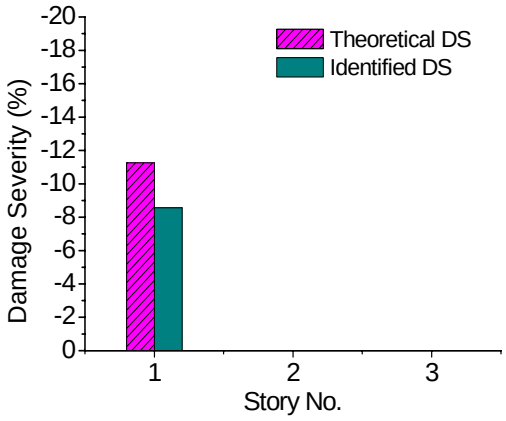

(b) Scenario 2

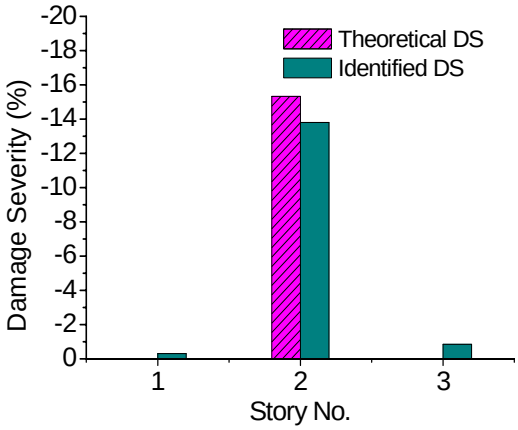

(c) Scenario 4

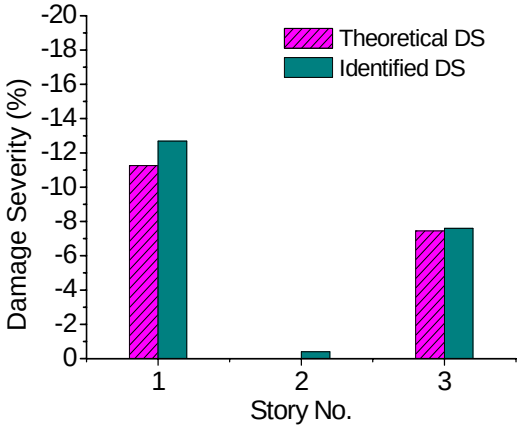

(d) Scenario 5

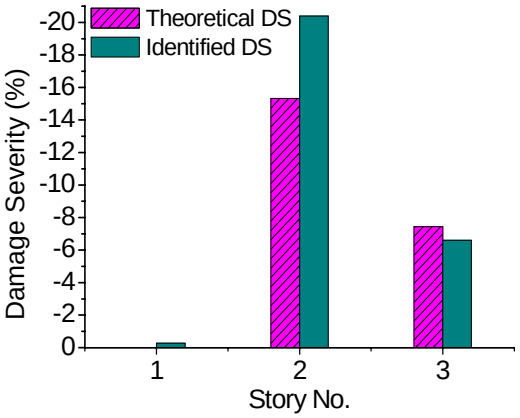

(e) Scenario 6

Figure 6.9 Identified results in the time domain using white noise excitations: (a) Scenario 1, (b) Scenario 2, (c) Scenario 4, (d) Scenario 5, (e) Scenario 6

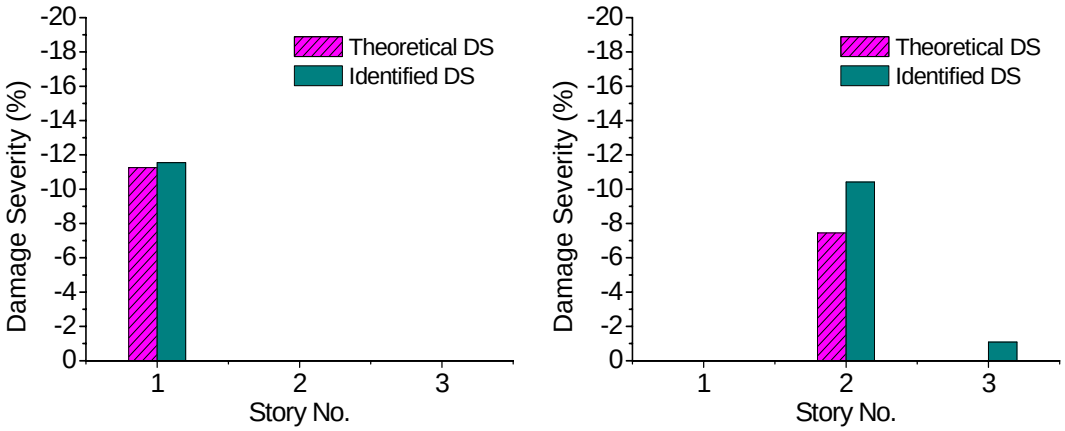

(a) Scenario 2 (b) Scenario 3

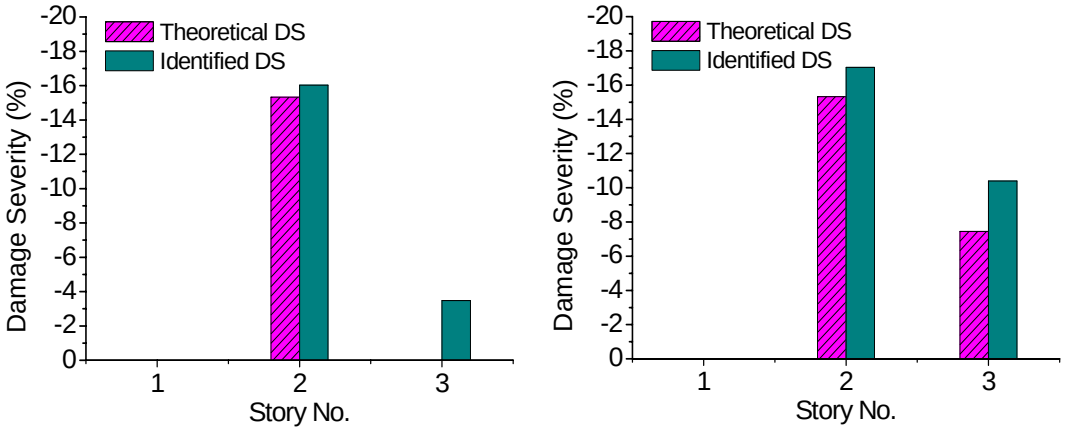

(c) Scenario 4 (d) Scenario 6

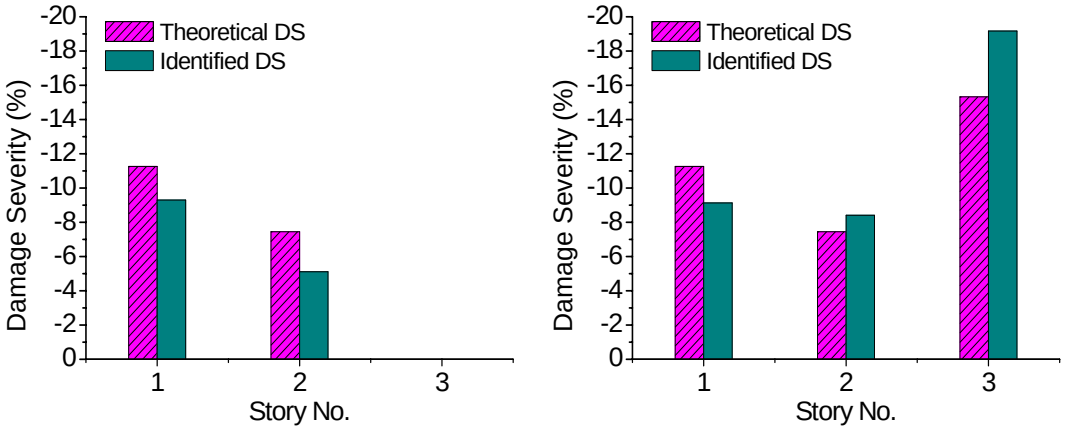

(e) Scenario 7 (f) Scenario 8

Figure 6.10 Identified results in the time domain using colored noise excitations: (a) Scenario 2, (b) Scenario 3, (c) Scenario 4, (d) Scenario 6, (e) Scenario 7, (f) Scenario 8

CHAPTER 7

STOCHASTIC DAMAGE DETECTION METHOD FOR STRUCTURES WITH PARAMATRIC UNCERTAINTIES

7.1 Introduction

In the previous Chapters 3, 4 and 5, the statistical moment damage detection (SMBDD) method has been proposed and numerically demonstrated to be feasible and effective for structural damage detection. Then, experimental investigation on this method in Chapter 6 further testified the proposed SMBDD method. Both the numerical analysis and the experimental investigation show that the proposed method is feasible and reliable for damage detection of building structures without uncertainties or random parameters. However, one of the main challenges of the practical application of a damage detection method to civil structures is that a significant amount of uncertainties such as modeling errors and measurement errors are inevitably involved in the damage detection procedure for civil structures. If the level of uncertainty is higher than or close to the level of actual changes of structural properties due to structural damage, the real information of structural damage will be concealed and the structural damage can not be accurately identified. For example, the existence of measurement noise may render less pronounced damage undetectable (negative falsity) or may identify some intact structural elements as damaged elements (positive falsity) (Doebling, *et al.*, 1998). The uncertainties existing in the structural model along with the errors in the measured vibration data limit the successful use of the deterministic damage detection methods. Housner

(1997) indicated that structural identification within a statistical framework appears to be a promising general approach to structural health monitoring of civil structures in view of inescapable data and modeling uncertainties.

Although many researchers have studied in the area of statistical structural damage identification and health monitoring based on vibration data, most of the statistical approaches still stay in primitive forms (Sohn, *et al.*, 2004). The representative approaches to detect structural damage with consideration of the uncertainties are the Bayesian methods (Beck and Katafygiotis, 1998; Katafygiotis and Beck, 1998; Vanik *et al.*, 2000; Beck and Au, 2002; Yuen and Katafygiotis, 2005), the Monte Carlo simulation (MCS) methods (Agbabian *et al.*, 1988; Banan *et al.*, 1994; Yeo *et al.*, 2000; Zhou *et al.*, 2003), the perturbation methods (Papadopoulos and Garcia, 1998; Xia *et al.*, 2002; Xia and Hao, 2003) and the statistical pattern recognition methods (Farrar *et al.*, 1999; Sohn *et al.*, 2001). For the Bayesian probabilistic approaches, the computation could become prohibitive when a large number of substructures of complex civil structures are assumed as damaged because substantive hypotheses should be examined to find more local maximum posterior probabilities and potentially to identify the correct damage event. The problem of computational complex also exists in the stochastic perturbation methods, in which various covariance matrices of updating parameters have to be calculated by the MCS method under many circumstances. The MCS methods are computationally intensive because it requires a large number of simulations to obtain an accurate and valid statistics. For the statistical pattern recognition methods, they can be divided into two classes: supervised learning and unsupervised learning. The unsupervised learning can be applied to data not containing examples from the damaged structure,

but this approach is inherently limited to identify presence of damage only. When data are available from both the undamaged and damaged structure, supervised learning approach can be taken to move forward to higher level damage identification to locate and quantify damage. However, the acquisition of data sets from the damaged structure in various damage states is often prohibitive for most applications. Furthermore, almost all of damage detection techniques with consideration of uncertainties assume the Gaussian distribution of a feature space, and establish decision making threshold values based on this normality assumption. Therefore, they do not always work effectively in dealing with uncertainty parameters which are not normally distributed. In addition, few, if any, of the current probabilistic damage detection methods can give complete probabilistic information such as the probability density function (PDF) of structural damage severity. Therefore, a new stochastic damage detection method is proposed in this chapter to locate structural damage and their corresponding damage severities in consideration of the random parameters or uncertainties involved in building structures.

Firstly, the basic equations and algorithm of the stochastic damage detection method are derived and presented. The stochastic damage detection method can be applied to civil structures with two stages. The first stage is to calculate the PDFs of the structural stiffness parameters at both the undamaged state and the damaged state. The second stage is to identify damage locations and their corresponding damage severities by calculating the probability of damage existence and the PDFs of damage severity indices. Numerical investigation is performed to demonstrate the proposed method through a three-story shear building structure. To simply illustrate the proposed method, only the first modal damping ratio of the building is adopted as

an independent random parameter, while the second modal damping ratio is fixed as a deterministic value and the third modal damping ratio is calculated from the first two modal damping ratios according to the Rayleigh damping assumption. The first modal damping ratio is set to be of a lognormal distribution in order to testify the applicability of the proposed method to non-Gaussian random parameters. Three damage scenarios of the shear building are explored. Numerical analysis results show that the proposed method is reliable and effective for structural damage detection when uncertainties or random errors are taken into account.

7.2. Stochastic Damage Detection Method

A new stochastic damage detection method is proposed and its formulae are derived in this section. The basic principle of the stochastic damage detection method is to identify the PDFs of stiffness parameters of a structure before and after the occurrence of damage using the measured building responses, and then to determine damage locations and their corresponding damage severities by calculating the probability function $P\left\{\hat{K}^u - \hat{K}^d \geq \alpha \times \hat{K}^u\right\}$ and its derivatives, where $\hat{K}^u$ is the identified stiffness of a component interested before damage occurrence, while $\hat{K}^d$ is the counterpart after the damage occurrence. α is a variable ranging from 0 to 100%.

7.2.1 Calculation of PDFs of structural stiffness parameters before and after damage

The first stage of the stochastic damage detection method focuses on the

identification of the PDFs of structural elemental stiffness parameters before and after damage. Intuitively, all modal updating methods can be combined with MCS method and perturbation method for such uncertainty propagation. However, MCS method and perturbation method are either of computational prohibitiveness particularly for large complex structures or only effective for dealing with Gaussian random parameters. In this regard, a new integrated algorithm is proposed to identify the PDFs of the structural stiffness parameters at the undamaged state $\hat{K}^u$ and the corresponding PDFs after the damage occurrence $\hat{K}^d$ by combining the Statistical Moment-Based Damage Detection (SMBDD) method (Zhang, et al., 2008 and Xu, et al., 2009) and the Probability Density Evolution (PDE) method (Li and Chen, 2004). One distinctive advantage of the SMBDD method is that it is not only sensitive to structural damage (or structural stiffness changes) but also insensitive to measurement noise, which has been numerically and experimentally demonstrated in the references. The PDE method can handle any kinds of uncertainty parameters and is more efficient than MCS method for uncertainty propagation. Hence, the PDFs of the structural elemental stiffness parameters before and after damage can be accurately and efficiently calculated by combing the two methods.

Without loss of generality, the equation of motion of a MDOF building structure with random parameters in the matrix form can be expressed as

$$\mathbf{M}\ddot{\mathbf{X}}(t)+\mathbf{C}(\boldsymbol{\Theta})\dot{\mathbf{X}}(t)+\mathbf{K}(\boldsymbol{\Theta})\mathbf{X}(t)=\mathbf{f}(t) \tag{7.1}$$

with the following deterministic initial condition

$$\mathbf{X}(t_0)=\mathbf{x}_0,\ \ \dot{\mathbf{X}}(t_0)=\dot{\mathbf{x}}_0 \tag{7.2}$$

where $\ddot{\mathbf{X}}$, $\dot{\mathbf{X}}$, $\mathbf{X}$ are the acceleration, the velocity and the displacement vector of *N* order; $\mathbf{f}(t)$ is the external excitation which is used to detect the structural damage,

$\mathbf{f}(t) = [f_1(t), f_2(t), \cdots, f_N(t)]$; **M**, **C** and **K** are the $N \times N$ mass matrix, damping matrix and stiffness matrix, respectively; $\boldsymbol{\Theta}$ is the random parameter vector of n_θ order which reflects the uncertainties in the structural identification procedure, with the known PDF of $p_{\boldsymbol{\Theta}}(\boldsymbol{\theta})$.

For every given value of the random parameter vector $\boldsymbol{\Theta}$, the structural stiffness parameters can be obtained by the SMBDD method. Detail description about the SMBDD method can be found elsewhere (Zhang, *et al.*, 2008 and Xu, *et al.*, 2009). Due to the random nature of $\boldsymbol{\Theta}$, the identified structural stiffness parameters are also stochastic and dependent on the random parameter $\boldsymbol{\Theta}$, denoted as $\mathbf{k}(\boldsymbol{\Theta})$. The PDE method that has been used successfully in many stochastic dynamical systems is employed here to obtain the PDFs of $\mathbf{k}(\boldsymbol{\Theta})$ because of its versatility and no computational intensiveness.

Construct a virtual random vector process for every elemental stiffness parameter.

$$Z_l(t) = k_l(\boldsymbol{\Theta}) \cdot t \tag{7.3}$$

where $k_l(\boldsymbol{\Theta})$ is the *l*th elemental stiffness parameter or the *l*th element of $\mathbf{k}(\boldsymbol{\Theta})$, there is

$$\dot{Z}_l = k_l(\boldsymbol{\Theta}) \tag{7.4}$$

For an engineering structure, the *l*th element stiffness parameter identified is existent, unique for every given value of $\boldsymbol{\Theta}$ and dependent on the random parameters $\boldsymbol{\Theta}$. So is the virtual random vector process $Z_l(t)$. According to the principle of preservation of probability, the joint PDF of $(Z_l(t), \boldsymbol{\Theta})$, denoted as $p_{Z_l\boldsymbol{\Theta}}(z, \boldsymbol{\theta}, t)$, satisfies the following probability density evolution equation (PDEE).

$$\frac{\partial p_{Z_l\boldsymbol{\Theta}}(z,\boldsymbol{\theta},t)}{\partial t}+\dot{Z}_l(\boldsymbol{\theta},t)\frac{\partial p_{Z_l\boldsymbol{\Theta}}(z,\boldsymbol{\theta},t)}{\partial z}=0 \tag{7.5}$$

Substitute Equation (7.4) into Equation (7.5), it gets

$$\frac{\partial p_{Z_l\boldsymbol{\Theta}}(z,\boldsymbol{\theta},t)}{\partial t}+k_l(\boldsymbol{\theta})\frac{\partial p_{Z_l\boldsymbol{\Theta}}(z,\boldsymbol{\theta},t)}{\partial z}=0 \tag{7.6}$$

with the following initial condition

$$p_{Z_l\boldsymbol{\Theta}}(z,\boldsymbol{\theta},t)|_{t=0}=\delta(z)p_{\boldsymbol{\Theta}}(\boldsymbol{\theta}) \tag{7.7}$$

where $\delta(\cdot)$ is the Dirac's function.

After solving the initial-value problem of Equations (7.6) and (7.7), the PDF of $Z_l(t)$ can be given by

$$p_{Z_l\boldsymbol{\Theta}}(z,\boldsymbol{\theta},t)|_{t=0}=\delta(z)p_{\boldsymbol{\Theta}}(\boldsymbol{\theta}) \tag{7.8}$$

Note that

$$k_l(\boldsymbol{\Theta})=Z_l(t)\big|_{t=1} \tag{7.9}$$

Therefore, the PDF of $Z_l(t)$ at time 1 is just the PDF of $k_l(\boldsymbol{\Theta})$ which is aimed to obtain.

The procedure to find the solution of the PDFs of structural elemental stiffness parameters before and after damage can be summarized as follows:

(1) Select the random parameters $\boldsymbol{\Theta}$ need to consider and obtain their probabilistic information in the domain $\Omega_{\boldsymbol{\Theta}}$ ($\Omega_{\boldsymbol{\Theta}}$ is the distribution domain of $\boldsymbol{\Theta}$). The considered random parameters may be Young's modulus, structural damping ratios, elemental mass parameters, external excitation parameters and any combination of these parameters or others;

(2) Construct the virtual random vector processes $\mathbf{Z}^u=\mathbf{k}^u(\boldsymbol{\Theta})\cdot t$ and

$\mathbf{Z}^d = \mathbf{k}^d(\boldsymbol{\Theta}) \cdot t$, where the superscripts '*u*' and '*d*' respectively represents the undamaged and damaged states. $\dot{\mathbf{Z}}^u = \mathbf{k}^u(\boldsymbol{\Theta})$ and $\dot{\mathbf{Z}}^d = \mathbf{k}^d(\boldsymbol{\Theta})$ are then simply derived.

(3) Discretize the random parameters $\boldsymbol{\Theta}$ into representative points $\boldsymbol{\theta}_q, q = 1, 2, \cdots, N_s$ in the domain $\Omega_{\boldsymbol{\Theta}}$; Denote the representative domain of each representative point $\boldsymbol{\theta}_q$ as V_q. The probability measure over this domain is assigned to this point and denoted as P_q.

$$P_q = \int_{V_q} p_{\boldsymbol{\Theta}}(\boldsymbol{\theta}) d\boldsymbol{\theta} \tag{7.10}$$

Clearly, $\sum_{q=1}^{N_s} P_q = 1$. The initial condition expressed by Equation (7.7) is discretized correspondingly as

$$p_{Z_l\boldsymbol{\Theta}}(z, \boldsymbol{\theta}_q, t)|_{t=0} = \delta(z) P(\boldsymbol{\theta}_q), \quad q = 1, 2, \cdots, N_s \tag{7.11}$$

(4) For every given discrete point $\boldsymbol{\theta}_q$, the structural stiffness vectors before and after the damage occurrence, $\mathbf{k}^u(\boldsymbol{\theta}_q)$ and $\mathbf{k}^d(\boldsymbol{\theta}_q)$, are identified respectively by the SMBDD method using measurement data at the two stages;

(5) Substitute the attained values of $k_l^u(\boldsymbol{\theta}_q)$ and $k_l^d(\boldsymbol{\theta}_q)$ in Step (4) into Equation (7.6) for the *l*th elemental stiffness parameter of the undamaged and damaged structure, respectively, and solve Equations (7.6) and (7.11) by the finite difference method to obtain $p_{Z_l^u}(z, \boldsymbol{\theta}_q, t)$ and $p_{Z_l^d}(z, \boldsymbol{\theta}_q, t)$, respectively, where Z_l^u and Z_l^d are respectively the *l*th element of $\mathbf{Z}^u$ and $\mathbf{Z}^d$;

(6) Repeat Steps (4) and (5) until $p_{Z_l^u}(z_l, \boldsymbol{\theta}_q, t)$ and $p_{Z_l^d}(z_l, \boldsymbol{\theta}_q, t)$ at every given discrete points, $\boldsymbol{\theta}_q, q = 1, 2, \cdots, N_s$, are obtained;

(7) Synthesize the results in Step (6) to respectively obtain $p_{Z_l^u}(z_l,t)$ and $p_{Z_l^d}(z_l,t)$ through the discretized version of Equation (7.10)

$$p_{Z_l}(z,t)=\sum_{q=1}^{N_s} p_{Z_l\Theta}(z,\boldsymbol{\theta}_q,t) \tag{7.12}$$

Finally, let t =1, the PDFs of k_l^u and k_l^d are obtained.

(8) Repeat Steps (5), (6) and (7) until PDFs of all structural elemental stiffness parameters are obtained;

7.2.2 Identification of damage locations and damage severities

The second stage of the stochastic damage detection method is to identify structural damage locations and their corresponding damage severities by employing the previously obtained PDFs of structural elemental stiffness parameters before and after damage. For simplicity, the *l*th elemental stiffness parameter identified is denoted as $\hat{K}$ in the following expression. Firstly, a probability function is defined and calculated as follows.

$$\begin{aligned} P\left\{\hat{K}^u-\hat{K}^d\ge\alpha\times\hat{K}^u\right\} &= P\left\{\hat{K}^d\le(1-\alpha)\times\hat{K}^u\right\} \\ &= \int_0^\infty\int_0^{(1-\alpha)\times\hat{K}^u} p(\hat{K}^d,\hat{K}^u)d\hat{K}^d d\hat{K}^u \\ &= \int_0^\infty\int_0^{(1-\alpha)\times\hat{K}^u} p(\hat{K}^d)\cdot p(\hat{K}^u)d\hat{K}^d d\hat{K}^u \\ &= \int_0^\infty[\int_0^{(1-\alpha)\times\hat{K}^u} p(\hat{K}^d)d\hat{K}^d]p(\hat{K}^u)d\hat{K}^u \end{aligned} \tag{7.13}$$

The probability function $P\left\{\hat{K}^u-\hat{K}^d\ge\alpha\times\hat{K}^u\right\}$ is the function of α, denoted as $G(\alpha)$. Its value will decrease along with the increase of α. Here we assume that $\hat{K}^u$ and $\hat{K}^d$ are independent to each other. As was mentioned before, the PDFs of structural stiffness parameters are dependent on the PDFs of the random

parameters $\boldsymbol{\Theta}$. Therefore, if there is no damage at the associated location the identified $\hat{K}^u$ and $\hat{K}^d$ should have the same PDF since the same uncertainties or random parameters are considered before and after damage occurrence. Under this situation, $\hat{K}^u$ and $\hat{K}^d$ are uniformly denoted as $\hat{K}$, and the value of $P\left\{\hat{K}^u - \hat{K}^d \geq \alpha \times \hat{K}^u\right\}$ at $\alpha = 0$, that is, the value of $P\left\{\hat{K}^u - \hat{K}^d \geq 0\right\}$ can be derived as follows.

$$\begin{aligned} P\left\{\hat{K}^u - \hat{K}^d \geq 0\right\} &= P\left\{\hat{K}^d \leq \hat{K}^u\right\} \\ &= \int_0^\infty \int_0^{\hat{K}^u} p(\hat{K}^d, \hat{K}^u) d\hat{K}^d d\hat{K}^u \\ &= \int_0^\infty \int_0^{\hat{K}^u} p(\hat{K}^d) \cdot p(\hat{K}^u) d\hat{K}^d d\hat{K}^u \\ &= \int_0^\infty [\int_0^{\hat{K}^u} p(\hat{K}^d) d\hat{K}^d] p(\hat{K}^u) d\hat{K}^u \\ &= \int_0^\infty [\int_0^{\hat{K}} p(\hat{K}) d\hat{K}] p(\hat{K}) d\hat{K} \\ &= \int_0^\infty F(\hat{K}) dF(\hat{K}) \\ &= \frac{1}{2}[F(\hat{K})]^2 \Big|_0^\infty = \frac{1}{2} \end{aligned} \tag{7.14}$$

where $F(\hat{K})$ is the distribution function of $\hat{K}$.

According to Equation (7.14), it can be concluded that when there is no damage at the location investigated, the value of $P\left\{\hat{K}^u - \hat{K}^d \geq 0\right\}$ should equal to 0.5. Otherwise, if there is damage at the location investigated, the PDF of $\hat{K}^d$ should offset toward the negative abscissa compared with the PDF of the stiffness parameter at the undamaged state, $\hat{K}^u$. Hence, the value of $P\left\{\hat{K}^u - \hat{K}^d \geq 0\right\}$ should be larger than 0.5. Therefore, whether structural damage occurs or not can be determined according to the values of $P\left\{\hat{K}^u - \hat{K}^d \geq 0\right\}$. When the value of $P\left\{\hat{K}^u - \hat{K}^d \geq 0\right\}$ is

larger than 0.5, there should be damage occurrence at the corresponding location and the larger the value of $P\left\{\hat{K}^u - \hat{K}^d \geq 0\right\}$, the higher probability the damage occurrence at this place.

In addition, once the probability function $P\left\{\hat{K}^u - \hat{K}^d \geq \alpha \times \hat{K}^u\right\}$ has been obtained, the derivative of $P\left\{\hat{K}^u - \hat{K}^d \geq \alpha \times \hat{K}^u\right\}$ in terms of α can be further calculated, which is also the function of the variable α. Rearrange the probability function $G(\alpha)$ as

$$\begin{aligned} G(\alpha) &= P\left\{\hat{K}^u - \hat{K}^d \geq \alpha \times \hat{K}^u\right\} \\ &= P\left\{\frac{\hat{K}^u - \hat{K}^d}{\hat{K}^u} \geq \alpha\right\} \\ &= 1 - P\left\{\frac{\hat{K}^u - \hat{K}^d}{\hat{K}^u} \leq \alpha\right\} \end{aligned} \tag{7.15}$$

Since $(\hat{K}^u - \hat{K}^d)/\hat{K}^u$ is the definition of structural damage severity, $P\left\{(\hat{K}^u - \hat{K}^d)/\hat{K}^u \leq \alpha\right\}$ is just the distribution function of structural damage severity, denoted as $F(\alpha)$. Therefore,

$$-G'(\alpha) = f(\alpha) \tag{7.16}$$

The negative derivative of $G(\alpha)$ is just the PDF of structural damage severity, denoted as $f(\alpha)$. Therefore, the value of α corresponding to the maximum of $f(\alpha)$ should be the most likely value of structural damage severity, denoted as β, which is straightforwardly set as the index of damage severity for structures with uncertainties. Therefore, according to the above deductions, not only structural damage locations but also their corresponding damage severities can be identified by the proposed stochastic damage detection method. The flowchart of the stochastic

damage detection method is presented in Figure 7.1. The feasibility and effectiveness of the new stochastic damage detection method are demonstrated by the following numerical investigation based on a three-story shear building structure.

7.3. Numerical Investigation

7.3.1 Numerical model

To evaluate the effectiveness of the stochastic damage detection method for building structures with uncertainties or of random parameters, the three-story shear building model shown in Figure 7.2 is investigated in this paper. The mass and horizontal stiffness coefficients of the three-story shear building model are respectively 350250 kg and 4728400 kN/m for the first story, 262690 kg and 315230 kN/m for the second story, and 175130 kg and 157610 kN/m for the third story. The mass of each floor is assumed to be invariant. Though more than one random parameter can be taken into account by the proposed method, it is sufficient for demonstrative purposes to consider only one random parameter of the building structure. In the following numerical investigation, the first modal damping ratio is selected as a random parameter due to its highly uncertainties or random errors in the identification of this parameter. The first damping ratio is approximated as a lognormal distribution with mean value $\overline{\xi}$ = 1% and the standard deviation σ of 10% of the mean value. The second modal damping ratio is fixed as 2.14%. The third modal damping ratio is calculated from the first two modal damping ratios according to the Rayleigh damping assumption. The ground acceleration is simulated as a colored white noise corresponding to the Kanai-Tajimi spectrum having parameters ω_g = 15.6 rad/sec

and ζ_g = 0.6. The magnitude is chosen such that the maximum absolute value of acceleration is 2.0 m/sec^2. To simulate the colored white noise excitation, a method of digital simulation random processes developed by Shinozuka and Jan (1972) is utilized. The duration of the excitation time history is 1000s with the sampling frequency of 256 Hz.

7.3.2 Numerical Analysis

In this section, three damage scenarios, Scenario 1, 2 and 3, are explored through the shear building model. Both Scenarios 1 and 2 have single damage at the second story but with different damage severities of 10% and 20%, respectively. Scenario 3 has the multi-damage at the first story and the third story respectively with the damage severities of 20% and 10%, respectively.

The PDFs of the horizontal stiffness parameters of the undamaged shear building structure are first identified according to the proposed algorithm in Section 2.1. The first modal damping ratio is discretized into 21 representative points in the domain $[\bar{\xi} - 3\sigma,\ \bar{\xi} + 3\sigma]$, as seen in Figure 7.3. For every given representative point, ξ_i, the horizontal stiffness parameters of the undamaged shear building are identified by using the SMBDD method. The discretized representative points ξ_i and the corresponding identified horizontal stiffness parameters of the undamaged shear building are listed in Table 7.1. Then respectively substitute the identified horizontal stiffness parameters into Equation (7.6) and solve it with the finite difference method. Following the procedure of the proposed algorithm in Section 2.1, the PDF of every story's horizontal stiffness parameter of the undamaged structure is finally obtained.

Likewise, the PDFs of the horizontal stiffness parameters for Scenarios 1, 2 and 3 are also identified and respectively presented in Figures 7.4, 7.5 and 7.6 in comparison with the identified PDFs of the horizontal stiffness parameters of the undamaged building. The solid red lines stand for the PDFs of the undamaged shear building, while the dotted blue lines stand for the counterparts of the damaged building.

Table 7.1 Identified stiffness parameters of the undamaged structure

No.	ξ_i	Story 1	Story 2	Story 3
1	0.0074	5287164800	354730240	177358680
2	0.0077	5229349800	350663220	175327720
3	0.0080	5149865300	345118050	172568980
4	0.0083	5061825300	338916160	169471800
5	0.0086	4984801200	342098900	164384060
6	0.0089	4926428000	298523950	148982510
7	0.0092	4869308900	315110140	169321590
8	0.0095	4810261300	294431810	146951340
9	0.0098	4751981000	292550670	146020970
10	0.0101	4695639400	312994980	156525780
11	0.0104	4641564200	289036760	144282060
12	0.0107	4595750600	287372210	143457670
13	0.0110	4553734200	285754670	142660310
14	0.0113	4508861000	299738810	149915870
15	0.0116	4460632400	296328830	148220130
16	0.0119	4412387000	292906480	146516850
17	0.0122	4365901500	289597900	144868940
18	0.0125	4322035500	286468230	143309600
19	0.0128	4280236400	283479780	141820230
20	0.0131	4240985400	280666700	140417760
21	0.0134	4204557200	276180710	139691580

As seen from Figures 7.4, 7.5 and 7.6, the stiffness values corresponding to the peak

values of the PDFs of an undamaged story before and after damage are almost at the same position. For a damaged story, the stiffness values corresponding to the peak values of the PDFs after damage are apparently smaller than those before damage occurrence. And the larger the damage severity, the more backward offset occurs between the PDFs of the damaged state and those of the undamaged state. This is verified by the identified results of Story 2 for Scenarios 1 and 2 which are respectively presented in Figure 7.4 (b) and Figure 7.5 (b). For the stories with damage in Scenario 3, say, Stories 1 and 3, the PDFs after damage apparently offset backward in comparison with that before damage occurrence, while the PDF of the horizontal stiffness parameter of Story 2 almost keeps unchanged. Therefore, the damage locations can be qualitatively determined according to the identified PDFs of structural elemental stiffness parameters before and after damage.

Then damage locations and their corresponding damage severities are quantitatively identified according to the following investigation. The probability functions $P\left\{K^u - K^d \geq \alpha \times K^u\right\}$ for Scenarios 1, 2 and 3 are calculated according to Equation (10) and plotted in Figures 7.7, 7.8 and 7.9, respectively. In Figure 7.7, the values of $P\left\{K^u - K^d \geq \alpha \times K^u\right\}$ at $\alpha = 0$, or the values of $P\left\{K^u - K^d \geq 0\right\}$, for the first and third stories are 50.84% and 50.81%, respectively, which indicates that the PDFs of the first and third stories' horizontal stiffness values change only marginally before and after damage occurrence. That is, the first and third stories have no damage. However, the corresponding value for the second story is 95.55% which is much larger than 0.5. It means the stiffness of the second story is apparently decreased or damaged.

For Scenario 2, it can be seen from Figure 7.5 that the PDFs of the first and third stories' horizontal stiffness values change very little before and after the damage occurrence. In addition, the values of $P\left\{K^u - K^d \geq 0\right\}$ for the first and third stories in Figure 7.8 are 55.82% and 55.85%, respectively, which are only a litter larger than 50%. On the other hand, the values of $P\left\{K^u - K^d \geq 0\right\}$ corresponding to the damage severities of 2% and 5% are theoretically calculated as 55.65% and 63.85%, respectively. Therefore, it can be deduced that the first and third stories of Scenario 2 either have no damage or have only marginal damage which is about 2%. More determinate conclusion can be made by calculating the derivative of $P\left\{K^u - K^d \geq \alpha \times K^u\right\}$ in the following section. However, for the second story, the value of $P\left\{K^u - K^d \geq 0\right\}$ is 99.99%, which can directly lead to the assured conclusion that the stiffness of the second story is definitely decreased or damaged. The probability functions $P\left\{K^u - K^d \geq \alpha \times K^u\right\}$ for Scenario 3 are presented in Figure 7.9. The values of $P\left\{K^u - K^d \geq 0\right\}$ for the first story, the second story and the third story are respectively 99.99%, 50.34% and 95.58%. Therefore, the first and third stories are determined as damage locations.

In order to provide more information about the structural damage for Scenarios 1, 2, and 3, the negative derivatives of the probability functions $P\left\{K^u - K^d \geq \alpha \times K^u\right\}$ or the PDFs of structural damage severity of every story are calculated and presented in Figures 7.10, 7.11, and 7.12, respectively. As seen from Figure 7.10, the damage severity of the second story can be determined as 10.0% according to the proposed index of damage severity. The identified damage severity is identical with the actual

value. The damage severities at the other two stories are identified as 0, which verifies the aforementioned conclusion that there is no damage at the first and third story for Scenario 1. According to Figure 7.11, the damage severities of the first, second and third stories for Scenario 2 are 1.0%, 20.5% and 0, respectively, which are very close to the true values, 0, 20% and 0. As seen from Figure 7.12, the identified damage severity values of the first and third stories of Scenario 3 are 20.5% and 10%, respectively, which are almost the same as the actual values, 20% and 10%. And the second story should have no damage according to the profile of Figure 7.12 (c). The identified damage severities of the three scenarios are compared with the real values in Figure 7.13. The identified results are identical with or very close to the real values. In summary, the analysis results show that the proposed stochastic damage detection method can accurately detect both damage locations and their corresponding damage severities when uncertainty or random parameters of building structures are taken into account. The feasibility and effectiveness of the proposed stochastic damage detection method are numerically demonstrated.

7.4 Concluding Remarks

A new stochastic damage detection method has been proposed in this paper for structural damage detection of building structures of random parameters or with uncertainties. Numerical investigation has been performed to demonstrate the feasibility and effectiveness of the proposed method in terms of a shear building structure, in which the first modal damping ratio is regarded as a random parameter with a lognormal distribution. Three damage scenarios were explored. For every damage scenario, the PDFs of structural stiffness parameters before and after damage

occurrence $\hat{K}^u$ and $\hat{K}^d$ were firstly identified by employing the proposed algorithm. Then the defined probability functions $P\left\{K^u - K^d \geq \alpha \times K^u\right\}$ and their negative derivatives were computed by making use of the identified PDFs of structural stiffness parameters before and after damage.

When the PDF of $\hat{K}^d$ offsets toward the negative abscissa of stiffness compared with the PDF of the undamaged stiffness parameter, $\hat{K}^u$, and the value of $P\left\{K^u - K^d \geq \alpha \times K^u\right\}$ at $\alpha = 0$ is larger than 0.5, the damage occurrence could be ascertained. Their corresponding damage severity values were accurately determined according to the maximum points of the negative derivatives of $P\left\{K^u - K^d \geq \alpha \times K^u\right\}$ (the PDFs of structural damage severities). Numerical analysis results show that not only damage locations but also damage severities can be correctly identified by the proposed method. The proposed method is effective and robust for structural damage detection when uncertainties or random parameters are taken into account.

In the next chapter, a framework of the reliability analysis will be developed by utilizing the SMBDD method in conjunction with the PDE method. The reliability of instrumented building structures will be evaluated based on the dynamic response measurements with consideration of uncertainties in measurements, structures and external excitations.

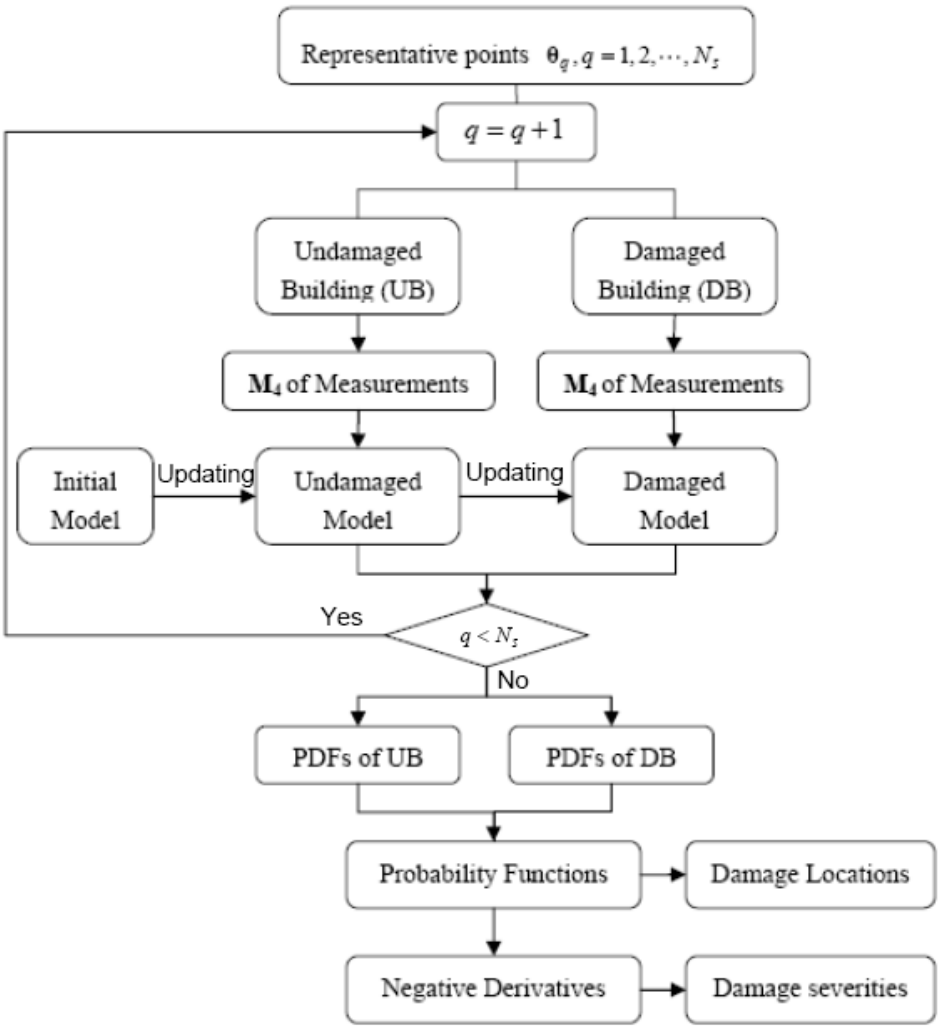

Figure 7.1 Flowchart of the stochastic damage detection method

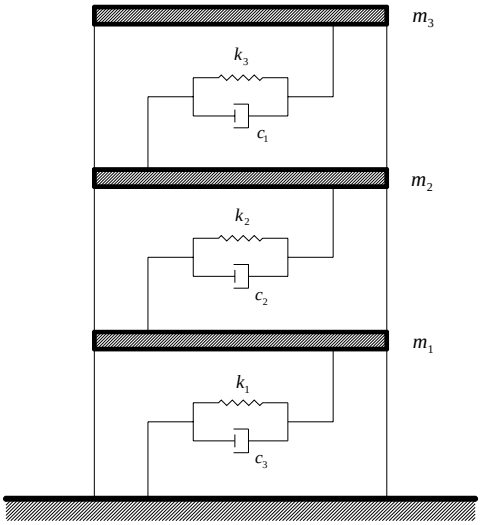

Figure 7.2 Three-story shear building model

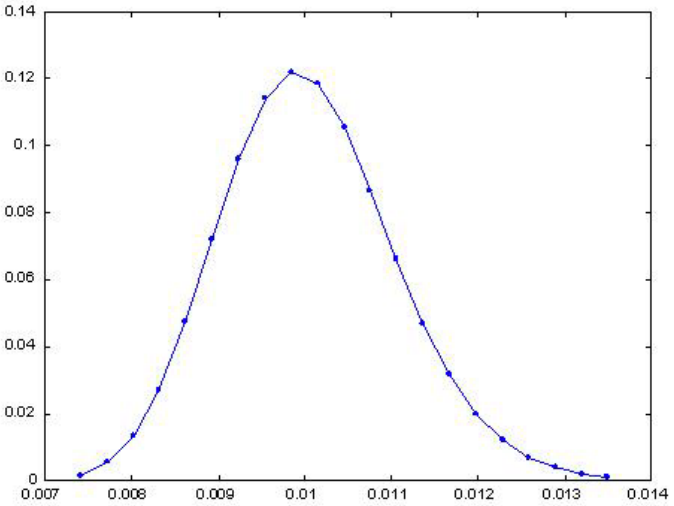

Figure 7.3 Representative points of the first damping ratio

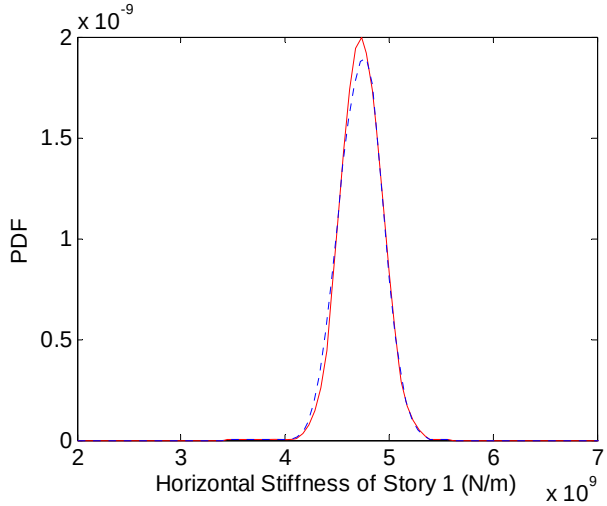

(a) Story 1

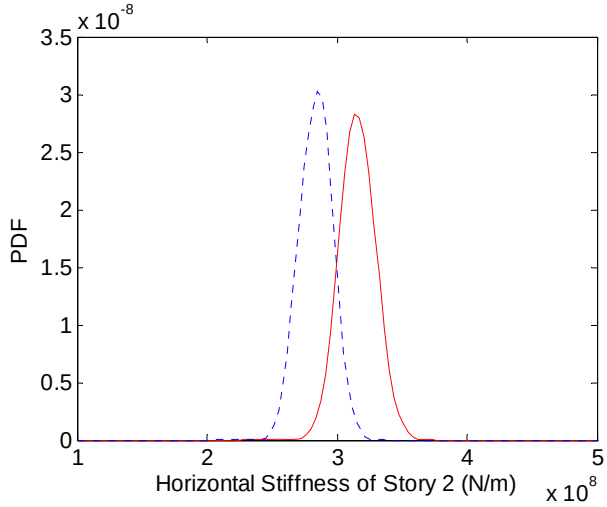

(b) Story 2

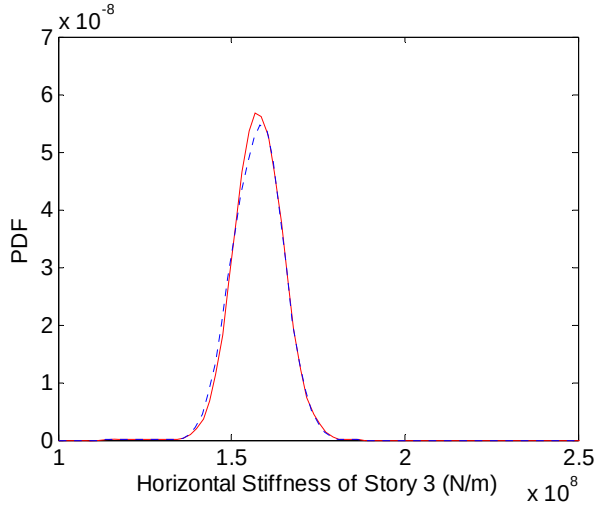

(c) Story 3

Figure 7.4 Comparison of identified PDFs of horizontal stiffness parameters before and after damage in Scenario 1: (a) Story 1, (b) Story 2, (c) Story 3

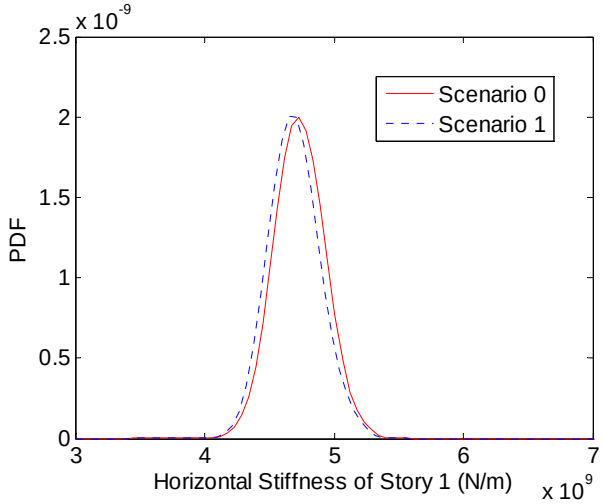

(a) Story 1

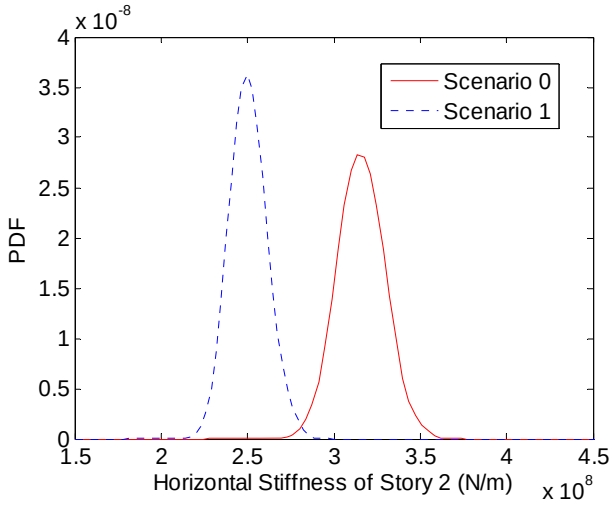

(b) Story 2

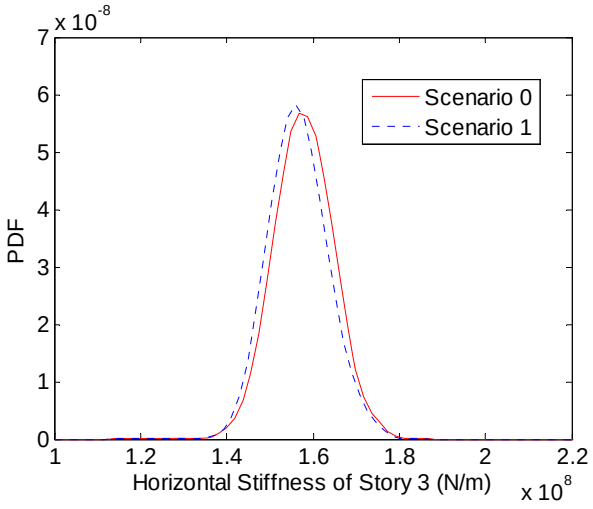

(c) Story 3

Figure 7.5 Comparison of identified PDFs of horizontal stiffness parameters before and after damage in Scenario 2: (a) Story 1, (b) Story 2, (c) Story 3

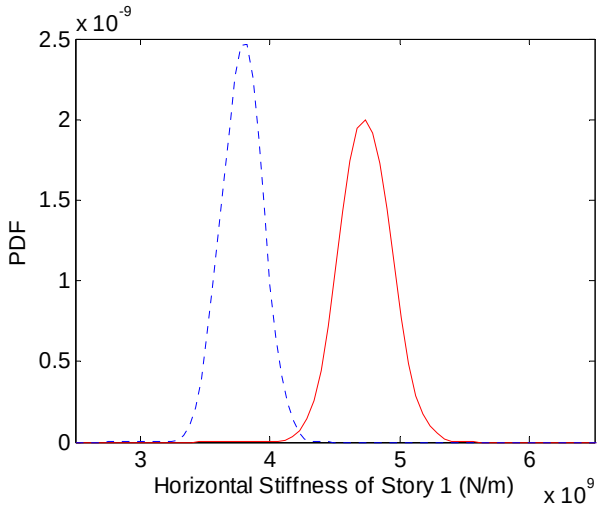

(a) Story 1

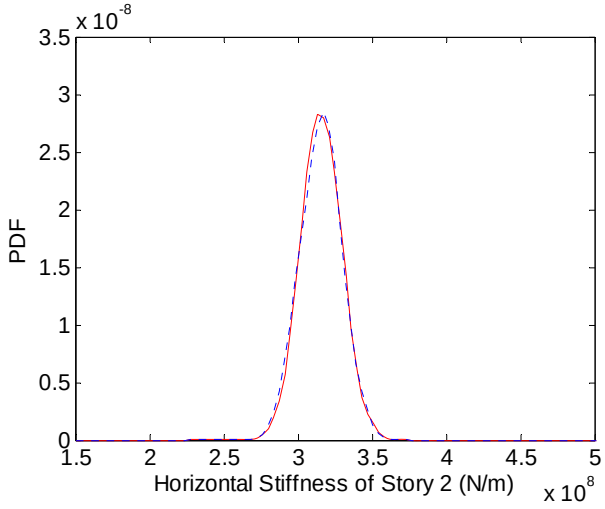

(b) Story 2

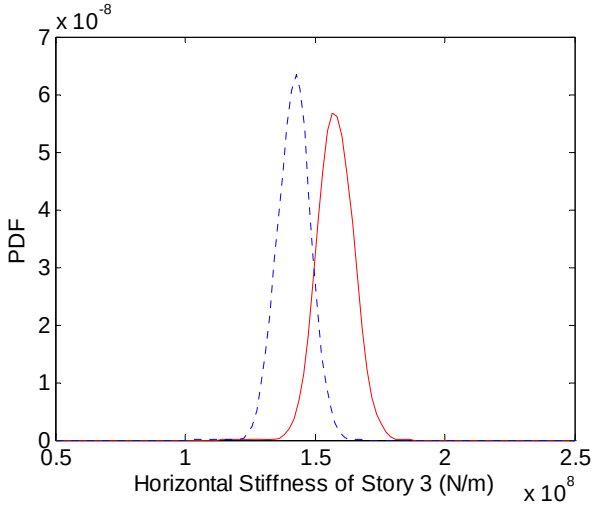

(c) Story 3

Figure 7.6 Comparison of identified PDFs of horizontal stiffness parameters before and after damage in Scenario 3: (a) Story 1, (b) Story 2, (c) Story 3

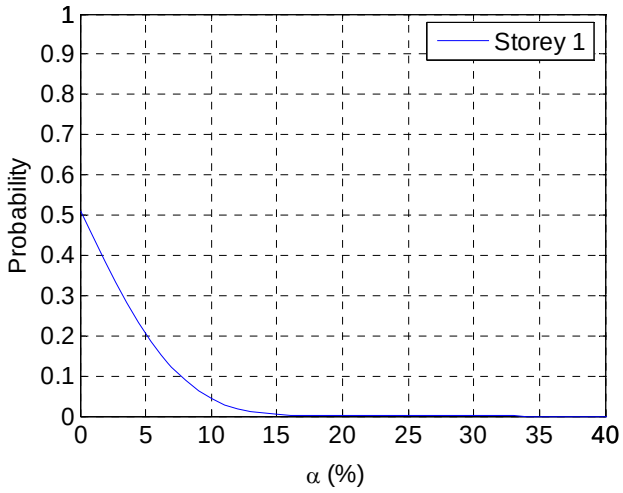

(a) Story 1

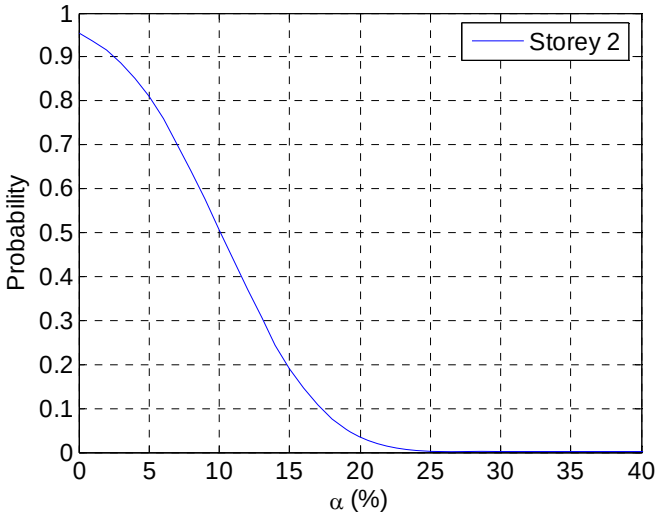

(b) Story 2

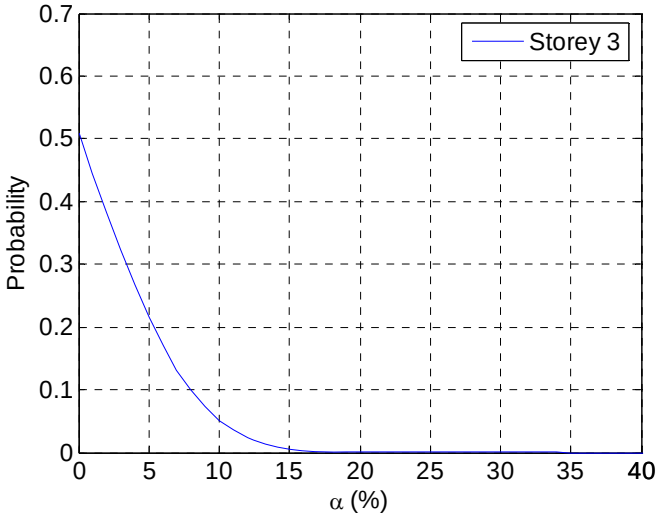

(c) Story 3

Figure 7.7 Probability functions $P\left\{K^u - K^d \geq \alpha \times K^u\right\}$ of every story in Scenario 1: (a) Story 1, (b) Story 2, (c) Story 3

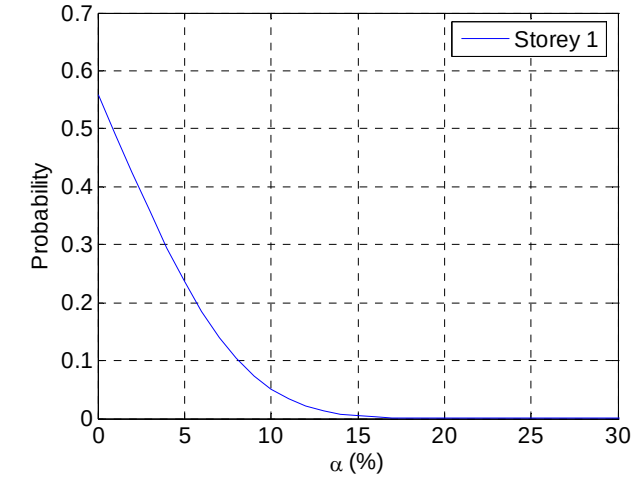

(a) Story 1

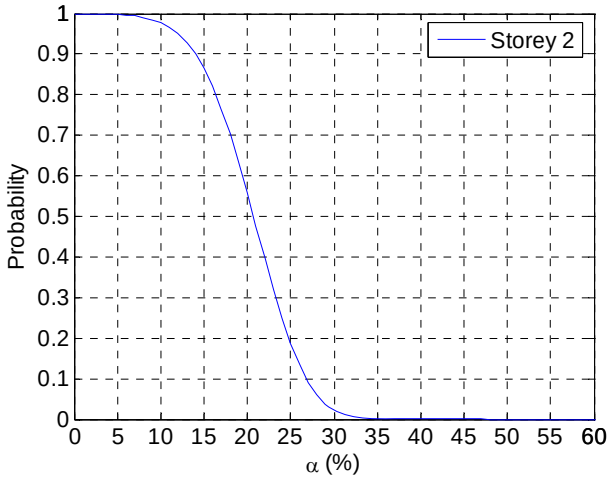

(b) Story 2

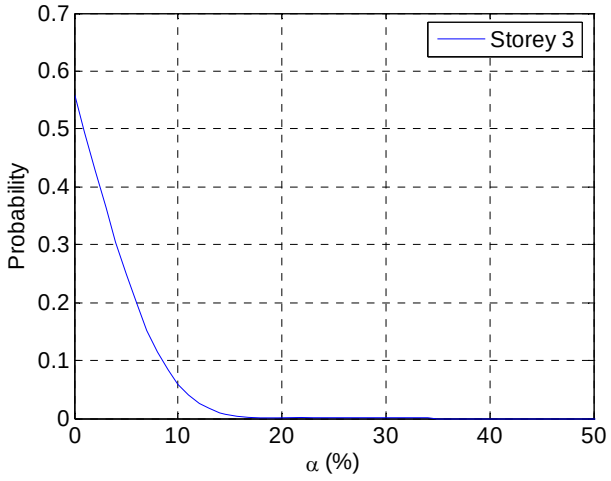

(c) Story 3

Figure 7.8 Probability functions $P\left\{K^u - K^d \geq \alpha \times K^u\right\}$ of every story in Scenario 2: (a) Story 1, (b) Story 2, (c) Story 3

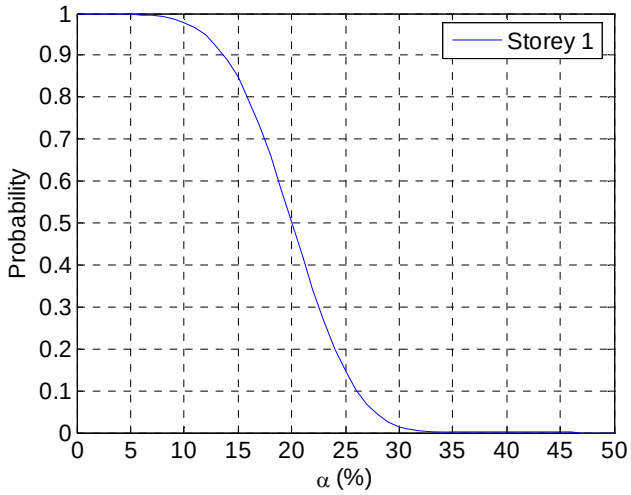

(a) Story 1

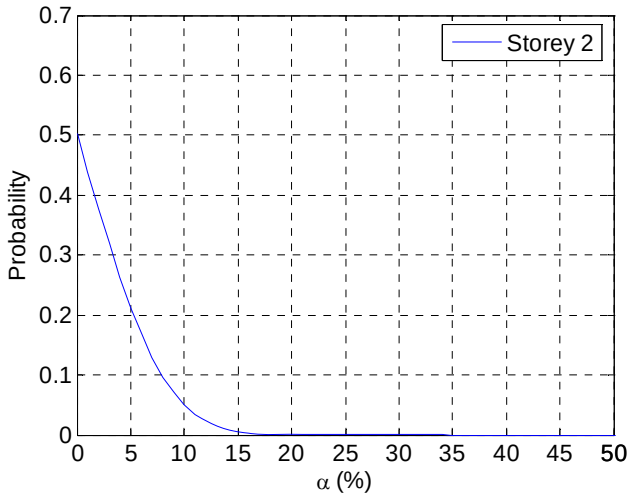

(b) Story 2

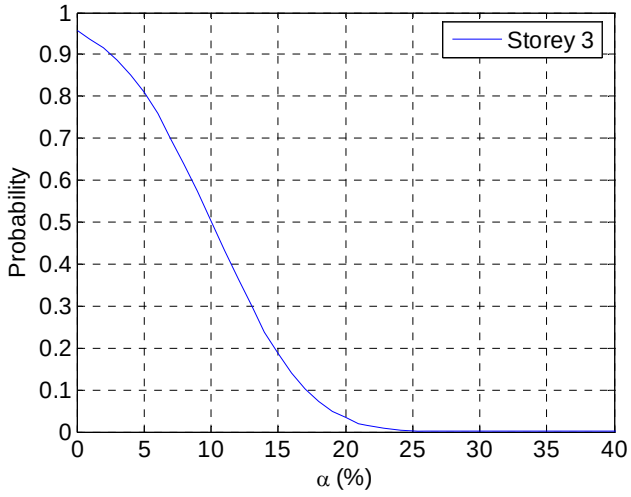

(c) Story 3

Figure 7.9 Probability functions $P\left\{K^u - K^d \geq \alpha \times K^u\right\}$ of every story in Scenario 3:

(a) Story 1, (b) Story 2, (c) Story 3

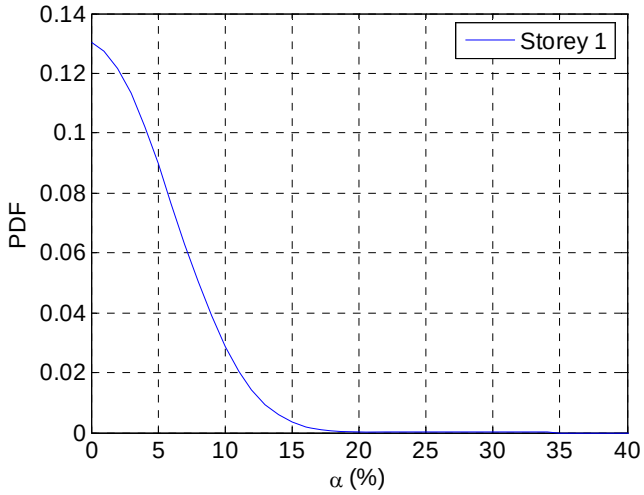

(a) Story 1

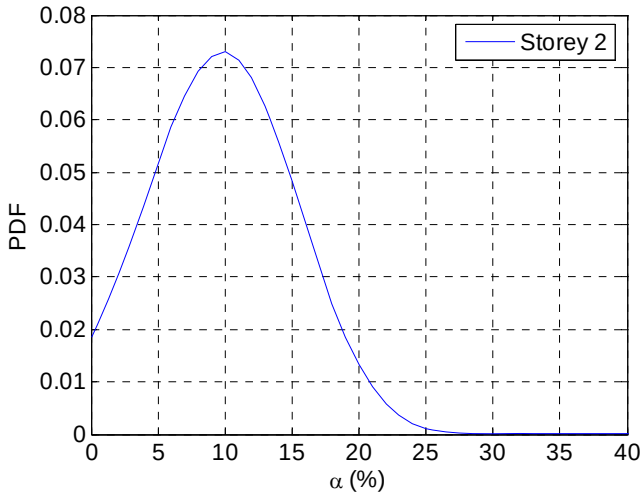

(b) Story 2

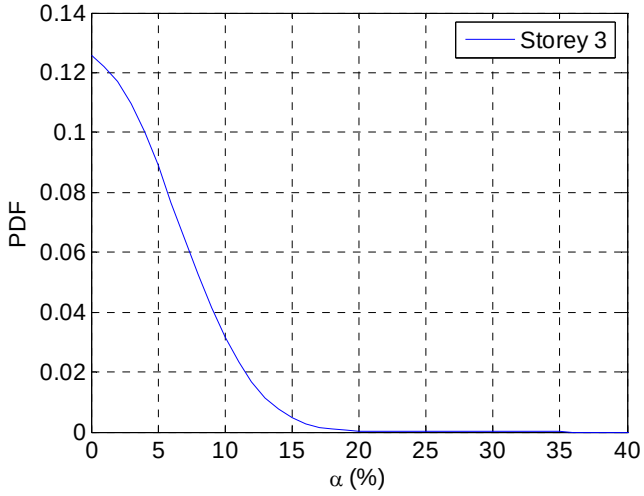

(c) Story 3

Figure 7.10 Derivatives of probability functions $P\left\{K^u - K^d \geq \alpha \times K^u\right\}$ in Scenario 1: (a) Story 1, (b) Story 2, (c) Story 3

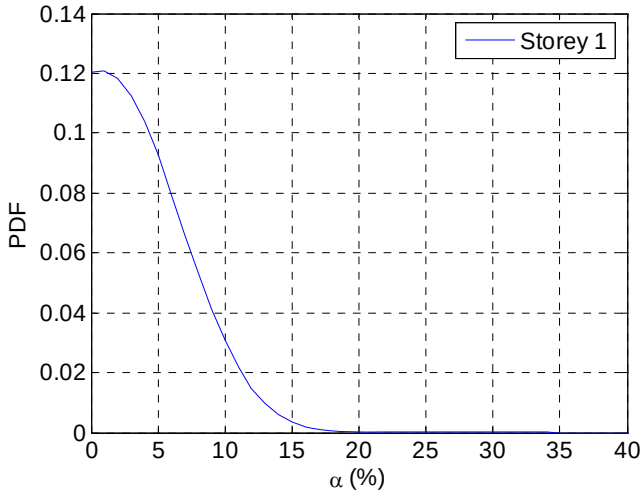

(a) Story 1

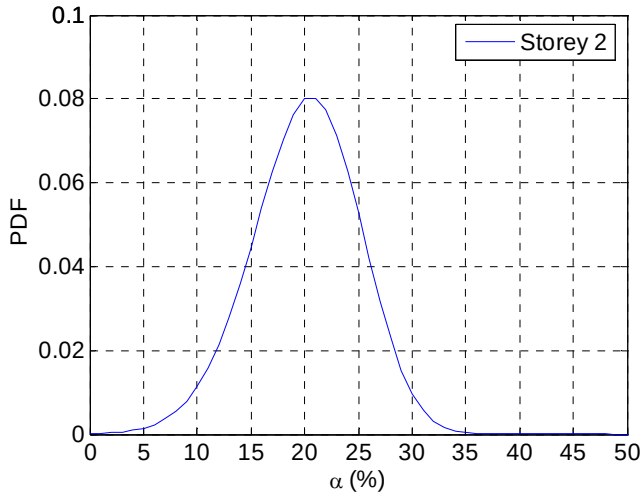

(b) Story 2

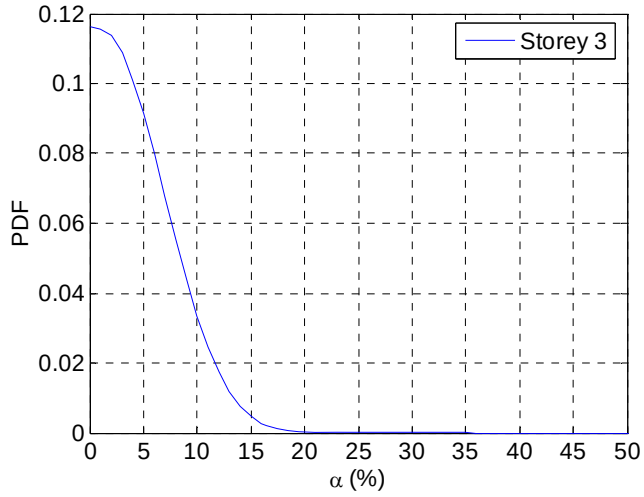

(c) Story 3

Figure 7.11 Derivatives of probability functions $P\left\{K^u - K^d \geq \alpha \times K^u\right\}$ in Scenario 2:

(a) Story 1, (b) Story 2, (c) Story 3

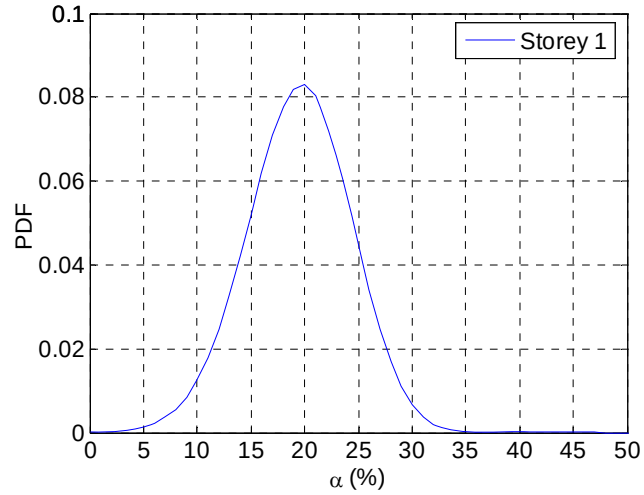

(a) Story 1

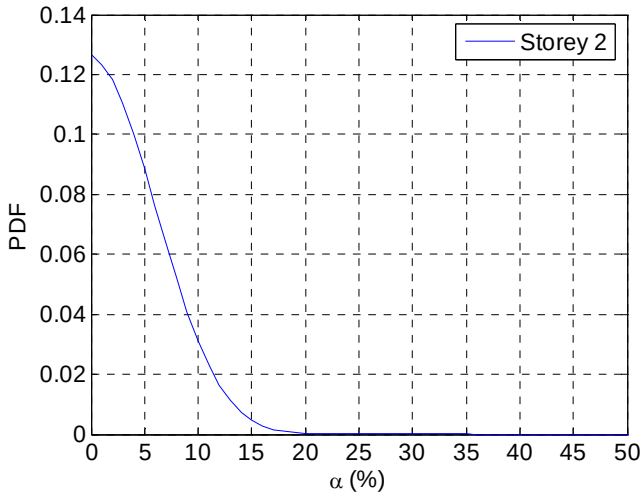

(b) Story 2

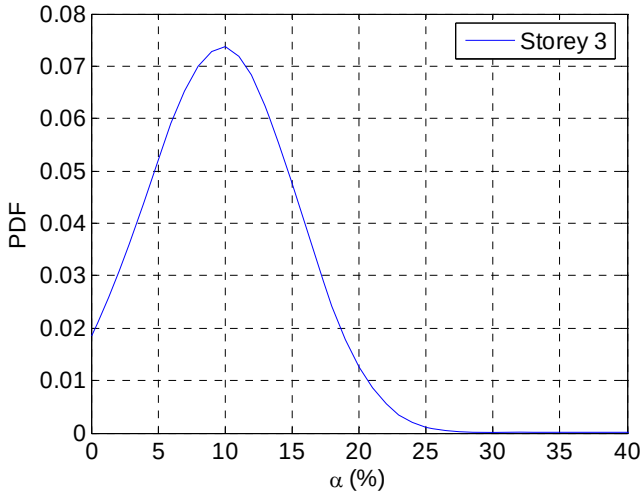

(c) Story 3

Figure 7.12 Derivatives of probability functions $P\left\{K^u - K^d \geq \alpha \times K^u\right\}$ in Scenario 3:

(a) Story 1, (b) Story 2, (c) Story 3

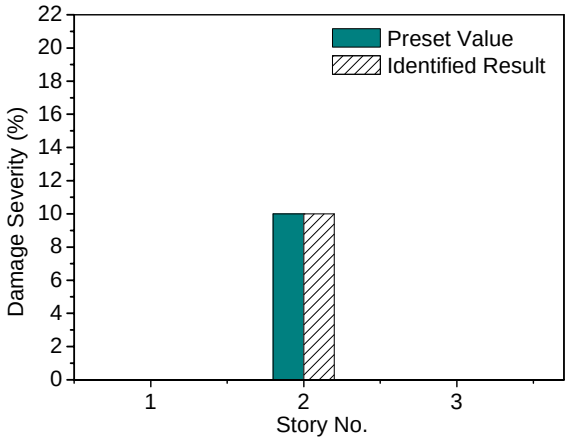

(a) Scenario 1

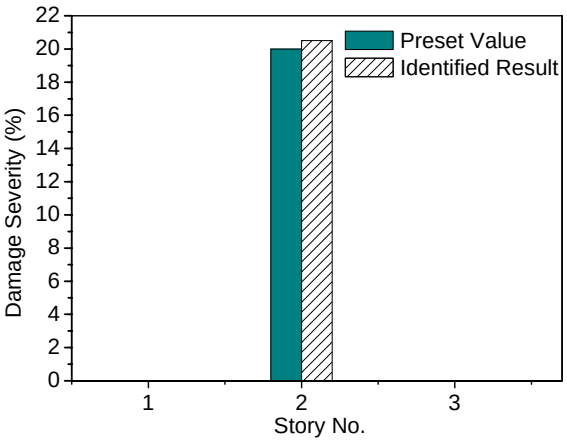

(b) Scenario 2

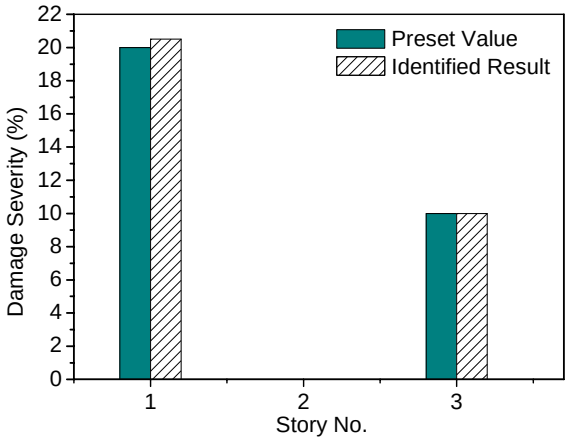

(c) Scenario 3

Figure 7.13 Identified damage severities in comparison with the real values: (a) Scenario 1, (b) Scenario 2, (c) Scenario 3

CHAPTER 8

RELIABILITY ANALYSIS OF STOCHASTIC BUILDING STRUCTURES

8.1 Introduction

The stochastic damage detection method has been proposed to consider the uncertainties involved in damage detection of building structures in Chapter 7. To further evaluate the reliability of the instrumented building structures, structural component probability and structural system probability will be investigated in this chapter. Although the development of structural damage detection has now attained some degree of maturity, the application of measured data of structural health monitoring system (SHMS) to structural reliability evaluation is still in its infancy. A gap between health monitoring technologies and structure integrity assessment impedes structure managers to benefit from measured data for inspection, maintenance and management exercises. In addition, in most of previous investigations, structural system identification and structural reliability assessment are treated separately. When uncertainties or random parameters are taken into account, the stiffness parameters of all the elements in a building structure identified are random parameters coupling with each other. Under this circumstance, it is prohibitive to evaluate structural reliability by the current reliability analysis methods for civil structures. This chapter therefore presents two integrated methods to evaluate structural dynamic reliability and structural system reliability, respectively. The integrated methods accept the measurement responses as input and produce as

output the reliability of the concerned instrumented structures, in which structural reliability analysis is coupled with structural system identification. Numerical investigation is conducted through a stochastic shear building structure whose stiffness parameters can not be directly utilized to evaluate structural reliability because they all are random parameters obtained by system identification with consideration of uncertainties and they couple with each other. Three damage scenarios of the stochastic shear building are also investigated. The external force of the building structure is an EL Centro excitation. Two cases are considered. In the first case, only the random parameters of the undamaged and damaged building structures are considered. In the second case, there are random parameters both in the structures and in the external force. Numerical analysis results show that the component reliability and the system reliability of the stochastic building structures are effectively evaluated by the proposed methods using limited measurement responses.

8.2 Component Reliability of Stochastic Building Structures

In this section, a new structural component reliability analysis method is proposed by integrating the SMBDD method and the probability density evolution equation (PDEE)-based absorbing boundary condition method (Chen and Li, 2005). The algorithm of the proposed method is presented for stochastic structures with only one limit state function or one specified failure mode. The system identification and structural reliability analysis are not treated separately in the algorithm of the proposed method. On the contrary, the structural reliability analysis is coupled with the structural system identification by directly using the probabilistic information of

the random parameters considered in the structural system identification other than the random stiffness parameters of all structural elements identified. The component reliability of a stochastic building structure without explicit system identification can thus be evaluated by the proposed method.

8.2.1 Governing equations of structural component reliability analysis

Without loss of generality, a building structure can be discretized into a MDOF system by the finite element method, and the equation of motion in the matrix form of the building structure can be expressed as

$$\mathbf{M}\ddot{\mathbf{X}}(t)+\mathbf{C}(\boldsymbol{\Theta})\dot{\mathbf{X}}(t)+\mathbf{K}(\boldsymbol{\Theta})\mathbf{X}(t)=\mathbf{g}(\boldsymbol{\Psi},t) \tag{8.1}$$

where $\ddot{\mathbf{X}}$, $\dot{\mathbf{X}}$, $\mathbf{X}$ are the acceleration, the velocity and the displacement vector of N order; $\mathbf{g}(\boldsymbol{\Psi},t)$ is a random or deterministic external force, where $\boldsymbol{\Psi}$ is the $n_{\boldsymbol{\Psi}}$ order random parameter vector with the known probability density function $p_{\boldsymbol{\Psi}}(\boldsymbol{\psi})$ which reflects the uncertainty in the excitation. If $\boldsymbol{\Psi}$ is deterministic, $\mathbf{g}(\boldsymbol{\Psi},t)$ stands for a deterministic dynamic excitation. $\mathbf{M}$, $\mathbf{C}$ and $\mathbf{K}$ are the $N \times N$ mass matrix, damping matrix and stiffness matrix, respectively; $\boldsymbol{\Theta}$ is the random parameter vector of n_θ order which reflects the uncertainty in the structural identification procedure, with the known probability density function $p_{\boldsymbol{\Theta}}(\boldsymbol{\theta})$. Evidently, due to the random nature of $\boldsymbol{\Theta}$, the identified structural stiffness is also a random stiffness matrix, denoted as $\mathbf{K}(\boldsymbol{\Theta})$. For every given value $\boldsymbol{\theta}$ of the random parameter vector $\boldsymbol{\Theta}$, the structural stiffness vector of the building structure can be identified by the SMBDD method, denoted as $\mathbf{k}_{\boldsymbol{\Theta}}(\boldsymbol{\theta})$. As usual, the structural responses have the following deterministic initial condition

$$\mathbf{X}(t_0) = \mathbf{x}_0, \quad \dot{\mathbf{X}}(t_0) = \dot{\mathbf{x}}_0 \tag{8.2}$$

In general, the dynamic reliability of the building structure under the dynamic excitation $\mathbf{g}(\mathbf{\Psi}, t)$ can be given by

$$R(t) = P\left\{X(\tau) \in \Omega_S, \ \tau \in [0, t]\right\} \tag{8.3}$$

where P{·} is the probability of the random event; Ω_S is the safe domain. Equation (8.1) means that the dynamic reliability is the total probability of a random event that are always in the safe domain over the time duration [0, t]. If the reliability is assessed through either the top displacement or one inter-story displacement of a building structure, the structural dynamic reliability can be expressed as

$$R(t) = P\left\{\left|X_{top}(\tau)\right| \le x_{B1}, \ \tau \in [0, t]\right\} \tag{8.4a}$$

or

$$R(t) = P\left\{\left|X_{floor}(\tau)\right| \le x_{B2}, \ \tau \in [0, t]\right\} \tag{8.4b}$$

where $X_{top}(t)$ is the displacement response of the building at the top, $X_{floor}(t)$ is the story drift investigated and x_{B1} or x_{B2} is the threshold of the displacement.

As mentioned before, for every given value $\boldsymbol{\theta}$ of the stochastic parameter vector $\mathbf{\Theta}$, the identified structural lateral stiffness vector is unique and denoted as $\mathbf{k}_{\mathbf{\Theta}}(\boldsymbol{\theta})$. Let $\mathbf{Z} = (\mathbf{\Theta}, \mathbf{\Psi})$, the joint PDF of $\mathbf{X}(t)$ and $\mathbf{Z}$ is denoted as $p_{\mathbf{XZ}}(x, \mathbf{z}, \mathbf{k}_{\mathbf{\Theta}}(\boldsymbol{\theta}), t)$, here $\mathbf{X}(t)$ may be displacement responses, internal forces, stress response, and others. The general probability density evolution equation is given as

$$\frac{\partial p_{\mathbf{XZ}}(x, \mathbf{z}, \mathbf{k}_{\mathbf{\Theta}}(\boldsymbol{\theta}), t)}{\partial t} + \dot{\mathbf{X}}(\mathbf{z}, t)\frac{\partial p_{\mathbf{XZ}}(x, \mathbf{z}, \mathbf{k}_{\mathbf{\Theta}}(\boldsymbol{\theta}), t)}{\partial x} = 0 \tag{8.5}$$

with the initial condition

$$p_{\mathbf{XZ}}(x,\mathbf{z},t)\Big|_{t=t_0} = \delta(x-x_0)\,p_{\mathbf{Z}}(\mathbf{z}) \tag{8.6}$$

Since Equation (8.3) means that the reliability is the total probability of the random events that are always in the safe domain over the time duration [0, t], once the random events enter the failure domain the related probability will never return to the safe domain. That is, the probability density transits one-direction outside the boundary. As a result, an absorbing boundary condition is imposed on Equation (8.5) as follows.

$$p_{\mathbf{XZ}}(x,\mathbf{z},t) = 0, \qquad x \in \Omega_{\mathrm{f}} \tag{8.7}$$

where Ω_{f} is the failure domain.

If the solution of the initial-boundary-value problem (8.5), (8.6) and (8.7) is $\breve{p}_{X\mathbf{Z}}(x,\mathbf{z},t)$, then the 'remaining' PDF is

$$\breve{p}_X(x,t) = \int_{\Omega_{\mathbf{Z}}} \breve{p}_{X\mathbf{Z}}(x,\mathbf{z},t)\mathrm{d}\mathbf{z} \tag{8.8}$$

and the structural dynamic reliability will be given by

$$R(t) = \int_{\Omega_S} \breve{p}_X(x,t)dx \tag{8.9}$$

where Ω_S is the safe domain. For the symmetrical double boundary problem, Equation (8.9) becomes

$$R(t) = \int_{-x_B}^{x_B} \breve{p}_X(x,t)dx \tag{8.10}$$

It can be seen from the above derivation that the probability flows like the water in a river with leaking dikes.

8.2.2. Numerical algorithm for structural component reliability analysis

Denote the stochastic variations as $\mathbf{Z}$ which includes two kinds of random parameters: the random parameters in the excitation $\boldsymbol{\Psi}$ and the structural random parameters $\boldsymbol{\Theta}$. The basic procedure to evaluate the dynamic reliability of a building structure is presented in Figure 8.1 and depicted as follows:

1. Discretize the stochastic variations $\boldsymbol{Z}$ into representative points $\mathbf{z}_i = (\boldsymbol{\theta}_q, \boldsymbol{\psi}_r),\ i = 1, 2, \cdots, N_z,\ q = 1, 2, \cdots, N_\theta,\ r = 1, 2, \cdots, N_\psi$ in the domain Ω_z, Denote the representative domain of each representative point as V_i. The probability measure over this domain is assigned to this point and denoted as P_i.

$$P_i = \int_{V_i} p_{\mathbf{Z}}(\mathbf{z}) d\mathbf{z} \tag{8.11}$$

Clearly, $\sum_{i=1}^{N_z} P_i = 1$. The initial condition expressed by Equation (8.6) is discretized correspondingly as

$$p_{\mathbf{XZ}}(x, \mathbf{z}_i, t)\Big|_{t=t_0} = \delta(x - x_0) P_i,\ i = 1, 2, \cdots, N_z \tag{8.12}$$

2. For every specific value of structural random parameter vector $\boldsymbol{\theta}_q$, the stiffness parameters of the undamaged or damaged building structure, $\mathbf{k}_{\boldsymbol{\Theta}}(\boldsymbol{\theta}_q)$, can be identified by the SMBDD method using the structural health monitoring system (SHMS)-recorded measurement data;
3. For a given $\mathbf{z}_i = (\boldsymbol{\theta}_q, \boldsymbol{\psi}_r)$ and its corresponding identified stiffness vector $\mathbf{k}_{\boldsymbol{\Theta}}(\boldsymbol{\theta}_q)$, calculate the velocity $\dot{\mathbf{X}}(\mathbf{z}_i, t)$ by solving Equation (8.1) with a deterministic numerical method;
4. Substitute $\dot{\mathbf{X}}(\mathbf{z}_i, t)$ into Equation (8.5), and solve the initial-boundary-value problem defined by Equations (8.5), (8.12) and (8.7) with the finite difference

method;

5. Repeat Steps 3 and 4 until $\breve{p}_{XZ}(x, \mathbf{z}_i, t)$ at every given discrete points, $\mathbf{z}_i, i = 1, 2, \cdots, N_z$, are obtained;
6. Synthesize the results in Step 5 to obtain $\breve{p}_X(x,t)$ through the discretized version of Equation (8.8)

$$\breve{p}_X(x,t) = \sum_{i=1}^{N_i} \breve{p}_{X\mathbf{Z}}(x, \mathbf{z}_i, t) \tag{8.13}$$

7. Carry out the numerical integration in Equation (8.9) to obtain the structural component reliability with respect to time *t*.

The deterministic structural stiffness identification is embedded in the procedure of structural component reliability evaluation in Step 2. Detailed information of the method to identify structural stiffness can be found in Chapters 3, 4 and 5. In Chapter 7, the identified stiffness values of $\mathbf{k}_{\Theta}(\boldsymbol{\theta})$ for every given discrete points of the stochastic parameters are utilized to calculate the distribution of the structural stiffness parameters and then detect structural damage. In this chapter, they are arrayed with their corresponding discrete points of the stochastic parameters to calculate the reliability of building structures.

8.3 System Reliability of Stochastic Building Structures

In this section, a new structural system reliability analysis method is proposed by integrating the SMBDD method and the PDEE-based equivalent extreme value method (Chen and Li, 2007). The algorithm of the integrated method is presented for stochastic structures with multi limit state functions. The structural system reliability

analysis is coupled with the structural system identification in the algorithm of the proposed method.

8.3.1 Governing equations of structural system reliability analysis

Generally speaking, the structural component reliability is such defined that only one limit state function is involved. In other words, only one specified failure mode is considered by the structural component reliability. For the reliability evaluation of a structure, we usually need to take into account more than one indices, or more than one failure modes. For instance, when the serviceability of a multi-story building structure is considered, not only the first inter-story drift is require not to exceed a threshold, but also all the other inter-story drifts are required not to exceed corresponding thresholds. In this case, a family of limit state functions should be considered

$$\begin{aligned} Y_1 &= g_1(\xi_1, \xi_2, \cdots, \xi_n) \\ Y_2 &= g_2(\xi_1, \xi_2, \cdots, \xi_n) \\ &\cdots \\ Y_m &= g_m(\xi_1, \xi_2, \cdots, \xi_n) \end{aligned} \tag{8.14}$$

For example, let us consider an N-story building structure under a random external excitation. It should be noted that all the stiffness parameters of the building structure are random parameters identified by using the SHMS-based measurement data with consideration of uncertainties or random parameters $\boldsymbol{\Theta}$. And the stiffness parameters are also coupling with each other. Obviously, the random nature of the stiffness parameters is caused by the random parameters $\boldsymbol{\Theta}$ considered in the structural system identification. To evaluate the system reliability of the building structure, the identified stiffness parameters can not be directly used. Otherwise, it will be

prohibitive to evaluate the structural system reliability especially for large civil building structures when a large number of random stiffness parameters should be considered. In this regards, a new structural system reliability analysis method is proposed which couples the structural system reliability analysis with the structural system identification by utilizing the probabilistic information of the random parameters $\boldsymbol{\Theta}$.

The equation of motion in the matrix form of the building structure is expressed as

$$\mathbf{M}\ddot{\mathbf{X}}(t)+\mathbf{C}(\boldsymbol{\Theta})\dot{\mathbf{X}}(t)+\mathbf{K}(\boldsymbol{\Theta})\mathbf{X}(t)=\mathbf{g}(\boldsymbol{\Psi},t) \tag{8.15}$$

with the following deterministic initial condition

$$\mathbf{X}(t_0)=\mathbf{x}_0,\ \ \dot{\mathbf{X}}(t_0)=\dot{\mathbf{x}}_0 \tag{8.16}$$

The meanings of the denotations in Equations (8.15) and (8.16) can be found in Section 8.2.1. The total random parameter vector in the structural system reliability analysis can be denoted as $\mathbf{Z}=(\boldsymbol{\Theta},\boldsymbol{\Psi})$. Due to the random nature of $\mathbf{Z}$, the dynamic responses of the building structure are also random processes. Denote the inter-story drifts from the floor to the top by $X_1(\mathbf{Z},t),X_2(\mathbf{Z},t),\cdots,X_N(\mathbf{Z},t)$, the heights of the stories by $h_1,h_2,\cdots,h_N$. The system reliability of the structure can be defined by

$$R=\Pr\left\{\bigcap_{j=1}^{N}\left\{\left|\frac{X_j(\mathbf{Z},t)}{h_j}\right|<\varphi_{\mathrm{b}},\ \ t\in[0,T]\right\}\right\} \tag{8.17}$$

where φ_{b} is the threshold of inter-story angle. For clarity, we define the dimensionless inter-story drift as

$$\bar{X}_j(\mathbf{Z},t)=\left|\frac{X_j(\mathbf{Z},t)}{h_j\varphi_{\mathrm{b}}}\right|,\ \ j=1,2,\cdots,N \tag{8.18}$$

Thus Equation (8.17) becomes

$$\begin{aligned} R &= \Pr\left\{\bigcap_{j=1}^{N}\left\{\overline{X}_j(\mathbf{Z},t) < 1,\ \ t \in [0,T]\right\}\right\} \\ &= \Pr\left\{\bigcap_{j=1}^{N}\left\{\overline{X}_{j,\max}(\mathbf{Z}) < 1\right\}\right\} \end{aligned} \tag{8.19}$$

where $\overline{X}_{j,\max}(\mathbf{Z}) = \max_{t\in[0,T]}\left\{\overline{X}_j(\mathbf{Z},t)\right\}$. Further, we define an equivalent extreme value by

$$\overline{X}_{\max}(\mathbf{Z}) = \max_{1\le j\le N}\left(\overline{X}_{j,\max}(\mathbf{Z})\right) \tag{8.20}$$

To evaluate the system reliability of the building structure, the PDF of the equivalent extreme value $\overline{X}_{\max}(\mathbf{Z})$ should be calculated. Introduce a virtual stochastic process

$$Y(\mathbf{Z},\tau) = \overline{X}_{\max}(\mathbf{Z})\cdot\tau \tag{8.21}$$

where τ is somewhat like the time and is called as the "virtual time". $Y(\tau)$ is a "virtual stochastic process" whose randomness comes from the random parameter vector $\mathbf{Z}$. The virtual stochastic process satisfy the conditions

$$Y(\mathbf{Z},\tau)\Big|_{\tau=0} = 0\,,\ \ Y(\mathbf{Z},\tau)\Big|_{\tau=1} = \overline{X}_{\max}(\mathbf{Z}) \tag{8.22}$$

Differentiating Equation (8.21) on both sides with regard to τ will yield

$$\dot{Y}(\mathbf{Z},\tau) = \overline{X}_{\max}(\mathbf{Z}) \tag{8.23}$$

The virtual stochastic process satisfies the following probability density evolution equation

$$\frac{\partial p_{Y\mathbf{Z}}(y,\mathbf{z},\tau)}{\partial\tau} + \dot{Y}(\mathbf{z},\tau)\frac{\partial p_{Y\mathbf{Z}}(y,\mathbf{z},\tau)}{\partial y} = 0 \tag{8.24}$$

with the initial condition [From Equation (8.16)]

$$p_{Y\mathbf{Z}}(y,\mathbf{z},\tau)\,|_{\tau=0} = \delta(y)p_{\mathbf{Z}}(\mathbf{z}) \tag{8.25}$$

where $p_{Y\mathbf{Z}}(y,\mathbf{z},\tau)$ is the joint PDF of Y and $\mathbf{Z}$, and $p_{\mathbf{Z}}(\mathbf{z})$ is the PDF of $\mathbf{Z}$.

Once the initial-value problem consisting of Equations (8.24) and (8.25) is solved, the PDF of $Y(\tau)$ will be given by

$$p_Y(y,\tau) = \int_{\Omega_{\mathbf{z}}} p_{Y\mathbf{Z}}(y,\mathbf{z},\tau)d\mathbf{z} \tag{8.26}$$

Note that $\bar{X}_{\max} = Y(\tau)_{\tau=1}$, the PDF of $Y(\tau)$ at time 1 is the PDF of $\bar{X}_{\max}$.

$$p_{\bar{X}_{\max}}(x) = p_Y(y,\tau)\,|_{\tau=1} \tag{8.27}$$

The integral on the PDF of this equivalent extreme value random variable will then give the system reliability and the probability of failure, i.e.

$$R = \Pr\left\{\bar{X}_{\max} < 1\right\} = \int_0^1 p_{\bar{X}_{\max}}(x)dx \tag{8.28}$$

$$P_{\mathrm{f}} = 1 - R \tag{8.29}$$

8.3.2. Numerical algorithm for structural system reliability analysis

The numerical algorithm to evaluate the system reliability of a building structure is presented in Figure 8.2 and depicted as follows:

1. Discrete the random parameter vector into representative points in the domain Ω_z, $\mathbf{z}_i = (\boldsymbol{\theta}_q, \boldsymbol{\psi}_r)$, $i = 1,2,\cdots,N_z$, $q = 1,2,\cdots,N_\theta$, $r = 1,2,\cdots,N_\psi$, and calculate the probability measure P_i for every representative point $\mathbf{z}_i$ by Equation (8.11);
2. For every given value $\boldsymbol{\theta}_q$ of the stochastic parameter vector $\boldsymbol{\Theta}$, the structural stiffness parameter vector can be identified by the SMBDD method using the SHMS-based measurement data, denoted as $\mathbf{k}_{\boldsymbol{\Theta}}(\boldsymbol{\theta}_q)$;
3. Substitute the given representative point $\mathbf{z}_q = (\boldsymbol{\theta}_q, \boldsymbol{\psi}_q)$ and the corresponding

stiffness matrix $\mathbf{K}(\boldsymbol{\theta}_q)$ obtained from the identified structural stiffness parameter vector $\mathbf{k}_{\boldsymbol{\Theta}}(\boldsymbol{\theta}_q)$ into Equation (8.1). The inter-story drifts and then the equivalent extreme value $\bar{X}_{\max}(\mathbf{z}_q)$ of the inter-story drifts of the building structure can be calculated for every given value $\mathbf{z}_i$ of the stochastic parameter vector $\mathbf{Z}$;

4. Substitute $\bar{X}_{\max}(\mathbf{z}_q)$ into Equation (8.24), and solve the discretized version of Equations (8.24) ~ (8.25) using the finite difference method;
5. Repeat Steps 2-4 until *i* equals to N_z;
6. Calculate the PDF of $Y(\tau)$ by the discretized version of Equation (8.26) and the PDF of $\bar{X}_{\max}$ is then obtained through Equation (8.27);
7. Carry out the numerical integration in Equation (8.28) to obtain structural system reliability. The failure probability can then be obtained through Equation (8.29).

The structural component reliability after an external excitation can also be calculated by integrating the SMBDD method and the PDEE-based equivalent extreme value method. Since

$$\begin{aligned} \mathrm{R}(T) &= \mathrm{P}\left\{ X_j(\mathbf{Z},\tau) \in \Omega_S,\ \tau \in [0,T] \right\} \\ &= \mathrm{P}\left\{ X_{j,\max}(\mathbf{Z}) \in \Omega_S \right\} \end{aligned} \tag{8.30}$$

where T is the total time duration of an external excitation, $X_{\max}(\mathbf{Z}) = \max_{t\in[0,T]} \left\{ X(\mathbf{Z},t) \right\}$.

Therefore, the only difference between structural component reliability after an external excitation in terms of the *j*th interested response and structural system reliability lies in that the PDF of the maximum value of the *j*th interested response $X_{j,\max}(\mathbf{Z})$ rather than the PDF of the equivalent extreme value of the whole

structure $\overline{X}_{\max}(\mathbf{Z})$ should be calculated in the aforementioned procedure. Hence, the corresponding component reliability and failure probability can be respectively evaluated by

$$\mathrm{R}_j = \mathrm{P}\left\{X_{j,\max} \in \Omega_S\right\} = \int_{\Omega_S} p_{X_{j,\max}}(x)dx \tag{8.31}$$

$$\mathrm{P}_{\mathrm{f},j} = 1 - \mathrm{R}_j, \quad j = 1,2,\cdots,N \tag{8.32}$$

8.4 Numerical Investigation

In this section, the undamaged stochastic shear building and its three damage scenarios, that is, Scenarios 1, 2 and 3 that have been investigated in Chapter 7, are employed to evaluate their structural component reliability under the earthquake excitation in the shape of EL Centro acceleration record in the E-W direction. The power spectral density function of the external excitation is estimated and presented in Figure 8.3. The dynamic properties of the four scenarios are analyzed and presented in Table 8.1 in which Scenario 0 stands for the undamaged shear building. Two cases are investigated here. In the first case, only the first modal damping ratio (ξ_1) is considered as a random parameter due to the uncertainty during the damping identification. In the second case, both the first modal damping ratio (ξ_1) and the peak acceleration ($a_{g\max}$) of the earthquake excitation are considered as two random parameters. It means that both the structure and the excitation are random. The details of the two cases are presented in Table 8.2.

Table 8.1 Dynamic properties of the four investigated scenarios

Scenario	Scenario 0			Scenario 1		
Frequency	3.447	7.372	19.155	3.342	7.241	19.085
Mode	1.0000	1.0000	1.0000	1.0000	1.0000	1.0000
	15.4786	13.6161	-0.0949	17.1223	15.1110	-0.0853
	32.3337	-9.8390	0.0063	33.5627	-11.6228	0.0057
Scenario	Scenario 2			Scenario 3		
Frequency	3.220	7.111	19.015	3.358	7.113	17.294
Mode	1.0000	1.0000	1.0000	1.0000	1.0000	1.0000
	19.1813	16.9775	-0.0757	12.5053	10.7809	-0.1197
	35.1855	-13.9395	0.0051	27.7643	-7.3556	0.0088

Table 8.2 Probability information of the random parameters

Case No.	Parameter	Distribution	Mean	C.O.V
1	ξ_1	Lognormal	0.01	0.1
2	ξ_1	Lognormal	0.01	0.1
	$a_{g\max}$	Normal	1.25 m/s^2	0.1

8.4.1 Numerical analysis of structural component reliability

In this section, the reliability is assessed through the top displacement or one inter-story displacement of building structures. In other words, only one limit state function is involved to evaluate structural component reliability. This kind of problem can be solved by the absorbing boundary condition method elaborated in Section 8.2.

8.4.1.1 Numerical investigation on Case A

For the first case, the procedure of evaluating the structural component reliability is depicted as follows. Firstly, measure the displacement responses of the undamaged or damaged structure under a white noise or colored noise excitation and calculate the fourth-order statistical moments of displacement responses. Then discretize the random parameter, the first modal damping ratio, into 21 representative points in the domain $[\bar{\xi}-3\sigma,\ \bar{\xi}+3\sigma]$. The discrete points are listed in Table 7.1 and presented in Figure 7.2. For every given representative point, ξ_i, the horizontal stiffness vector of the undamaged or damaged shear building is identified in the frequency domain by the SMBDD method. The identified results corresponding to each representative point, ξ_i, can be found in Table 7.1.

For every given discrete damping ratio, after the horizontal stiffness values of the undamaged or damaged shear building structure are identified, calculate the corresponding velocity responses $\dot{\mathbf{X}}(\boldsymbol{\theta},t)$ of the displacement of the top floor or the story drifts of the structure under the EL Centro earthquake excitation. After that, solve the initial-boundary-value problem defined by Equations (8.5), (8.6) and (8.7) with the finite difference method. Finally, carry out the numerical integration in Equations (8.8) and (8.9) for reliability assessment.

For Case A, the reliability defined with the boundary of top displacement in the time duration [0, 18s] is presented in Table 8.3. It can be seen from Table 8.3 that the reliability increases for every scenario when the threshold enlarges. Take Scenario 2 as an example. When the threshold of the top displacement ranges from 0.013m to

0.017m, the dynamic reliability of the damaged shear building in the time duration [0, 18s] increases from 11.65% to 99.33%. In addition, the undamaged structure has the higher reliability than the three damage scenarios for every threshold in Table 8.3.

Comparing the results of Scenarios 1 and 2 in Table 8.3, the conclusion can be made that when the concerned damage scenarios have the same damage locations, the larger the damage severity values are, the lower component reliability the damaged structure has. However, the reliability of Scenarios 3 which has both damage of 20% at the first story and damage of 10% at the third story is larger than that of Scenarios 2 which only has single damage of 20% at the second story. This may be explained as follows. As seen from Figure 8.3 that the power spectral density of the EL Centro excitation almost equals to zero when frequency is larger than 15Hz. The third mode frequencies of the undamaged shear building and the three damage scenarios are all larger than 15Hz, which means that the third mode responses are filtered by the EL Centro excitation. Only the first two modes take action in the displacement responses. In addition, the first two mode frequencies of Scenario 3 are respectively 3.358 and 7.113 which are respectively larger than the first two mode frequencies of Scenario 2, 3.220 and 7.111. That is, if the third mode does not take action, the damaged structure of Scenario 2 is more flexible than the damaged structure of Scenario 3. Therefore, when the component reliability is defined by the threshold of top displacement, Scenario 2 should have lower reliability than Scenario 3. This has been demonstrated by the results in Table 8.3. The statement can be made that when the component reliability is defined by the threshold of the top displacement response of the building structure, the component reliability depends on the dynamic properties of the structure, the external excitation and the threshold.

Table 8.3 Reliability of Case A in terms of different thresholds of the top displacement

Threshold (mm)	Reliability (%)			
	Scenario 0	Scenario 1	Scenario 2	Scenario 3
13.0	98.75	81.27	11.65	84.88
14.0	99.95	89.89	21.97	93.08
15.0	100.00	96.58	38.19	97.81
15.5	100.00	98.99	51.45	99.30
16.0	100.00	99.96	73.30	99.95
17.0	100.00	100.00	99.33	100.00

The component reliability of each story defined by different thresholds of each story drift is presented in Tables 8.4~8.6. Since the horizontal stiffness value of the first story of the undamaged shear building is much larger than that of the other two stories, which is 15 times of that of the second story and 30 times of that of the third story, the threshold of the first story drift is set to be much smaller than those of the other two story drifts.

Table 8.4 Reliability of Case A in terms of different thresholds of story drift 1

Threshold (mm)	Reliability (%)			
	Scenario 0	Scenario 1	Scenario 2	Scenario 3
0.4	69.61	55.21	4.52	5.80
0.5	99.89	91.25	54.85	73.45
0.6	100.00	100.00	100.00	96.59
0.7	100.00	100.00	100.00	100.00

Table 8.5 Reliability of Case A in terms of different thresholds of story drift 2

Threshold (mm)	Reliability (%)			
	Scenario 0	Scenario 1	Scenario 2	Scenario 3
6.0	99.90	73.92	2.69	96.95
7.0	100.00	96.89	17.62	100.00
8.0	100.00	100.00	53.21	100.00
9.0	100.00	100.00	100.00	100.00

Table 8.6 Reliability of Case A in terms of different thresholds of story drift 3

Threshold (mm)	Reliability (%)			
	Scenario 0	Scenario 1	Scenario 2	Scenario 3
6.0	53.15	46.40	11.60	10.23
7.0	97.59	86.31	43.70	64.22
8.0	100.00	100.00	99.86	94.28
9.0	100.00	100.00	100.00	100.00

It can be seen form Tables 8.4~8.6 that the component reliability of every story increases for every scenario when the threshold enlarges. Take Scenario 2 in Table 8.6 for example, when the threshold ranges from 6mm to 9mm, the component reliability of the damaged shear building increases from 11.60% to 100.00%. In addition, the reliability of the undamaged structure has the highest value for every threshold in Tables 8.4~8.6.

It can also be seen from Table 8.4 that although Scenarios 1 and 2 have no damage at the first story, the component reliability values of the first story in Scenarios 1 and 2 are still apparently decreased. And the larger the damage severity at the second story, the lower the component reliability of the first story of the damaged structure. Likewise, as seen from Table 8.6 that although Scenarios 1 and 2 have no damage at

the third story, the component reliability values of the third story in Scenarios 1 and 2 are still apparently decreased. And the larger the damage severity at the second story, the lower the component reliability of the third story of the damaged structure. The component reliability of each story is not only dependent on the horizontal stiffness of itself but also concerned with the dynamic properties of the whole structure.

Similarly, although the first story of Scenario 3 has the damage of 20%, the component reliability of the first story in Scenario 3 is generally higher than that in Scenario 2 which has no damage at the first story according to Table 8.4. And the component reliability of the third story in Scenario 3 which has damage of 10% at the third story is sometimes higher than that in Scenario 2 which has no damage at the third story instead according to Table 8.6. The statement can be made that when the component reliability of each story is defined by the threshold of the corresponding story drift of the undamaged or damaged building structure, the component reliability depends on its own horizontal stiffness, the dynamic properties of the whole structure, the properties of the external excitation and the threshold.

Furthermore, the component reliability of Scenario 2 defined by different thresholds of the top displacement in the time interval [4s, 6s] is presented in Figure 8.4. The component reliability of the second story in Scenario 2 defined by different thresholds of Story Drift 2 in the time interval [0, 16s] is presented in Figure 8.5. The changes of these component reliabilities of the damaged structure during the earthquake excitation can be seen in Figures 8.4 and 8.5.

8.4.1.2 Numerical investigation on Case B

For the second case, the procedure of evaluating the structural component reliability is depicted as follows. Firstly, measure the displacement responses of the undamaged or damaged structure under a colored noise excitation and calculate the fourth-order statistical moments of story drifts. Then discretize the stochastic variations $\mathbf{Z}$ into representative points in the domain Ω_z and denote the abbreviation of the lattice point as $\mathbf{z}_1 = (\boldsymbol{\theta}_1, \boldsymbol{\psi}_1)$, $\mathbf{z}_2 = (\boldsymbol{\theta}_2, \boldsymbol{\psi}_2)$, $\cdots$, $\mathbf{z}_{n_z} = (\boldsymbol{\theta}_{n_z}, \boldsymbol{\psi}_{n_z})$, where $\boldsymbol{\Theta}$ is the first modal damping ratio whose uncertainty is considered in the structural identification and the reliability analysis and $\boldsymbol{\Psi}$ is the random maximum acceleration of the EL Centro earthquake excitation. In the analysis, $\boldsymbol{\Theta}$ and $\boldsymbol{\Psi}$ are independent to each other. Detailed probabilistic information about them can be found in Table 8.2. In the numerical analysis, the random parameter vector $\mathbf{Z}$ is discretized into 441 representative points as presented in Figure 8.6.

For every given discrete point, $\boldsymbol{\theta}_q$, the horizontal stiffness vector of the investigated shear building can be identified by the SMBDD method. After that, for every given discrete point $\mathbf{z}_q = (\boldsymbol{\theta}_q, \boldsymbol{\psi}_q)$, calculate the corresponding velocity responses $\dot{\mathbf{X}}(\mathbf{z}_q, t)$ of the displacement of the top floor and the story drifts of the structure under the EL Centro earthquake excitation. Solve the initial-boundary-value problem defined by Equations (8.5), (8.6) and (8.7) with the finite difference method and carry out the numerical integration in Equations (8.8) and (8.9), the structural component reliability defined by top displacement or story drifts can be finally carried out.

For Case B, the calculated reliability defined with the boundary of top displacement

of the undamaged structure and the damaged structure after the EL Centro earthquake excitation is listed in Table 8.7. As seen form Table 8.7, the reliability increases for every scenario when the threshold enlarges. Take Scenario 2 in Table 8.7 as an example, when the threshold ranges from 0.013m to 0.017m, the dynamic reliability of the damaged shear building increases from 16.85% to 69.03%. In addition, the reliability of the undamaged structure is the highest for every threshold. The reliability decreases for the damaged structure with Scenarios 1 and 2. The larger the damage severity at the second story, the lower the reliability of the damaged structure. For the same reason as has been explained in Case A, although Scenario 3 has both the damage of 20% at the first story and the damage of 10% at the third story, its reliability defined by the threshold of the top displacement is still larger than that of Scenario 2.

Table 8.7 Reliability of Case B in terms of different thresholds of the top displacement

Threshold (m)	Reliability (%)			
	Scenario 0	Scenario 1	Scenario 2	Scenario 3
0.0130	90.90	74.48	16.85	76.81
0.0140	97.32	86.96	30.77	89.20
0.0150	99.42	93.97	49.49	95.43
0.0160	99.91	97.54	69.03	98.25

The component reliability values of Story 1, 2 and 3 defined with the threshold of the corresponding story drift are respectively presented in Table 8.8~8.10 for Case B. It can be seen form Tables 8.8~8.10, the reliability increases for every scenario when the threshold enlarges. Taking Scenario 2 in Table 8.8 as an example, when the threshold ranges from 6mm to 9mm, the reliability of the damaged shear building increases from 4.70% to 88.46%. In addition, the reliability of the undamaged

structure is the highest for every threshold in Tables 8.8~8.10.

Table 8.8 Reliability of Case B in terms of different thresholds of story drift 1

Threshold (m)	Reliability (%)			
	Scenario 0	Scenario 1	Scenario 2	Scenario 3
0.0005	98.40	89.69	55.94	60.10
0.0006	99.99	99.22	95.67	93.00
0.0007	100.00	99.99	99.95	99.21
0.0008	100.00	100.00	100.00	99.96

Table 8.9 Reliability of Case B in terms of different thresholds of story drift 2

Threshold (m)	Reliability (%)			
	Scenario 0	Scenario 1	Scenario 2	Scenario 3
0.006	93.19	63.63	4.70	92.90
0.007	99.80	92.21	22.83	99.37
0.008	100.00	99.05	58.52	99.97
0.009	100.00	99.94	88.46	100.00

Table 8.10 Reliability of Case B in terms of different thresholds of story drift 3

Threshold (m)	Reliability (%)			
	Scenario 0	Scenario 1	Scenario 2	Scenario 3
0.006	50.68	46.21	15.98	19.28
0.007	88.09	82.75	49.79	60.38
0.008	98.83	96.55	85.48	88.90
0.009	99.96	99.64	98.20	98.07

Although Scenarios 1 and 2 have no damage at the first story, the component reliability values of the first story in Scenarios 1 and 2 are still apparently decreased according to Table 8.8. And the larger the damage severity at the second story, the lower the component reliability of the first story of the damaged structure. Likewise,

although Scenarios 1 and 2 have no damage at the third story, the component reliability values of the third story in Scenarios 1 and 2 are still apparently decreased with the increase of the damage severity at the second story according to Table 8.10.

Similarly, although Scenario 3 has both the damage of 20% at the first story and the damage of 10% at the third story, its component reliability values of the first story and the third story are generally close to or higher than those of Scenario 2 according to Tables 8.8 and 8.10. The component reliability of each story is not only dependent on its own horizontal stiffness but also concerned with the dynamic properties of the whole structure, the external excitation and the threshold value.

The dynamic reliability of Scenario 2 defined by different thresholds of the top displacement and the component reliability of the third story defined by different thresholds of Story drift 3 in Scenario 2 is respectively presented in Figures 8.7 and 8.8 for Case B. The changes of the component reliability during the duration of the external excitation can clearly observed from these figures.

8.4.1.3 Effects of more uncertainties on structural reliability

The undamaged or damaged stochastic shear building structures investigated above are identical for Case A and Case B. The only difference between them lies in that the external excitation of Case A is deterministic while the peak acceleration of the external excitation is a random parameter for Case B. It means that both the structure and the external excitation are stochastic in Case B: two random parameters are considered for the latter. To investigate the effect of multiple random parameters on structural reliability, the analytical results of Case A and Case B are further studied

and compared.

By comparing the results in Table 8.3 with those in Table 8.7, it can be seen that the reliability of Case B in terms of different thresholds of the top displacement is lower than that of Case A for Scenarios 0, 1 and 3. However, different observation is made for Scenario 2: when the thresholds are small (13mm, 14mm and 15mm), the corresponding reliability of Scenario 2 which is relatively low improves with the increase of random parameters from Case A to Case B. On the other hand, when the threshold is 16mm, the corresponding reliability of Scenario 2 which is relatively high decreases form 73.30% (Case A) to 69.03% (Case B). A similar result is also observed for the component reliability in terms of different thresholds of Story Drift 2 by comparing the values in Table 8.5 with those in Table 8.9.

According to Equation (8.31), the component reliability values calculated in Tables 8.3 and 8.7 depend on the distribution of the maximum value of the top displacement response. Theoretically speaking, when more uncertainties (random parameters) are considered, the degree of dispersion of the maximum value should increase. That is, the probability density function (PDF) of the maximum value of the top displacement response should become flatter as schematically shown in Figure 8.9(a). Their cumulative distribution functions (CDFs) (see Figure 8.9(b)) have a point of intersection. When a threshold is less than the intersection point, structural reliability becomes higher when more uncertainties are considered. Otherwise, structural reliability should decrease on the contrary.

To demonstrate this conclusion, the actual PDFs of the extreme value of the top

displacement during the external excitations for Scenario 2 are respectively calculated for Case A and Case B and presented in Figure 8.10(a). Their CDFs are also calculated and presented in Figure 8.10 (b). It can be seen from Figure 8.10(a) that when more uncertainties are considered, the distribution of the maximum value of the top displacement becomes more dispersive and flatter. In Figure 8.10(b), the CDFs of Case A and Case B really have a point of intersection. When thresholds are 13mm, 14mm and 15mm, structural component reliability increases from Case A to Case B, while it decreases for the threshold of 16mm. The results are consistent to those presented in Tables 3 and 5. In addition, the PDFs and CDFs of the maximum value of the top displacement for Scenario 3 are also respectively calculated for Case A and Case B and presented in Figure 8.11. As seen from Figure 8.11(a), the distribution of the maximum value of the top displacement for Scenario 3 also becomes more dispersive and flatter. Furthermore, all the thresholds (13mm~16mm) locate at the right side of the intersection point of the CDFs in Figure 8.11(b). Therefore, the reliability becomes lower when more uncertainties are considered for Case B, which is also demonstrated by the results in Tables 8.3 and 8.7. In conclusion, when more uncertainties are considered, the higher structural reliability should decrease, and on the contrary the lower structural reliability should increase.

8.4.2 Numerical analysis of structural system reliability

In addition, when the multi-story shear building structure is required that all the inter-story drifts do not exceed the corresponding threshold, a family of limit state functions should be considered. In other words, the system reliability of the structure should be evaluated under this situation. The proposed algorithm aforementioned in Section 8.3 will be employed here to evaluate the system reliability of the building

structure in the following numerical analysis. In the following numerical analysis, the threshold for all story drifts is set as 7mm.

8.4.2.1 Numerical investigation on Case A

The probability density function (PDF) and cumulative distribution function (CDF) of the extreme value for the undamaged structure are presented in Figure 8.12. In Figure 8.12(b), the abscissa can be understood as the threshold and the ordinate gives their corresponding reliability. The failure probability can then be obtained by Equation (26). The analysis results of the system failure probability in Case A are listed in Table 8.11 and compared with the component failure probability of each story obtained by the same method.

Table 8.11 System failure probability versus component failure probability of every story in Case A (%)

Failure Probability	Scenario 0	Scenario 1	Scenario 2	Scenario 3
Story 1	0.00	0.00	0.00	0.00
Story 2	0.00	2.35	80.19	0.00
Story 3	1.28	12.97	53.45	32.63
The Whole Structure	1.28	12.97	80.19	32.63

It can be seen that the failure probability of the whole structure equals to the maximum value of those of story drifts. For example, Story 3 in Scenario 1 has the maximum failure probability of 12.97% and the failure probability of the whole structure is also 12.97%. This means that Story 3 is the weakest link in the damaged structure with Scenario 1 and the probability of the whole structure is dependent on

the weakest link. For Scenario 2 and 3, the weakest links respectively exist at Story 2 and Story 3 and the failure probability values are respectively 80.19% and 32.63%. The investigated shear building is a special case which satisfies the weakest link assumption. Otherwise, the failure probability of the whole structure should be larger than the maximum of the component failure probabilities of all stories, or the system reliability should be smaller than the minimum component reliability of all stories.

8.4.2.2 Numerical investigation on Case B

The analysis results of the system failure probability in Case B are listed in Table 8.12 and compared with the component failure probability of each story obtained by the same method. It can be seen that the system failure probability of the whole structure equals the maximum component failure probability of all stories. In addition, the system failure probability of the undamaged structure has the lowest value. The system failure probability increases with the increase damage severity at the second story in Scenarios 1 and 2. That is, the larger the single damage severity at the second story, the lower system reliability of the damaged structure. However, the system reliability of Scenario 3 is higher than that of Scenario 2 for the same reason as has been explained in Section 8.4.1.1. The system reliability depends on the dynamic properties of the undamaged and damaged building structure, the external excitation and the limit state functions.

Table 8.12 System failure probability versus component failure probability of every story in Case B (%)

Failure Probability	Scenario 0	Scenario 1	Scenario 2	Scenario 3
Story Drift 1	0.00	0.00	0.00	0.00
Story Drift 2	0.12	5.83	72.13	0.45
Story Drift 3	9.91	14.79	46.90	35.09
The Whole Structure	9.91	14.79	72.13	35.09

8.5 Conclusions

Two integrated methods have been proposed to respectively evaluate structural component reliability and structural system reliability in this chapter. The structural reliability analysis is coupled with structural system identification in the two integrated methods. Firstly, the method to evaluate the component reliability of stochastic structures with only one limit state function has been proposed based on the SMBDD method in conjunction with the PDEE-based absorbing boundary condition method. The governing equations and the numerical algorithm of the component reliability analysis method have been presented. Then, the method to evaluate system reliability of stochastic structures with multi limit state functions has been developed by integrating the SMBDD method with the PDEE-based equivalent extreme value method. The governing equations and the numerical algorithm of the structural system reliability analysis method have also been presented in this chapter.

Numerical investigation has been conducted to evaluate structural component reliability and structural system reliability of a three-story shear building structure and its three damage scenarios by using the two proposed methods. Two cases have

been explored. In the first case, only the first modal damping ratio is considered as a random parameter. In the second case, both the structural random parameter and the maximum acceleration of the EL Centro excitation are taken into account in the reliability analysis. The first modal damping ratio and the maximum acceleration of the EL Centro excitation are both regarded as random parameters in the second case.

The structural component reliability defined by the threshold of top displacement or each story drift has been analyzed for the undamaged shear building and its three damage scenarios. The analysis results show that the structural component reliability increases for the undamaged shear building and the three damage scenarios when the threshold of the top displacement or one story drift enlarges. In addition, the undamaged shear building has the highest reliability. For the damage scenarios at the same locations, the larger damage severity the lower reliability of the damaged shear building.

The analysis results of the structural system reliability defined by multi limit state functions have also been obtained by using the proposed method. Then the system failure probability values of the undamaged shear building and the three damage scenarios are calculated and compared with the component failure probability of each story. The results of comparison show that the failure probability of the whole structure is always larger than or equal to that of one story.

Therefore, the proposed reliability analysis methods can handle the problem that the stiffness parameters of the concerned structure are all random parameters obtained by system identification and coupled with each other by directly using the probabilistic

information of the random parameters considered in system identification and the SHMS-based measurement data. The structural dynamic reliability and structural system reliability of stochastic building structures can be effectively evaluated by the proposed methods.

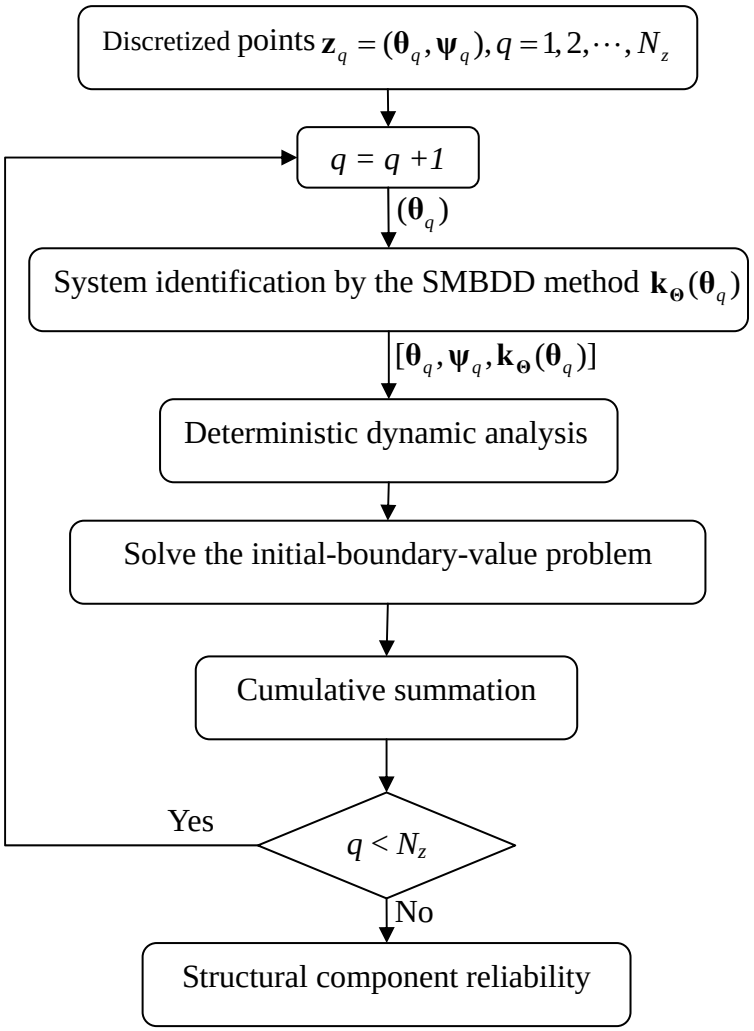

Figure 8.1 Procedure of the structural component reliability analysis method

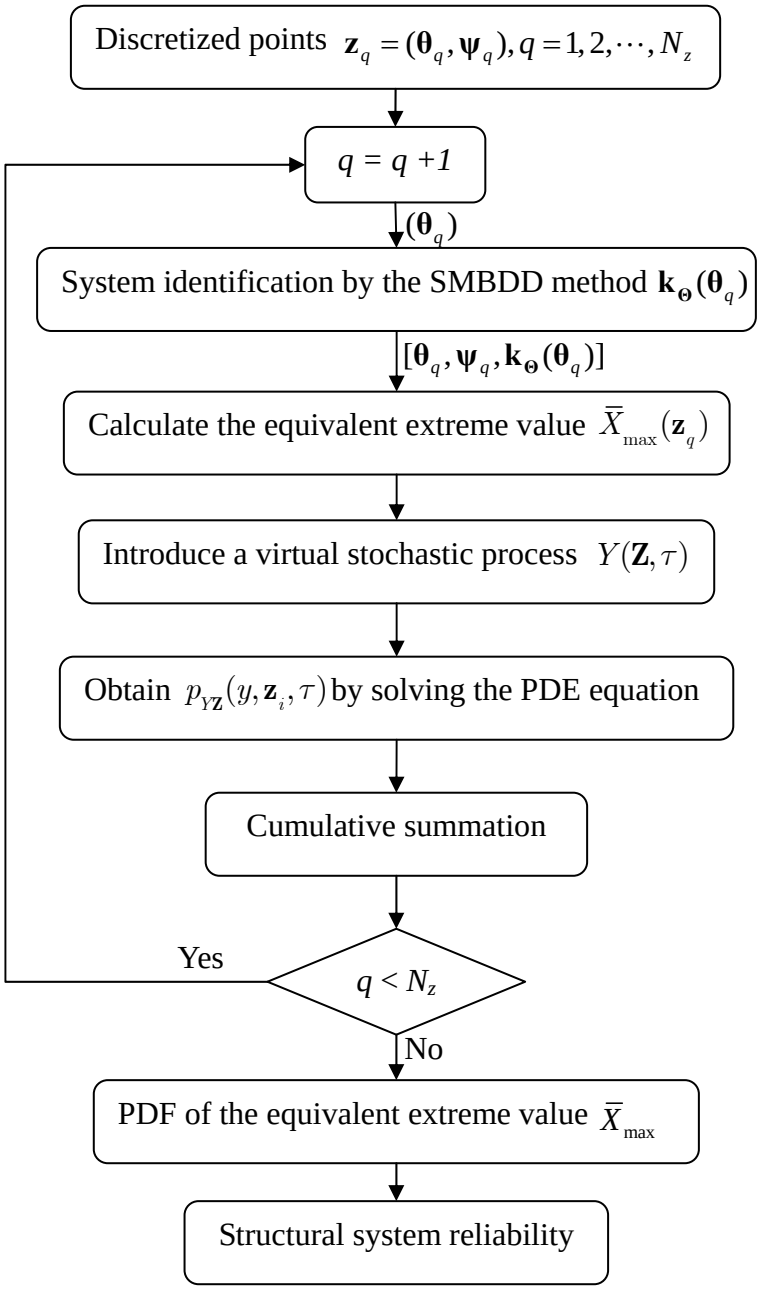

Figure 8.2 Procedure of the structural system reliability analysis method

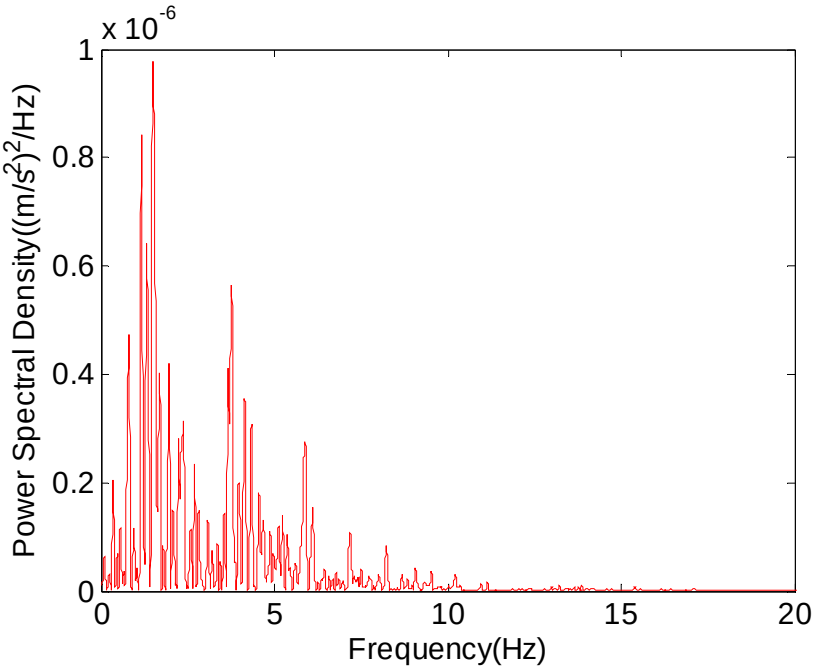

Figure 8.3 Power spectral density of the EL Centro excitation

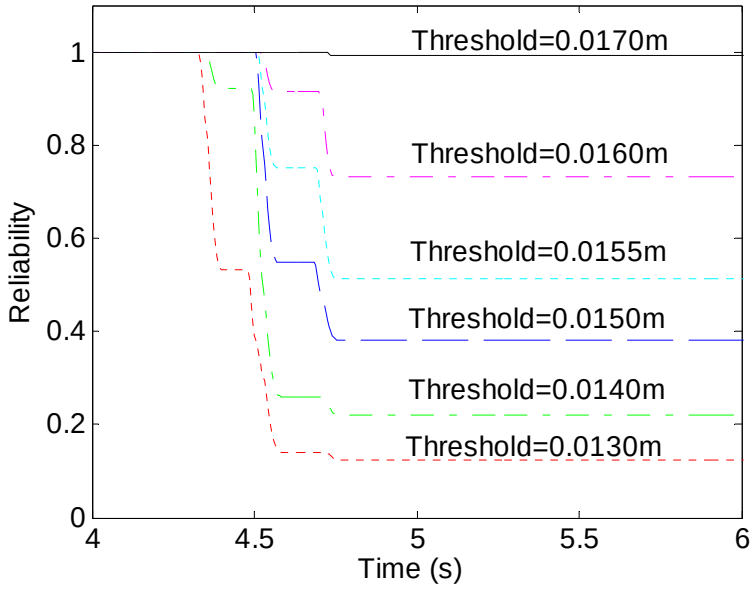

Figure 8.4 Time dependent reliability of Scenario 2 in terms of different thresholds of the top displacement in Case A

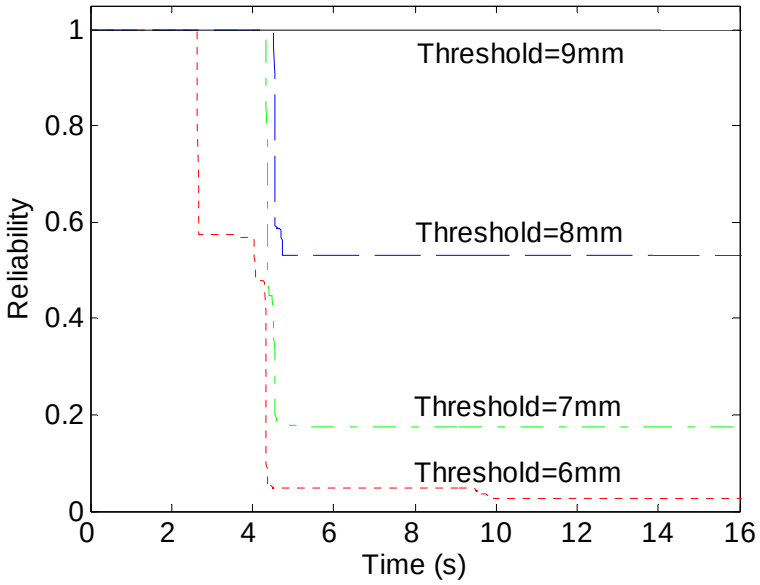

Figure 8.5 Time dependent reliability of the second story of Scenario 2 in terms of different thresholds of Story Drift 2 in Case A

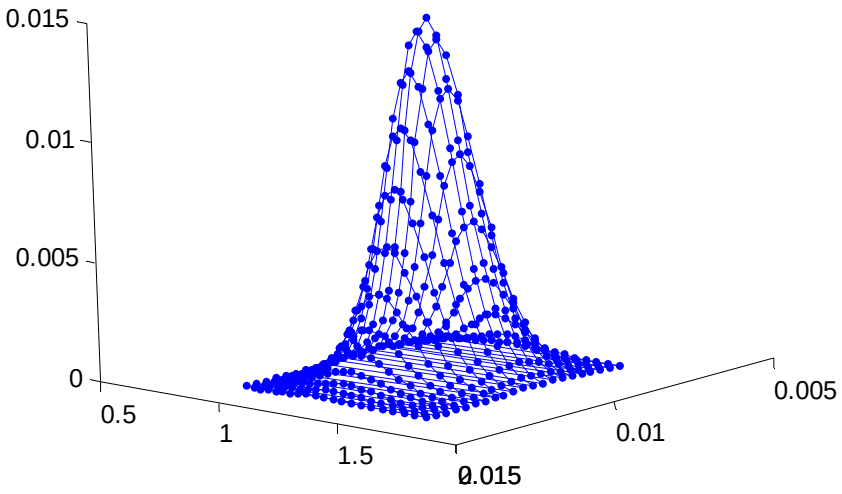

Figure 8.6 Representative points of Case B

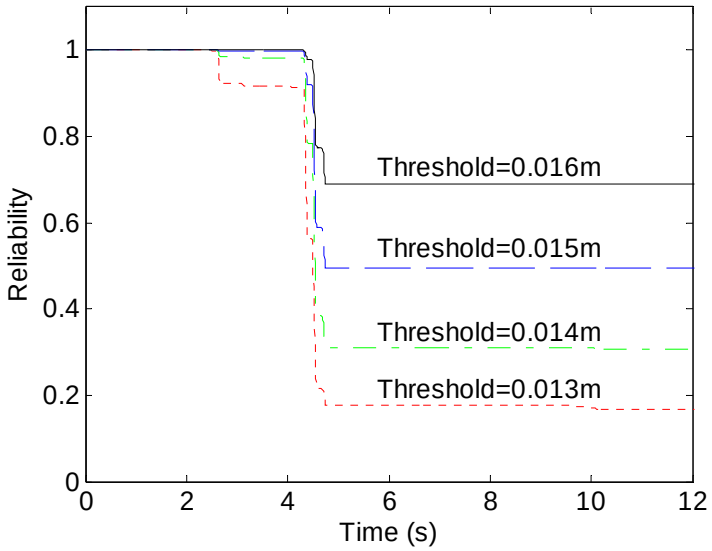

Figure 8.7 Time dependent reliability of Scenario 2 in terms of different thresholds of the top displacement in Case B

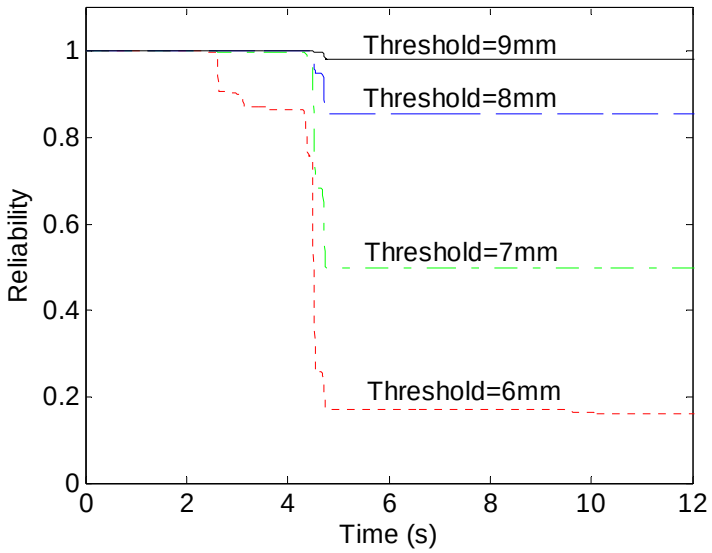

Figure 8.8 Time dependent reliability of the third story of Scenario 2 in terms of different thresholds of Story Drift 3 in Case B

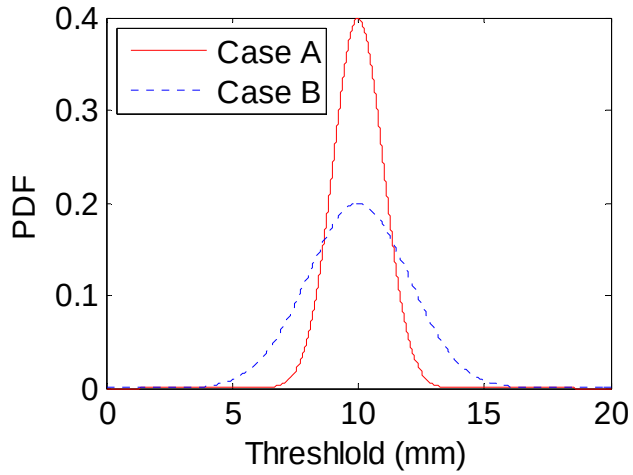

(a) PDFs

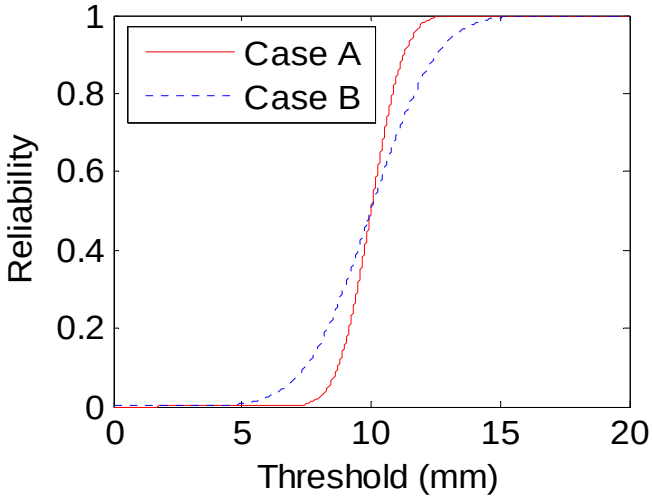

(b) CDFs

Figure 8.9 Schematic View of PDFs and CDFs with different degrees of dispersion

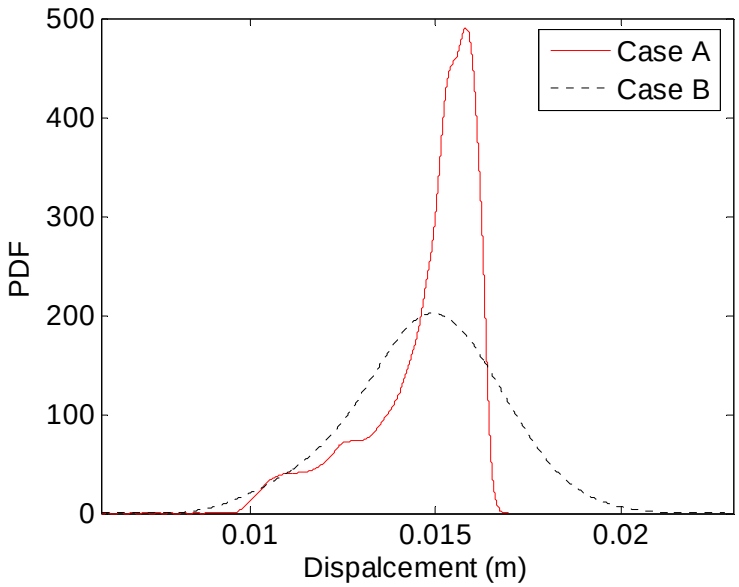

(a) PDFs

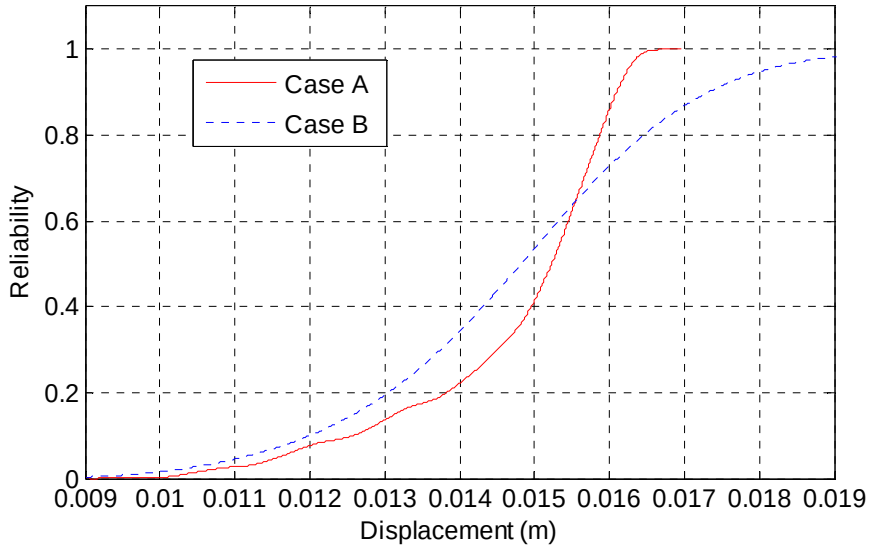

(b) CDFs

Figure 8.10 Comparison of PDFs and CDFs of the maximum value of the top displacement of Scenario 2 between Case A and Case B: (a) PDFs; (b) CDFs

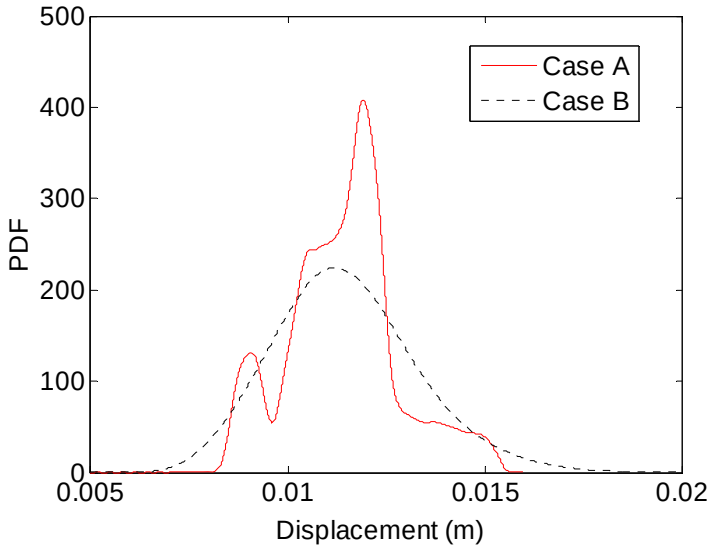

(a) PDFs

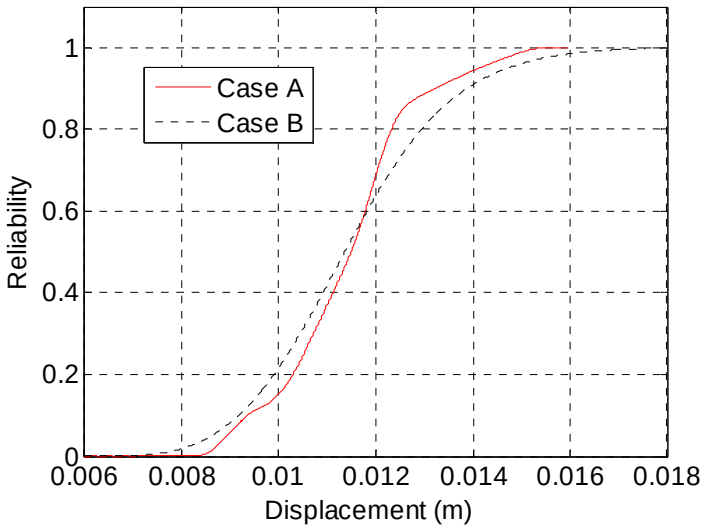

(b) CDFs

Figure 8.11 Comparison of PDFs and CDFs of the maximum value of the top displacement of Scenario 3 between Case A and Case B: (a) PDFs; (b) CDFs

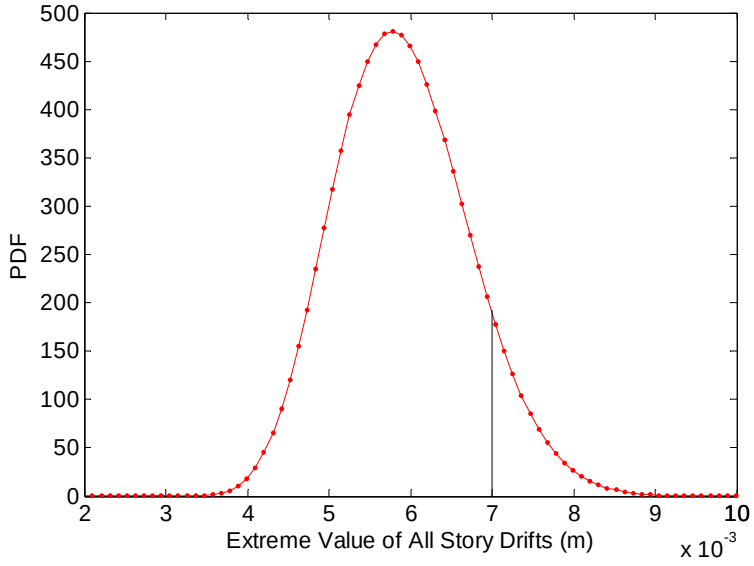

(a) PDF

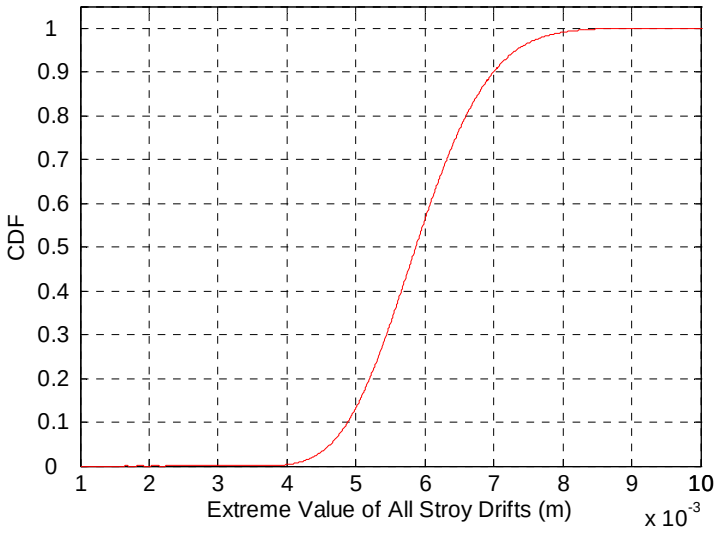

(b) CDF

Figure 8.12 PDF and CDF of the extreme value for the undamaged structure: (a) PDF, (b) CDF

CHAPTER 9

CONCLUSIONS AND RECOMMENDATIONS

9.1 Conclusions

This dissertation has established a framework in which novel stochastic approaches in consideration of the uncertainties involved in measurements, structures and external excitations are proposed to effectively detect damage of building structures and assess their reliability. Firstly, a new statistical moment-based damage detection (SMBDD) method was proposed in the frequency domain. Extensive numerical investigation demonstrated that the proposed method is not only sensitive to structural local damage but also insensitive to measurement noise. Then, the proposed method was extended in the frequency domain in three aspects: the types of building structures, the types and locations of random external excitation and the number of structural responses measured. Extensive numerical examples were presented to demonstrate the feasibility and effectiveness of the generalized SMBDD method. The algorithm of the SMBDD method has also been developed in the time domain. Various damage scenarios were investigated by the generalized SMBDD method in the time domain for different building structures. The application of the proposed method to non-Gaussian excitations was also explored in the time domain. This dissertation then experimentally investigated the SMBDD method both in the frequency domain and in the time domain through shaking table tests. After that, the research work on structural damage detection has made further progress by proposing a new stochastic damage detection method based on the generalized SMBDD method in consideration of random parameters or uncertainties which are

inescapable for civil structures. Finally, two integrated methods have been proposed to respectively evaluate component reliability and system reliability of stochastic structures whose stiffness parameters of all elements identified are random parameters and coupled with each other.

The main contributions of this thesis and the conclusions reached are summarized as follows:

1. Establishment of the Novel Statistical Moment-Based Damage Detection Method

A new structural damage detection method has been proposed in the frequency domain based on the statistical moments of displacement responses of a shear building structure. Firstly, the sensitivity of statistical moments of different responses to structural damage and the effect of measurement noise on the quality of identified results were theoretically analyzed through a single-story shear building under white noise ground excitation. It is found that the relative change of the statistical moment of structural displacement response is two times more sensitive to the relative change of building stiffness than those of velocity and acceleration. In addition, the higher order statistical moments are more sensitive to structural damage than that of the natural frequency and the second-order moment. However, the higher statistical moments may not be numerically stable. As a result, the fourth-order moment of displacement response has been proposed as a new damage index by the proposed method, which makes a tradeoff between the sensitivity to structural damage and the numerical stability to random excitation. Theoretical analysis results of the single-story shear building show that the new method is sensitive to structural damage. Even when the damage severity is only 2%, the identified result is almost the same as

the actual value. In addition, the proposed method is insensitive to measurement noise. Even when the noise intensity is as high as 15%, the maximal relative error of identified damage severity values for various damage cases of the shear building is only 1.88%.

Then various damage scenarios of a three-story shear building were numerically investigated by the proposed SMBDD method in the frequency domain. Numerical results show that the fourth order moments of story drifts can be used to accurately identify both damage locations and damage severities for all the damage scenarios concerned. Furthermore, a significant advantage of the proposed damage detection method has been manifested that it is insensitive to measurement noise. Even when the measurement noise intensity is as high as 15%, the SMBDD method still gives highly reliable results on damage severities and damage locations of the multi-story shear building structure. The feasibility and robustness of the proposed method have been demonstrated through the multi-story shear building.

2. Extension of the SMBDD Method in the Frequency Domain

Further study has advanced the SMBDD method in the frequency domain to make it more general for any type of building structures under any type of random excitation as long as it complies with the Gaussian distribution. The SMBDD method has also been extended from the necessity of complete measurements of all DOFs to the proper selection of measurements of incomplete DOFs. Various damage scenarios of a MDOF shear building structure, a high-rise building and a frame structure have been investigated by using colored noise excitations at different locations and selected measurement responses. The effect of measurement noise on the quality of

identified results has also been investigated for all the damage scenarios concerned by numerically contaminating the external excitations and the measured responses with white Gaussian random noises. Numerical analysis results show that the damage locations and severities of all the concerned various damage scenarios can be identified satisfactorily even though the structural responses used are incomplete and the measurement noise has a high noise-to-signal ratio of 15%. The feasibility and effectiveness of the generalized SMBDD method have been demonstrated by the satisfactorily results of the extensive numerical examples.

3. Extension of the SMBDD Method in the Time Domain

The SMBDD Method has been further extended to the time domain for building structures under Gaussian or non-Gaussian external excitations. The algorithm of the SMBDD method in the time domain has been proposed. Various damage scenarios of different damage locations and damage severities of shear buildings, high-rise buildings and frame structures have been numerically investigated. The effect of measurement noise has also been considered by contaminating measured dynamic responses and external excitations with Gaussian white noise for all the concerned damage scenarios. Numerical results demonstrate that the generalized SMBDD method is feasible and effective for building structures under either Gaussian or non-Gaussian excitations in the time domain. Even when the measurement noise intensity is as high as 15%, the structural damage locations of various damage scenarios with incomplete measurements are accurately identified no matter whether the external excitation is of Gaussian distribution or not. Furthermore, the identified damage severities are exactly equal to the real values when measurement noise is not considered. Otherwise, when measurement noise is considered, the precision of the

identified damage severities in the time domain is similar with that in the frequency domain. Nevertheless, the requirement of proper optimization methods in model updating is required for the generalized SMBDD method in the time domain.

4. Experimental Investigation of the SMBDD Method

The SMBDD method has been experimentally examined both in the frequency domain and in the time domain. Three shear building models were constructed for the shaking table tests under either band-limited white noise excitation or the Kanai-Tajimi filtered white noise (colored noise) excitation. The background noise intensity of about 8% to 10% of the peak ground acceleration was involved in the shake table tests. A total of eight damage scenarios of different damage locations and severities were created on the three building models to examine the feasibility and accuracy of the proposed damage detection method by using white noise and colored noise ground excitations. Firstly, the experimental data were analyzed by the proposed method in the frequency domain. It was found that the identified results from the two different white noise ground excitations were very close to each other for all the damage scenarios concerned. The damage locations and severities of either single damage case or multi-damage case could be identified correctly by the proposed method, even for the minor damage cases. Although the theoretical damage severity values may be different from the real damage severity values, the fact that the identified damage severity values are close to the theoretical values still demonstrates the feasibility and effectiveness of the SMBDD method. Then, the experimental data were analyzed by the proposed method in the time domain. The damage locations of either single damage case or multi-damage case were also accurately identified by the proposed method in the time domain, even for the minor damage cases.

Furthermore, the identified damage severities are close to both the theoretical values and those identified by the proposed method in the frequency domain. It can be concluded that the proposed SMBDD method is feasible and robust both in the frequency domain and in time domain.

5. Development of the Stochastic Damage Detection Method

Another contribution of the dissertation is that a new stochastic damage detection method has been proposed for structural damage detection of building structures of random parameters or with uncertainties. New damage indices have been proposed to not only determine damage locations but also identify damage severities in the stochastic damage detection method. The new stochastic damage detection method can handle building structures with both Gaussian and non-Gaussian random parameters. Numerical investigation has been performed to examine the feasibility and effectiveness of the proposed method in terms of a shear building structure, in which the first damping ratio is regarded as a random parameter with a lognormal distribution. Three damage scenarios have been considered. Numerical analysis results show that not only damage locations but also damage severities can be correctly identified by the proposed method. The proposed method is effective and robust for structural damage detection when uncertainties or random parameters are taken into account.

6. Establishment of a Framework to Evaluate Component and System Reliability of Building Structures

A framework has been established for evaluating component and system reliability of building structures whose stiffness parameters are all random parameters obtained by

system identification and coupled with each other. By directly using the probabilistic information of the random parameters considered in system identification and the SHMS-based measurement data, the structural component reliability and structural system reliability of stochastic building structures can be effectively evaluated by the proposed methods. Structural component reliability and structural system reliability of a three-story shear building structure and its three damage scenarios were respectively evaluated by the two proposed methods. Two cases were explored. In the first case, only the first modal damping ratio was considered as a random parameter. In the second case, both the structural random parameter and the maximum acceleration of the EL Centro excitation were taken into account in the reliability analysis. The first modal damping ratio and the maximum acceleration of the EL Centro excitation are both regarded as random parameters in the second case. The analysis results show that the undamaged shear building has the highest reliability compared with that of the damaged shear building with different damage scenarios. For the damage scenarios at the same locations, the larger damage severity the lower reliability of the damaged shear building. In addition, with the increase of the threshold of top displacement or one story drift, the structural reliability correspondingly increases for both the undamaged shear building and the damaged shear building. For the structural system reliability defined with multi limit state functions, similar analysis results were obtained by the proposed method. Analysis results also show that the failure probability of the whole structure is always larger than or equal to that of one story. Therefore, the reliability of a stochastic structure without explicit damage identification can be obtained by the proposed reliability assessment methods using limited measurement responses.

9.2 Recommendations

Studies have been made in the development of methodologies for damage detection and reliability assessment of instrumented building structures using monitoring data in this thesis. Most of the proposed methods are general and can be developed and applied to other engineering structures. In this section, recommendations are provided for further research and exploration.

(i) Development of the optimization method utilized in the SMBDD method

In the proposed SMBDD method, the nonlinear least square method is utilized to update structural stiffness parameters both in the frequency domain and in the time domain. Although good results have been obtained for almost all the concerned cases, the limitation of the optimization algorithms themselves that they will not always converge to global optimization will jeopardize the effectiveness and feasibility of the proposed SMBDD method to detect structural damage, especially for large complex structures. Therefore, it would be of value to find more efficient and reliable optimization algorithms to ensure the robustness of the SMBDD method.

(ii) Experimental investigation on the proposed SMBDD method for more complicate structural models

In the thesis, shaking table tests have been conducted to demonstrate the feasibility and effectiveness of the proposed SMBDD method through shear building models. Nevertheless, before this method can be applied to real structures the experimental investigation on more complicate structures, such as a three-dimensional frame structures with incomplete measurements, is necessary to further experimentally examine the proposed method.

(iii) Numerical investigation of the stochastic damage detection method for cases with multi random parameters

A framework of the stochastic damage detection method with consideration of the uncertainties or random parameters has been established in the thesis. To illustrate the proposed method, the modal damping ratios are considered as random parameters because the identification of the modal damping ratios involves many uncertainties in reality. For the sake of simplification, only the first damping ratio is assumed as a random parameter with a lognormal distribution. Theoretically speaking, the proposed method can solve the problem of structural damage detection with multiple random parameters or uncertainty factors. Therefore, it is necessary to further investigate the proposed method through damage detection cases with multiple random parameters.

(iv) Study on the probabilistic distribution of the stochastic parameters involved in civil structures

In the numerical investigation of the proposed stochastic damage detection method, the stochastic parameters are assumed to be lognormal distribution, which may be different from the actual situations of real structures. To further understanding the uncertainties of existing structures, it is of value to conduct research and give a statistical description of the concerned random parameters for some kind of structure.

(v) **Experimental investigation and application of the stochastic damage detection methods**

The shaking table tests conducted in this study can be utilized to further evaluate the effectiveness of the proposed stochastic damage detection method. Firstly, the

distribution of the damping ratios could be identified by the Bootstrapping schemes (Kijewski and Kareem, 2002). Then the stochastic damage detection method can be utilized to identify the damage locations and damage severities of the damaged shear building models, and its effectiveness could be evaluated by comparing the identified results with the real values. Once the feasibility and effectiveness of the stochastic damage detection method have been experimentally demonstrated, it can be further applied to real structures according to the following suggested procedures for two different situations. Firstly, if the probabilistic distribution of the random parameters is known, the algorithms proposed in Chapter 7 can be directly utilized to detect structural damage. Otherwise, the PDFs of the structural stiffness parameters at the undamaged state, $\hat{K}^u$, or those after the earthquake, $\hat{K}^d$, should be identified through extensive sampling monitoring data or by Bootstrapping schemes. Then, the PDFs of the structural stiffness parameters can be estimated and structural damage locations and damage severities can be determined according to the proposed method.

References

Acharjee S and Zabaras N (2006). Uncertainty propagation in finite deformations – a spectral stochastic Lagrangian approach, *Computing Methods in Applied Mechanics and Engineering*, 195: 2289–2312.

Agbabian MS, Masri SF, Miller RK and Caughey TK (1988). A system identification approach to the detection of changes in structural parameters, *Structural Safety Evaluation Based on System Identification Approach*, Friedrick Vieweg & Son, Wiesbaden, 341-356.

Alvandi A, Cremona C (2006). Assessment of vibration-based damage identification techniques, *Journal Sound and Vibration*, 292: 179-202.

Ang AHS and Tang WH (1984). *Probability concepts in engineering planning and design -decision, risk and reliability*, Volume II, Wilcy, New York.

Ang AHS, Abdelnour J, Chaker AA (1975). Analysis of activity networks under uncertainty, *Journal of Engineering Mechanics*, ASCE, 101(EM4):373–87.

Araki Y and Hjelmstad KD (2001). Optimum sensitivity-based statistical parameters estimation from modal response, *AIAA Journal*, 39: 1166-1174.

Au FTK, Cheng YS, Tham LG and Bai ZZ (2003). Structural damage detection based on a micro-genetic algorithm using incomplete and noisy modal test data, *Journal of Sound and Vibration*, 259(5): 1081-1094.

Au SK and Beck JL (2001). First excursion probabilities for linear systems by very efficient importance sampling, *Probabilistic Engineering Mechanics*, 16: 193–207.

Banan MR, Banan MR and Hjelmstad KD (1994). Parameter estimation of structures from static response I: computational aspects, *Journal of Structural Engineering*, ASCE, 120: 3243-3258.

Baroth J, Bodé L, Bressolette PH, Fogli M (2006). SFE method using Hermite polynomials: an approach for solving nonlinear mechanical problems with uncertain parameters, *Computer Methods in Applied Mechanics and Engineering*, 195:6479–6501.

Baroth J, Bressolette PH, Chauvière C, Fogli M (2007). An efficient SFE method using Lagrange polynomials: application to nonlinear mechanical problems with uncertain parameters, *Computer Methods in Applied Mechanics and Engineering*, 196:4419–4429.

Beck JL and Katafygiotis LS (1998). Updating models and their uncertainties I: Bayesian statistical framework, *Journal of Engineering Mechanics*, ASCE, 124, 455-461.

Beck JL and Au SK (2002). Baysian updating of structural models and reliability using Markov chain Monte Carlo simulation, *Journal of Engineering Mechanics-ASCE*, 128(4):380-391.

Bjerager P (1988). Probability integration by directional simulation, *Journal of Engineering Mechanics*, ASCE, 14:1285-1302.

Bernard P (1998). Stochastic linearization: what is available and what is not, *Computers and Structures*, 67: 9–18.

Berveiller M, Sudret B, Lemaire M (2006). Stochastic finite element: a non-intrusive approach by regression, *Journal of Computational Mechanics*, 15: 81–92.

Breitung K (1984). Symptotic approximations for multinormal integrals, *Journal of Engineering Mechanics*, ASCE, 110(3): 357–366.

Brenner CE, Bucher C (1995). A contribution to the SFE-based reliability assessment of nonlinear structures under dynamic loading. *Probabilistic Engineering Mechanics*, 10:265–273.

Bucher CG (1988), Adaptive sampling--an iterative fast Monte Carlo procedure, *Structural Safety*, 5:119-126

Byrd RH, Schnabel RB and Shultz GA (1988), Approximate Solution of the Trust Region Problem by Minimization over Two-Dimensional Subspaces, *Mathematical Programming*, 40: 247-263.

Cambou B (1977). Application of First Order Uncertainty Analysis in the Finite Element Method in Linear Elasticity, *Proceedings of Second International Conference on Application of Statistics and Probability in Soil and Structural Engineering*, London, England.

Chaudhry Z and Ganino AJ (1994). Damage detection using neural networks-an initial experimental study on debonded beams, *Journal of Intelligent Material Systems and Structures*, 5: 585-589.

Chen JB and Li J (2005). Dynamic response and reliability analysis of nonlinear stochastic structures, *Probabilistic Engineering Mechanics*, 20:33-44.

Chen JB and Li J (2007). The extreme value distribution and dynamic reliability analysis of nonlinear structures with uncertain parameters, Structural Safety, 29: 77-93.

Chen JJ, Duan BY, Zeng YG (1997). Study on dynamic reliability analysis of the structures with multi-degree-of freedom. *Computers and Structures*, 62(5):877-881.

Chou JH and Ghaboussi J (2001). Genetic algorithm in structural damage detection, *Computers and Structures*, 79:1335-1353.

Christensen PT, Murotsu Y (1986). *Application of structural systems reliability theory*, Berlin, Heidelberg, New York, Tokyo, Springer-Verlag.

Clough RW, Penzien J (1993). *Dynamics of Structures* (2nd edition). McGraw-Hill: New York.

Cobb RG and Liebst BS (1997). Structural damage identification using assigned partial eigenstructure, *AIAA Journal*, 35: 152-158.

Collins JD, Hart GC, Hasselman TK and Kennedy B (1974). Statistical identification of structures, *AIAA Journal*, 12: 185-190.

Cramer H (1966). On the intersections between the trajectories of a normal stationary stochastic process and a high level, *Arkiv för Matematik,* 6: 337-349.

Crandall SH (1970). First-crossing probabilities of the linear oscillator. *Journal of Sound and Vibration,* 12: 285-299.

Dennis JE, Gay DM and Welsch RE (1981), An adaptive nonlinear least-squares algorithm, *ACM Transactions on Math. Software*, 7: 348-368.

Deodatis G. and Shinozuka M (1988). Stochastic FEM Analysis of Nonlinear Dynamic Problems, *Stochastic Mechanics*, Princeton University, Princeton, N.J., 3:27-54.

Deodatis G. and Shinozuka M (1991). Weighted Integral Method II: Response Variability and Reliability, *Journal of Engineering Mechanics*, ASCE, 117 (8):1865-1877.

Ditlevsen O (1979). Narrow reliability bounds for structural systems, *Journal of Structural Mechanics*, 7:453–72.

Doebling SW, Farrar CR and Goodman RS (1997). Effects of measurement statistics on the detection of damage in the Alanosa Canyon Bridge, *Proceedings of the 15th International Modal Analysis Conference*, Orlando, FL, February 3-6, 919-929.

Doebling SW, Farrar CR, Prime MB (1998). A summary review of vibration-based damage identification methods, *The Shock and Vibration Digest*, 30: 91-105.

Doebling SW, Farrar CR, PrimeM B (2001). A summary review of vibration-based damage identification , *The Shock and Vibration Digest*, 30 (2):91-105.

Engelund S and Rackwitz R (1993). A benchmark study on importance sampling techniques in structural reliability, *Structural Safety*, 12(4): 255–276.

Farrar CR, Baker WE, Bell TM, Cone KM, Darling TW, Duffel TA, Eklund A and Migliori A (1994). *Dynamic Characterization and Damage Detection in the I-40 Bridge Over the Rio Grande*, Los Alamos National Laboratory report, LA-12767-MS.

Farrar CR and Jauregui DA (1998). Comoareative study of damage identification algorithms applied to a bridge: I. experiment, *Smart Materials and Structures*, 7:704-719.

Farrar CR and Doebling SW (1998). A comparison study of modal parameter confidence intervals computed using the Monte Carlo and Bootstrap techniques, *Proceedings of the 16th International Modal Analysis Conference*, Santa Barbara, CA, February, 936-944.

Farrar CR, Duffey TA, Doebling SW and Nix DA (1999). A statistical pattern recognition paradigm for vibration-based structural health monitoring, *2nd*

International Workshop on Structural Health Monitoring, Stanford University, Stanford, 764-773.

Feng YS (1989). A method for computing structural system reliability with high accuracy, *Computer & Structures*, 33(1):1–5.

Field Jr RV, Grigoriu M (2004). On the accuracy of the polynomial chaos approximation, Probabilist. *Journal of Engineering Mechanics*, 19:65–80.

Fisher RA, Tippett LHC (1928). Limiting forms of the frequency distribution of the largest and smallest member of a sample, *Proceedings of the Cambridge Philosophical Society*, 24:180–90.

Fox CHJ (1992). The location of defects in structures: a comparison of the use of natural frequency and mode shape data, *Proceedings of the 10th International Modal Analysis Conference*, Society for Experimental Mechanics, Bethel, 552-558.

Fonseca JR, Friswell MI, Mottershead JE and Lees AW (2005). Uncertainty identification by the maximum likelihood method, *Journal of Sound and Vibration*, 288, 587-599.

Foo J, Yosibash Z, Karniadakis GE (2007). Stochastic simulation of riser-sections with uncertain measured pressure loads and/or uncertain material properties, *Computer Methods in Applied Mechanics and Engineering*, 196:4250–4271.

Friswell MI (1989). The adjustment of structural parameters using a minimum variance estimator, *Mechanical Systems and Signal Processing*, 3: 143-155.

Friswell MI and P enny JET (1997). Is damage location using vibration measurements practical, *Damage Assessment of Structures Using Advanced Signal Processing Procedures: DAMAS 97*, Dulieu-Smith JM, Staszewski WJ and Worden K(editors), Sheffield Academic Press, Sheffield, 351-362.

Friswell MI, Penny JET and Garvey SD (1998). A combined genetic and eigensensitivity algorithm for the location of damage in structures, *Computers and Structures*, 69: 547-556.

Ghanem R (1999). Ingredients for a general purpose stochastic finite elements implementation, *Computer Methods in Applied Mechanics and Engineering*, 168:19–34.

Ghanem R (1999). The non-linear Gaussian spectrum of lognormal stochastic processes and variables, *Journal of Applied Mechanics,* ASME, 66:964–973.

Ghanem R, Spanos PD (2003). *Stochastic Finite Elements: A Spectral Approach*, Springer-Verlag, Berlin, Second edition, Dover Publications, New York.

Ghanem RG., Kruger RM (1996). Numerical solution of spectral stochastic finite element systems, *Computer Methods in Applied Mechanics and Engineering*, 129:289–303.

Grigoriu M (1984). Crossings of non-Gaussian translation process. *Journal of Engineering Mechanics*, 110(4):610–20.

Grigoriu M (1998). Simulation of stationary non-Gaussian translation processes. *Journal of Engineering Mechanics*, 124(2):121–6.

Gumbel EJ (1958). *Statistics of extremes*. Columbia University Press.

Handa K and Anderson K (1981). Application of Finite Element Method in the Statistical Analysis of Structures, *International Conference on Structural Safety and Reliability*, Elsevier.

Harbitz A (1986). An efficient sampling method for probability of failure calculation. *Structural Safety,* 3 (2):109-115.

Hart GC and Collins JD (1970). The Treatment of Randomness in Finite Element Modeling, *SAE Shock and Vibrations Symposium*, Los Angeles, CA, Oct., 2509-2519.

Hart GC and Yao JTP (1977), System identification in structural dynamics, *Journal of the Engineering Mechanics Division*, ASCE, 103: 1089-1104.

Hohenbichler M and Rackwitz R (1988). Improvement of second-order reliability estimates by importance sampling, *Journal of Engineering Mechanics*, ASCE, 114:2195-2199

Housner GW, Bergman LA, et al. (1997). Structural control: past, p resent and future, *Journal of Engineering Mechanics*, 123 (9): 897-971.

Hou Z, Noori M and Amand RS (2000). Wavelet-based approach for structural damage detection, *Journal of Engineering Mechanics*, 126(7): 677-683.

Jensen H, Iwan WD (1992). Response of systems with uncertain parameters to stochastic excitation. *Journal of Engineering Mechanics*, 118(5):1012–1025.

Imregun M and Visser WJ (1991). A review of model updating techniques, *Shock and Vibration Digest*, 23: 9-20.

Iwan WD, Huang CT (1996). On the dynamic response of non-linear systems with parameter uncertainty. *International Journal of Non-Linear Mechanics*, 31: 631–645.

Jensen H, Iwan WD (1992). Response of systems with uncertain parameters to stochastic excitation, *Journal of Engineering Mechanics*,118: 1012–1025.

Juan C, Dyke JS and Erik AJ (2000). Health monitoring based on component transfer functions, *Advances in Structural Dynamics*, Elsevier Science Ltd., Oxford, UK, 11, 997-1004.

Karamchandani A and Cornell CA (1991). Adaptive hybrid conditional expectation approaches for reliability estimation, *Structural Safety*, 11: 59-74.

Kareem A and Hseih J (1986). Reliability analysis of concrete chimneys under wind loading, *Journal of Wind Engineering and Industrial Aerodynamics*, 25(1): 93-112.

Kareem A (1988a). Aerodynamic response of structures with parametric uncertainties, *Structural Safety*, 5: 205-225.

Kareem A (1988b). Effect of parametric uncertainties on wind excited structural response, *Journal of Wind Engineering and Industrial Aerodynamics*, 30: 233-241.

Kareem A (1990). Reliability Analysis of Wind Sensitive Structures, *Journal of Wind Engineering and Industrial Aerodynamics*, 33: 495-514.

Katafygiotis LS and Beck JL (1998). Updating models and their uncertainties II: model identifiability, *Journal of Engineering Mechanics*, 124: 463-467.

Kawano K, Venkataramana K (1999). Dynamic response and reliability analysis of large offshore structures. *Computer Methods in Applied Mechanics and Engineering*, 168: 255-272.

Kijewski T and Kareem A (2002). On the reliability of a class of system identification techniques: insights from bootstrap theory, *Structural Safety*, 24:261-280.

Kleiber M and Hien TD (1992). *The Stochastic Finite Element Method: Basic Perturbation Technique and Computer Implementation*, Wiley, New York.

Klosner JM, Haber SF, Voltz P (1992). Response of non-linear systems with parameter uncertainties, *International Journal of Non-Linear Mechanics*, 27(4): 547–563.

Ko JM, Wong CW and Lam HF (1994). Damage detection in steel framed structures by vibration measurement approach, *Proceedings of the 12th International Modal Analysis Conference*, Society for Experimental Mechanics, Bethel, 280-286.

Lam HF, Ko JM and Wong CW (1995). Detection of damage location based on sensitivity analysis, *Proceedings of 13th International Modal Analysis Conference*, 1499-1505.

Law SS, Waldron P and Taylor C (1992). Damage detection of a reinforced concrete bridge deck using the frequency response function, *Proceedings of 10th International Modal Analysis Conference*, 772-778.

Li J (1996). *Stochastic structural systems-analysis and modeling*, Beijing, Science Press.

Li J and Roberts JB (1999a). Stochastic structural system identification, Part1: mean parameter estimation, *Computational Mechanics*, 24: 206-210.

Li J and Roberts JB (1999b). Stochastic structural system identification, Part2: variance parameter estimation, *Computational Mechanics*, 24: 211-215.

Li J and Chen JB (2003). The probability density evolution method for analysis of stochastic structural dynamic response. *Acta Mechanica Sinica*, 35: 437–442.

Li J, Chen JB (2003). Probability density evolution method for dynamic response analysis of stochastic structures, Advances in Stochastic Structural Dynamics, *Proceedings of the Fifth International Conference on Stochastic Structural Dynamics*, Hangzhou, China, August.

Li J, Chen JB (2004). Probability density evolution method for dynamic response analysis of structures with uncertain parameters, *Computational Mechanics*, 34: 400-409.

Li J, Chen JB (2006). The probability density evolution method for dynamic response analysis of non-linear stochastic structures, *International Journal for Numerical Methods in Engineering*, 65:882–903.

Li J, Chen JB and Fan WL (2006). The equivalent extreme-value event and evaluation of the structural system reliability, *Structural Safety*, 29: 112-131.

Link M (2001). Updating of analytical models – review of numerical procedures and application aspects, *Structural Dynamics @2000: Current Status and Future Directions*, Ewins DJ, Inman DJ (editors), Research Studies Press, Philadelphia, 193-223.

Liu SC and Yao JTP (1978), Structural identification concept, *Journal of the Structural Division*, ASCE, 104: 1845-1858.

Liu PL (1995). Identification and damage detection of trusses using modal data, *Journal of Structural Engineering*, ASCE, 121: 599-608.

Liu WK, Besterfield G and Belytschko T (1988). Transient probabilistic systems. *Computing Methods in Applied Mechanics and Engineering*, 67(1): 27–54.

Lucor D, Su CH, Karniadakis G.E (2004). Generalized polynomial chaos and random oscillators, *International Journal for Numerical Methods in Engineering*, 60:571–596.

Klosner JM (1992), Haber SF, Voltz P. Response of non-linear systems with parameter uncertainties, *International Journal of Non-Linear Mechanics*, 27: 547–563.

Maes MA, Breitung K and Upuis D J (1993), Symptotic importance sampling, *Structural Safety*, 12:167- 186

Madsen HO and Tvedt L (1990). Methods for time-dependent reliability and sensitivity analysis, *Journal of Engineering Mechanics*, 16:2118-2135.

Mares C and Surace C (1996). An application of genetic algorithms to identify damage in elastic structures, *Journal of Sound and Vibration*, 195: 195-215.

Matthies HG., Brenner CE, Bucher CG. and Soares CG. (1997). Uncertainties in Probabilistic Numerical Analysis of Structures and Solids-Stochastic Finite Elements, *Structural Safety*, 19 (3): 283-336.

Mayes RL (1992). Error localization using mode shapes – an application to a two link robot arm, *Proceedings of the 10th International Modal Analysis Conference*, Society for Experimental Mechanics, Bethel, 886-891.

Mckay MD, Beckman RJ and Conover WJ (2000). A comparison of three methods for selecting values of input variables in the analysis of output from a computer code, *Technometrics*, 42(1): 55-61.

Melchers RE (1987). *Structural reliability analysis and prediction*, Halsted Prcss, New York.

Melchers RE (1990). Radial importance sampling for structural Reliability, *Journal of Engineering Mechanics*, ASCE,116:189-203.

Melchers RE and Tang LK (1984). Dominant failure modes in stochastic structural systems, *Structural safety*, 2(2):127-143.

Montgomery DC (1976), *Design and analysis of experiments*, John Wiley & Sons Incorporation.

Mohan PS, Nair PB, Keane AJ (2008). Multi-element stochastic reduced basis methods, *Computing Methods in Applied Mechanics and Engineering*, 197:1495–1506.

Mottershead JE and Friswell MI (1993), Model updating in structural dynamics: a survey, *Journal of Sound and Vibration*, 167: 347-375.

Murotsu Y, Okada H, Yonezawa M, Grimmelt M and Taguchi K (1981). Automatic generation of stochastically dominant modes of structural failure in frame structure, *Bulletin of University of Osaka Prefecture*, Series A, 30: 85-101.

Nair PB, Keane AJ (2002). Stochastic reduced basis methods, *AIAA Journal,* 40:1653–1664.

Nakagiri S and Hisada T (1982). Stochastic Finite Element Method Applied to Structural Analysis with Uncertain Parameters, *Proceedings of the International Conference on FEM,* August, 206-211.

Natke HG (1988), Updating computational models in frequency domain based on measured data: a survey, *Probabilistic Engineering Mechanics*, 3, 28-35.

Natke HG and Yao JTP (1988). *Structural Safety Evaluation Based on System Identification Approach*, Friedrick Vieweg & Son, Wiesbaden.

Natke HG (1991). Error localization within spatially finite-dimensional models, *Computational Mechanics,* 8: 153-160.

Ndambi MJM (2002), *Damage assessment in reinforced concrete beams by damping analysis*, Ph.D dissertation, Mechanics of Materials and Constructions, Vrije University, Brussel, Belgium.

Nordal H, Cornell CA and Karamchandani A (1987). A structural system reliability case study of an eight-leg steel jacket offshore production platform, *Marine Structural reliability symposium,* Arlington, Virginia.

Nouy A, Clément A, Schoefs F, Mo N (2008), An extended stochastic finite element method for solving stochastic partial differential equations on random domains, *Computing Methods in Applied Mechanics and Engineering*, 197: 4663-4682.

Papadopoulos L and Garcia E (1998). Structural damage identification: a probabilistic approach, *AIAA Journal*, 36: 2137-2145.

Pandey AK, Biswas M, Samman MM (1991). Damage detection from changes in curvature mode shapes, *Journal Sound and Vibration*,145: 321-332.

Pandey AK and Biswas M (1994), Damage detection in structures using changes in flexibility, *Journal of Sound and Vibration*, 169: 3-17.

Park S, Stubbs N and Sikorsky C (1997). Linkage of nondestructive damage evaluation to structural system reliability, *Smart Systems for Bridges, Structures and Highways*, Stubbs N(editor), The International Society for Optical Engineering, Bellingham, 234-245.

Powell A (1958). On the fatigue failure of structures due to vibration excited by random pressure fields, *Journal of the Acoustical Society of America*, 30(12):1130–1135.

Rackwitz R (2001). Reliability analysis - a review and some perspectives, *Structural Safety*, 23 (4) : 365 – 395

Ratcliffe CP (1997). Damage detection using a modified Laplacian operator on mode shape data, *Journal of Sound and Vibration*, 204: 505-517.

Rice OC (1944), Mathematical analysis of random noise, *Bell System Technical Journal*, ASCE, 23:282-332.

Ricles JM and Kosmatka JB (1992). Damage detection in elastic structures using vibratory residual forces and weighted sensitivity, *AIAA Journal*, 30: 2310-2316.

Rizos PF, Aspragathos N and Dimarogonas AD (1990). Identification of crack location and magnitude in a cantilever beam from the vibration modes, *Journal of Sound and Vibration*, 138 (3): 381-388.

Rytter A(1993). *Vibration Based Inspection of Civil Engineering Structures*, Ph.D Thesis, Department of Building Technology and Structural Engineering, Aalborg University, Denmark.

Rubenstein RY, (1981). *Simulation and the Monte Carlo method*, Wiley, New York.

Sachdeva SK, Nair PB, Keane AJ (2006). Comparative study of projection schemes for stochastic finite element analysis, *Computing Methods in Applied Mechanics and Engineering*, 195:2371–2392.

Salane HJ, Baldwin JW (1990). Identification of modal properties of bridges, *Journal of Structural Engineering*, 116: 2008-2021.

Salawu OS (1997). Detection of Structural Damage through Changes in Frequency: A Review, *Engineering Structures*, 19: 718-723.

Salawu OS (1997). An integrity index method for structural assessment of engineering structures using modal testing, *Insight: The Journal of the British Institute of Non-Destructive Testing*, 39(1): 126-137.

Salawu OS and Williams C (1994). Damage location using vibration mode shapes. *Proceedings of 12th International Modal Analysis Conference*, 933-939.

Salawu OS and Williams C (1995). Bridge assessment using forced-vibration testing, *Journal of Structural Engineering*, ASCE, 121: 161-173.

Sanayei M and Saletnik MJ (1996a), Parameter estimation of structures from static strain measurements I: formulation, *Journal of Structural Engineering*, ASCE, 122: 555-562.

Sanayei M and Saletnik MJ (1996b). Parameter estimation of structures from static strain measurements II: error sensitivity analysis, *Journal of Structural Engineering*, ASCE, 122: 563-572.

Schevenels M, Lombaert G., Degrande G. (2004). Application of the stochastic finite element method for Gaussian and non-Gaussian systems, *Proceedings of ISMA Conference*, 3299-3313.

Schuëller GI (1997). A State-of-the-Art Report on Computational Stochastic Mechanics, *Journal of Probabilistic Engineering Mechanics*, 12 (4):197-313.

Shi ZY, Law SS, and Zhang LM (2000). Optimum sensor placement for structural damage detection, *Journal of Engineering Mechanics*, ASCE, 126: 1173-1179.

Shinozuka M (1972). Monte-Carlo solution of structural dynamics, *Comput Struct*, 2: 655-674.

Shinozuka M and Deodatis G. (1988). Response Variability of Stochastic Finite Element Systems, *Journal of Engineering Mechanics*, 114 (3): 499-519.

Shinozuka M (1983). Basic analysis of structural safety, *Journal of Strutural Engineering*, ASCE, 109: 721-740.

Smyth AW, Masri SF, Caughey TK and Hunter NF (2000). Surveillance of mechanical systems on the basis of vibration signature analysis, *Journal of Applied Mechanics*, ASME, 67: 540-551.

Sohn H and Law KH (1997). A Bayesian probabilistic approach for structure damage detection, *Earthquake Engineering and Structural Dynamics*, 26: 1259-1281.

Sohn H, Farrar CR, Hunter NF, Worden K (2001). Structural health monitoring using statistical pattern recognition techniques, *Journal of Dynamic Systems Measurement and Control-Transactions of the ASME*, 123(4): 706-711.

Sohn H, Farrar CR, Hemez FM, Shunk DD, Stinemates DW, and Nadler BR (2004). *A review of structural health monitoring literature: 1996-2001*, Report No. LA-13976-MS, Los Alamos National Laboratory, Los Alamos, New Mexico.

Soong TT (1973). *Random Differential Equations in Science and Engineering*, Academic Press, New York, London.

Spanos PD, and Ghanem R (1989). Stochastic finite element expansion for random media, *Journal of Engineering Mechanics*, ASCE, 115: 1035-1053.

Spencer BF Jr. (1988). Elishakoff I. Reliability of uncertain linear and nonlinear systems, *Journal of Engineering Mechanics*, 114(1):135–149.

Stubbs N and Kim JT (1996), Damage localization in structures without baseline modal parameters, *AIAA Journal*, 34, 1644-1649.

Stubbs N, Park S, Sikorsky C and Choi S (1998). A methodology tonondestructively evaluate the safety of offshore platforms, *Proceedings of the 8th International Offshore and Polar Engineering Conference*, The International Society of Offshore and Polar Engineers, California, 71-79.

Stubbs N, Park S, Sikorsky C, and Choi S (2000). A global non-destructive damage assessment methodology for civil engineering structures, *International Journal of System Science*, 31: 1361-1373.

Sudret B, Kiureghian AD (2000). *Stochastic finite element methods and reliability: a state-of-the-art report*, Report No. UCB/SEMM-2000/08, University of California at Berkeley, USA.

Sudret B, Kiureghian AD (2002). Comparison of finite element reliability methods, *Probabilistic Engineering Mechanics*, 17:337–348.

Sun Z and Chang CC (2002). Structural damage assessment based on wavelet packet transform, *Journal of Structural Engineering*, ASCE, 130(7): 1055-1062.

Syski R (1967). *Stochastic differential equations in modern nonlinear equations*, McGraw-Hill: New York.

Tang LK and Melchers RE (1987). Dominant mechanisms in stochastic plastic frames, *Reliability engineering & system safety*, 18(2):101-115.

Titurus B, Friswell MI and Starek L (2003a). Damage detection using generic elements, Part I: model updating, *Computers and Structures*, 81: 2273-2286.

Titurus B, Friswell MI and Starek L (2003b). Damage detection using generic elements, Part II: damage detection, *Computers and Structures*, 81: 2287-2299.

Tognarelli MA, Zhao J, Rao KB, Kareem A (1997). Equivalent statistical quadratization and cubicization for nonlinear system, *Journal of Engineering Mechanics*, 123(5):512–523.

Toki K, Sato T and Kiyono J (1989). Identification of structural parameters and input ground motion from response time histories, *The Journal of Structural Engineering/Earthquake Engineering*, JSCE, 6(2): 413-421.

Topole KG and Stubbs N (1995). Nondestructive damage evaluation of a structure from limited modal parameters, *Earthquake Engineering and Structural Dynamics*, 24: 1427-1436.

Tsou P and Shen MHH (1994). Structural damage detection and identification using neural networks, *AIAA Journal*, 32 (1): 176-183.

Tvedt L (1990). Distribution] of quadratic forms in normal space, application to structural reliability, *Journal of Engineering Mechanics*, 116(6): 1183–1197.

Vanik MW, Beck JL and Au SK (2000). Bayesian probabilistic approach to structural health monitoring, *Journal of Engineering Mechanics-ASCE*, 126(7): 738-745.

Vanmarcke EH (1972). Properties of spectral moments with applications to random vibration, *Journal of Engineering Mechanics*, 98:425–46.

Vanmarcke EH (1973). Matrix form formulation of reliability analysis and reliability-based design, *Computers and Structures*, 3: 757-770.

Vincent B, Hu J and Hou Z (1999). Damage detection using empirical mode decomposition and a comparison with wavelet analysis, *Proceedings of 2nd*

Iternational Workshop on Structural Health Monitoring, Stanford University, Stanford, CA, 891-900.

Wang Z, Au FTK and Cheng YS (2008). Statistical damage detection based on frequencies of sensitivity-enhanced structures, *International Journal of Structural Stability and Dynamics*, 8(2): 231-255.

Wen YK and Chen HC (1987). On fast integration for time variant structural reliability, *Probabilistic Engineering Mechanics* , 2:156-162.

West WM (1984). Illustration of the use of modal assurance criterion to detect structural changes in an orbiter test specimen, *Proceedings of Air Force Conference on Aircraft Structural Integrity*, 1-6.

Witherell CE (1994). *Mechanical Failure Avoidance: Strategies and Techniques*, McGraw-Hill, New York.

Wong FS and Yao JTP (2001). Health monitoring and structural reliability as a value chain, *Computer-Aided Civil and Infrastructure Engineering*, 16: 71-78.

Worden K, Farrar CR, Manson G, Park G (2005). Fundamental axioms of structural health monitoring. *Structural Health Monitoring 2005: Advancements and Challenges for Implementation*, Chang FK (editor), DEStech Publications, Lancaster, Pennsylvania, 26-41.

Wu X, Ghaboussi J and Garrett JH (1992). Use of neural networks in detection of structural damage, *Computers and Structures*, 42(4), 649-659.

Wu D and Law SS (2004). Damage localization of plate structures from uniform load surface curvature, *Journal of Sound and Vibration*, 276, 227-244.

Xia PQ and Brownjohn JMW (2003). Residual stiffness assessment of structurally failed reinforced concrete structure by dynamic testing and finite element model updating, *Experimental Mechanics*, 43: 372-378.

Xia Y and Hao H (2001). A genetic algorithm for structural damage detection based on vibration data, *Proceedings of 19th International Modal Analysis Conferences, Kissimmee*, FL, 1381-1387.

Xia Y, Hao H, Brownjohn JMW and Xia PQ (2002). Damage identification of structures with uncertain frequency and mode shape data, *Earthquake Engineering and Structural Dynamics*, 31: 1053-1066.

Xia Y and Hao H (2003). Statistical damage identification of structures with frequency changes, *Journal of Sound and Vibration*, 263, 853-870.

Xiu D, Karniadakis GE (2002). The Wiener–Askey polynomial chaos for stochastic differential equations, SIAM, *Journal of Scientific Computing*, 24:619–644.

Xu YL and Chen J (2004). Structural damage detection using empirical mode decomposition: experimental investigation, *Journal of Structural Engineering*, ASCE, 130(11): 1279-1288.

Xu YL, Zhu HP and Chen J (2004), Damage detection of mono-coupled multistory buildings: Numerical and experimental investigations, *Structural Engineering and Mechanics*, 18**(**6): 709-729.

Xu XF (2007). A multiscale stochastic finite element method on elliptic problems involving uncertainties, *Computing Methods in Applied Mechanics and Engineering*, 196:2723–2736.

Xu YL, Zhang J & Li JC (2009), Experimental investigation on statistical moment-based structural damage detection method, *Journal of Structural Health Monitoring*, accepted for publication.

Yang JN and Lei Y (1999). Identification of natural frequencies and damping ratios of linear structures via Hilbert transform and empirical mode decomposition,

Proceedings of International Conference on Intelligent Systems and Control, IASTED/Acta press, Anaheim, California, 310-615.

Yao JTP (1979). Damage assessment and reliability evaluation of existing structures, *Engineering Structures*, 1: 245-251.

Yao JTP (1983). Damage evaluation for structural reliability assessment, *Nuclear Engineering and Design*, 75: 205-212.

Yao JTP (1985). *Safety and Reliability of Existing Structures*, Pitman Advanced Publication Program, Boston.

Yao GC, Chang KC, and Lee GC (1992). Damage diagnosis of steel frames using vibrational signature analysis, *Journal of Engineering Mechanics*, 118 (9): 1949-1961.

Yao JTP and Natke HG (1994). Damage detection and reliability evaluation of existing structures, *Structural Safety*, 15: 3-16.

Yeo I, Shin S, Lee HS and Chang SP (2000). Statistical damage assessment of framed structures from static responses, *Journal of Engineering Mechanics*, ASCE, 126: 414-421.

Yuen MMF (1985). A numerical study of the eigen-parameters of a damaged cantilever, *Journal of Sound and Vibration*, 103: 301-310.

Yuen KV and Katafygiotis LS (2005). Model updating using noisy response measurements without knowledge of the input spectrum, *Earthquake Engineering and Structural Dynamics*, 34: 167-187.

Zimmerman DC and Kaouk M (1992). Eigenstructure assignment approach for structural damage detection, *AIAA Journal*, 30: 1848-1855.

Zimmerman DC and Smith SW (1992). Model refinement and damage location for intelligent structures, *Intelligent Structural Systems*, Tzou, HS, and Anderson, GL (editors), Kluwer Academic Publishers, Boston, Massachusetts, 403-452.

Zimmerman DC (2006). Statistical confidence using minimum rank perturbation theory, *Mechanical Systems and Signal Processing*, 20: 1155-1172.

Zhang J, Xu YL, Xia Y and Li J (2008). A new statistical moment-based structural damage detection method, *Structural Engineering and Mechanics-An International Journal*, 30(4): 445-466

Zhou J, Feng X and Fan YF (2003)**.** A probabilistic method for structural damage identification using uncertain data, *Structural Health Monitoring and Intelligent Infrastructure*, Wu ZS and Abe M (editors), A.A. Balkma, Lisse, 487-492,